12-2016

Evaluation of 1,4-Dioxane Biodegradation Under Aerobic and Anaerobic Conditions

Francisco J. Barajas Rodriguez
Clemson University, rbaraja@clemson.edu

EVALUATION OF 1,4-DIOXANE BIODEGRADATION UNDER AEROBIC AND ANAEROBIC CONDITIONS

A Dissertation
Presented to
the Graduate School of
Clemson University

In Partial Fulfillment
of the Requirements for the Degree
Doctor of Philosophy
Environmental Engineering and Earth Science

---

by
Francisco J. Barajas Rodríguez
December 2016

Accepted by:
Dr. David L. Freedman, Committee Chair
Dr. Ronald W. Falta
Dr. Kevin T. Finneran
Dr. Harry D. Kurtz, Jr.
Dr. Lawrence C. Murdoch

ABSTRACT

Used mainly as a solvent stabilizer, 1,4-dioxane is present at many sites contaminated along with chlorinated solvents and other chemical compounds. Considered a probable human carcinogen by the U.S. Environmental Protection Agency, this contaminant has raised considerable concerns because of its potential adverse effects on health. Therefore, remediation of 1,4-dioxane has gained importance, and although there are several approaches for its treatment, such as *ex situ* physicochemical processes, bioremediation is a key alternative because it is a low energy demanding process. Anaerobic conditions are present at most contaminated sites, however, there is insufficient scientific evidence for anaerobic biodegradation of 1,4-dioxane. On the other hand, aerobic biodegradation of 1,4-dioxane has been widely studied under metabolic and cometabolic conditions. Nevertheless, limited information is known about the rate of 1,4-dioxane cometabolism with substrates, such as propane, that can be used for *in situ* bioremediation. Bacteria that grow on 1,4-dioxane have a low affinity for the contaminant since their half saturation coefficient (*Ks*) values are often high, but the contaminant half saturation coefficients (*Kc*) associated with cometabolism are usually lower. However, kinetic parameters for cometabolic biodegradation of 1,4-dioxane with a non-toxic and convenient substrate such as propane have not been evaluated. Based on the gaps in the scientific literature, and in order to expand the understanding of 1,4-dioxane biodegradation and its potential *in situ* bioremediation applications, the objectives of this study included: 1) Estimate the kinetic parameters for 1,4-dioxane metabolism and for cometabolism by propane-oxidizing bacteria that are relevant to field applications in bioremediation; and 2)

Evaluate the potential for *in situ* bioremediation of a 1,4-dioxane plume using metabolic and cometabolic biosparging and bioaugmentation, based on simulations using a subsurface transport model; and 3) Evaluate the potential for anaerobic biodegradation of 1,4-dioxane.

To achieve the first objective, kinetic parameters for aerobic cometabolic biodegradation of 1,4-dioxane by propane-oxidizing bacteria were evaluated for a pure culture, *Rhodococcus ruber* ENV425, and a mixed culture, ENV487. The 1,4-dioxane metabolizer *Pseudonocardia dioxanivorans* CB1190 was also tested for its kinetic parameters. Kinetics for metabolic and cometabolic biodegradation of 1,4-dioxane were successfully modeled using modified Monod equations. Results indicate that the propanotrophic bacteria have lower half saturation constants (K_C = 6.05 ± 0.26 and 3.25 ± 0.05 mg COD L^{-1}) for 1,4-dioxane than CB1190 (K_S = 11.5 ± 0.4 mg COD L^{-1}). Other parameters measured included the biomass yield (Y) for propane and 1,4-dioxane, transformation capacity (T_C), half saturation coefficients for oxygen (K_{SO} and K_{CO}), biomass decay coefficient (b), and substrate utilization rates (k_S and k_C). Coinhibition parameters (K_{iS} and K_{iC}) between propane and 1,4-dioxane were also estimated. Batch simulations showed that cometabolism is more advantageous than metabolism when the initial concentration of 1,4-dioxane is low (~1 mg L^{-1}) and that both processes are heavily impacted by dissolved oxygen concentrations less than 2 mg L^{-1}.

The second objective was achieved by simulating the effect of biodegradation reactions on a 1,4-dioxane subsurface plume treated with biosparging and bioaugmentation. The effect of the injection rates of propane, biomass and oxygen as well

as the initial 1,4-dioxane concentrations were evaluated in terms of the time to reach an average 1,4-dioxane level of 1 μg L^{-1}, as well as the percentage of 1,4-dioxane that underwent biodegradation. Data from a biosparging pilot study at Vandenburg Air Force base was used to calibrate the model as it applied to propanotrophic cometabolism. The simulation results indicated that propanotrophic cometabolism achieves remediation at a faster rate when the initial 1,4-dioxane concentration is less than 7.5 mg L^{-1}; lower concentrations do not support enough growth of microbes that grow of 1,4-dioxane to adequately offset the effect of cell decay. A continuous supply of propane to support cometabolism negates the effect of cell decay. The model provides a framework for comparing metabolic and cometabolic approaches to *in situ* bioremediation at other sites.

To achieve the third objective, microcosms were prepared with groundwater and sediment from two contaminated sites at which the field data suggest that 1,4-dioxane is undergoing anaerobic biodegradation. The groundwater contains high levels of acetone and isopropanol, which ensure anaerobic conditions. High levels of halogenated solvents are also present. The microcosms were amended with uniformly labeled [^{14}C]-1,4-dioxane to characterize degradation products. Amendments included Fe(III) oxide, Fe(III)-ethylene-diaminetetraacetic acid (Fe(III)-EDTA), anthraquinone disulfonate (AQDS), sulfate and oxygen. Following four years of incubation, biodegradation of many of the halogenated solvents was observed, as was iron reduction, sulfate reduction, and methanogenesis. However, there was no significant evidence to support biodegradation of 1,4-dioxane under anaerobic conditions, although partial mineralization in aerobic microcosms was observed. Further laboratory studies are needed to determine the

feasibility of anaerobic biodegradation of 1,4-dioxane. Until then, aerobic treatment remains the only viable bioremediation alternative.

DEDICATION

This dissertation is dedicated to my mother, Josefina Barajas; my grandfather, Jose Barajas; and family members and friends who have shown their support along the pursuit of this Ph.D. degree. This work could not have been done without their continuous and unconditional encouragement.

ACKNOWLEDGEMENTS

I would like to express my sincere gratitude to my adviser Dr. David L. Freedman for all his guidance, patience, and help that he showed during my pursuit of the doctoral degree, as well as his valuable mentorship inside and outside of the laboratory. I would also like to acknowledge my committee members Dr. Ronald W. Falta, Dr. Kevin T. Finneran, Dr. Harry Kurtz and Dr. Lawrence C. Murdoch for their guidance and input in this research.

I would like to give my special thanks to Dr. Lawrence C. Murdoch for his important contribution to the subsurface contaminant transport simulations work; Dr. Robert Steffan, Sheryl Stregel and David Lippincott for providing information and assistance on field data from the 1,4-dioxane bioaugmentation study at the Vandenberg Air Force Base site; and Dr. Shaily Mahendra at UCLA for providing the bacteria isolate *Pseudonocardia dioxanivorans* CB1190 to conduct part of the kinetic modeling study.

I would also like to thank Dr. Leo Lehmicke and Hargis and Associates, Inc. for providing financial and logistical support to conduct the anaerobic microcosms study for 1,4-dioxane biodegradation.

I would like to acknowledge the Mexican Science and Technology National Council (Consejo Nacional de Ciencia y Technologia, CONACYT) for their financial support during the first four years of pursuit of the Ph.D. degree.

I would like to thank my lab mates at Clemson University, i.e., Rong Yu, Angel A. Ramos, Anthony T. Reid, Hari S. Peethambaram, Han Wang, etc. for providing collaborative and friendly environment in the laboratory environment. I would also like to

thank the Dr. Kevin T. Finneran and Dr. Tanju Karanfil research group members for their valuable support and mentoring during my research activities.

TABLE OF CONTENTS

Page

LIST OF ABBREVIATIONS

Acronym	Definition
AQDS	Anthraquinone -2,6-disulfonate
COD	Chemical oxygen demand
DCA	Dichloroethane
DCE	Dichloroethylene
DCM	Dichloromethane
EDTA	Ethylenediaminetetraacetic acid
EPA	Environmental Protection Agency
GC	Gas chromatography
HPLC	High performance liquid chromatography
IPA	Isopropyl alcohol
MTBE	Methyl-*tert*-butyl ether
TBA	*Tert*-butyl alcohol
TCA	Trichoroethane
THF	Tetrahydrofuran
VAFB	Vandenberg Air Force Base
VC	Vinyl Chloride
VOC	Volatile organic compound

1. INTRODUCTION

1.1 Background

Chlorinated solvents were used for different industrial applications for decades,, mostly related to degreasing of metals to clean electronic equipment, semiconductors, precision instruments and aircraft hardware, and also for uses such as extraction of oils, textile cleaning, production of pharmaceuticals and preparation of inks and paints (Mohr, 2010a). Solvent stabilizers were used to protect solvents from physical and chemical conditions which could lead to hydrolysis, oxidation or condensation reactions that deteriorate the quality of the solvent. Solvent stabilizers, such as 1,4-dioxane, are present at most contaminated sites where chlorinated solvents were released to the environment. 1,4-Dioxane was first identified in 1863 (Lourenço, 1863) and became commercially available in the late 1920s. In the past, 1,4-dioxane was not considered to be a contaminant of concern and remediation focused mostly on the chlorinated solvents and other contaminants. However, recent studies show that 1,4-dioxane is an animal carcinogen and a probable human carcinogen, which led the Environmental Protection Agency (EPA) to reconsider 1,4-dioxane's status as an emerging contaminant (EPA, 2012).

The most important application of 1,4-dioxane was as a stabilizer of 1,1,1-trichloroethane (1,1,1-TCA) in aluminum containers. Therefore, 1,4-dioxane is usually associated with 1,1,1-TCA spills and has been detected at more than 50 Superfund sites (Mohr, 2010a). However, since 1,4-dioxane has also been used as an industrial solvent, some contaminated sites where chlorinated solvents are absent have 1,4-dioxane present as

the main contaminant (Mohr, 2010a). It is also found as an impurity in a variety of products such as antifreeze and aircraft deicing fluids, deodorants, shampoos, detergents, paints and varnishes (EPA, 2012; Mohr, 2010a). 1,4-Dioxane is also present in a variety of cosmetic products because it is a byproduct in the process of ethoxylation in the production of surfactants and in the production of polyethylene terephthalate (Hartung, 1989; Mohr, 2010a). In addition, it is present in some foods such as coffee and shrimp, although it is not clear if this occurrence is natural or due to the presence of 1,4-dioxane in surface water and groundwater used for irrigation (Hartung, 1989). 1,4-Dioxane levels that range from 5 to 6 ppm have been reported in polysorbate compounds used as an emulsifier in ice cream and other frozen desserts; the polymerization of these chemicals from polyoxyethylene involves trace levels of 1,4-dioxane as an impurity (Mohr, 2010a). 1,4-Dioxane is also used as a solvent for inks, adhesives, fats, waxes, cellulose esters, ethers and resins.

The occurrence of 1,4-dioxane in groundwater appears to be larger than previously anticipated. In California alone, a multisite survey showed that 1,4-dioxane has been detected at more than 194 sites out of more than 2,000 surveyed, from which 95% of them had chlorinated solvents present (Adamson et al., 2014). According to the survey, the plumes of 1,4-dioxane have an average concentration of 365 $\mu g\ L^{-1}$ and a median length of 269 m, which are frequently shorter than those of chlorinated solvents. The survey also reveals that 1,4-dioxane has not been identified at sites where chlorinated solvents could be associated with its presence. The data mining done in the California survey and monitoring results from the Air Force indicate that natural attenuation of 1,4-dioxane is occurring at some of the sites, where maximum site concentrations decreased 0.59 orders

of magnitude (Adamson et al., 2015). Attenuation rates of 1,4-dioxane that were confirmed at 22 sites were similar to the rates for 1,1-dichloroethylene (1,1-DCE) and trichloroethylene (TCE), and lower than for 1,1,1-TCA. Monitoring well data from the Air Force showed that attenuation frequency was similar to those observed in California. These findings indicate that dilute plumes of 1,4-dioxane may undergo natural attenuation. Nevertheless, this is not a universal situation, which raises the question as to what forms of active remediation should be used.

1,4-Dioxane moves rapidly in groundwater and does not volatilize very quickly from surface waters. 1,4-Dioxane is weakly retarded in soil because of its low adsorption to soil particles and it tends to move quickly from soil to groundwater. In addition, previous studies suggest that 1,4-dioxane is relatively resistant to biodegradation and does not bioconcentrate along the food chain (EPA, 2012; Mohr, 2010a).

Monitoring of 1,4-dioxane in surface waters has not been comprehensive in the United States, although several studies have been done with detection limits as low as 0.15 $\mu g\ L^{-1}$. One of the studies was conducted by the Lawrence Livermore National Laboratory for groundwater in the area of Sacramento, California. A total of 108 wells were analyzed with a detection limit of 0.2 $\mu g\ L^{-1}$; three samples had levels below 1 $\mu g\ L^{-1}$ (Mohr, 2010a). Another study done in the Kanagawa Prefecture in Japan showed levels of 1,4-dioxane between 0.2 and 1.5 $\mu g\ L^{-1}$ in tap water. 1,4-Dioxane was detected in 90% of the wells sampled, with the highest concentration levels ranging from 50 to 95 $\mu g\ L^{-1}$ (Mohr, 2010a). According to EPA, estimates of 1,4-dioxane releases to the environment from 1988 to 2004

indicate that out of 28 million pounds transferred to treatment facilities, 15 million pounds were released (Mohr, 2010a).

Because 1,4-dioxane is present as a byproduct in several consumer products such as shampoos, liquid dishwashing and laundry soaps, this contaminant can be present in wastewater. This was confirmed in samples from Michigan and Japan (Mohr, 2010a). In the City of Ann Arbor, Michigan, 1,4-dioxane was found at levels of 3 $\mu g\ L^{-1}$ in the influent to a wastewater treatment plant and the concentration was 2 $\mu g\ L^{-1}$ in effluent samples. In Japan, a wastewater treatment plant had 16 $\mu g\ L^{-1}$ in its influent and 11 $\mu g\ L^{-1}$ in its effluent. The sources of 1,4-dioxane in the Japanese wastewater were industrial pollution and surfactants. In the US, 1,4-dioxane was detected in three out of 100 sewage samples (Mohr, 2010a).

1,4-Dioxane has also been detected in the vicinity of landfills, including leachate, groundwater, landfill gas, and landfill gas condensate. According to a survey by EPA, the mean concentration of 1,4-dioxane in leachate from all municipal landfills was 118 $\mu g\ L^{-1}$ (Mohr, 2010a).

1.2 Health Risks

Exposure to 1,4-dioxane can occur during its manufacture or use as a stabilizer or solvent, via inhalation, ingestion of contaminated food or water, and dermal contact (EPA, 2012; Hartung, 1989). The most common route of exposure is inhalation and its distribution is uniform and rapid in the lung, liver, kidney, spleen, colon and skeletal muscle tissue. The highest risk of exposure is for workers at industrial sites that can inhale 1,4-dioxane repeatedly. Short term effects include irritation of the eyes, throat, nose and lungs as well

as vertigo, anorexia and headache. Long term exposure effects include dermatitis, eczema, drying and cracking of the skin and liver and kidney damage. 1,4-Dioxane has no known genotoxic or reproductive effects, although some studies on rats have shown that the developing fetus may be a target of toxicity. In terms of carcinogenicity, EPA has classified 1,4-dioxane as a probable human carcinogen by all routes of exposure (Hartung, 1989).

1.3 Physicochemical Properties

1,4-Dioxane is a cyclic ether that is produced by the dehydration of ethylene glycol or derived from ethylene oxide (Mohr, 2010a). Its structure consists of a ring of four carbons containing two oxygen atoms placed opposite each other resulting in two ether functional groups. The compound is completely miscible in water and most organic solvents, with an octanol-water partition coefficient, log K_{ow}, from -0.42 to -0.07. Its bioconcentration factor varies from 0.28 to 0.52 and its dimensionless Henry's constant is 1.96×10^{-4} (Mohr, 2010a). These properties make 1,4-dioxane highly mobile in subsurface environments and difficult to breakdown or strip out of water.

1.4 Bioremediation Relevance

1,4-Dioxane has become an increasingly important remediation target. Physicochemical techniques are available for ex situ treatment, but the associated costs are often considered prohibitive. Extracting groundwater for ex-situ treatment is generally regarded as ineffective for mass removal, and ex-situ treatment typically relies on energy and/or chemical intensive processes such as sonication, UV light, or use of strong oxidants. *In situ* remediation is a more appealing approach, especially if bioremediation can be used.

However, *in situ* bioremediation is hampered by a lack of information on the most effective strategy. Bioremediation is a potential alternative for cleanup of sites that are contaminated with 1,4-dioxane. A large amount of laboratory evidence supports biodegradation of this contaminant by microorganisms under aerobic conditions. Several fungi and bacteria have been discovered that oxidize 1,4-dioxane to CO_2 (Li et al., 2010; Mahendra and Alvarez-Cohen, 2006; Nakamiya et al., 2005; Parales et al., 1994; Pugazhendi et al., 2015; Sei et al., 2013; Sun et al., 2011) having several intermediate products such as 2-hydroxyethoxyacetaldehyde, 2-hydroxyethoxy acetic acid, and ethylene glycol (Figure 1-1). In contrast, there is limited evidence in the scientific literature for anaerobic biodegradation of 1,4-dioxane (Shen et al., 2008).

Metabolic aerobic biodegradation of 1,4-dioxane by a number of bacterial cultures has been studied, as well as cometabolic biodegradation associated with growth on several primary substrates. Several kinetic parameters, such as half saturation constants, maximum specific biodegradation rates, and biomass yields have been determined for aerobic metabolic biodegradation of 1,4-dioxane by mixed and pure cultures (Mahendra and Alvarez-Cohen, 2006). However, less is known about the kinetics of biodegradation of 1,4-dioxane under cometabolic conditions, especially with primary growth substrates, such as propane, that could be applied for *in situ* bioremediation, as opposed to primary growth substrates that are toxic, such as tetrahydrofuran (THF). Although cometabolism of 1,4-dioxane with propane as primary substrate has been observed (Skinner et al., 2009; Sun et al., 2011; Vainberg et al., 2006; Zenker et al., 2002), there is a lack of detailed information about the kinetic parameters for propane-oxidizing bacteria that degrade 1,4-dioxane, as

well as a comparison of the performance of these cometabolic kinetic parameters with those from metabolic biodegradation in field applications. To address this issue, the research presented in this dissertation fills those gaps by providing a kinetic model that describes cometabolic biodegradation of 1,4-dioxane by an enrichment culture (ENV487) and a pure culture (*Rhodococcus ruber* ENV425) that use propane as their primary growth substrate. The model consists of kinetic parameters estimated via laboratory experiments based on the approach used by Chang and Criddle (1997). The kinetic parameters were then used in a groundwater model to compare cometabolic biodegradation of 1,4-dioxane to metabolic biodegradation under simulated subsurface conditions.

This study also evaluated anaerobic biodegradation of 1,4-dioxane. The motivation for doing so came from field observations at two contaminated industrial sites. At these sites, the disappearance of a plume of 1,4-dioxane cannot be explained by dilution or any other physical process, and therefore, biodegradation was hypothesized as the mechanism. Field evidence indicates the plumes are anaerobic. To test this hypothesis, a series of microcosms containing sediment and groundwater from the sites were prepared, incubated anaerobically, and monitored over time. [^{14}C]-1,4-dioxane was added to determine the extent of biodegradation and the potential daughter products over time.

1.5 Biodegradability of Other Ether Compounds

Since 1,4-dioxane is an ether compound, it is important to review the biodegradability of related compounds that fall into this category. Ethers are organic compounds that present a higher challenge for biodegradation than many other hydrocarbons. Nevertheless, several microorganisms have been discovered that degrade

and, in some cases, grow on these types of compounds. Some of these microorganisms are able to degrade 1,4-dioxane cometabolically when grown on another ether compound.

1.5.1 Tetrahydrofuran

Biodegradation of THF has been well studied. THF is a cyclic ether composed of five carbon atoms, with a structure similar to that of 1,4-dioxane. A number of bacteria are able to grow on this compound. For example, Bernhardt and Diekman (1991) isolated and characterized the first aerobic bacterium able to grow on THF as a sole carbon source, *Rhodococcus* strain 219. A different microorganism, *Pseudonocardia* sp. strain K1, was isolated from a wastewater treatment plant and is capable of using THF as a sole source of carbon and energy under aerobic conditions (Kohlweyer et al., 2000). This bacterium grows with a doubling time of 14 h at a THF concentration of 20 mM and neutral pH, and it also grows on diethyl ether, polyethylene glycol and on two potential THF degradation products: γ-butyrolactone and 4-hydroxybutyrate. Strain K1 transforms THF with the involvement of a binuclear iron-containing monooxygenase (THFmo) which oxidizes THF to 2-hydroxytetrahydrofuran (Vainberg et al., 2006).

Cometabolism of THF and other ether compounds has been observed. Vainberg et al. (2006) studied the biodegradation of multiple ether pollutants such as THF, 1,4-dioxane, 1,3-dioxolane, *bis*-2-chloroethylether and MTBE by *Pseudonocardia* sp. strain ENV478. The enrichment culture was grown on THF and then exposed to the ether compounds and was able to degrade all of them. The best rates of biodegradation of 1,4-dioxane were achieved when the culture was previously grown on THF; however, the culture was also able to degrade 1,4-dioxane after being grown on sucrose, lactate, yeast extract, 2-propanol

and propane. The daughter product of 1,4-dioxane degradation was hydroxyethoxy acetic acid.

Optimization of the culture conditions for THF degradation resulted in isolation of a novel bacterium, *Rhodococcus* sp. YYL (Yao et al., 2009). This microorganism tolerates high concentrations of THF (up to 200 mM). The conditions tested to optimize THF biodegradation were pH, media concentrations of phosphorus ($K_2HPO_4 \cdot 3H_2O$), ammonia (NH_4Cl) and yeast extract (growth factors), and it was found that three trace elements that significantly increased THF biodegradation were found (Mg^{2+}, $Zn^{2+}$and Fe^{2+}) whereas the optimum values for pH, NH_4Cl, $K_2HPO_4 \cdot 3H_2O$, and yeast extract were 8.26, 1.80, 0.81 and 0.06 g L^{-1}, respectively.

Under anaerobic conditions, THF is considered a recalcitrant compound (Battersby and Wilson, 1989). A comprehensive study by Hongwei et al. (2004) showed the potential for anaerobic biodegradation of 47 aliphatic organic compounds, including 1,4-dioxane and THF, which were classified as poorly biodegradable. The key molecular structure variables involved in this assessment were total energy and molecular diameter, which were directly proportional to the potential for anaerobic biodegradation.

1.5.2 Methyl tert-Butyl Ether

Biodegradation of MTBE under aerobic conditions is well documented. Several cultures that originated from different environments can partially degrade or completely mineralize MTBE, either by using it as a sole energy and carbon source or through cometabolic processes. MTBE is biodegraded into *tert*-butyl alcohol (TBA) by a monooxygenase enzyme. Eventually, TBA is degraded to CO_2 (Deeb et al., 2000).

Anaerobic biodegradation of MTBE under *in situ* and laboratory conditions has been reported (Finneran and Lovley, 2001; Wilson et al., 2005; Yeh and Novak, 1994). Yeh and Novak (1994) found that MTBE, ethyl *tert*-butyl ether and TBA were biodegraded under sulfate reducing, denitrifying and methanogenic conditions. MTBE was the most recalcitrant to biodegradation whereas TBA was the easiest to degrade. MTBE and ETBE degradation was observed in sediments with low organic matter and a pH around 5.5, however, the co-existence of ethanol or other readily biodegradable compounds was inhibitory to MTBE and ETBE biodegradation.

The presence of humic substances and Fe(III) improved the biodegradation of MTBE under anaerobic conditions in sediments from a petroleum contaminated aquifer and in aquatic sediments (Finneran and Lovley, 2001). Microcosms without Fe(III) and humic substances did not show degradation of MTBE in aquifer soils. Using [^{14}C]-MTBE, the biodegradation products were identified as CO_2 and methane. TBA was also degraded to CO_2 and methane in aquatic sediments. In both soil types, the lag period prior to the onset of MTBE biodegradation was 250-300 days.

Even though ether type compounds are generally considered to be recalcitrant under anaerobic conditions, recent research on anaerobic biodegradation of MTBE indicates that it is possible to enhance this process under conditions commonly found in subsurface environments. Analogous to MTBE, the recent findings on aerobic and anaerobic biodegradation of 1,4-dioxane suggest that this compound could potentially be biodegraded in contaminated aquifers under the appropriate conditions.

1.5 Objectives

The overall objective of this dissertation was to evaluate metabolic and cometabolic biodegradation of 1,4-dioxane under anaerobic and aerobic conditions. The research filled several gaps in the literature by addressing the following specific objectives:

1) Determine the kinetic parameters for aerobic cometabolism of 1,4-dioxane by the propane-oxidizers *Rhodococcus ruber* ENV425 and mixed culture ENV425 as well as for metabolism by the isolate *Pseudonocardia dioxanivorans* CB1190. This objective is addressed in Chapter 2.

2) Compare bioremediation of a subsurface 1,4-dioxane plume under cometabolic conditions using ENV425 and under metabolic conditions using CB1190 by performing simulations with a contaminant transport model in groundwater. This objective is addressed in Chapter 3.

3) Evaluate the anaerobic biodegradation of 1,4-dioxane by performing a microcosm study using sediment and groundwater obtained from two former industrial sites impacted with 1,4-dioxane, chlorinated solvents, acetone, and isopropyl alcohol (IPA). This objective is addressed in Chapter 4.

This research investigated the biodegradation of 1,4-dioxane under anaerobic and aerobic conditions. The evaluation of anaerobic biodegradation was performed first. One of the motivations to study anaerobic biodegradation stems from field observations from two former industrial contaminated sites. Such observations indicate that anaerobic attenuation of 1,4-dioxane is occurring *in situ* because: 1) the sites are anaerobic due to the high chemical oxygen demand (COD) levels; and 2) 1,4-dioxane is disappearing faster than

expected. Based on these observations, the hypothesis of anaerobic biodegradation being responsible for attenuation of 1,4-dioxane at these sites was formulated.

Born from the necessity to explore other alternatives for *in situ* bioremediation of 1,4-dioxane, and in order to fill gaps in the scientific literature, a study of the kinetic parameters for cometabolism of 1,4-dioxane under aerobic conditions by propane-oxidizing bacteria was conducted. The potential advantage of using propane-oxidizers rests with the low cost and availability of propane as a primary substrate for *in situ* applications. Propane is not a toxic compound and it is less hazardous than some other primary substrates studied for 1,4-dioxane cometabolism. The kinetic parameters for cometabolism of 1,4-dioxane of the propane-oxidizing bacteria were compared with those from cultures that use 1,4-dioxane as a sole source of carbon and energy. To achieve this, objectives #1 and #2 needed to be satisfied. Completion of objective #1 provided an estimate of the required kinetic parameters, as well as a mathematical model that describes the kinetics of cometabolism of 1,4-dioxane by the propane-oxidizing bacteria. The model considers simultaneous and non-simultaneous cometabolism, co-inhibition between propane and 1,4-dioxane, and the limiting effect of oxygen on biodegradation rates. Objective #2 was achieved by evaluating the performance of metabolic and cometabolic bacteria and using the kinetic parameters obtained from the experimental data in a transport model that describes subsurface contamination with 1,4-dioxane. The model was tested at different concentrations of 1,4-dioxane and for different dimensions of the contaminant plume. In so doing, conditions that may be advantageous to implementing cometabolism were defined.

1.6 Figure for Chapter 1

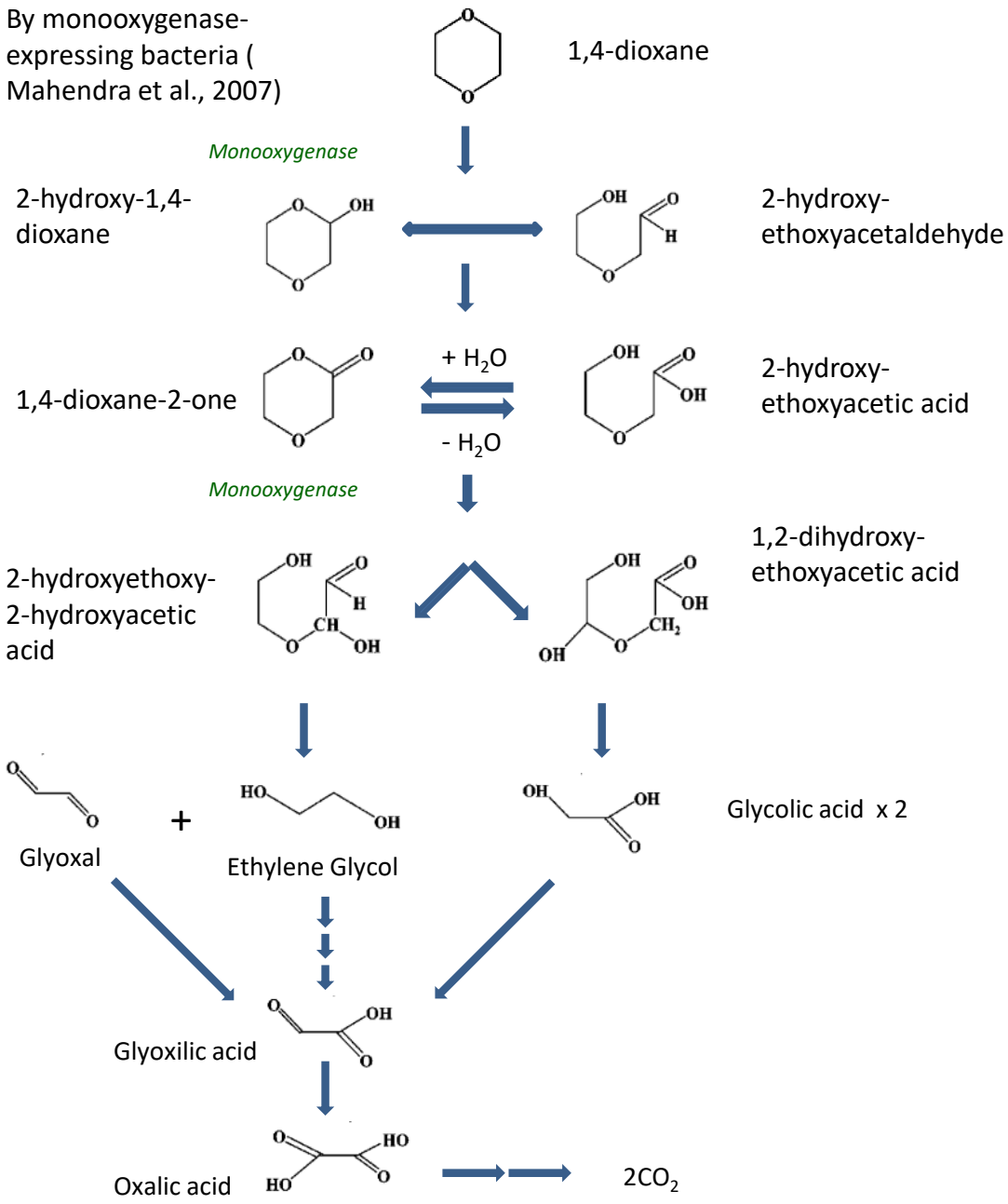

Figure 1-1 Pathway for aerobic biodegradation of 1,4-dioxane by strain CB1190 (Mahendra et al., 2007).

2. KINETICS OF 1,4-DIOXANE BIODEGRADATION UNDER AEROBIC AND ANAEROBIC CONDITIONS

2.1 Abstract

Bioremediation of groundwater contaminated with 1,4-dioxane may be achieved via bioaugmentation with cultures that use the contaminant as a growth substrate or by cultures that grow on a primary substrate such as propane and consume 1,4-dioxane via cometabolism. To evaluate these approaches requires a comprehensive understanding of the kinetics of both processes. Laboratory experiments were performed with suspended growth cultures to determine 16 Monod kinetic coefficients that describe consumption of 1,4-dioxane as a primary substrate by *Pseudonocardia dioxanivorans* CB1190 and cometabolism of 1,4-dioxane by the propanotrophic mixed culture ENV487 and by the propanotroph *Rhodococcus ruber* ENV425. Yields for the propanotrophs were approximately twice as high as for CB1190, as were the endogenous decay coefficients. Maximum specific growth rates, determined under intrinsic conditions, were highest for ENV425, followed by ENV487 and CB1190. Half saturation constants for 1,4-dioxane were approximately two to four times lower for the propanotrophic cultures compared to CB1190. Propane was significantly inhibitory to 1,4-dioxane biodegradation, but the reverse did not occur. The effect of oxygen concentration on metabolisms and cometabolism was incorporated; the propanotrophs exhibited a higher affinity for oxygen when degrading 1,4-dioxane in comparison to CB1190, although their affinity for oxygen was lower when growing on propane. Once all 16 kinetic parameters were determined, the

full kinetic model was used to simulate batch biodegradation of 1,4-dioxane. The propanotrophs decreased 1,4-dioxane from 1,000 to 1 μg L^{-1} in less time than the CB1190 when the initial biomass concentration was 0.74 mg COD L^{-1}; metabolic biodegradation was favored at higher initial biomass concentrations and higher initial 1,4-dioxane concentrations. The effect of dissolved oxygen on 1,4-dioxane biodegradation became apparent with all three cultures when the dissolved oxygen concentration fell below approximately 1.5 mg L^{-1}. The kinetic model provides a framework for comparing *in situ* biodegradation of 1,4-dioxane via bioaugmentation with cultures that use the contaminant as a growth substrate to those that achieve biodegradation via cometabolism.

2.2 Introduction

The emerging contaminant 1,4-dioxane has been detected at many sites across the U.S. (Adamson et al., 2014; Mohr, 2010b), usually in the presence of chlorinated solvents (Anderson et al., 2012). Since 1,4-dioxane is a probable human carcinogen and is highly miscible in water (Mohr, 2010a), special attention has been given to its presence in subsurface aquifers where it poses a health risk to the public, prompting the need of remediation approaches to achieve clean up goal levels. Although previously considered a recalcitrant compound, laboratory and field evidence support mineralization of 1,4-dioxane by microorganisms under aerobic conditions, whether by its use as a carbon and energy source (Kelley et al., 2001; Kim et al., 2009; Li et al., 2010; Mahendra and Alvarez-Cohen, 2005; Mahendra and Alvarez-Cohen, 2006; Nakamiya et al., 2005; Pugazhendi et al., 2015; Sun et al., 2011) or via cometabolism following growth on a primary growth substrate (Mahendra and Alvarez-Cohen, 2006; Vainberg et al., 2006; Zenker et al., 2002).

Metabolic processes are often considered advantageous for *in situ* biodegradation on the basis of higher rates of transformation, reduced risk of clogging due to excessive biomass growth, reduced oxygen demand, and reduced concern from not having to inject and distribute a primary substrate. For example, maximum specific biodegradation rates of up to 68 mg 1,4-dioxane COD mg biomass COD^{-1} d^{-1} have been reported for *Pseudonocardia dioxanivorans* CB1190, which uses the contaminant as a sole source of carbon and energy (Mahendra and Alvarez-Cohen, 2006). Studies of cometabolism with THF serving as the primary growth substrate show maximum specific biodegradation rates up to 0.58 mg 1,4-dioxane COD mg biomass COD^{-1} d^{-1} (Vainberg et al., 2006; Zenker et al., 2002). Nevertheless, cometabolic biodegradation may be advantageous for dilute plumes of 1,4-dioxane. In these instances, the low concentration of 1,4-dioxane may not be sufficient to support growth. An extensive survey by Adamson et al. (2014) indicates that the majority of contaminated sites have 1,4-dioxane levels below 1,800 μg COD L^{-1}.

Cometabolism of 1,4-dioxane can be achieved with several primary substrates, including propane, methane, toluene, and THF. Metabolism of a primary substrate induces formation of monooxygenases that initiate the oxidation of 1,4-dioxane (Mahendra and Alvarez-Cohen, 2006). There are several advantages associated with using propane for *in situ* cometabolic bioremediation; it is widely available, relatively inexpensive, and is non-toxic in comparison to substrates such as THF or toluene. Cometabolism of 1,4-dioxane with propane as a primary growth substrate has been observed in laboratory studies (Skinner et al., 2009; Sun et al., 2011; Vainberg et al., 2006; Zenker et al., 2002) as well as *in situ*, at a contaminated field site in which propane biosparging and bioaugmentation

with the culture *Rhodococcus ruber* ENV425 were applied (Lippincott et al., 2015). Nevertheless, there is limited information on the kinetic properties of propanotrophs, as well as no systematic comparison of the performance of cometabolic and metabolic biodegradation of 1,4-dioxane. Although the half saturation constant, biomass yield and maximum specific biodegradation rate have been reported for CB1190 (Mahendra and Alvarez-Cohen, 2006), the experimental conditions used were closer to extant than intrinsic (Grady et al., 1996; Kovárová-Kovar and Egli, 1998), i.e., the parameters were measured at relatively high concentrations of biomass to 1,4-dioxane. However, intrinsic conditions are more adequate to characterize reproducible kinetic parameter of bacteria cultures because such parameters become independent of the culture's history (Kovárová-Kovar and Egli, 1998).

The objectives of this study were to measure the kinetics of propane metabolism and 1,4-dioxane cometabolism by a mixed (ENV487) and a pure (ENV425) culture of propanotrophs under intrinsic conditions, and to measure the kinetics of 1,4-dioxane by CB1190 under intrinsic conditions. In both cases, the effect of dissolved oxygen concentration was incorporated. The resulting parameters were used in batch simulations of biodegradation, to explore the effect of the initial concentration of 1,4-dioxane, the initial biomass concentration, and dissolved oxygen concentration, on the time required to biodegrade 1,4-dioxane to 1.82 μg COD L^{-1}.

2.3 Modeling Aspects

The Monod-based kinetic model used in this study is applicable to cometabolism of a non-growth substrate (1,4-dioxane) in the presence or absence of a primary growth substrate

(propane), as originally proposed by Chang and Criddle (1997) for methanotrophic cometabolism of trichloroethylene. Equations 2-1 to 2-5 comprise the full model for metabolic and cometabolic biodegradation of 1,4-dioxane:

$$\frac{dS}{dt} = -q_{SMAX} \cdot \frac{S}{K_S\left(1+\frac{C}{K_{iC}}\right)+S} \cdot \frac{O - O_{SMIN}}{K_{SO} + O - O_{SMIN}} \cdot \frac{1}{\beta} \cdot X \qquad 2\text{-}1$$

$$\frac{dC}{dt} = -q_{CMAX} \cdot \frac{C}{K_C\left(1+\frac{S}{K_{iS}}\right)+C} \cdot \frac{O - O_{CMIN}}{K_{CO} + O - O_{CMIN}} \cdot X \qquad 2\text{-}2$$

$$\frac{dO}{dt} = -q_{COMAX} \cdot \frac{C}{K_C\left(1+\frac{S}{K_{iS}}\right)+C} \cdot \frac{O - O_{CMIN}}{K_{CO} + O - O_{CMIN}} \cdot \frac{1}{\beta} \cdot X \qquad 2\text{-}3$$

$$- q_{SOMAX} \cdot \frac{S}{K_S\left(1+\frac{C}{K_{iC}}\right)+S} \cdot \frac{O - O_{SMIN}}{K_{SO} + O - O_{SMIN}} \cdot \frac{1}{\beta} \cdot X$$

$$\frac{dX}{dt} = Y \cdot \beta \cdot \frac{dS}{dt} - bX - \frac{dC}{dt} \cdot \frac{1}{T_C} \qquad 2\text{-}4$$

$$\beta = \frac{V_l + H'V_g}{V_l} \qquad 2\text{-}5$$

where S is the concentration of growth substrate, C is concentration of non-growth substrate, X is the concentration of biomass, O is the concentration of dissolved oxygen, Y is the yield, K_S is the half saturation coefficient for growth substrate, K_C is the half saturation coefficient for non-growth substrate, q_{SMAX} is the maximum specific growth

substrate degradation rate, q_{CMAX} is the maximum specific non-growth substrate degradation rate, b is the endogenous decay coefficient, T_C is the transformation capacity, K_{iS} is the co-inhibition coefficient for the effect of growth substrate on non-growth substrate, K_{iC} is the co-inhibition coefficient for the effect of non-growth substrate on growth substrate degradation, K_{SO} is the half saturation coefficient for oxygen during growth substrate utilization, K_{CO} is the half saturation coefficient for oxygen during cometabolism of non-growth substrate, O_{SMIN} is the lowest level of oxygen achievable during biodegradation of growth substrate, O_{CMIN} is the lowest level of oxygen achievable during degradation of the non-growth substrate, q_{SOMAX} is the maximum specific oxygen utilization rate during biodegradation of the growth substrate, q_{COMAX} is the maximum specific oxygen utilization rate during degradation of non-growth substrate, β is the ratio of total mass in the bottle ($V_l \cdot C_l + V_g \cdot C_g$) to the mass in the aqueous phase ($V_l \cdot C_l$), V_l is the volume of liquid in a bottle, V_g is the volume of gas in a bottle, and H' is Henry's Law constant. Inclusion of dissolved oxygen is essential for capturing its impact on both metabolic and co-metabolic biodegradation of 1,4-dioxane, as described previously for other substrates (Rashid and Kaluarachchi, 1999; Semprini and McCarty, 1991a; Semprini and McCarty, 1991b).

2.4 Materials and Methods

2.4.1 Chemicals

1,4-Dioxane (99%) was obtained from Aldrich, oxygen (99.5%) from National Welders, nitrogen (99.99%) from National Welders, propane (99.5%) from Airgas, and

dichloromethane (DCM, 99.95%) from Omnisolve. Reagents for the protein assay included a MicroBCA kit (Thermo Scientific®), sodium hydroxide (ACS grade) from Amresco Inc., sodium bicarbonate (99.7%) from J.T. Baker and hydrochloric acid (ACS grade) from EMD Chemicals. All other chemicals used were reagent grade or equivalent in purity.

2.4.2 Cultures

Two propane-oxidizing cultures were obtained from CB&I. A pure culture, *Rhodococcus ruber* strain ENV425, was received on an agar plate and transferred to basal salts mineral medium (BSM) amended with 12 mM of sodium lactate. ENV487, a mixed consortium, was received in BSM. The composition of BSM (Hareland et al., 1975) was modified in order to reduce the amount of organic chelator (nitrilotriacetic acid, NTA). Experiments with BSM containing 12.9 mM NTA indicated that NTA served as a growth substrate; with a reduced level of NTA (1.3 mM), growth was not detectable but enough was present to prevent precipitation of trace metals.

Both propanotrophic cultures were grown at room temperature (22-24 °C) in 2.6 L glass bottles containing 1.5 L of BSM and 20% propane/80% air (v/v) in the headspace. The bottles were capped with screw caps lined with a Teflon septum. The bottles were incubated at room temperature on a shaker table. Oxygen in the headspace was maintained above 5% during biomass growth by periodic addition of pure oxygen.

Pseudonocardia dioxanivorans CB1190 was obtained from the University of California at Los Angeles. Colonies from agar plates were transferred to bottles containing ammonium mineral salts medium amended with 100 mg L^{-1} (182 mg COD L^{-1}) of 1,4-dioxane. The bottles were sealed with a gray butyl rubber septum and screw cap and

incubated on a shaker table at room temperature. The culture was maintained by transferring it periodically to fresh AMSM with concentrations of 1,4-dioxane of up to 500 mg L^{-1} (910 mg COD L^{-1}), as well as to agar plates with AMSM and 1,4-dioxane.

After growing the cultures in their respective media, harvesting was done when microbial activity was close to the stationary phase (Appendix A, Figure 6-1) to obtain the inoculum used in the experiments. It is assumed that bacteria cells harvested during this phase are still expressing the necessary enzymes to carry out cometabolism. In addition, centrifugation during harvesting removes any dissolved primary growth substrate.

2.4.3 Experimental Approach

A sequential approach was used to determine the kinetic parameters, similar to that one described by Chang and Criddle (1997). Most of the parameters were estimated independently to reduce uncertainty. For example, in the case of μ_{MAX} and K_S, μ_{MAX} should be determined first and then it can be used to fit for K_S. If both parameters are fit at the same time, there is a chance of obtaining multiple solutions.

Table 2-2 and Table 2-3 specifies which equations were fit to determine a parameter, which previously determined parameters were used as part of the fitting process, the initial concentrations of biomass, propane and/or 1,4-dioxane, and the number of replicates. Data was collected from batch assays performed at room temperature (22-24 °C), in 160 mL serum bottles with 100 mL of liquid, unless specified otherwise. The conversion of mass per bottle to aqueous phase concentration of propane was determined with equation 2-5, using a Henry's Law constant of 1.4 x 10^{-3} mol L^{-1} atm^{-1} (Sander, 1999); Henry's Law constant for 1,4-dioxane is sufficiently low (Mohr, 2010a) that it was

assumed to be zero. Biomass, propane and 1,4-dioxane are reported in terms of COD units. The conversion factors are 1.42 mg COD mg biomass^{-1} (Grady et al., 2011), 3.63 mg COD mg propane^{-1}, and 1.82 mg COD mg 1,4-dioxane^{-1}.

2.4.4 Yield and Endogenous Decay Coefficients

Yields for the propanotrophic cultures and CB1190 were measured by inoculating serum bottles with a low concentration of biomass and monitoring the increase in protein as the substrate was consumed. Yields were determined from the slope of cumulative biomass formed versus substrate consumed.

To determine endogenous decay coefficients, the propanotrophs and CB1190 were grown in 2.5 media L bottles containing 1.5 L of liquid by repeated additions of substrate until the biomass concentration reached 420 mg COD L^{-1}. The biomass was then continuously aerated by sparging with air in the absence of substrate. The rate of oxygen uptake was measured several times over a period of 9-14 days using a dissolved oxygen polarographic probe (Orion 5 Star, Thermo Scientific®). The biomass decay coefficient was calculated from the slope of the line between the natural logarithm of the oxygen uptake rate and incubation time (Grady et al., 2011).

2.4.5 Monod Kinetic Coefficients

Batch depletion data for propane and 1,4-dioxane were used to determine maximum growth rates (μ_{MAX}) and half saturation constants. Propanotrophic cells were harvested from 2.5 L bottles during the stationary phase of growth by centrifugation at (10,750x*g*, 15 min) and re-suspended in BSM. Serum bottles were inoculated with a low concentration of

culture and a high concentration of substrate (Table 2-2 and Table 2-3) and consumption of substrate was monitored over time. Assuming endogenous decay is negligible during periods of exponential growth, the substrate concentration (propane or 1,4-dioxane) is high relative to the half saturation constant, and the initial biomass concentration is low relative to the new amount formed, maximum growth rates were determined using the following equation:

$$dS/dt = \mu_{MAX} \cdot S_u \qquad 2\text{-}6$$

where S_u is the cumulative uptake of propane or 1,4-dioxane over time. When the integrated form of this equation is plotted (ln S_u versus time), the slope equals $\mu_{MAX.}$ To ensure that intrinsic conditions prevailed, this means, that bacteria performance was not affected by the environmental conditions, the initial ratio of substrate to biomass was ≥ 20 on a COD basis (Grady et al., 1996). Based on μ_{MAX} and Y, the maximum specific substrate utilization rates for propane and 1,4-dioxane were calculated:

$$q_{SMAX} = \mu_{MAX}/Y \qquad 2\text{-}5$$

Half saturation constants for the growth substrates (K_S) were determined by fitting substrate depletion data (from the same bottles used to determine μ_{MAX}) to equations 2-1 and 2-4 (for ENV487 and CB1190) (Table 2-2 and Table 2-3). For the initial experiments, the biodegradation equations focused on biomass growth and substrate consumption and were simplified by keeping oxygen in excess and setting the non-growth substrate concentration to zero (absence of cometabolism).

2.4.6 Non-growth Substrate Coefficients

Propanotrophic cells were harvested from 2.5 L bottles during the stationary phase of growth by centrifugation (10,750 x *g*, 15 min) and re-suspended in BSM (426 mg COD L^{-1}). 1,4-Dioxane was added at varying concentrations (14.5 to 36.4 mg COD L^{-1}), in the absence of propane. q_{CMAX} and K_C were determined by simultaneously fitting the batch depletion data for 1,4-dioxane to equations 2-2 and 2-4 (Table 2-2). The initial 1,4-dioxane concentration was low enough such that it was depleted to below detection. An initial estimate for T_C was obtained by adding enough 1,4-dioxane to triplicate bottles (182 mg COD L^{-1}) so that it was not all consumed and recording the amount consumed; T_C was estimated (1.6 and 1.00 mg 1,4-dioxane COD mg biomass COD^{-1} for ENV425 and ENV487, respectively) based on the mass of 1,4-dioxane consumed and the initial mass of cells present.

Additional experiments were performed in the same manner but at higher initial 1,4-doixane concentrations (182-1456 mg COD L^{-1}). The complete data set (i.e., bottles with only the propanotrophic cultures and 1,4-dioxane) was fit to equations 2-2 and 2-4 (with oxygen not limiting) to arrive at final values for q_{CMAX}, K_C and T_C (which changed only 2.1% from the initial estimate for ENV425 and 32% for ENV487).

To determine the co-inhibition coefficient for the effect of propane on 1,4-dioxane utilization (K_{iS}), propanotrophic cells were harvested during the stationary phase of growth as described above. Experiments in triplicate bottles were prepared with varying initial concentrations of propane (0, 1.8, 3.6, 7.2, or 14.4 mg COD L^{-1}) and a single concentration of 1,4-dioxane (22 mg COD L^{-1}). Batch depletion data for 1,4-dioxane and propane were

fit to equations 2-1, 2-2, and 2-4 (with oxygen not limiting) to estimate K_{iS} (Table 2-2), using an initial estimate ($8.5x10^3$ and $1x10^8$ mg COD L^{-1} for ENV425 and ENV487, respectively) for the effect of 1,4-dioxane on propane utilization (K_{iC}).

To determine K_{iC}, propanotrophic cells were harvested during the stationary phase of growth as described above. Experiments in triplicate bottles were prepared with varying initial concentrations of 1,4-dioxane (0, 182, 364, 655 and 1456 mg COD L^{-1}) and a single concentration of propane (42 mg COD L^{-1}). Batch depletion data for 1,4-dioxane and propane were fit to equations 2-1, 2-2, and 2-4 (with oxygen not limiting) to estimate K_{iC} (Table 2-2) using the estimate for K_{iS} as input. Using the initial estimates for K_{iS} and K_{iC}, the fitting process with each data set was repeated, until the estimates for both parameters converged.

2.4.7 Coefficients for Oxygen

Propanotrophic cells were harvested from 2.5 L bottles during the stationary phase of growth by centrifugation at (10,750x*g*, 15 min) and re-suspended in BSM (426 mg COD L^{-1}). Triplicate serum bottles were inoculated with culture and a sufficient level of propane (42 mg COD L^{-1}) or 1,4-dioxane (937 mg COD L^{-1}) so that it was in excess in comparison to the initial 6-10 mg L^{-1} of dissolved oxygen (Table 2-2). To estimate K_{SO}, batch depletion data for oxygen, propane and 1,4-dioxane were fit to equations 2-1, 2-3, and 2-4. The maximum specific oxygen utilization rate (q_{SOMAX}) was calculated directly from the zero order portion of the oxygen depletion data. The minimum oxygen concentration (O_{SMIN}) was calculated based on the final three oxygen measurements; linear regression was used to demonstrate that the slope of the best fit line through these data points was not

significantly different from zero (p<0.05). Values of K_{SO} and O_{SMIN} for CB1190 were determined similarly with 1,4-dioxane as the primary growth substrate (Table 2-3).

A similar approach was used for determination of the oxygen half saturation coefficient associated with cometabolism of 1,4-dioxane (K_{CO}). Triplicate bottles were set up with 9 mg L^{-1} of dissolved oxygen, 420 mg L^{-1} of propanotrophic biomass, and 182 mg COD L^{-1} of 1,4-dioxane (Table 2-2). The volume of the liquid phase was increased (144 mL) and the headspace decreased (16 mL) in order to achieve a mass of 1,4-dioxane in excess of the initial mass of oxygen. Batch depletion data for oxygen were fitted to equations 2-2, 2-3, 2-4 and 2-5 to estimate K_{CO}. The maximum specific oxygen utilization rates (q_{COMAX}) and minimum oxygen concentration (O_{SMIN}) were determined as described above for metabolic conditions.

2.4.8 Analytical Techniques

1,4-Dioxane was monitored by gas chromatographic (GC) analysis of aqueous filtered samples (0.2 µm PTFE); 350 µL was dispensed into a GC vial with a 500 µL glass insert. Samples (1.0 µL) were injected on a Hewlett Packard 5890 Series II GC, equipped with a flame ionization detector and a 60-m x 0.32-mm ZB-624 capillary column (Phenomenex). Hydrogen served as the carrier gas (2.0 mL min^{-1}). The temperature program was 40 ºC for 5 min, increased to 90 ºC at 6.0 ºC min^{-1} and held for 5 min. The injector and detector temperatures were 180 ºC and 260 ºC, respectively. The detection limit was 45 µg COD L^{-1} (25 µg L^{-1}).

Lower concentrations of 1,4-dioxane were analyzed using a micro-frozen extraction procedure adapted from Li et al. (2011). Filtered samples (3.0 mL) were added

to glass vials (4.0 mL) containing DCM (0.6 mL), providing a 5:1 volumetric ratio of water to DCM. The vials were capped with a Teflon-faced rubber septa and screw caps and agitated for 15 s. The vials were placed at a 45° angle, with the DCM in contact with the septum, and transferred to a freezer (-20 °C) for at least 1 hour. After the water froze, 200 µL from the DCM phase was removed rapidly (to prevent the DCM was warming and volatizing) and placed into a GC vial. The GC method used to quantify 1,4-dioxane in DCM was the same as mentioned above, except that the injection volume was increased to 3.0 µL. The detection limit was 90 µg COD L^{-1} (50 µg L^{-1}).

Oxygen levels were monitored in headspace samples (0.5 mL) using a Hewlett Packard 5890 Series II GC equipped with a thermal conductivity detector and a MS-5A 60/80 Mesh Molecular Sieve column (Alltech). Helium served as the carrier and reference gas (34 Ml min^{-1}). The temperature program was isothermal at 60 °C for 5 min. The injector and detector temperatures were 150 °C and 100 °C, respectively. The response from the GC was calibrated to the dissolved oxygen concentration. The detection limit for this method was 66 µg L^{-1}.

Propane was quantified by injecting a headspace sample (0.5 mL) onto a Hewlett Packard 5890 Series II GC equipped with a flame ionization detector and a 2.44-m x 3.175-mm column packed with 1% SP-1000 on 60/80 Carbopak B (Supelco). Nitrogen was the carrier gas (30 mL min^{-1}). The column temperature was isothermal (80 °C) for 3 min. The injector and detector temperatures were 200 °C. The detection limit was 2.1 mg COD L^{-1} (0.58 mg L^{-1}).

Protein was quantified using a modified version of the MicroBCA assay (Thermo Scientific®). Bovine serum albumin (BSA) was used as a standard. Samples (0.9 mL) were mixed with sodium hydroxide (0.1 mL, 10 M) by vortexing and placed in a water bath (90 ºC, 10 min). Aliquots of the lysate were neutralized (pH 6.5-7.5) using HCl (80-95 µL, 11.64 M) and bicarbonate (0.5 mL, 0.5 mM $NaHCO_3$). Samples (1 mL) were then mixed with MicroBCA Working Reagent (1 mL), incubated in a water bath (60 ºC, 1 h), cooled (25 min), and checked for absorbance (Genesys 20 UV-visible spectrophotometer, Thermo Scientific®) at 562 nm. Protein was assumed to constitute 50% of the mass of biomass (Grady et al., 2011). A correlation was determined between direct absorbance (600 nm) measurements of biomass in medium and protein concentrations, permitting the use of absorbance to estimate protein levels.

2.4.9 Numerical Methods

Aquasim® 2.0 was used to fit batch depletion data to the model equations (Reichert, 1994) The simplex method was used for initial optimization, followed by the secant method to obtain the standard error (Verce and Freedman, 2001). Weighting of the data was used to capture the effect of low concentration data for K_S and K_C (Neter et al., 1996; Verce and Freedman, 2001). Most of the parameters were determined sequentially and independently (Chang and Criddle, 1997). When a simulation required use of previously determined parameters (e.g., determination of T_C required Y, b, q_{SMAX}, q_{CMAX}, K_S, and K_C), those parameters were allowed to vary within their 95% confidence interval during fitting. Initial concentrations for propane and 1,4-dioxane were allowed to vary within 10% of

measured values. This method resulted in low uncertainties throughout the parameters estimation.

2.5 Results and Discussion

2.5.1 Yield, Endogenous Decay, and Monod Kinetic Coefficients

Yields and decay coefficients were measured first (Table 2-4), as these were required inputs for determining other coefficients. Similar *Y* and *b* values were obtained for ENV425 and ENV487 but were higher compared to CB1190 (Appendix A, Figure 6-1Figure 6-2 and Figure 6-3). Other studies have also reported yields for growth on ethers that are lower in comparison to other hydrocarbons (Bruce et al., 2013).

The μ_{max} for ENV425 is approximately twice that compared to ENV487 and CB1190 (Figure 2-1). The maximum substrate utilization rate for CB1190 growing on 1,4-dioxane was intermediate to that for ENV425 and ENV487 growing on propane. Mahendra and Alvarez-Cohen (Mahendra and Alvarez-Cohen, 2006) reported a q_{SMAX} value for CB1190 equal 55 mg of 1,4-dioxane COD mg biomass COD^{-1} d^{-1} to that is more than 30-fold higher than the value measured in this study of 2.11 mg of 1,4-dioxane COD mg biomass COD^{-1} d^{-1}. Variability in kinetic coefficients among different studies is attributable, at least in part, to the history of the culture (Grady et al., 1996; Harder and Dijkhuizen, 1984), parameter identifiability (Grady et al., 1996), and the nature of the assay, e.g., batch or chemostat (Kovárová-Kovar and Egli, 1998). In this study, μ_{max} (and by extension q_{SMAX}) was determined under batch intrinsic conditions, i.e., the ratio of initial substrate to biomass was greater than 20 (COD basis), while Mahendra and Alvarez-Cohen

used extant conditions, as well as a higher temperature (30 ºC versus 22-24 ºC). A q_{SMAX} value of 52 mg of 1,4-dioxane COD mg biomass COD^{-1} d^{-1} for CB1190 was obtained when the same experimental approach used by Mahendra and Alvarez-Cohen was followed (Appendix A, Figure 6-4).

Once q_{SMAX} values were established, the batch depletion data were fit to equations 2-1, 2-4 and 2-5 to obtain K_S (Figure 2-1). The K_S value of 11.5 ± 0.4 mg COD L^{-1} for CB1190 determined in this study is an order of magnitude lower than a K_S of 291 ± 80 mg COD L^{-1} reported by Mahendra and Alvarez-Cohen (2006), most likely a consequence of the different experimental conditions used. Half saturation coefficients for the propanotrophs were 11 to 20 mg COD L^{-1}; these values are an order of magnitude lower (mixed culture; (Chang and Alvarez-Cohen, 1995)) and higher (*Mycobacterium vaccae* JOB5; (Wilcox et al., 1995)) compared to previously reported studies. The model fit for ENV425 notably deviated from the data at propane concentrations below 2 mg COD L^{-1}. The Blackman equation (Heijnen and Romein, 1995) provides a better fit at low concentrations (Appendix A, Figure 6-5). Nevertheless, equation 2-1 provides a better fit for a broader range of initial substrate concentrations, which was especially relevant for the coinhibition coefficients.

2.5.2 Non-growth Substrate Coefficients

The maximum specific biodegradation rates and half-saturation constants for 1,4-dioxane as the non-growth substrate (q_{CMAX}) were obtained from batch biodegradation experiments in the absence of propane (Figure 2-2, Table 2-4, Table 2-3). The propanotrophs consumed 1,4-dioxane at about one half the maximum specific rate as CB1190. K_C values (6.05 ± 0.26 and 3.25 ± 0.05 mg COD L^{-1}) are two to four times lower

than the K_S value for metabolic degradation of 1,4-dioxane by CB1190 (11.5 ± 0.4 mg COD L^{-1}) (Table 2-4). The q_{CMAX} and K_C values determined in this study fall within the range of found in the literature (Mahendra and Alvarez-Cohen, 2006; Roy et al., 1994; Zenker et al., 2002), which vary by three orders of magnitude, depending on the experimental approach and type of primary growth substrate used.

Transformation capacities (T_C) were estimated using biodegradation data for 1,4-dioxane at different initial concentrations (Figure 2-3). T_C satisfied the full range of data, although at intermediate concentrations (~55-75 mg COD L^{-1}), equations 2-2, 2-4, and 2-5 tended to over-predict the rate (Fig. 3a, 3b). No self-inhibition was observed for cometabolism of 1,4-dioxane at high concentrations, in the absence of propane. The T_C values for ENV425 and ENV487 are within the range for other monooxygenase-expressing cultures (0.56-5.9 mg of 1,4-dioxane COD mg biomass COD^{-1} (Mahendra and Alvarez-Cohen, 2006)); however, out of 11 cultures reported, only two have T_C values above 0.97.

The coefficient that describes inhibition of 1,4-dioxane biotransformation by propane (K_{iS}) was estimated from an experiment in which propane and 1,4-dioxane were simultaneously present for ENV487 (Fig. 4a, 4b) and ENV425 (Appendix A, Fig. Figure 6-6 and Figure 6-7). The effect of propane on 1,4-dioxane is evident. The estimated K_{iS} values were 0.65 and 0.74 mg COD L^{-1} for ENV425 and ENV487, respectively. Zenker et al. (2002) reported a similar co-inhibition coefficient for a mixed culture that grew on THF as its primary substrate. To determine the co-inhibition coefficient for the presence of 1,4-dioxane on propane utilization (K_{iC}), data from treatments containing an initial propane concentration of 36.3 mg COD L^{-1} and various initial 1,4-dioxane concentrations (up to

1,600 mg COD L^{-1}) were used for ENV487 (Figure 2-4c, Figure 2-4d) and ENV425 (Appendix A, Figure 6-8). 1,4-Dioxane had a relatively minor inhibitory effect on propane utilization, especially at concentrations that are typical for most groundwater plumes (i.e., ≤100 mg L^{-1}). Consequently, the values for K_{iC} (Table 2-4) were as high as to be insignificant contributors to propane utilization (equation 2-1) and oxygen utilization (equation 2-3). Zenker et al. (2002) reported an even higher K_{iC} value for a THF grown culture.

The model for cometabolism developed by Chang and Criddle (1997) included a transformation yield (T_Y), which increases the specific non-growth substrate utilization rate according to the amount of primary substrate consumed. Inclusion of T_Y did not improve the model fits for cometabolism of 1,4-dioxane and therefore it was not included in equation 2-2. Nevertheless, T_Y may be calculated as the product of T_C and Y, giving values of 0.82 and 1.0 mg of 1,4-dioxane COD mg of propane COD^{-1} for ENV425 and ENV487, respectively. Zenker et al. (2002) reported a T_Y of 4.2 mg 1,4-dioxane COD mg of THF COD^{-1}. T_Y values for cometabolism of chlorinated ethenes using methane as the primary substrate are one or two orders of magnitude lower (Anderson and McCarty, 1997), indicating that cometabolism of 1,4-dioxane is a more efficient process.

2.5.3 Coefficients for Oxygen

Batch depletion data used to determine oxygen utilization coefficients for ENV487 and CB1190 (Figure 2-5, Appendix A, Figure 6-9) indicate that Substrate utilization slowed as oxygen decreased below detection (~0.10 mg L^{-1}; ENV487) or reached a minimum (0.36 mg L^{-1}; CB1190). The half saturation coefficients for oxygen in the

presence of growth substrate (K_{SO}) were similar (1.5 to 2.3 mg L^{-1}), as were the maximum specific oxygen utilization rates (q_{SOMAX}; Table 2-4).

During cometabolism of 1,4-dioxane by the propanotrophic cultures, oxygen consumption ceased at 0.26-0.29 mg L^{-1}, resulting in cessation of 1,4-dioxane consumption (Figure 2-6). Propanotrophs have a slightly lower threshold oxygen concentration than CB1190. The batch depletion data for oxygen and 1,4-dioxane were used to estimate K_{CO} values, which were similar for ENV425 and ENV487 and an order of magnitude lower than the oxygen half saturation coefficient for CB1190. The maximum specific oxygen utilization rate for ENV487 during cometabolism of 1,4-dioxane (q_{COMAX}) was approximately twice as high as for ENV425 (Table 2-4).

2.5.4 Batch Simulations

The kinetic coefficients (Table 2-4) were used in equations 2-1 to 2-4 to compare 1,4-dioxane biodegradation via metabolism and propane-induced cometabolism under batch conditions. At initial concentrations of 1800 µg COD 1,4-dioxane COD L^{-1} (corresponding to 1000 µg L^{-1}), 0.74 mg biomass COD L^{-1}, propane at either 10% or 100% of saturation (338 mg COD L^{-1}), and oxygen at saturation, CB1190 consumed 1,4-dioxane at a higher rate than ENV487 until the concentration reached 380-420 µg COD L^{-1} (Figure 2-7a). This is consistent with CB1190 having a higher maximum specific utilization rate but a higher half-saturation coefficient, as well as the preference of ENV487 to consume propane before 1,4-dioxane. Selection of 0.74 mg biomass COD L^{-1} was based on an estimate from the mass of cells added in a bioaugmentation field study described by Lippincott et al. (2015) where propane was used as the primary growth substrate.

Saturation concentrations of propane are achievable, although lower levels are also likely depending on the radius of influence of an injection well (Lippincott et al., 2015).

The initial biomass concentration has an impact on this comparison, which was made based on the time to reach a hypothetical remediation goal of 1.8 µg COD 1,4-dioxane COD L^{-1}. When the initial conditions are 1800 µg 1,4-dioxane COD L^{-1}, propane at either 10% or 100% of saturation (338 mg COD L^{-1}), and oxygen at saturation, the propanotrophic culture reaches the goal faster at biomass levels below 8 mg COD L^{-1}, while CB1190 is faster at higher initial biomass levels (Figure 2-7b). This is consistent with the propanotrophic cultures having higher growth rates and higher yields. The simulation for CB1190 stops at an initial biomass concentration of ~6 mg COD L^{-1}; below this level, endogenous decay exceeds growth and degradation of 1,4-dioxane slows or ceases. Using a lower endogenous decay coefficient for CB1190 shifts the simulation to the left, making metabolic degradation more competitive at lower initial biomass levels (Appendix A, Figure 6-10).

The initial 1,4-dioxane concentration also has a significant impact on the time to achieve a hypothetical remediation goal of 1.8 µg COD 1,4-dioxane COD L^{-1}. When the initial conditions are 8 mg biomass COD L^{-1}, propane at either 10% or 100% of saturation (338 mg COD L^{-1}), and oxygen at saturation, ENV487 reaches the goal faster when the initial concentration of 1,4-dioxane is below ~17-27 mg COD L^{-1} (Figure 2-7c). Higher 1,4-dioxane concentrations favor the growth of CB1190 while cometabolic degradation is hampered by the need to consume greater amounts of propane. This simulation is also impacted by the endogenous decay rate; a lower value for CB1190 makes metabolic

degradation more competitive at lower initial concentrations of 1,4-dioxane (Appendix A, Figure 6-10c).

The effect of oxygen concentration was evaluated for an initial 1,4-dioxane concentration of 1.8 μg COD L^{-1}, propane at either 10% or 100% of saturation, and biomass at either 0.74 or 15 mg COD L^{-1} (Figure 2-8). The higher biomass level was selected on the basis of having a condition where CB1190 outperformed the cometabolic bacteria; this occurs when the initial biomass concentration is above 8 mg COD L^{-1} as shown in Figure 2-7b. The time to reach a hypothetical remediation goal of 1.8 μg COD 1,4-dioxane COD L^{-1} increased significantly at oxygen concentrations below 1-2 mg L^{-1}. The propanotrophic cultures was less inhibited by lower oxygen levels at the lower initial biomass concentrations (Figure 2-8a, Figure 2-8b), while CB1190 was reached the remediation goal more quickly at the higher initial biomass concentration. Other studies report a similar impact of low DO levels on *in situ* biodegradation (Borden et al., 1989; Chiang et al., 1989; Wilson and Bouwer, 1997). The results reinforce the importance of the role of DO in the performance of metabolic and cometabolic bioremediation strategies.

2.6 Conclusions

A Monod kinetic model was able to describe the characteristics of the cultures' growth and cometabolic transformation capabilities. Several parameters, such as yields, decay coefficients, and 1,4-dioxane specific biodegradation rates were of the same order of magnitude between the propane-oxidizing cultures. Half saturation constants for ENV425 were twice as high as for ENV487. The affinity towards 1,4-dioxane was higher in the propanotrophic cultures than in CB1190. There was no self-inhibition on

cometabolic biodegradation of high concentrations of 1,4-dioxane and T_C values were in the upper range when compared to another study for 1,4-dioxane cometabolism by other cultures. 1,4-Dioxane cometabolic biodegradation rates were slower than that of CB1190, but within range of what is reported for cometabolism. In terms of the effect oxygen concentration, the propane-oxidizing cultures had relatively high K_{SO} but low K_{CO} values. CB1190 had a lower affinity towards oxygen in the presence of 1,4-dioxane when compared to the propanotrphic cultures. In addition, the minimum oxygen concentrations were absent for the propanotrphic cultures in the presence of propane or lower than CB1190 when considering the presence of 1,4-dioxane. For cometabolism of 1,4-dioxane, inhibition caused by propane on biodegradation of 1,4-dioxane was significantly higher than inhibition caused by 1,4-dioxane on the utilization of propane. The inhibition was a consequence of the preference of the cultures to use propane for growth; once propane levels decreased, 1,4-dioxane biodegradation intensified. For practical purposes, 1,4-dioxane did not inhibit the growth of the propanotrophic cultures.

Simulations of metabolic and cometabolic biodegradation of 1,4-dioxane at low DO levels demonstrated that the initial biomass concentration is a key variable to be considered for *in situ* remediation of 1,4-dioxane by metabolic and cometabolic bacteria. This applies when the DO is limited and the 1,4-dioxane concentration is in the vicinity of 1.82 mg COD L^{-1}. An adequate amount of propane is essential to achieve robust growth of the propanotrophic cultures and therefore sufficient enzymatic activity to degrade 1,4-dioxane below clean up goal levels under limited DO conditions. The kinetic model used in this study is useful to predict the biodegradation extent of 1,4-dioxane under idealized

batch conditions for the metabolic and cometabolic biodegradation. The preference for metabolic or cometabolic biodegradation of 1,4-dioxane depends the conditions indicated, as well as on the specific transport conditions in the subsurface environment in which bioremediation is to be applied.

2.7 Tables for Chapter 2

Table 2-1 Nomenclature

β	Factor to convert dissolved growth substrate to total mass of growth substrate (mg COD per bottle mg COD dissolved^{-1})
b	Biomass decay coefficient (d^{-1})
C	Non-growth substrate concentration (mg COD L^{-1})
H'	Henry's Law constant ([gas concentration in M] [aqueous concentration in M^{-1}])
K_C	Half saturation coefficient for non-growth substrate (mg COD L^{-1})
K_{CO}	Half saturation coefficient for oxygen for non-growth substrate (mg COD L^{-1})
K_{iC}	Co-inhibition coefficient from growth substrate (mg COD L^{-1})
K_{iS}	Co-inhibition coefficient from non-growth substrate (mg COD L^{-1})
K_S	Half saturation coefficient for growth substrate (mg COD L^{-1})
K_{SO}	Half saturation coefficient for oxygen for growth substrate (mg COD L^{-1})
O	Oxygen concentration (mg COD L^{-1})
O_{CMIN}	Minimum threshold oxygen concentration for non-growth substrate (mg COD L^{-1})
O_{SMIN}	Minimum threshold oxygen concentration for growth substrate (mg COD L^{-1})
q_{CMAX}	Maximum specific non-growth substrate biodegradation rate (d^{-1})
q_{COMAX}	Maximum specific oxygen utilization rate for non-growth substrate (d^{-1})
q_{SMAX}	Maximum specific growth substrate utilization rate (d^{-1})
q_{SOMAX}	Maximum specific oxygen utilization rate for growth substrate (d^{-1})
S	Growth substrate concentration (mg COD L^{-1})
T_C	Transformation capacity (mg of 1,4-dioxane COD mg of biomass COD^{-1})
V_l	Volume of liquid in a bottle (L)
V_g	Volume of gas in a bottle (L)
X	Biomass concentration (mg COD L^{-1})
Y	Biomass yield (mg of biomass COD mg of substrate COD^{-1})

Table 2-2 Experimental conditions for determining kinetic parameters of propanotrophic cultures ENV425 and ENV487

				Initial Concentration (mg COD L^{-1})			
Parameter	**Equations**	**Simplifications**	**Required Inputs**	**Biomass**	**Propane**	**1,4-Dioxane**	**Replicates**
Y	-	-	-	8.5	44	-	3
b	-	-	-	420	0	-	3
μ_{MAX}	2-6	-	Y	8.5	44	-	3
q_{SMAX}	2-7	-	μ_{MAX}, Y	-	-	-	-
K_S	2-1, 4, 5	$O>>O_{SMIN}$, $O>>K_{SO}$, $C=0$	Y, b, q_{SMAX}	8.5	44	-	3
q_{CMAX}	2-2, 4, 5	$O>>O_{SMIN}$, $O>>K_{SO}$, $S=0$	b	420	-	14.5-36.4	6
K_C	2-2, 4, 5	$O>>O_{SMIN}$, $O>>K_{SO}$, $S=0$	b	420	-	16.4	3
T_C	2-2, 4, 5	$O>>O_{SMIN}$, $O>>K_{SO}$, $S=0$	b	420	-	182	18
K_{iS}	2-1, 2, 4, 5	$O>>O_{SMIN}$, $O>>K_{SO}$	q_{SMAX}, q_{CMAX}, K_S, K_C, Y, b, K_{iC}, T_C,	420	1.8-14.5	16.4	10
K_{iC}	2-1, 2, 4, 5	$O>>O_{SMIN}$, $O>>K_{SO}$	q_{SMAX}, q_{CMAX}, K_S, K_C, Y, b, K_{iS}, T_C,	420	36	18-1,456	4
O_{SMIN}	-	-	-	420	44	900	3
O_{CMIN}	-	-	-	8.5	-	170	3
q_{SOMAX}	-	-	-				3
q_{COMAX}	-	-	-				3
K_{SO}	2-1, 3, 4, 5	$C=0$	q_{SMAX}, K_S, O_{SMIN}, q_{SOMAX}, b	8.5	44	514	3
K_{CO}	2-2, 3, 4, 5	$S=0$	q_{CMAX}, K_C, q_{COMAX}, O_{CMIN}, b, T_C	420	-	935	3

Table 2-3 Experimental conditions for determining kinetic parameters of CB1190

Parameter	Equations	Simplifications	Required Inputs	Initial Concentration (mg COD L^{-1})			Replicates
				Biomass	Propane	1,4-Dioxane	
Y	-	-	-	27	-	360	3
b	-	-	-	420	-	0	3
μ_{MAX}	2-6	-	Y	57	-	1360	3
q_{SMAX}	2-7	-	μ_{MAX}, Y	-	-	-	-
K_S	2-1, 4	$O>>O_{SMIN}$, $O>>K_{SO}$, C =0	Y, b, q_{SMAX}	57	-	1360	3
O_{SMIN}	-	-	-	8.5	-	900	3
q_{SOMAX}	-	-	-	8.5	-	900	3
K_{SO}	2-1, 3, 4	C = 0	b, Y, μ_{SMAX}, K_S, O_{SMIN}, q_{SOMAX}	8.5	-	900	3

Table 2-4 Results for kinetic coefficients [a]

Parameter	Units[b]	ENV425	ENV487	CB1190
Y	mg COD mg COD^{-1}	0.56 ± 0.09	0.61 ± 0.06	0.35 ± 0.07
b	d^{-1}	0.11 ± 0.02	0.14 ± 0.04	0.05 ± 0.01
μ_{MAX}	d^{-1}	1.53 ± 0.16	0.85 ± 0.08	0.74 ± .06
q_{SMAX}	mg COD mg COD^{-1} d^{-1}	2.73 ± 0.18	1.39 ± 0.07	2.11 ± 0.07
K_S	mg COD L^{-1}	20.1 ± 1.4	11.5 ± 0.2	11.5 ± 0.4
q_{CMAX}	d^{-1}	0.87 ± 0.08	0.92 ± 0.01	-
K_C	mg COD L^{-1}	6.05 ± 0.26	3.25 ± 0.05	-
T_C	mg COD mg COD^{-1}	1.46 ± 0.07	1.64 ± 0.23	-
K_{iS}	mg COD L^{-1}	0.65 ± 0.06	0.74 ± 0.03	-
K_{iC}	mg COD L^{-1}	$2.1\text{x}10^{10} \pm 1.9\times10^{17}$	$7.7\times10^{3} \pm 2.3\times10^{3}$	-
O_{SMIN}	mg COD L^{-1}	0[c]	0[c]	0.36 ± 0.03
O_{CMIN}	mg COD L^{-1}	0.26 ± .04	0.29 ± 0.08	-
q_{SOMAX}	mg O_2 mg COD^{-1} d^{-1}	1.41 ± 0.20	1.05 ± 0.012	1.39 ± 0.02
q_{COMAX}	mg O_2 mg COD^{-1} d^{-1}	0.22 ± 0.004	0.39 ± 0.004	-
K_{SO}	mg COD L^{-1}	2.18 ± 0.30	2.27 ± 0.09	1.52 ± 0.03
K_{CO}	mg COD L^{-1}	0.32 ± 0.11	0.35 ± 0.06	-

[a] ±95% confidence interval, using the standard error from Aquasim; intervals for q_{SMAX} and T_Y calculated by propagation of error from the standard errors for μ_{MAX}, Y, and T_C. Parameters were determined at room temperature (22-24 °C).

[b] Conversion factors for COD units: 1.82 mg COD mg 1,4-dioxane^{-1}, 3.63 mg COD mg propane^{-1}, 1.42 mg COD mg biomass^{-1}.

[c] Detection limit was 66 µg L^{-1}.

2.8 Figures for Chapter 2

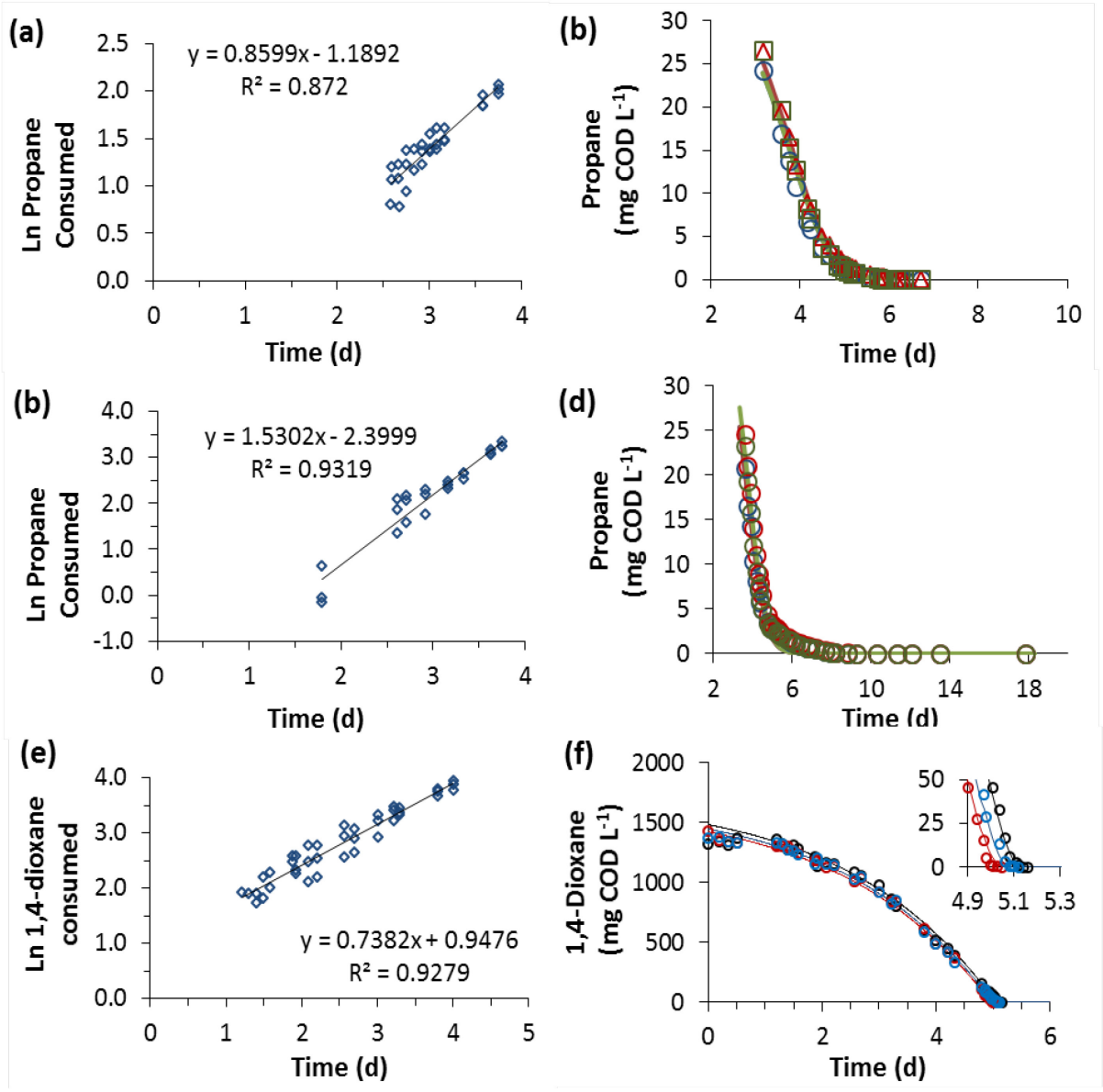

Figure 2-1 Estimation of K_S and μ_{MAX} for: (a, b) mixed culture ENV487, (c, d) isolate *Rhodococcus ruber* ENV425, and (e, f) 1,4-dioxane metabolizer isolate *Pseudonocardia dioxanivorans* CB1190. Symbols represent measured values from triplicate bottles whereas lines describe model fittings.

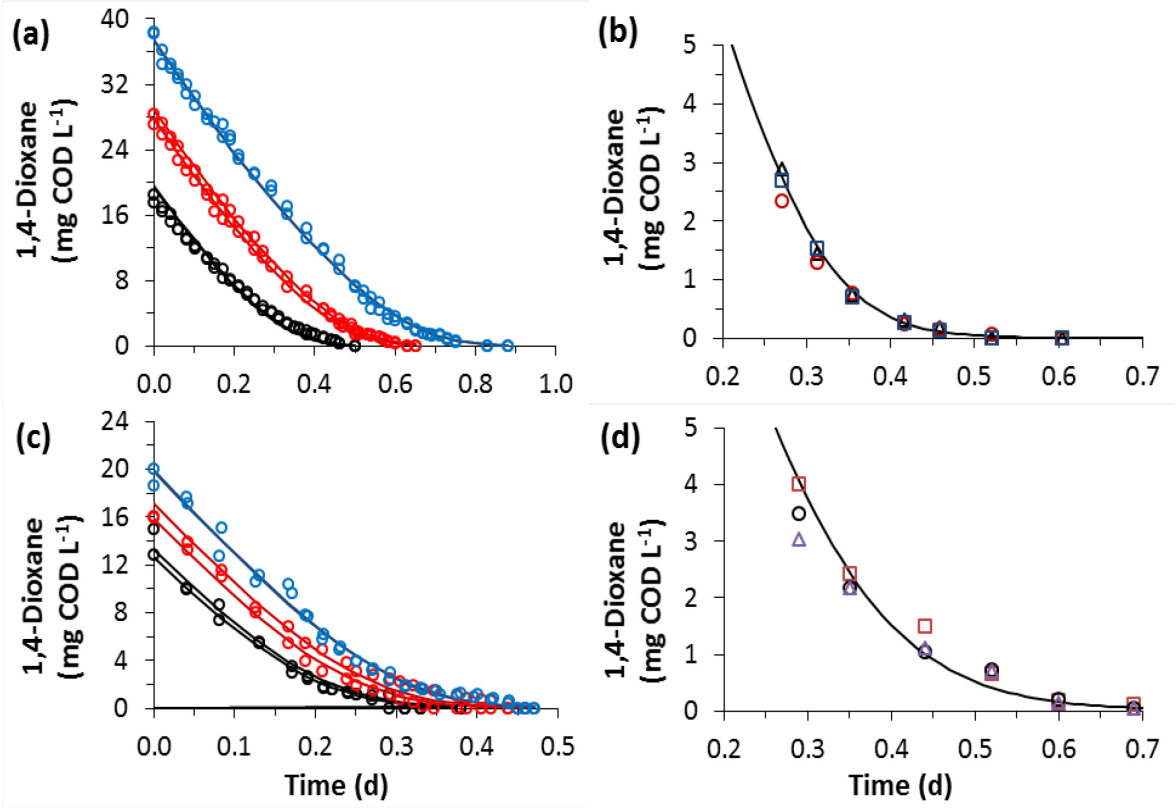

Figure 2-2 Estimation of K_C and q_{CMAX} for: (a, b) mixed culture ENV487, and (c, d) isolate *Rhodococcus ruber* ENV425.

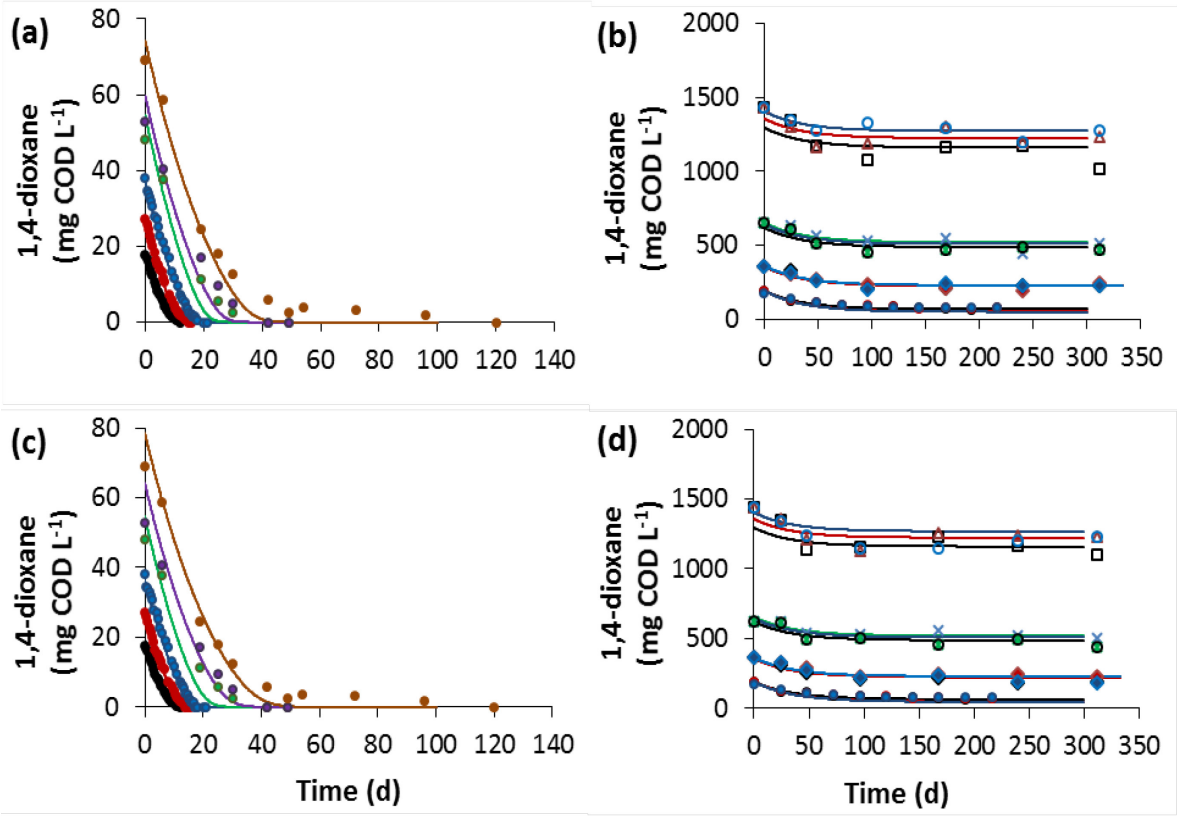

Figure 2-3 Estimation of *Tc* at low and high concentrations of 1,4-dioxane for: (a, b) mixed culture ENV487, and (c, d) isolate *Rhodococcus ruber* ENV425.

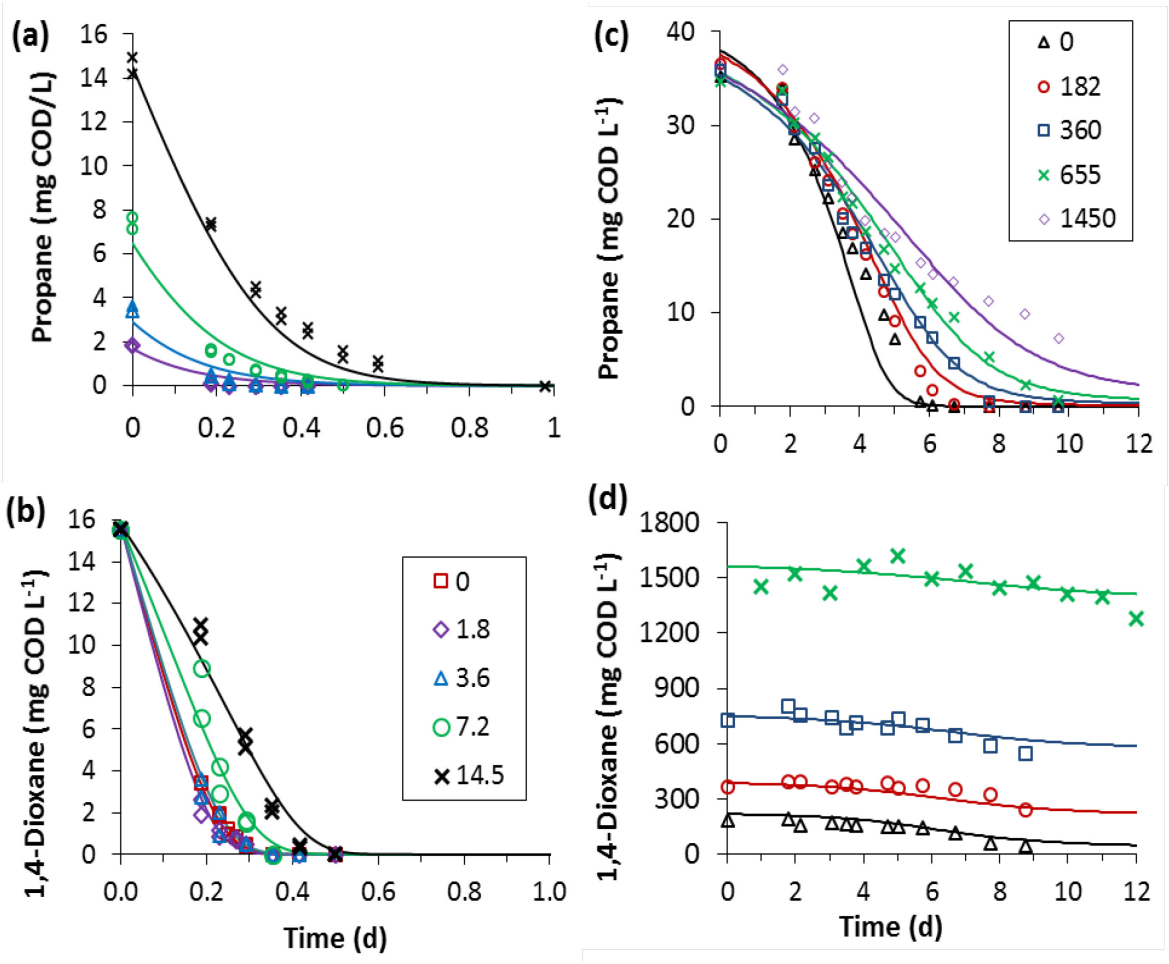

Figure 2-4 1,4-Dioxane and propane data used to estimate the coinhibition coefficients for: (a, b) propane inhibition on 1,4-dioxane degradation (K_{iS}) and (c, d) 1,4-dioxane inhibition on propane utilization (K_{iC}) for ENV487. Symbols represent experimental data for duplicates (a, b) or single bottles (c, d). Symbols in (b) represent initial propane concentrations; in (c), initial 1,4-dioxane concentrations (mg COD L^{-1}).

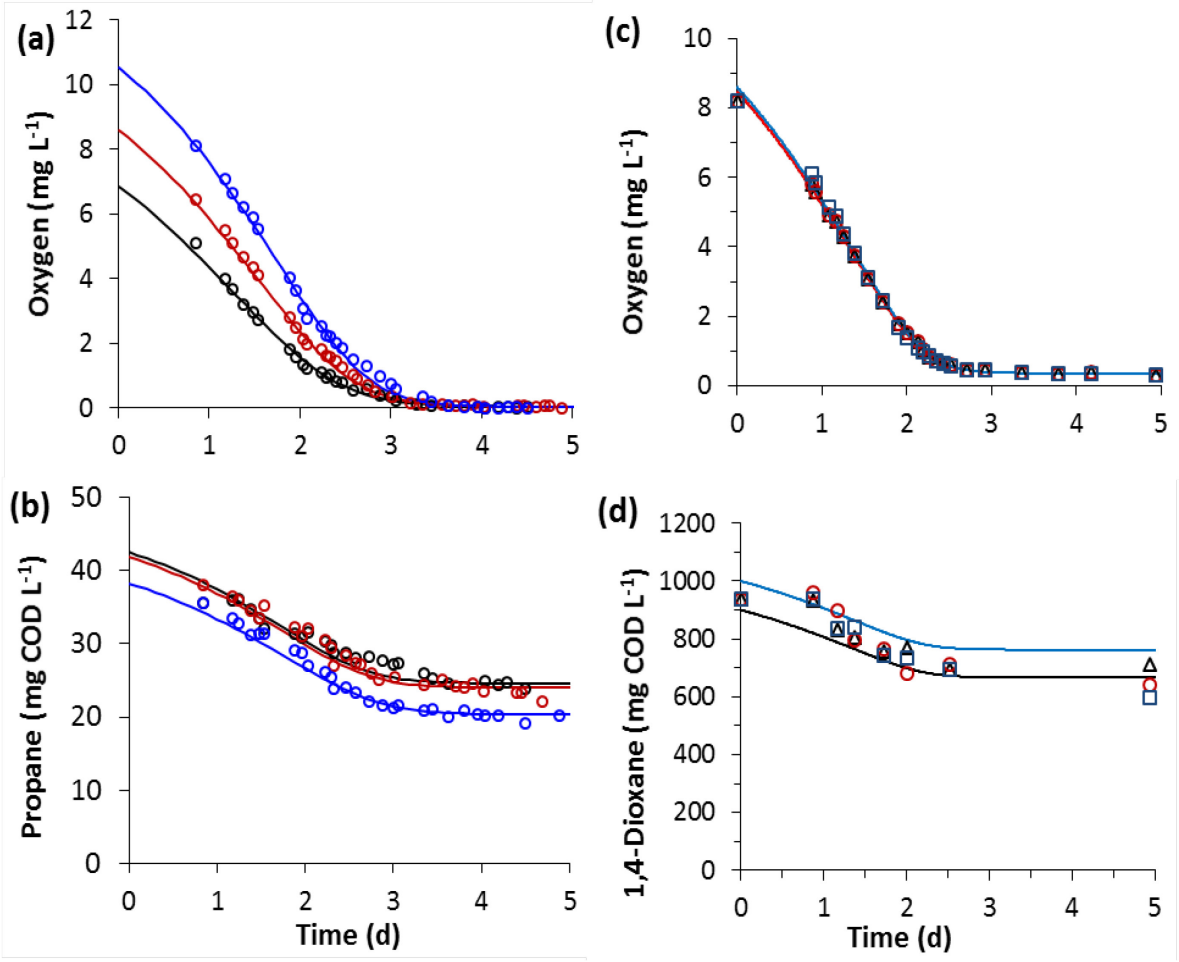

Figure 2-5 Oxygen and growth substrate batch depletion data used for the estimation of K_{SO} and q_{SOMAX} for: (a, b) ENV487 and (c, d) CB1190.

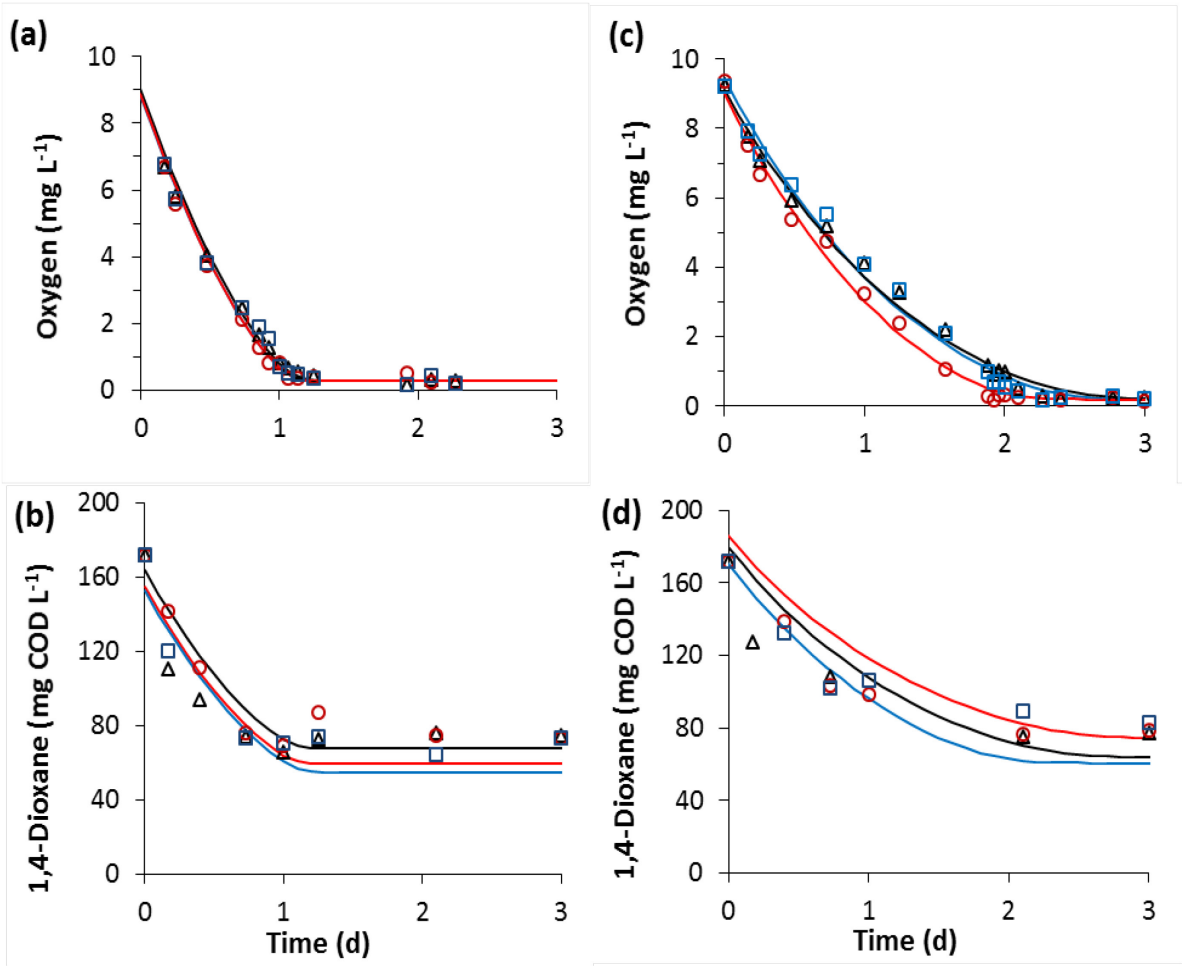

Figure 2-6 Oxygen and 1,4-dioxane batch depletion data used for the estimation of K_{CO} and q_{COMAX} for: (a, b) mixed culture ENV487 and (c, d) *Rhodococcus ruber* ENV425. Different symbols represent different bottles and different color lines represent model fits to each bottle.

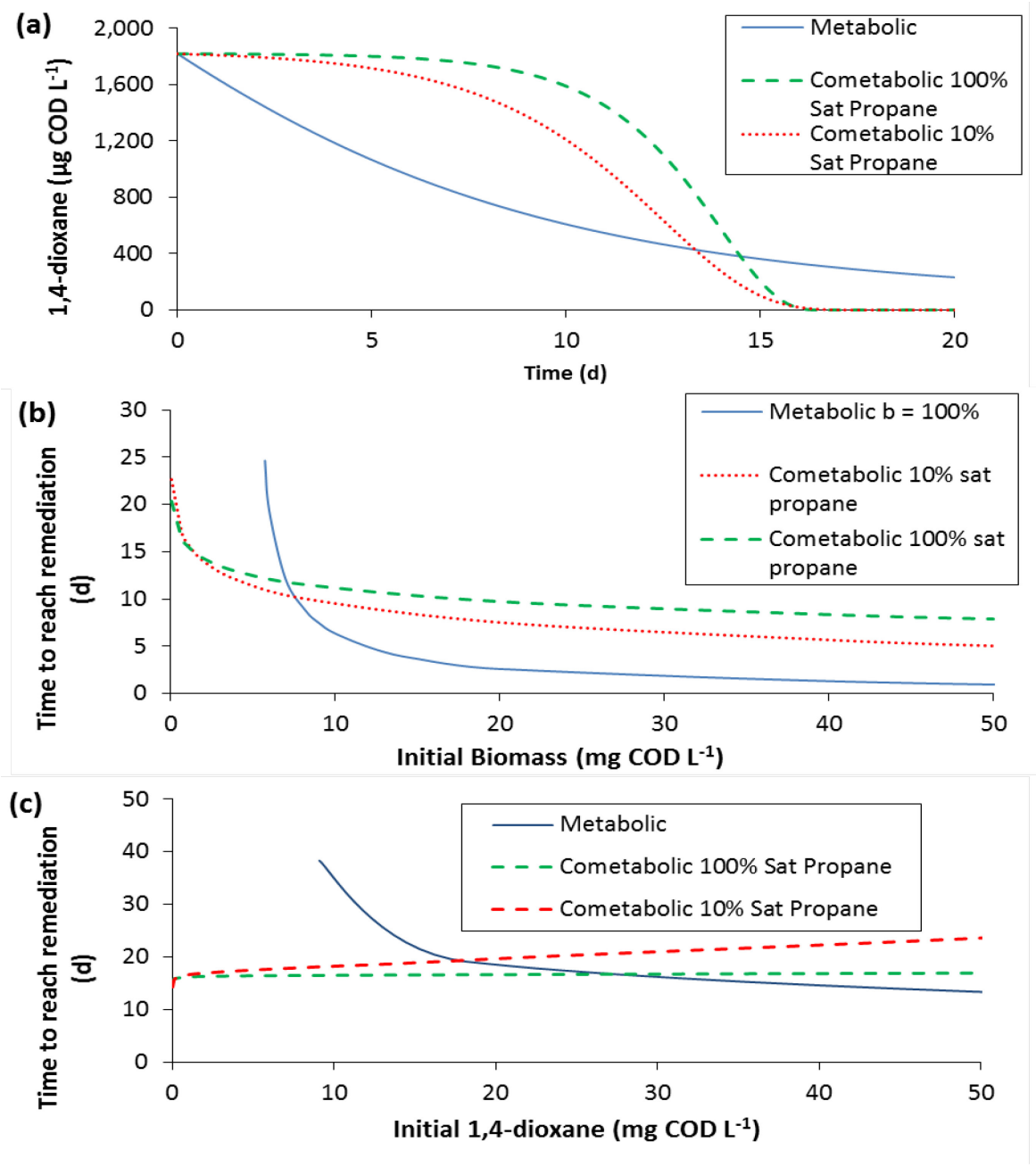

Figure 2-7 Batch simulations using the kinetic model for metabolic (solid line) and cometabolic (dashed lines) ENV487 to predict: (a) biodegradation of an initial concentration of 1,4-dioxane of 1,820 µg COD L^{-1}; the time to achieve a remediation goal to reach 1.82 µg COD L^{-1} (1 µg L^{-1}) with respect to the initial biomass (b) and 1,4-dioxane (c) concentrations. The initial propane concentration is 100% (long dash) and 10% (short dash) the saturation concentration. The initial biomass concentration was 0.74 mg COD L^{-1} for (a) and (c). The initial 1,4-dioxane concentration is 1,820 µg COD L^{-1} in panel (b).

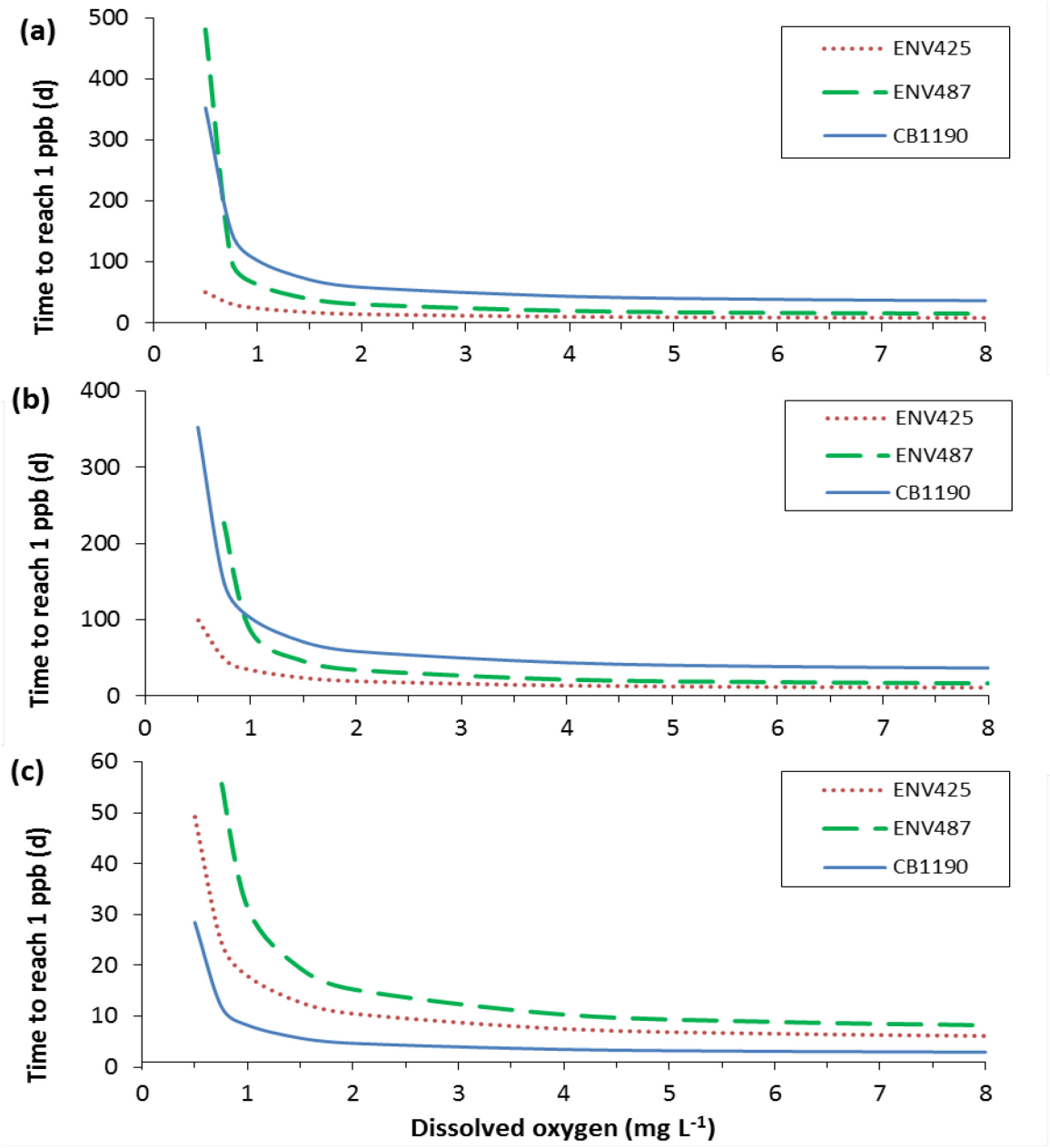

Figure 2-8 Batch simulations in Aquasim to determine the effect of steady dissolved oxygen concentration on the time to achieve a 1,4-dioxane remediation goal equivalent to 1 µg L^{-1} for: mixed culture ENV487 (long dashed line), *Rhodococcus ruber* ENV425 (short dashed line), and *Pseudonocardia dioxanivorans* CB1190 (solid line). Initial 1,4-dioxane concentration is 1.82 mg COD L^{-1}. Other initial conditions are: (a) propane = 100% saturation, biomass = 0.74 mg COD L^{-1} ; (b) propane = 10% saturation, biomass = 0.74 mg COD L^{-1}; (c) propane = 10%, biomass = 15 mg COD L^{-1}.

3. SIMULATIONS OF *IN SITU* BIODEGRADATION OF 1,4-DIOXANE UNDER METABOLIC AND COMETABOLIC CONDITIONS

3.1 Abstract

A wide variety of microbes are capable of aerobically biodegrading 1,4-dioxane via metabolism or cometabolism. Bioremediation with microbes that metabolize 1,4-dioxane has several advantages, including a reduced likelihood of clogging the aquifer, lower oxygen demand, and no need to provide a primary substrate. However, the concentration of 1,4-dioxane in most plumes is below 1,000 μg L^{-1}, which may not support metabolic biodegradation at a sufficiently high rate. Cometabolism could be an alternative for *in situ* remediation of dilute plumes of 1,4-dioxane. Even though aerobic biodegradation of 1,4-dioxane has been proven under laboratory conditions, an assessment tool is needed to evaluate its performance under *in situ* conditions. The objective of this study was to compare the performance of metabolic and cometabolic bacteria under *in situ* conditions for bioremediation of 1,4-dioxane.

A finite element contaminant transport model was developed to simulate metabolic and cometabolic bioremediation of 1,4-dioxane via bioaugmentation and biosparging. The model geometry is two-dimensional with Cartesian coordinates. The model incorporates advection, diffusion and biodegradation reactions described by multi-substrate Monod kinetics and coinhibition effects. The transport model with biodegradation was coupled to an approximated steady-state air sparging simulation used to distribute gas species in the aquifer. The model was calibrated with monitoring well data for 1,4-dioxane and propane from a pilot study at the Vandenberg Air Force Base (VAFB), where bioremediation was

carried out via cometabolism by propanotrophic bacteria. In this field study, air and propane were injected in cycles into a confined aquifer to support bioaugmentation with the propanotrophic culture *Rhodococcus ruber* ENV425. The model geometry was constructed based on the characteristics of this site.

For metabolic degradation, the model simulated bioaugmentation with *Pseudonocardia dioxanivorans* CB1190 and sparging with air alone. However, to the author's knowledge, there are no available data published on pilot studies for metabolic bioaugmentation of 1,4-dioxane.

Kinetic parameters that describe biodegradation of 1,4-dioxane were determined in a prior laboratory study (described in Chapter 2) using both types of bioaugmentation cultures. Sensitivity analysis was performed for several model parameters. To achieve the objective of this study, a comparative analysis was performed to evaluate bioremediation by metabolism and cometabolism of 1,4-dioxane. The conditions varied were: 1) initial concentration of 1,4-dioxane; 2) biomass injection rate; 3) oxygen injection rate; and 4) propane injection rate (for cometabolism). The metrics used to compare metabolic and cometabolic bioremediation performance were the time to achieve an average 1,4-dioxane concentration of 1 $\mu g\ L^{-1}$ and the percentage of biodegradation that occurred after 10 years.

The simulation results were significantly impacted by parameters such as the biomass decay coefficient. A decay rate value 10 times lower than what was measured in batch experiments was needed in order to calibrate the model to field data from VAFB. It was also necessary to reduce the maximum specific 1,4-dioxane biodegradation rate by 50% with respect to the experimentally determined value. This was likely a consequence

of measuring the rate in the laboratory in the absence of chlorinated ethenes and ethanes, while they were present at VAFB and are known to inhibit aerobic biodegradation of 1,4-dioxane. The model was also affected by variations in the biomass dispersion coefficient. Simulation results indicated that bioremediation of 1,4-dioxane using cometabolism was more effective when the initial 1,4-dioxane concentration was below 10 mg L^{-1}. Between initial concentrations of 0.5 and 7.5 mg L^{-1}, the time to achieve 1 µg/L was at least one order of magnitude higher for CB1190. The gap between cometabolism and metabolism lessened at initial 1,4-dioxane concentrations below 0.5 mg L^{-1}, since the impact of decay on survival of CB1190 diminished when less substrate needed to be removed. The rate of biomass injection (8.4×10^{-8} to 8.4×10^{-5} kg COD m^{-2} s^{-1}) had a significantly greater impact on the time to reach 1 µg L^{-1} with CB1190 compared to the ENV425, since the primary substrate for cometabolism (propane) was provided in excess. The oxygen injection rate (2.0×10^{-6} to 2.0×10^{-3} kg COD m^{-2} s^{-1}) had a greater impact on the percentage of biodegradation for metabolism of 1,4-dioxane. Increasing the propane injection rate (3.54×10^{-7} to 3.54×10^{-4} kg COD m^{-2} s^{-1}) significantly reduced remediation times for cometabolism, although this effect plateaued at the higher rates. The model used in this study was calibrated to a specific site, but it provides a general framework for comparing the performance of metabolic and cometabolic bioremediation of 1, 4-dioxane at other sites with different *in situ* conditions.

3.2 Introduction

1,4-Dioxane has become an important target for remediation due to its status as a probable human carcinogen and its presence at numerous contaminated sites across the

U.S. (Adamson et al., 2014). *In situ* biodegradation of 1, 4-dioxane is an alternative to energy intensive physicochemical techniques. Laboratory studies have shown aerobic biodegradation can be achieved by metabolic and cometabolic processes (Mahendra and Alvarez-Cohen, 2006; Sei et al., 2013; Zenker et al., 2002).

Even though several microbial cultures that degrade 1,4-dioxane metabolically or cometabolically have been well studied under laboratory conditions (Li et al., 2010; Mahendra et al., 2007; Mahendra and Alvarez-Cohen, 2005; Nakamiya et al., 2005; Parales et al., 1994; Pugazhendi et al., 2015; Sei et al., 2013), there has been no systematic evaluation of their performance under *in situ* conditions. In addition, most of the studies for cometabolism of 1,4-dioxane involve the use of toxic compounds as primary substrates, including THF and toluene (Mahendra and Alvarez-Cohen, 2006; Skinner et al., 2009; Zenker et al., 2002).

Cometabolism of other contaminants such as chlorinated aliphatic hydrocarbons has been demonstrated in field applications where methane or propane served as the primary growth substrate delivered via air sparging (Frascari et al., 2015). Moreover, bioremediation of methyl tert-butyl ether (MTBE) has also been demonstrated in an *in situ* propane cometabolic air sparging application (Steffan et al., 1997). Similarly, cometabolism of 1,4-dioxane has been performed by air sparging using propane as the primary substrate followed by bioaugmentation with the propane-oxidizing culture *Rhodococcus ruber* ENV425 at Site 24, VAFB, CA (Lippincott et al., 2015); reductions of up to 99% for 1,4-dioxane at different monitoring wells were observed as well as final concentrations below 2 $\mu g\ L^{-1}$.

The performance of microbial cultures may be different under field conditions when compared to their results in laboratory studies. Pilot studies are one tool used to evaluate a strategy such as bioaugmentation for *in situ* applications. However, pilot studies can be costly. An intermediate approach between the laboratory and field scale applications is the use of model simulations. In order to achieve that, a subsurface contaminant transport model must be coupled with a kinetic model that describes biodegradation of 1,4-dioxane. The simplest approaches to modeling biodegradation of organic contaminants utilize zero or first order kinetics, however, a more realistic alternative is the use of Monod kinetics combined with inhibition terms.

Biodegradation models that include multiple biodegradation pathways and substrates have been described (Hunter et al., 2001). Several software codes such as BIORXNTRN (Hunter et al., 2001), BIOMOC (Essaid and Bekins, 1997), MIN3P (Mayer et al., 2001), and MISER (Chen et al., 2013) have been applied to simulate mass transport and biodegradation of contaminants. BIOMOC allows for multiple chemical compounds with a Monod model for biodegradation and includes noncompetitive, competitive and biomass inhibition factors. MIN3P is capable of simulating multiple substrates, terminal electron acceptors and inhibition. MISER has been used to simulate biodegradation of chlorinated solvents by two microbial populations with lactate serving as the electron donor, as well as inhibition and capabilities for multiple chemical compounds.

In situ cometabolism of chlorinated aliphatics has been simulated using Monod kinetics for methane-oxidizing bacteria (Semprini and McCarty, 1991a; Semprini and McCarty, 1991b). Monod kinetics were coupled to a 1-D transport model that considered

advection, dispersion and sorption. The kinetic model included terms to express the effect of oxygen-limiting conditions on the rate of growth substrate and contaminant biodegradation, as well as competitive inhibition terms. The model simulations predicted concentrations of methane, vinyl chloride (VC), *trans*-1,2-DCE and *cis*-1,2-DCE that were similar to field data.

Despite the variety of cases in which transport models have been coupled to biodegradation models, no attempt to evaluate metabolic and cometabolic *in situ* bioremediation of 1,4-dioxane by numerical modeling has been published. Accurately describing the biodegradation kinetics in a transport model should include various substrate interactions, including coinhibition; this can have a significant impact on the rate and extent of biodegradation of the contaminant, which will not likely be captured by the use of simplified first order reaction rates.

The purpose of this study was to compare the performance of *in situ* metabolic and cometabolic bioremediation of 1,4-dioxane by coupling a subsurface transport model to a biodegradation kinetic model that used kinetic parameters obtained in laboratory batch experiments. The kinetic model describes biodegradation of 1,4-dioxane by *Rhodococcus ruber* ENV425, which uses propane as growth substrate. It also describes metabolic biodegradation by the culture *Pseudonocardia dioxanivorans* CB1190. The focus of this study was to evaluate the differences in bioremediation outcomes that are the product of biodegradation by cultures that use 1,4-dioxane as a growth substrate and those that grow on propane and cometabolize 1,4-dioxane.

The model was implemented with Comsol due to the software's capacity to couple different physics or processes such as flow in porous media, contaminant transport and biodegradation kinetics. The comparison of metabolism and cometabolism included simulations in which four conditions were varied: initial 1,4-dioxane concentration, biomass injection rate, oxygen injection rate, and propane injection rate. Initial 1,4-dioxane concentration is important since the growth and decay of CB1190 is proportional to the amount of 1,4-dioxane available. Biomass injection rates are important because of the practical challenges involved in delivering the injection slurry, as well as the effect it may have on growth of the culture and subsequent biodegradation of 1,4-dioxane. Oxygen injection rate is relevant because the dissolved oxygen concentration impacts the cultures differently, based on differences in their oxygen utilization coefficients. Lastly, propane injection rates impact the growth rate of the propanotrophs and therefore the rate of cometabolism.

3.3 Pilot Study

The model was calibrated with field data obtained from an air sparging and bioaugmentation case study (Lippincott et al., 2015) in which the propane-oxidizing culture ENV425 was used to degrade 1,4-dioxane to concentrations below 2 μg L^{-1}. The site is underlain by a shallow aquifer of silty fine sand and a deep aquifer formed from well-graded sand with gravel (25 to 27 m below ground surface). The aquifers are separated by a low permeability clay layer approximately 1 m thick. The hydraulic gradient at the site was not significant. The injection and monitoring wells were located in the deep aquifer where bioaugmentation occurred. Sparging was used to deliver oxygen and propane into

the aquifer. Four monitoring wells (MW-5B, MW-34B, MW-47B and SW-2B) were placed several meters away from the sparging well (Figure 3-1).

It is important to note that there is an error in Figure 3 of Lippencott et al. (2015), regarding the y-axis units that correspond to propane concentration. The units of propane concentration displayed are mg L^{-1}, however, the correct propane concentration units are µg L^{-1}. (D. Lippincott, personal communication, July 7, 2016). A second error was also spotted in the same paper: in Figure 6, the symbols are switched between monitoring wells 5B and 2B.

Sparging to deliver oxygen between day 0 and day 37 was done by a once daily injection of 45 min of air at a rate of 0.28 m^3 min^{-1}. On day 37, the sparging frequency was increased to 6 daily cycles of 0.28 m^3 min^{-1} for 36 min each. Propane injection started on day 29 as part of the 45 min daily injection and then increased on day 37 as part of the 36 min, 6 cycles per day injection routine. All of the biomass (36 L of slurry) was injected on day 41 from the same injection well used for sparging.

Based on the sparging rates, the volume of air injected each day was 12.8 m^3 d^{-1} during the first 29 days, and 60.4 m^3 d^{-1} for the rest of the sparging operation. If we assume that the total volume of the aquifer is 275 m^3 based on the estimated radius of influence by Lippincott (2015) of 8 m and a 1.37 m thickness, then the pore volume would be 82.6 m^3 based on a typical porosity value of 0.3. This volume of water would be displaced by air just after 6.4 days of sparging. Therefore, there must be leakage of gas going upward through the confining layer. This could happen due to discontinuities and fractures in the clay layer. Under low sparging rates, stratification of air under certain soil layers could

occur, however for high sparging rates, air can breakthrough some of these layers (Johnson et al., 2001). In addition, gas venting was observed in the monitoring wells (D. Lippincott, personal communication, January 18, 2016), so a portion of the gas could have escaped this way if the wells were not capped properly.

Sparging produces a transient gas distribution that reaches its maximum right before the air is turned off (Figure 3-2a). As gas moves away from the sparging well, the majority will be located in the upper levels of the aquifer, forming a layer of gas right below the clay layer. The shape of the gas plume is determined by the porous medium properties such as the intrinsic permeability, as well as multiphase flow parameters such as the capillary entry pressure and the capillary retention curve, which can be described by Brooks and Corey parameters (Brooks and Corey, 1964). The gas leakage rate through this confining layer determines how far the gas layer spreads in the radial direction.

After the air is shut down, some of the gas will be dissolved while some of it will be leaked. Since no more air is being sparged during this stage, the water that was initially pushed away comes back and fills the pores again, until the sparging is turned on again (Figure 3-2b). This cycling of sparging generates movement of water or recirculation, which creates water mixing. This mixing increases advection and dispersion of the species involved, especially biomass. Gas species (propane and oxygen) are delivered mainly by advection in the gas phase, and are then dissolved in the liquid phase via mass transfer, limited by their solubility in water.

Within 245 days of operation at VAFB, bioremediation of 1,4-dioxane was evident. Monitoring well data indicated a decrease in propane in all of the wells a few days after

bioaugmentation started, confirming that the propanotrophic culture was active. In addition, a decrease in 1,4-dioxane was observed in three of the monitoring wells, but remained unchanged in well MW-5B (Lippincott et al., 2015).

3.3 Conceptual Model

The scope of the model simulations performed in this study was to compare the performance of metabolic and cometabolic bacteria under equal environmental conditions, while incorporating differences in thier kinetic characteristics. Since field data from VAFB are available for cometabolic biodegradation of 1,4-dioxane, the model was tailored to these site conditions. Delivery of oxygen and propane was simulated by an approximated air sparging model. It is outside of the scope of this study to provide a complete air sparging model; however, certain elements of the process were used to approximate the distribution of propane and oxygen in the aquifer such that they were in good agreement with the field data.

Air sparging systems have been widely studied (Johnson et al., 2001; Lundergard and Andersen, 1993; McCray and Falta, 1996, 1997; Sellers and Schreiber, 1992; Suthersan, 1999). Gas flow in porous media has also been studied under laboratory conditions to determine the shape of a gas plume (Ji et al., 1993). Numerical simulations have been developed to assess the performance of injection of air in air sparging systems (Benner et al., 2000; Lundergard and Andersen, 1993; McCray and Falta, 1997).

For this study, the flow of water and gas in porous media was simulated in a hydrogeological setting based on the pilot study at VAFB (Lippincott et al., 2015). The air sparging conditions in the pilot study were approximated under two assumptions. First,

gravity effects were approximated by dividing the aquifer thickness into five uniform segments and the average capillary pressure in each layer was calculated. This capillary pressure was used in the model to calculate the relative permeabilities of the fluids and the phase saturations. Therefore, the model does not describe any flow in the vertical direction. Second, the air sparging process was at steady state. The justification for this assumption is that even though the air was injected in cycles, the frequency and parameters of the injections remained unchanged in the long term (Lundergard and Andersen, 1993). Also, because there was upward leakage of air through the confining layer, the same amount of air that entered the aquifer was either consumed for biodegradation or left through leakage. The benefit of this assumption is that an average daily constant rate replaced the cycle injections and therefore its implementation in the simulation was significantly simplified, as opposed to having six daily injections over multiple years of simulation. One disadvantage of this approach is that groundwater mixing does not occur and its velocity is negligible since there was a fixed gas distribution. Therefore, movement of biomass in the water phase had to be adjusted independently of the water velocity. This was done by adjusting a diffusion-like parameter to account for biomass dispersion and was calibrated using the 1,4-dioxane depletion data.

The model geometry is based on Cartesian coordinates, with a plan-view in the x and y directions, and a two dimensional circular shape with a 1,4-dioxane plume similar to the one described in the pilot study at VAFB; an injection well was located at the center of the domain (Figure 3-1). The screened area of the sparging well was 0.21 m^2 based on a height of 1.37 m and a radius of 0.025 m.

Air entered at the injection well and traveled away from it; the flow was driven by the injection gas pressure and upward gas leakage that occured due to fractures and discontinuities in the confining layer. This resulted in water and gas saturations that depend on the injection pressure and gas leakage rate (Figure 3-3). The air and water pressures are related by the Brooks and Corey equations and determine the saturation and relative permeability of the gas and the water phases (Brooks and Corey, 1964). The gases, oxygen (O_{gas}) and propane (S_{gas}), entered the domain at the injection well in the gas phase where most of their movement occurred; they were then transferred to the water phase via a mass transfer process, which was controlled by the aqueous concentration and solubility of the gaes.

The reactive transport model predicted concentrations in the water phase for the four species involved in cometabolism: 1,4-dioxane (C), dissolved propane (S), dissolved oxygen (O), and biomass (X). For the metabolic simulations, propane was omitted. Only propane (S_{gas}) and oxygen (O_{gas}) were predicted for the gas phase. The model was calibrated with monitoring data from the pilot study. The plume of 1,4-dioxane was divided into three uniform concentration zones of 1100, 550 and 100 $\mu g\ L^{-1}$.

Mass transfer from the gas to the water phase was modulated by the concentrations in the gas and aqueous phase, a global mass transfer coefficient,and the solubility of the species. Adsorption and volatilization were ignored because 1,4-dioxane does not adsorb to a significant extent and its Henry's law constant is comparatively low. Biomass transport was dependent on the adjusted diffusion-like coefficient for the water phase; other

mechanisms that impact the transport of biomass, such as adsorption, straining and settling, were not included in the model.

Biomass decay is a critical parameter that influences the survivability of bacteria. Under controlled laboratory conditions, the decay coefficient is considered constant. However, under certain environmental conditions, such as low-substrate or starvation conditions, physiological changes in biomass can slow down the endogenous decay rate (Lobos et al., 2005; Lu et al., 2007). This is especially important for bioaugmentation with a culture that grows on the contaminant when the initial concentration of the contaminant is below the level needed for growth to offset decay.

A second parameter of high importance is the maximum specific rate of 1,4-dioxane biodegradation. The kinetic model used in this study did not incorporate the inhibitory effects of co-contaminants such as chlorinated ethenes and chlorinated ethanes. Furthermore, the variability in kinetic parameters for biodegradation of organic contaminants is evident in the literature (Chambon et al., 2013; Kovárová-Kovar and Egli, 1998). Consequently, it was reasonable to assume that the biomass decay coefficient and maximum specific biodegradation rate used for modeling purposes were different from those that were determined under laboratory conditions.

3.3.1 Governing equations: Water and Gas Flow

The flow of the water and gas phase was described by the conservation of mass equation under assumed steady state conditions:

$$\nabla \cdot (\rho_i \vec{u}_i) = \varepsilon_i \dot{S}_i \qquad 3\text{-}6$$

where the subscript "i" refers to the fluid phase, ρ_i is the density of the fluid (kg m^{-3}), $\vec{u}_i$ is the Darcy's volumetric flux (m s^{-1}), $\dot{S}_i$ is a sink or source mass rate (kg m^3 s^{-1}), and ε_i is the effective porosity (dimensionless). The movement of fluid in porous media is described by Darcy's law for laminar flow:

$$\vec{u}_i = -\frac{k_{ri}k}{\mu_i}(\nabla P_i) \qquad 3\text{-}2$$

where k_{ri} is the relative permeability of the fluid (dimensionless), k is the intrinsic permeability of the aquifer (m^2), μ_i is the fluid's viscosity (Pa·s), and ∇P_i is the pressure gradient (Pa m^{-1}). The source of gas mass in the aquifer was provided as an inlet pressure that generated a mass flux on the well screen. The gas sink was dependent on the gas pressure and a reference pressure (the initial gas pressure). The gas leakage term was regulated by a conductance coefficient (C_n). The leakage rate is:

$$\dot{S}_g = -C_n\left(P_g - P_{g\_initial}\right) \qquad 3\text{-}3$$

where $\dot{S}_g$ is the gas leak rate (kg m^3 s^{-1}), C_n is the conductance coefficient (s m^{-2}), and P_g and $P_{g\_initial}$ are the gas and reference gas pressures (Pa), respectively. For the gas and water fluids, equation 3-1 becomes:

$$\nabla \cdot \left[\rho_g\left(-\frac{k_g}{\mu_g}\left(\nabla P_g\right)\right)\right] = -\varepsilon C_n\left(P_g - P_{g\_initial}\right) \qquad 3\text{-}1$$

$$\nabla \cdot \left[\rho_w\left(-\frac{k_w}{\mu_w}(\nabla P_w)\right)\right] = 0 \qquad 3\text{-}2$$

The effective fluid permeability is defined as the product between the intrinsic permeability (k), and the relative permeability of the fluid (k_{ri}). The relative permeability is expressed as a function of the capillary pressure according to the Brooks and Corey equation (Brooks and Corey, 1964):

$$k_{rg} = \left[1 - \frac{P_{EC}}{P_C}^{\lambda}\right]^2 \left[1 - \left(\frac{P_{EC}}{P_C}\right)^{2+\lambda}\right] \quad 3\text{-}3$$

$$k_{rw} = \left(\frac{P_{EC}}{P_C}\right)^{2+3\lambda} \quad 3\text{-}4$$

The entry gas capillary pressure (P_{EC}) is a parameter specific to the porous medium and is defined as the pressure needed to have air flow (Johnson et al., 2001). Lambda (λ) depends on the pore size distribution of the medium (Brooks and Corey, 1964). For gas pressure values above the water pressure, the capillary pressure is defined as:

$$P_c = P_g - P_w - P_{EC} \qquad P_g > (P_w + P_{EC}) \quad 3\text{-}5$$

$$P_c = P_{EC} \qquad P_g < (P_w + P_{EC}) \quad 3\text{-}6$$

The effective porosity in each fluid phase takes into account total porosity and phase saturation:

$$\varepsilon_i = \varepsilon \cdot S_i \quad 3\text{-}7$$

where ε is the aquifer porosity and S_i is the phase saturation. The water and gas phase saturations are:

$$S_w = \left(\frac{P_{EC}}{P_C}\right)^{\lambda} \qquad P_C \geq P_{EC} \quad 3\text{-}8$$

$$S_w = 1 \qquad P_C \leq P_{EC}$$

$$S_g = 1 - \left(\frac{P_{EC}}{P_C}\right)^{\lambda} \quad P_C \geq P_{EC} \quad 3\text{-}9$$

$$S_g = 0 \qquad\qquad P_C \leq P_{EC}$$

Therefore, the effective porosities for each fluid are:

$$\varepsilon_{water} = \varepsilon \cdot \left(\frac{P_{EC}}{P_C}\right)^{\lambda} \tag{3-10}$$

$$\varepsilon_{gas} = \varepsilon \cdot \left[1 - \left(\frac{P_{EC}}{P_C}\right)^{\lambda}\right] \tag{3-11}$$

The model is two dimensional and does not physically include the thickness of the aquifer. This is valid because the aquifer from the field study is relatively thin. The capillary pressures at five different heights within the aquifer were calculated to characterize gas saturation due to the increase in hydrostatic pressure with depth. Each height yields a different hydrostatic water pressure which then determined five capillary pressures. The capillary pressures were averaged over depth and those values were used to calculate the relative permeabilities and the phase saturations.

3.3.2 Governing Equations: Solute Transport and Biodegradation

The transport was described using:

$$\frac{d\varepsilon_w C}{dt} = -\nabla \cdot (\vec{u}_w C) + \nabla \cdot \left(\left(\varepsilon_w \cdot (D^C_{e,w} + D^C_{h,w})\right)\nabla C\right) - q_C \cdot X \tag{3-12}$$

$$\frac{d\varepsilon_w S}{dt} = -\nabla \cdot (\vec{u}_w S) + \nabla \cdot \left(\left(\varepsilon_w \cdot (D^S_{e,w} + D^S_{h,w})\right)\nabla S\right) - q_S \cdot X + \dot{S}_S \tag{3-13}$$

$$\frac{d\varepsilon_w O}{dt} = -\nabla \cdot (\vec{u}_w O) + \nabla \cdot \left(\varepsilon_w \cdot (D^O_{e,w} + D^O_{h,w})\nabla O\right) - q_O \cdot X + \dot{S}_O \tag{3-14}$$

$$\frac{d\varepsilon_w X}{dt} = -\nabla \cdot (\vec{u}_w X) + \nabla \cdot \left(\left(\varepsilon_w \cdot (D^X_{e,w} + D^X_{h,w})\right)\nabla X\right) - q_X \cdot X \tag{3-15}$$

where C, S, O and X are the contaminant, growth substrate, oxygen and biomass concentrations in the water phase, respectively; $\vec{u}_w$ is the groundwater velocity; ε_w is the effective water pore volume; $D^i_{e,w}$ and $D^i_{h,w}$ are the effective diffusivity and the dispersion coefficients in the water phase; q_C, q_S, q_O and q_X are the specific biodegradation rates for the contaminant, substrate, oxygen and biomass species, respectively, described by a modified Monod equations with kinetic parameters determined under laboratory conditions in Chapter 2. $\dot{S}_S$ and $\dot{S}_O$ are the mass transfer source terms for growth substrate and oxygen, respectively.

For the gas phase, only two species were considered and no biodegradation occurs. Therefore, the equations are:

$$\frac{d\varepsilon_g S_{gas}}{dt} = -\nabla \cdot \left(\vec{u}_g S_{gas}\right) + \nabla \cdot \left(\left(\varepsilon_g \cdot (D^S_{e,g} + \alpha_g \vec{u}_g)\right)\nabla S_{gas}\right) - \dot{S}_S \qquad 3\text{-}16$$

$$\frac{d\varepsilon_g O_{gas}}{dt} = -\nabla \cdot \left(\vec{u}_g O_{gas}\right) + \nabla \cdot \left(\left(\varepsilon_g \cdot (D^O_{e,g} + \alpha_g \vec{u}_g)\right)\nabla O_{gas}\right) - \dot{S}_O \qquad 3\text{-}17$$

where S_{gas} and O_{gas} are the gas concentrations for propane and oxygen, respectively; $\dot{S}_S$ and $\dot{S}_O$ are the propane and oxygen gas sinks due to dissolution in the water phase, respectively; ε_{gas} is the gas porosity and α is the dispersivity in the gas phase, respectively; and $D^O_{e,gas}$ and $D^S_{e,gas}$ are the effective diffusivities of oxygen and propane in the gas phase, respectively. The mass transfer rate term for oxygen and propane is defined as:

$$\dot{S}_S = K^S_{GW}\left(S_{gas} - H_S S\right) \qquad S < Sol_S \qquad 3\text{-}18$$

$$\dot{S}_S = 0 \qquad S \geq Sol_S$$

$$\dot{S}_O = K_{GW}^{O}\left(O_{gas} - H_O O\right) \qquad O < Sol_O \qquad 3\text{-}19$$

$$\dot{S}_O = 0 \qquad O \geq Sol_O$$

where K_{GW}^{S} and K_{GW}^{O} are the global mass transfer coefficients for propane and oxygen, respectively; H_S and H_O are the Henry's law constants for propane and oxygen, respectively; and Sol_S and Sol_O are the solubilities for propane and oxygen, respectively.

Monod equations accounting for coinhibition between substrate and non-growth substrate were used for cometabolism of 1,4-dioxane, as described in Chapter 2. The kinetic parameters adjusted for a temperature of 15 ºC are summarized in Table 3-2.

3.2.3 Boundary and Initial Conditions

The initial gas pressure was set equal to the hydrostatic pressure, allowing a smooth start to the numerical simulations. The initial concentrations of propane and oxygen in the gas phase were zero. The initial concentrations of propane, oxygen, and biomass in the water phase were zero. The initial 1,4-dioxane concentration consisted of three concentration zones of 1100, 550, and 100 µg L^{-1} located at the same position as described in the pilot study (Figure 3-1).

The hydrostatic water pressure was 45,000 Pa. For the gas phase, an injection pressure of 7,000 Pa was specified at the injection well for the first 37 days, and then increased to 14,000 Pa for the rest of the simulation (Table 3-3). This increase was made to be consistent with the increase in the air sparging injection cycles used in the pilot study. The outer boundary of the model was open flow to allow gas, water and species to move away from the model domain (Figure 3-1). The fluxes of propane used were 1.01×10^{-5} kg

COD m^2 s^{-1} between days 29 and 37 and 8.09×10^{-5} kg COD m^2 s^{-1} from day 37. The fluxes of oxygen were 5.34×10^{-3} kg COD m^2 s^{-1} during the first 37 days and 2.56×10^{-2} kg COD m^2 s^{-1} from day 37. The flux of biomass added was 1.68×10^{-5} kg COD m^2 s^{-1} between day 41 and day 42. Biomass addition was simulated as an injection spread over one 24 h period.

3.4 Model Implementation

Comsol version 5.2 was used to implement the model calibration and to perform the analysis to assess the effect of different parameters on the time to achieve a bioremediation goal. Calibration of the model to the data observed in the field demonstration at VAFB was used as a baseline scenario. One of the reasons for using Comsol is its ability to incorporate the complex biodegradation kinetics and to readily couple a gas and water flow model.

3.4.1 Model calibration

Calibration was done by adjusting parameters so that the model adequately predicted the 1,4-dioxane concentrations observed in the field at four monitoring wells. There was no data available for the gas distribution from the pilot study. Therefore, the flow was calibrated to match the aqueous propane distribution observed in the field. The propane field concentrations showed a similar pattern among all the monitoring wells. The pattern consisted of an increase in propane from day 29 to day 41 followed by a decrease until the concentration approached zero by day 100. 1,4-Dioxane concentrations decreased below 2 μg L^{-1} at two of the monitoring wells by day 150 (Lippincott et al., 2015). Monitoring well MW-5B did not show any decrease in 1,4-dioxane, however, well MW-

34B exhibited a fast decrease. Wells MW-5B and MW-34B are at similar distances from the injection well, however, the field data shows that biodegradation occurred only in one of them. Parameters such as k, ε, P_{EC}, λ, remained fixed during calibration and were set based on the type of porous media described in the pilot study. $K_{G,W,O,}$ and $K_{G,W,S}$ were chosen based on the mass transfer values of oxygen and propane, respectively. The parameters that were adjusted to match the propane distribution included $D_{h,W,S}$, α, ε and C_n. 1,4-Dioxane biodegradation data was used to adjust b, q_{CMAX}, $D_{h,W,X}$, $D_{h,W,C}$, $D_{h,W,O,}$ and $K_{G,W,O}$. The range of values considered for each parameter are given in section 3.5.2, under sensitivity analysis.

P_{g_sparge} and C_n were adjusted to obtain a mass flux of air that is similar to the amount of air added in the pilot study (6.44 x 10^{-4} kg m^{-1} s^{-1}). These are essential because they control the gas flux and therefore the advective transport of oxygen and propane.

The dispersion of propane and oxygen in the gas phase was defined as:

$$D_h = \alpha_g \vec{u}_g \qquad 3\text{-}20$$

where D_h is the hydrodynamic dispersion coefficient, and α_g is the dispersivity in the gas phase. For contaminant transport parameters in the water phase, the dispersion coefficients $D_{h,W,S}$, $D_{h,W,C}$, $D_{h,W,O}$, and $D_{h,W,X}$ were manually adjusted to match the pilot study data.

Each parameter was adjusted by using the parametric sweep tool in Comsol. An initial adjustment of the parameters described above was done manually until it was determined by visual inspection that the model reasonably fit the field data from the monitoring wells. Subsequently, optimization of the parameters was done by using the optimization physics node available in Comsol. This optimization procedure provided for

a quantitative assessment of the calibration by calculating the sums of squared errors between the field data and the predicted concentrations of 1,4-dioxane for each of the four wells.

3.4.2 Numerical Implementation

To solve the gas and water flow models, two "Darcy flow" nodes were used in Comsol. These modules were coupled via the Brooks and Corey equations. In the gas phase Darcy flow module, the sparge gas pressure was specified at the boundary representing the well's circumference. The gas leak term was implemented as a "mass source/sink" node that covered the entire model domain. The dependent variable was the gas pressure (P_g). In the water phase, the biomass flux was specified in the same circumference boundary of the injection. The dependent variable was water pressure (P_w). These two modules were run simultaneously to generate a gas and water distribution at steady state. The velocity fields, relative permeabilities and effective porosities obtained from this simulation were used as input or initial conditions for the contaminant transport model.

The "Transport of Diluted Species in Porous Media" node was used in Comsol to solve the contaminant transport equations. One node was used for the transport of gas species in the gas phase, and another one for the transport in the aqueous phase. Advection and dispersion were the only transport mechanisms enabled and volatilization and adsorption were ignored. The dependent variables were the chemical species already described: S, C, O and X for the water phase and S_gas and O_gas for the gas phase. In the "Porous Media Transport Properties" node, porosity, diffusion and dispersion coefficients were entered as user defined. For the gas phase, dispersion of oxygen and propane was

modeled by the fluid velocity ($\vec{u}_g$) multiplied by a dispersivity value (α). Soil was chosen as the solid material and water and air were chosen as the fluids from the Comsol library.

Mass transfer between the gas and aqueous phases was enabled for oxygen and propane. In the gas contaminant transport node, mass transfer was defined as a sink term covering all of the model domain. In the water contaminant transport module, a "mass source" node was used containing the same mass transfer rate term (Equations 3-18 and 3-19).

The kinetic parameters, step functions, Brooks and Corey equations, biodegradation Monod expressions, dispersion, and mass transfer rate equations were stated in the "Definitions" node. Geometric ellipses were used to define the 1,4-dioxane plumes. In addition, geometric points were added in locations that match the position of the monitoring wells from the pilot study with respect to the injection well.

A fluid-dynamics, triangular meshing (Figure 3-4) of the domain was customized in order to refine the grid in the 1,4-dioxane plume. The mesh was refined as a boundary mesh for the domain containing the injection well; this was done to have a smooth mesh element size transition from the well boundary to the rest of the domain. The rest of the mesh was set as free triangular.

Two "studies" with a time-dependent solver were set up to run the simulations. A "study" in Comsol is a solver or set of solvers to be used for the numerical simulations. The solver time units were set in days.

For Study 1, the Darcy flow modules for the gas and the water phases were run; the first simulation range was 0 to 41 days with a maximum time step of 0.1 d and the second

range was 42 to 150 d with a maximum time step of 5 d. This allowed for the flow model to reach steady state conditions.

For Study 2, the gas and water "Transport of Species in Porous Media" modules were run simultaneously. This study used Study 1 solutions to provide for values for variables not solved in Study 2, such as velocity fields and effective porosities. The simulation time was split in two ranges: range 1 from 0 to 45 d with a maximum time step of 1 d and range 2 from 46 to 245 d with a maximum time step of 5 d. This was done to improve the post-processing of the data when long simulation times were used. The final simulation time was the same remediation time used in the case study in which bioaugmentation was performed. Whenever necessary, the total simulation time was extended. Regarding the solver properties, the absolute tolerance was 0.001 for the dependent variables and the solver used was PARDISO.

A parametric sweep was utilized for the parameters described for the sensitivity analysis (Table 3-5). The metrics considered to compare such variations were the time to achieve a remediation goal of 1 μg L^{-1}, percent of 1,4-dioxane removed, and sums of squared errors.

Data sets for each well and line plots displaying concentration versus time were obtained after each simulation and compared to the predicted concentrations of propane and 1,4-dioxane against the observed field data, thereby allowing calculation of residuals. Surface plots were also generated which provided an overall perspective of changes in species concentrations in the aquifer.

After the model was manually calibrated, an optimization module was set up by the gradient based method Levenberg-Marquadt. The objective function for optimization was the minimization of the residual sums of squared errors between the predicted and measured concentrations of 1,4-dioxane. There were a total of four objective functions based on the four sums of squared errors corresponding to each monitoring well. A baseline model was obtained when the calibration and optimization were completed. The baseline model was subsequently modified to study the effect of initial conditions on achieving 1,4-dioxane bioremediation goals.

3.4.3 Comparison between Metabolism and Cometabolism

After performing the model calibration and sensitivity analysis of the model parameters, the performance of CB1190 (grows on 1,4-dioxane) and the propanotroph ENV425 (cometabolizes 1,4-dioxane) was compared. Variations in the initial 1,4-dioxane concentrations and propane, oxygen and biomass input fluxes were performed to evaluate their effect on bioremediation. The initial concentration of 1,4-dioxane was varied from 0.1 to 100 times the baseline value, equivalent to 0.1 to 100 mg L^{-1} in the source zone. The biomass injection rate was varied from 0.5 to 500%, the oxygen injection rate from 0.1 to 100% and the propane injection rate from 0.5 to 100% with respect to the baseline values. The same two metrics used in the sensitivity analysis were followed, i.e., the time to achieve an average 1,4-dioxane concentration of 1 μg L^{-1} and percentage of contaminant degraded after 10 years. This comparison was the main outcome of the present study.

3.5 Results

3.5.1 Model Calibration: Cometabolic Bioremediation

The parameters adjusted to achieve the calibration of the propane data were k, ε, Brooks and Corey parameters (P_{EC} and λ), C_n, $D_{h,W,S}$, and α (Table 3-1). Along with k and C_n, P_{g_sparge} was adjusted to generate a mass flux of 6.44 x 10^{-4} m s^{-1} of air into the aquifer at the injection well boundary, which corresponds to the observed gas flux in the pilot study. Distributions of k_{rg}, ε_g, and $\vec{u}_g$ in the aquifer were obtained as a solution from this simulation (Figure 3-5).

The model closely followed the rise in propane concentrations after its addition on day 29 (Figure 3-6). The predicted propane concentration reached approximately 250 and 210 µg L^{-1} for wells 47B and 2B which are located closest to the injection well, however, the highest measured concentration was 110 µg L^{-1} in these wells. A similar pattern was observed for the distant wells in which the predicted peak concentration of propane was ~95 and ~130 µg L^{-1} and the measured peak concentration was no higher than 65 and 75 µg L^{-1}, respectively. The model also predicted the consumption of propane that followed the addition of biomass on day 42. However, the decrease in propane concentration is slower for the simulated prediction since it took between 300 and 400 d to reach zero whereas the field data had a sudden decrease and reached the detection limit in less than 50 days.

The model fits the 1,4-dioxane field data from the monitoring wells near the injection well better than for the more distant wells (Figure 3-7). According to the field data, biodegradation of 1,4-dioxane was similar in the two monitoring wells located near

the injection well (i.e. 47B and 2B). 1,4-Dioxane concentrations decreased at approximately the same time in both of these wells. By 210 days of operation, 1,4-dioxane levels fell below 2 μg L^{-1}. This was not the case for the more distant monitoring wells (5B and 34B). Even though those wells were at similar distances from the injection well, they were located in opposite directions. Monitoring well 5B did not show any significant decrease in 1,4-dioxane during biosparging, however, well 34B showed a decrease in concentration from 136 to 8.9 μg L^{-1} in only 61 days.

Fitting of the 1,4-dioxane data from the pilot study was the primary criterion for adjusting the transport and kinetic parameters for model calibration. After an adequate trend on propane concentration rise and decrease was predicted by the model, parameters such as $D_{h,W,X}$, $D_{h,W,C}$, $D_{h,W,O}$, b, and q_{CMAX} were adjusted. The total sums of squared errors for the four wells was 4.6×10^{-6} (kg COD m^{-3})^2. However, it is important to look at the sums of squared errors from each well, since the initial concentrations varied among them. Well 5B had an initial 1,4-dioxane concentration of 555 μg L^{-1} (1×10^{-3} kg COD m^{-3}) and well 34B started at 135 μg L^{-1} (2.4×10^{-4} kg COD m^{-3}). The closest wells, 47B and 2B, had initial concentrations of 1,090 μg L^{-1} (2×10^{-3} kg COD m^{-3}) and 997 μg L^{-1} (1.8×10^{-3} kg COD m^{-3}), respectively. The sum of squared errors for well 34B was 8.2×10^{-8} (kg COD m^{-3})^2 and for 5B it was 3.04×10^{-6} (kg COD m^{-3})^2. Even though the initial concentration of well 5B is five times higher than 34B, its sum of squared errors is four orders of magnitude higher. In order to decide on the most adequate model fit, attention was paid mostly to wells 47B and 2B, which are in the highest 1,4-dioxane concentration zone. The sums of squared errors for wells 47B and 2B were 2.7×10^{-7} (kg COD m^{-3})^2 and 1.41×10^{-6} (kg COD m^{-3})^2,

respectively. Considering only wells 47B and 2B, the sum of squared errors calculated was 1.65×10^{-6} (kg COD m^{-3})^2 for the calibrated parameters.

3.5.2 Sensitivity Analysis

A sensitivity analysis was performed for each parameter to investigate their effects on 1,4-dioxane biodegradation. The simulation time was extended to 10 years in order to capture long term trends. Table 3-5 shows the range of parameters selected and the effects the parameters had on the outcome of the simulation. The ranges chosen to vary b, q_{MAX}, and K_{iS} were based on the values obtained from batch experiments in the laboratory; b was varied from 0 to 100% of the laboratory value to explore the full range from absence to decay in a suspended batch culture, whereas q_{MAX} was varied from 10 to 100% and K_{iS} from 1 to 1000%.

The dispersion coefficients were varied according to the equivalent dispersion values that would result from the dispersivity and a hypothetically expected water velocity, which could vary at least between 2×10^{-5} to 2×10^{-3} m s^{-1} (Harter, 2003). In addition, typical dispersivity values vary depending on the porous medium, flow rate and characteristic length that is modeled. Dispersivity in soils has been observed to vary up from two to three orders of magnitude (Gelhar et al., 1992), from 0.03 to 0.33 of the distance traveled (Vanderborght and Vereecken, 2007). Therefore, the typical hydrodynamic dispersion coefficients vary between 2×10^{-7} to 2×10^{-4} m^2 s^{-1}. In addition, hydrodynamic dispersion coefficients of similar orders of magnitude have been applied or measured in the literature (Hornberger et al., 1992; Semprini and McCarty, 1991a). The ranges used for the

sensitivity analysis of the hydrodynamic dispersion coefficients in water cover those values reported in the literature and vary three to four orders of magnitude.

For transport of propane and oxygen in the gas phase, the dispersivity was varied between 0.016 and 0.333 of the value of the characteristic length used in the model. Lastly, porosity values were varied between 0.1 and 0.5, which is a range that includes the porosities of unconsolidated materials such as sand, gravel, and clays (Manger, 1963).

The transport model closely followed the field data for 1,4-dioxane from the two monitoring wells (47B and 2B) closest to the injection well when using values for q_{CMAX} and b that are 50% and 10%, respectively, of those determined in the laboratory with suspended growth cultures (Figure 3-7). A significant impact from b on the percentage of 1,4-dioxane biodegraded after 10 years and the time to reach an average concentration of 1 μg L^{-1} was observed. When b was set above 25% of the experimentally determined value, the average 1,4-dioxane concentration decreased, although at a slower rate. The concentration of 1,4-dioxane did not reach 1 μg L^{-1} even after 10 years (Appendix B, Figure 6-11). A concentration of 1 μg L^{-1} was only reached when b was between 0 and 10% of the laboratory determined value. The percentage of 1,4-dioxane that was biodegraded after 10 years decreased to 20% when b was 100% of the experimental value, revealing its highly significant long-term impact.

When the laboratory determined value of q_{CMAX} was used, 1,4-dioxane was consumed at too high a rate compared to the observed field data. This parameter was adjusted to 50% of its experimental value to improve the model fit. Lowering q_{CMAX} to 10% of the experimental value increased the time to achieve 1 μg L^{-1} from 3.5 to 6.7 years.

However, the impact on the percentage of 1,4-dioxane that was biodegraded after 10 years was insignificant, although it took three years longer to reach 1 µg L^{-1} when q_{CMAX} was decreased to 10% of the experimentally determined value.

K_{iS} was varied between 1 and 1000% of the experimentally determined value; the lower K_{iS}, the higher the inhibition effect. The results indicated that K_{iS} does not have a significant effect on the percentage of 1,4-dioxane biodegraded after 10 years; this remained at 100% for all values of K_{iS}, indicating that remediation was achieved within 10 years, regardless of propane inhibition (Appendix B, Figure 6-15).

$D_{h,W,X}$ was varied over several orders of magnitude and had a negative effect on the percentage of 1,4-dioxane biodegraded when its value was below 1×10^{-8} m^2 s^{-1}. For the lowest value tested, 1×10^{-9} m^2 s^{-1}, there was no biodegradation of 1,4-dioxane (Appendix B, Figure 6-16). Regarding the effects of $D_{h,W,X}$ on the time to reach the remediation goal, a value of 1×10^{-6} m^2 s^{-1} resulted in the fastest rate of biodegradation. A considerable difference in remediation times was observed between 1×10^{-8} m^2 s^{-1} (which required more than 40 years) and 5×10^{-8} m^2 s^{-1} (which achieved the remediation goal in 4.0 years). When dispersion was higher than 1×10^{-6} m^2 s^{-1}, complete biodegradation was still achieved after 10 years.

$D_{h,W,C}$ had a moderate effect on the percentage of contaminant biodegraded after 10 years. For a $D_{h,W,C}$ of 5×10^{-8} to 1×10^{-7} m^2 s^{-1}, the percentage of 1,4-dioxane biodegraded dropped to 96% (Appendix B, Figure 6-18). Correspondingly, the remediation goal was of 1 µg L^{-1} was not achieved within 10 years. For low values (1×10^{-9} to 1×10^{-8} m^2 s^{-1}), the difference in time to achieve the remediation goal was 0.9 years (Appendix B, Figure 6-

18b). For a value of 1×10^{-6} m^2 s^{-1}, the average concentration dropped below 1 μg L^{-1} after 5.3 years and the percentage of biodegradation increased to 100%.

$D_{h,W,S}$ and $D_{h,W,O}$ in water did not have a significant effect on the time to achieve the remediation goal or the percentage of 1,4-dioxane biodegraded after 10 years. Changing these parameters by several orders of magnitude changed the time to reach the 1,4-dioxane target of 1 μg L^{-1} by only 0.05 year (Appendix B, Figure 6-20 and Figure 6-21).

Varying α had a low to significant impact on biodegradation of 1,4-dioxane. The most significant impact was observed when α was decreased from 3.0 to 0.05 m, which increased the time to achieve the remediation goal from 4.0 to 4.8 years (Appendix B, Figure 6-23 and Figure 6-24). However, there was no impact on the percentage of 1,4-dioxane biodegradation after 10 years.

Changes in ε strongly affected the time to achieve the remediation goal: for a value of 0.1, the remediation time was 1.6 years, whereas for a value of 0.5 the time was 7.0 years (Appendix B, Figure 6-26). Since the mass of 1,4-dioxane present for a given plume concentration depends on the pore space volume, there is more mass of contaminant when ε is larger, and therefore it takes longer to biodegrade it.

3.5.3 Metabolic Bioremediation

The same approach for sensitivity analysis was used to evaluate the effect of several parameters on bioremediation of 1,4-dioxane by CB1190. A strong effect by *b* was observed (Appendix B, Figure 6-12). The goal to reach a concentration of 1 μg L^{-1} of 1,4-dioxane was not achieved except when the *b* was zero. This reflects the competing processes of growth and decay, in an environment with a low initial substrate

concentration. The percentage of 1,4-dioxane biodegraded was also strongly affected by decay; when 100% of the experimentally determined *b* value was used, only 34% of the contaminant was degraded.

q_{SMAX} was varied from 10 to 100% of the laboratory determined value (Appendix B, Figure 6-14). A moderate effect was observed when 10% of q_{SMAX} was used, which lowered the percentage of contaminant degraded to 80%. As expected, the remediation goal was not reached since decay limited the amount of viable biomass.

$D_{h,W,X}$ had a significant effect on the percent of 1,4-dioxane biodegraded after 10 years (Appendix B, Figure 6-17). For the lowest $D_{h,W,X}$ value, only 43% of 1,4-dioxane was biodegraded and it took 3.7 years to achieve the remediation goal. In contrast, for a $D_{h,W,X}$ value of 2×10^{-6} m^2 s^{-1}, the time to reach the remediation goal was only 0.61 year. A $D_{h,W,X}$ value of 1×10^{-5} m^2 s^{-1} resulted in no growth of biomass and therefore no biodegradation of 1,4-dioxane.

$D_{h,W,C}$ had a moderate effect on the percentage of biodegradation after 10 years (Appendix B, Figure 6-19). In this case, a lower value yielded better removal of 1,4-dioxane; the most significant drop in biodegradation occurred when $D_{h,W,C}$ was decreased from 5×10^{-9} to 1×10^{-7} m^2 s^{-1}. When $D_{h,W,C}$ was high, the plume became less stable and some of the contaminant mass moved away from the biomass, thereby escaping biodegradation.

$D_{h,W,O}$ and α did not have a significant effect on biodegradation of 1,4-dioxane, since the amount of oxygen added into the aquifer was always in excess (Appendix B, Figure 6-22 and Figure 6-25).

Lastly, ε had a limited effect on the percentage of biodegradation of 1,4-dioxane by CB1190 after 10 years (Appendix B, Figure 6-27). For a porosity of 0.1, 99.8% of 1,4-dioxane was degraded, whereas for an ε of 0.5 this decreased to 89.1% The same reasoning that applied to the propanotrophic culture applies here, i.e., a higher ε means there is more pore space and therefore more mass of contaminant for the same concentration plume. The higher the mass of contaminant present, the longer it takes to biodegrade it. For an ε of 0.1, the remediation goal of 1 μg L^{-1} was achieved in 1.7 years.

3.5.4 Effect of the Initial Concentration of 1,4-Dioxane

The performance of CB1190 was strongly influenced by the initial 1,4-dioxane concentration (Figure 3-8). At a contaminant concentration of 0.1 mg L^{-1}, the remediation goal was achieved after two years and the percentage of biodegradation after 10 years of simulation was 92%. As the initial concentration of 1,4-dioxane increased, the percentage of biodegradation approached 100%; however, for initial concentrations between 0.5 and 7.5 mg L^{-1}, the time to 1 μg L^{-1} exceeded 40 years. When the initial concentration increased to 10 mg L^{-1}, the time to reach the remediation goal abruptly decreased to 1.8 years. The larger mass of 1,4-dioxane available made it possible to sustain growth of CB1190.

Simulations with the propanotrophic culture ENV425 were performed with a constant input of propane at the same rate used in the field study, as well as an input rate that varied proportionally to the initial concentration of 1,4-dioxane. ENV425 performed better than CB1190 when the initial 1,4-dioxane concentration was less than or equal to 7.5 mg L^{-1}. ENV425 was able to degrade close to 100% of the contaminant after 10 years, except when the initial concentration of 1,4-dioxane was 100 mg L^{-1}. At an initial 1,4-

dioxane concentration of 7.5 mg L^{-1} and lower, the time to reach 1 µg L^{-1} ranged from ~1.4 to ~5.6 years, with very little effect . However, as the concentration of 1,4-dioxane increased above 7.5 mg L^{-1}. The propane addition rate only had an impact on the remediation time at initial 1,4-dioxane levels of 10 mg L^{-1} and above, when a constant rate became insufficient to sustain a high enough rate of cometabolism.

ENV425 outperformed the CB1190 for low concentrations of 1,4-dioxane because CB1190 did not have enough carbon and energy to grow as fast as the cometabolic bacteria. However, the roles were reversed for 1,4-dioxane plumes above 7.5 mg L^{-1} since more carbon and energy were available for CB1190 to grow and thus achieve high enough biodegradation rates to offset the impact of decay.

3.5.5 Effect of Biomass Injection Rate

The effect of the biomass injection rate on the performance of metabolic and cometabolic biodegradation of 1,4-dioxane was evaluated (Figure 3-9), with all other conditions unchanged from the baseline. The extent of biodegradation improved as the injection rate of CB1190 increased. Biodegradation percentages increased from 77% to 99% between the lowest and highest biomass injection rates. The impact on the time to reach 1 µg L^{-1} of 1,4-dioxane was much less gradual; the time to reach the goal was only below 40 years at the highest injection rate (8.4×10^{-5} kg COD m^{-2} s^{-1}).

There was no significant effect of the biomass injection rate on the percentage of contaminant biodegraded after 10 years (Figure 3-9) for ENV425, which remained close to 100%. In addition, the effect on the time to reach 1 µg L^{-1} was moderate, with remediation times ranging from 3.6 and 4.9 years. Cometabolic biomass growth and

performance was more strongly dependent on the amount of propane available, which was constant. The metabolic bacteria were highly affected by the biomass injection rate because of the low concentration 1,4-dioxane used in these simulations (i.e., 1 mg L^{-1}).

3.5.6 Effect of Propane Injection Rate

The effect of the propane injection rate was evaluated on the performance of ENV425. Injection rates were varied by several orders of magnitude relative to baseline conditions (Figure 3-10), from 3.54×10^{-7} to 3.54×10^{-4} kg COD m^2 s^{-1}. The percentage of 1,4-dioxane biodegradation was strongly affected only when the propane injection rate decreased below 1.77×10^{-5} kg COD m^{-2} s^{-1}, with only 57% removal at the lowest injection rate (Figure 3-10a).

A similar effect was observed on the time to reach 1 μg L^{-1} of 1,4-dioxane. Below an injection rate of 2.48×10^{-5} kg COD m^{-2} s^{-1}, the remediation goal was not achieved within 40 years (Figure 3-10b). At higher propane injection rates, the time to reach 1 μg L^{-1} decreased noticeably and then levelled off at 2.2 years.

3.5.7 Effect of the Oxygen Injection Rate

The percentage of 1,4-dioxane biodegradation by CB1190 after 10 years decreased from a baseline of 95% to 57% when the oxygen injection rate decreased from 2.02×10^{-3} kg COD m^{-2} s^{-1} to 5.05×10^{-6} kg COD m^{-2} s^{-1}; no biodegradation occurred at the lowest injection rate of 2.02×10^{-6} kg COD m^{-2} s^{-1} (Figure 3-11a). ENV425 was not affected as significantly; the percentage of biodegradation was above 96% at an oxygen injection rate

of 5.05×10^{-6} kg COD m^{-2} s^{-1} and then decreased to 51% when the rate was 2.02×10^{-6} kg COD m^{-2} s^{-1}.

CB1190 did not reach the remediation goal within 40 years for any of the oxygen rates evaluated. This was expected since the target was not reached at the highest injection rate evaluated, which was also the baseline value. The effect on ENV425 was more evident; the time to reach the remediation goal decreased from above 40 years for the lowest rate down to 17.5 years for an injection rate of 5.05×10^{-6} kg COD m^{-2} s^{-1}, then levelled off as the injection rate increased to 1.01×10^{-5} kg COD m^{-2} s^{-1} and above (Figure 3-11b). The results indicate that the pilot study at VAFB was performed at an adequate oxygen injection rate.

3.6 Discussion

The discrepancies between the model prediction for 1,4-dioxane concentrations in the distant wells, 5B and 34B, with respect to the field data measurements may be attributable to heterogeneities in the aquifer that provide more open channels for propane and biomass to move towards 34B. Similarly, heterogeneities such as clay lenses amy be blocking the flow of propane towards MW-5B, thus preventing biomass growth. The model assumes that the porous medium between the injection well and the monitoring wells is homogeneous, therefore, its biodegradation prediction is an intermediate case of the observed concentrations in both distant wells.

A significant discrepancy between the model prediction and the field data was the rate at which propane decreased in the monitoring wells. The model predicted much more gradual decreases than what was observed in the field. The sudden decreases observed in

the field may be a consequence of the difficulty in measuring low concentrations of dissolved gases in situ.

Growth of the propanotrophs was strongly affected by the decay rate under the pilot study conditions. The field propane concentrations were two orders of magnitude lower than the half saturation constant measured in the laboratory, therefore, the lower the propane concentrations, the slower the biodegradation rate. Biological kinetic parameters can vary widely under in situ conditions (Chambon et al., 2013; Kovárová-Kovar and Egli, 1998) and changes in the physiological state of biomass under such conditions suggest that lower decay rates may occur when the primary growth substrate is available at low concentrations (Lobos et al., 2005; Perez-Padilla, 1996).

Another kinetic parameter that had a major impact on the rate of 1,4-dioxane biodegrations was q_{CMAX}. The need to reduce this the maximum rate of substrate utilization in the simulations, compared to the value measured in the laboratory, may be attributable to the presence of co-contaminants along with 1,4-dioxane at VAFB. Chlorinated aliphatic compounds are inhibitory to aerobic biodegradation of 1,4-dioxane, (Mahendra et al., 2013), yet their effect was omitted in the kinetic model used in this study. The reduction in q_{CMAX} incorporates this inhibitory effect, which was further revealed by the sensitivity analysis (Appendix B, Figure 6-13). The adjustment to q_{CMAX} slowed the rate of biodegradation; nevertheless, given enough time, the majority of the 1,4-dioxane mass was still degraded because there was enough biomass growth due to the continuous supply of propane. In the case of the CB1190, the equivalent parameter adjusted was q_{SMAX}. This rate affected biomass growth strongly and had a compounding effect on 1,4-dioxane

biodegradation because growth CB1190 depended only on the concentrations of 1,4-dioxane and oxygen, as opposed to the cometabolic case in which biomass growth was largely independent of 1,4-dioxane.

Biodegradation of 1,4-dioxane was slowed initially due to inhibition by propane shortly after bioaugmentation; however, once enough ENV485 had grown on the propane, biodegradation of 1,4-dioxane started. Low values of K_{iS} (i.e., less than 10%, which means higher inhibition) impacted the time it takes to achieve the remediation goal; nevertheless, the difference was moderate when compared to effects related to b and q_{CMAX}.

The effect of $D_{h,W,X}$ on the percentage of biodegradation after 10 years was only relevant for the lowest value evaluated, at which point there was not enough contact between the bacteria and 1,4-dioxane. As expected, the faster the biomass moved away from the injection well, the easier it was for biomass to catch up with the propane and oxygen and thus achieve higher growth rates. The trend for CB1190 was similar, with decreasing remediation times as dispersion of biomass increased. Since higher biomass dispersion allowed bacteria to reach the 1,4-dioxane faster, biomass growth was promoted earlier and therefore the remediation time was reduced. However, when biomass dispersion was set too high, the biomass moved past the substrate and resulted in poor performance.

It is important to note that biomass movement was approximated in this study by adjusting the dispersion coefficient in the water phase. It would be more accurate to model biomass movement as a function of the groundwater velocity, as well as the properties of the bacterial cells that impact transport, e.g., straining, settling and attachment. This would require that special attention be given to the groundwater flow conditions generated during

biosparging, and to the regional groundwater flow, as well as the type of culture injected. Transport of 1,4-dioxane degrading bacteria should be assessed in more detail in future work.

The effect of $D_{h,W,C}$ on bioremediation performance showed that there was a range of values in which biodegradation slowed down, resulting in the time to reach the remediation goal exceed 40 years. It is unclear why biodegradation improved with the fastest $D_{h,W,C}$; this may be related to early contact between biomass and the 1,4-dioxane plume as some of the 1,4-dioxane mass moved more rapidly towards the injection well. The effects of the 1,4-dioxane dispersion coefficient are strongly dependent on the shape, size and location of the contaminant plume with respect to the injection well because these determine the probability of contact between biomass and the contaminant. Similarly to $D_{h,W,X}$, dispersion of 1,4-dioxane was adjusted to match the pilot study biodegradation data. In general, movement of 1,4-dioxane will depend on groundwater mixing induced by the sparging operation. Additional research is needed for simulate remediation of larger 1,4-dioxane plumes, especially those in which there is an appreciable flow of groundwater. For example, large plumes would likely require use of multiple sparging wells to create a barrier that intercepts downgradient movement of the 1,4-dioxane.

Changes in α in the gas phase did not affect bioremediation outcomes because the amount of propane and oxygen injected in the system were in excess to the required input. Transport of these gas species was more dependent on the gas velocity and the gas distribution in the aquifer.

The simulation results indicated that the initial concentration of the 1,4-dioxane plume shifted the advantage between CB1190 and ENV425. When 1,4-dioxane was below 0.25 mg L^{-1}, the performance of CB1190 became more competitive. The biomass injected was high enough to degrade this low concentration of 1,4-dioxane, even if the cells could not benefit from any net growth. This further emphasizes the importance of the value of *b*. A higher *b* would further reduce the competitiveness of CB1190. Maintaining a constant ratio of propane to 1,4-dioxane was important for concentrations of 1,4-dioxane higher than 10 mg L^{-1}. Adding a corresponding amount of propane improved the performance of ENV425 for high concentrations of 1,4-dioxane plumes, however, cometabolic biodegradation was still outcompeted by CB1190.

The amount of ENV425 biomass injected in the pilot study was sufficient to promote biodegradation and achieve the remediation goal even if the growth substrate was limited. The performance of ENV425 depended more strongly on the amount of propane injected over time than in the inoculum size. In contrast, CB1190 was significantly dependent on the amount of biomass injected because its growth substrate, 1,4-dioxane, was fixed and at a low concentration.

The propane injection rate utilized in the field pilot study was in excess with respect to the amount needed to biodegrade 1,4-dioxane and promote biomass growth. Results also indicate that there are diminishing returns with respect to remediation times when injection rates become excessive. The temptation to use a high rate of propane injection is considerable, since the cost of the propane is modest compared to the total cost of remediation. In addition to achieving little added benefit, the risk of aquifer clogging due

to excessive propanotrophic growth is also considerable, although that was not included in the simulations.

Variations in oxygen injection rates suggest that CB1190 was affected more strongly than ENV425. ENV425 was more resilient to decreases in oxygen injection rates, however, its performance was strongly hindered at the lowest oxygen injection rate evaluated. These results are consistent with the lower oxygen half saturation constant for ENV425 versus CB1190 found in the laboratory experiments (Chapter 2), and the fact that ENV425 does not have a minimum oxygen concentration for 1,4-dioxane biodegradation. Since the propanotrophic culture has a higher affinity for oxygen, it was less impacted at lower concentrations.

One of the more important outcomes from this study was the significant variability in reaching a remediation goal of 1 $\mu g\ L^{-1}$, depending on basic considerations such at the inhibitory effect of co-contaminants, the decay rate, and the initial concentration of 1,4-dioxane. Use of bioaugmentation requires that special attention be given to the physiological state of the bacteria being injected.

Considering the potential for bioremediation times in excess of several years, a cost-benefit analysis should be performed to determine if other remediation approaches are preferable, e.g., hydraulic control of the plume combined with ex-situ treatment such as advanced oxidation. Operating a sparging system for more than several years could become costly compared to a more energy-intensive but short-term physicochemical approach.

3.7 Conclusions

A steady state air sparging flow model was successfully coupled to a contaminant transport model that included Monod kinetics for 1,4-dioxane biodegradation by metabolic and cometabolic processes. The air sparging model was able to predict the flows of gas and water by simulating relative permeabilities and gas and water saturations in response to an injection pressure. Gas flow in the aquifer achieved a steady state that reasonably predicted the gas flow at the VAFB site. Simulation results from the air sparging model were used as initial conditions for the contaminant transport model.

The coupled models were calibrated using the site's monitoring data for 1,4-dioxane. The model predicted the correct trend for propane distribution but predicted a slower rate of propane consumption than what was observed in the field trial at VAFB. The reason for a slower rate of propane consumption is not yet known but may be related to the difficulty of accurately sampling dissolved gasses. The model predicted the decrease in 1,4-dioxane concentration in the two closest monitoring wells; however, the model was less accurate for predicting 1,4-dioxane in the two monitoring wells furthest from the source zone. One of these wells showed no biodegradation while the other one started biodegradation 150 days earlier than what the model predicted. The model predicted a trend between these extremes. The different behaviors in those wells may have been a consequence of preferential flow paths created during air sparging and aquifer heterogeneities.

A sensitivity analysis of several parameters used in the model showed that the biomass decay rate had a significant impact on bioremediation outcomes with respect to

both the percentage of biodegradation after 10 years and the time to achieve an average 1,4-dioxane concentration of 1 μg L^{-1}. The effect was largest for CB1190, such that for most of the simulations a remediation goal of 1 μg L^{-1} was not achieved even after 40 years. The biomass dispersion coefficient in the water phase also had a significant impact on the performance of both cultures. With ENV425, the closer the spread of biomass to that of oxygen and propane, the shorter the remediation time. For CB1190, shorter remediation times occurred when the biomass was distributed closest to the 1,4-dioxane.

The maximum specific 1,4-dioxane biodegradation rate also had a significant effect on the time to reach 1 μg L^{-1} and a somewhat lesser impact on the percentage of 1,4-dioxane consumed. Other parameters that had a significant effect were the biomass dispersion rate in water and aquifer porosity. Dispersion coefficients in the water phase for 1,4-dioxane, oxygen and propane had a low impact on bioremediation performance, as did the dispersivities for propane and oxygen in the water phase.

The performance of CB1190 was compared to ENV425 under several scenarios. Varying the initial concentration of the 1,4-dioxane plume indicated that CB1190 outperformed ENV425 at levels greater than or equal to 10 mg L^{-1}. On the other hand, ENV425 was more effective at 1,4-dioxane concentrations below 10 mg L^{-1}. For concentrations below 0.25 mg L^{-1}, the viability of CB1190 improved, although ENV425 still required shorter remediation times.

Biomass injection rates had a strong effect on the metabolism of 1,4-dioxane in terms of the percent biodegradation achieved after 10 years. Cometabolic biodegradation

was not affected by the biomass injection rate because continuous addition of propane allowed for growth throughout the treatment zone.

Oxygen injection rates had a more significant effect on the performance of CB1190 than ENV25. However, both cultures were negatively affected by the lowest oxygen injection rate evaluated.

Cometabolic biodegradation of 1,4-dioxane was reduced when the propane injection rate was reduced several fold below the baseline level. When adequate propane was provided, remediation times improved and further increases to the propane injection rate became unnecessary. These results indicated there is an optimum rate of propane injection to achieve bioremediation of 1,4-dioxane. The simulations suggested that propane was added in excess during the VAFB pilot study.

The model developed for this study represents a novel tool for assessing the performance of metabolic and cometabolic bacteria for *in situ* bioremediation of 1,4-dioxane. The effectiveness of each bioremediation strategy depends strongly on aquifer permeability, dispersion (groundwater mixing), biomass movement, biomass decay, competitive inhibition, the initial concentration of 1,4-dioxane, and biomass, oxygen and propane injection rates. The results from this study indicate that gas sparging with air and propane coupled to bioaugmentation with a propanotrophic culture will achieve a faster rate of remediation than air sparging and bioaugmentation with a culture that metabolically biodegrades 1,4-dioxane, as long as the initial concentration of 1,4-dioxane is less than or equal to 7.5 mg L^{-1}. That is the case for the majority of 1,4-dioxane plumes that have been characterized thus far.

3.8 Tables for Chapter 3

Table 3-1 Nomenclature.

Parameter	Description
b	Biomass decay coefficient
q_{CMAX}	Maximum specific 1,4-dioxane biodegradation rate
$D_{h,W,S}$	Propane dispersion coefficient in water
$D_{h,W,C}$	1,4-Dioxane dispersion coefficient in water
$D_{h,W,O}$	Oxygen dispersion coefficient in water
$D_{h,W,X}$	Biomass dispersion coefficient in water
α_S	Propane dispersivity constant in gas
α_O	Oxygen dispersivity constant in gas
k	Intrinsic permeability
ε	Aquifer porosity
P_{EC}	Gas entry pressure
λ	Brooks and Corey lambda
$P_{sparge1}$	Gas sparge pressure
$P_{sparge2}$	Gas sparge pressure
C_n	Gas leak coefficient
$K_{GW,S}$	Propane overall mass transfer coefficient
$K_{GW,O}$	Oxygen overall mass transfer coefficient

Table 3-2 Kinetic parameters used for simulations of biodegradation of 1,4-dioxane in Comsol.*

Parameter	Units	ENV425	CB1190
K_S	kg COD m^{-3}	2.52×10^{-2}	1.15×10^{-2}
μ_{MAX}	s^{-1}	7.48×10^{-6}	3.61×10^{-6}
q_{SMAX}	kg COD kg COD^{-1} s^{-1}	1.33×10^{-5}	1.00×10^{-5}
Y	kg COD kg COD^{-1}	0.56	0.35
K_C	kg COD m^{-3}	6.05×10^{-3}	-
q_{CMAX}	kg COD kg COD^{-1} s^{-1}	4.24×10^{-6}	-
b	s^{-1}	5.49×10^{-7}	2.59×10^{-7}
K_{SO}	kg COD m^{-3}	1.17×10^{-3}	1.52×10^{-3}
q_{SOMAX}	kg COD kg COD^{-1} s^{-1}	1.87×10^{-7}	3.37×10^{-7}
O_{SMIN}	kg m^{-3}	0	3.56×10^{-4}
T_C	kg COD kg COD^{-1}	1.46	-
K_{iS}	kg COD m^{-3}	4.60×10^{-4}	-
K_{iC}	kg COD m^{-3}	1.80×10^{6}	-
K_{CO}	kg m^{-3}	3.66×10^{-4}	-
q_{COMAX}	kg COD kg COD^{-1} s^{-1}	2.58×10^{-7}	-
O_{CMIN}	kg m^{-3}	2.24E-04	-

* Parameters were adjusted from the laboratory value (23 ºC) to the aquifer temperature (15 ºC) by a conversion factor, *CF*, where $CF=\theta^{(T1-T2)}$ and $\theta=1.09$ (Grady et al., 2011).

Table 3-3 Model boundary conditions.

Variable	Units	Value	Condition
$P_{g\_sparge1}$	Pa	7,000	0 < t < 29 d
$P_{g\_sparge2}$	Pa	14,000	t > 29 d
$P_{g\_initial}$	Pa	45,000	t > 0 d
P_g	Pa	45,000	R = 30 m
P_w	Pa	45,000	R = 30 m
N_{S_gas1}	kg COD m^{-2} s^{-1}	1.01×10^{-5}	29 < t <37 d
N_{S_gas2}	kg COD m^{-2} s^{-1}	8.09×10^{-5}	t > 37 d
N_{O_gas1}	kg COD m^{-2} s^{-1}	5.34×10^{-3}	0 < t < 37 d
N_{O_gas2}	kg COD m^{-2} s^{-1}	2.56×10^{-2}	t > 37 d
N_{X_water}	kg COD m^{-2} s^{-1}	1.68×10^{-5}	41 < t < 42 d

Table 3-4 Parameters for model calibration.

Parameter	Units	Value
b*	s^{-1}	5.46×10^{-8}
q_{CMAX}*	kg COD kg COD^{-1} s^{-1}	5.02×10^{-6}
$D_{h,W,S}$*	m^2 s^{-1}	1.00×10^{-6}
$D_{h,W,C}$*	m^2 s^{-1}	1.00×10^{-8}
$D_{h,W,O}$*	m^2 s^{-1}	1.00×10^{-6}
$D_{h,W,X}$*	m^2 s^{-1}	5.00×10^{-8}
α*	m	3
k	m^2	2.30×10^{-13}
ε	-	0.3
P_{EC}	Pa	300
λ	-	2
C_n*	s m^{-2}	5.00×10^{-8}
$K_{GW,S}$	s^{-1}	3.29×10^{-4}
$K_{GW,O}$	s^{-1}	1.3×10^{-2}

*These parameters were varied and adjusted to achieve the calibration.

Table 3-5 Sensitivity analysis showing the impact of model parameters on the biodegradation percentage and remediation time for ENV425 and CB1190.

		ENV425		CB1190		
Parameter	**Units**	**Impact on biodegradation percentage***	**Impact on remediation time***	**Impact on biodegradation percentage**	**Impact on remediation time**	**Range varied**
b	s^{-1}	Significant	Significant	Significant	-	$0 – 5.5\times10^{-7}$
q_{CMAX}	kg COD kg COD^{-1} s^{-1}	Low	Significant	Moderate	-	2.1×10^{-7} - 2.1×10^{-6}
$D_{h,W,S}$	m^2 s^{-1}	Low	Low	NR	NR	1×10^{-9} - 1×10^{-5}
$D_{h,W,C}$	m^2 s^{-1}	Low	Significant	Moderate	-	1×10^{-9} - 1×10^{-6}
$D_{h,W,O}$	m^2 s^{-1}	Low	Low	Low	-	1×10^{-7} -1×10^{-4}
$D_{h,W,X}$	m^2 s^{-1}	Significant	Significant	Significant	Significant	1×10^{-9} -1×10^{-5}
α_S	m	Low	Moderate	NR	NR	0.05 - 10
α_O	m	Low	Low	Low	Low	.05 - 10
k	m^2	Significant	Significant	Low	-	5×10^{-14} - 5×10^{-12}
K_{iS}	kg COD m^{-3}	Low	Moderate	NR	NR	4.6×10^{-6} - 4.6×10^{-1}
ε	-	Low	Significant	Moderate	-	0.1 - 0.5

* A significant impact corresponds to a change in the time to reach the remediation goal and/or the percentage of 1,4-dioxane degraded by more than 30% relative to the baseline case. A moderate impact corresponds to change between 5 and 30% relative to the baseline case. A low impact corresponds to a change less than 5% relative to the baseline case. A dash indicates a change to the parameter had no impact on the outcome. NR (not relevant) indicates the parameter pertains to the propanotrophic culture and not CB1190.

3.9 Figures for Chapter 3

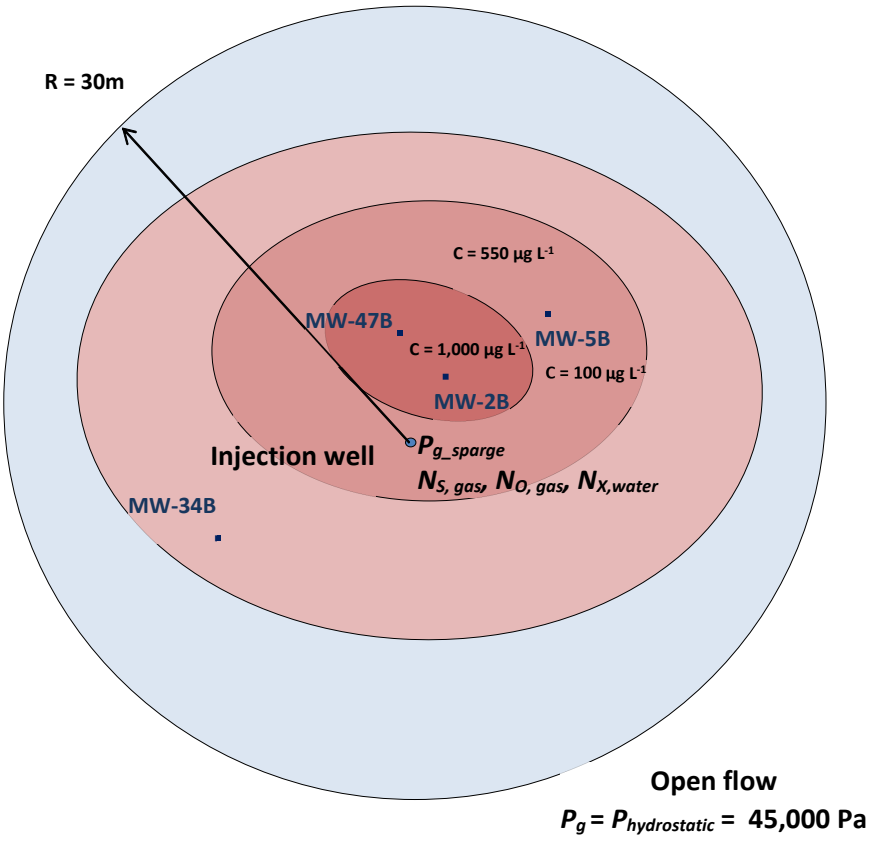

Figure 3-1 Plan view of the geometry of the conceptual model for a plume of 1,4-dioxane in groundwater at the VAFB site, showing the location of the injection and monitoring wells. Values for P_g, P_{g_sparge}, $N_{S,gas}$, $N_{O,gas}$, and $N_{x,water}$ are shown in Table 3-3.

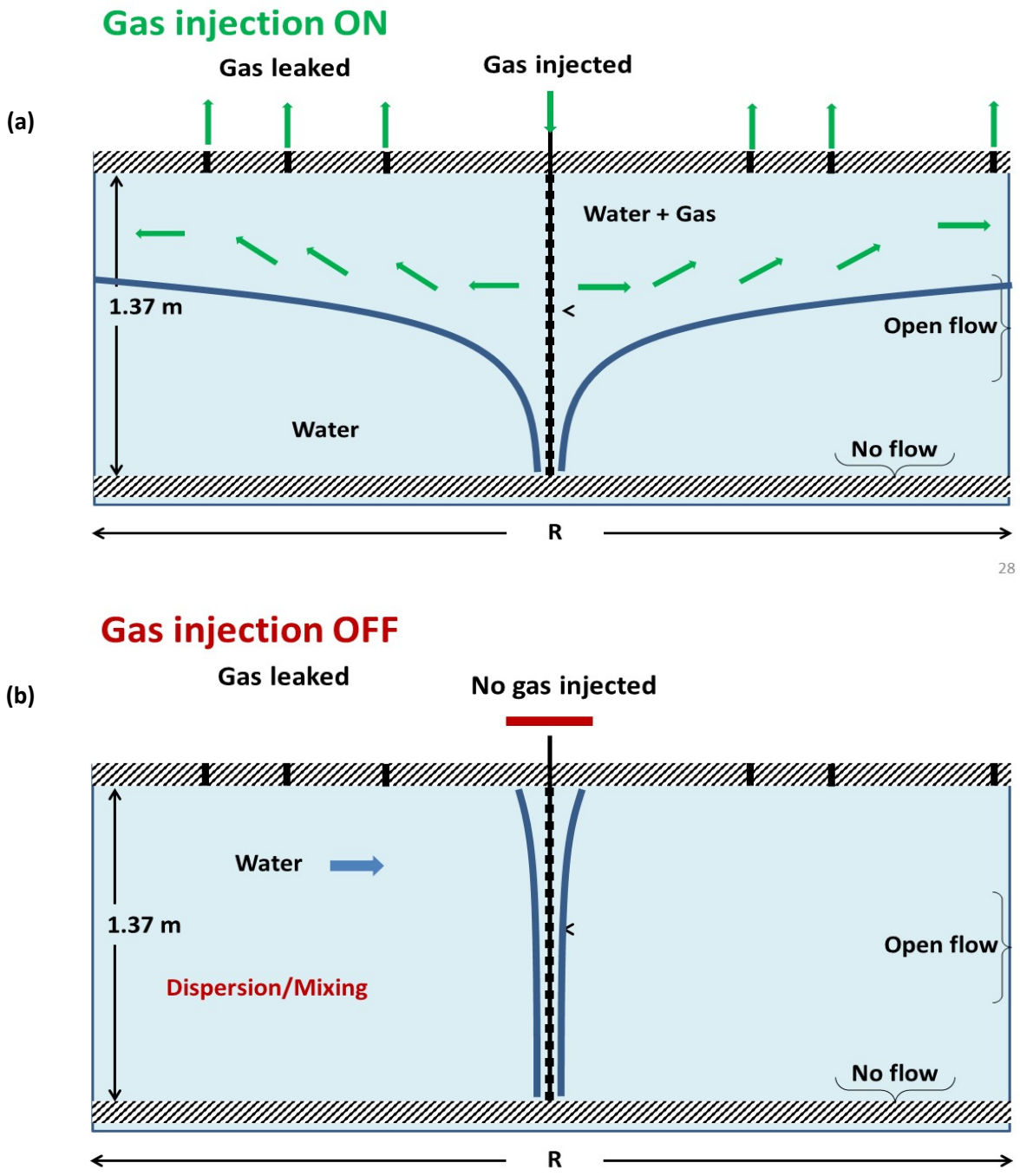

Figure 3-2 Cross sectional describing the pilot study air sparging process in a confined aquifer. Gas leaks through fractures in the confining layer. The expansion and collapse of the gas plume generates water mixing.

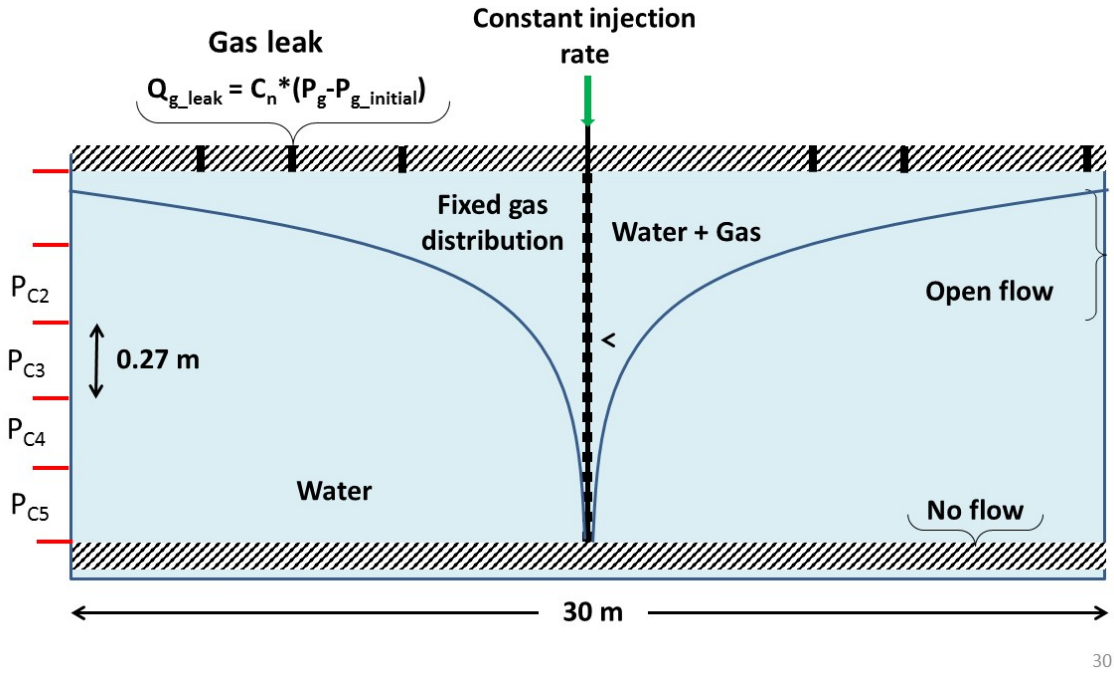

Figure 3-3 Cross sectional schematic view of the assumptions used in the conceptual model. The gas distribution is fixed because air flow is at steady state.

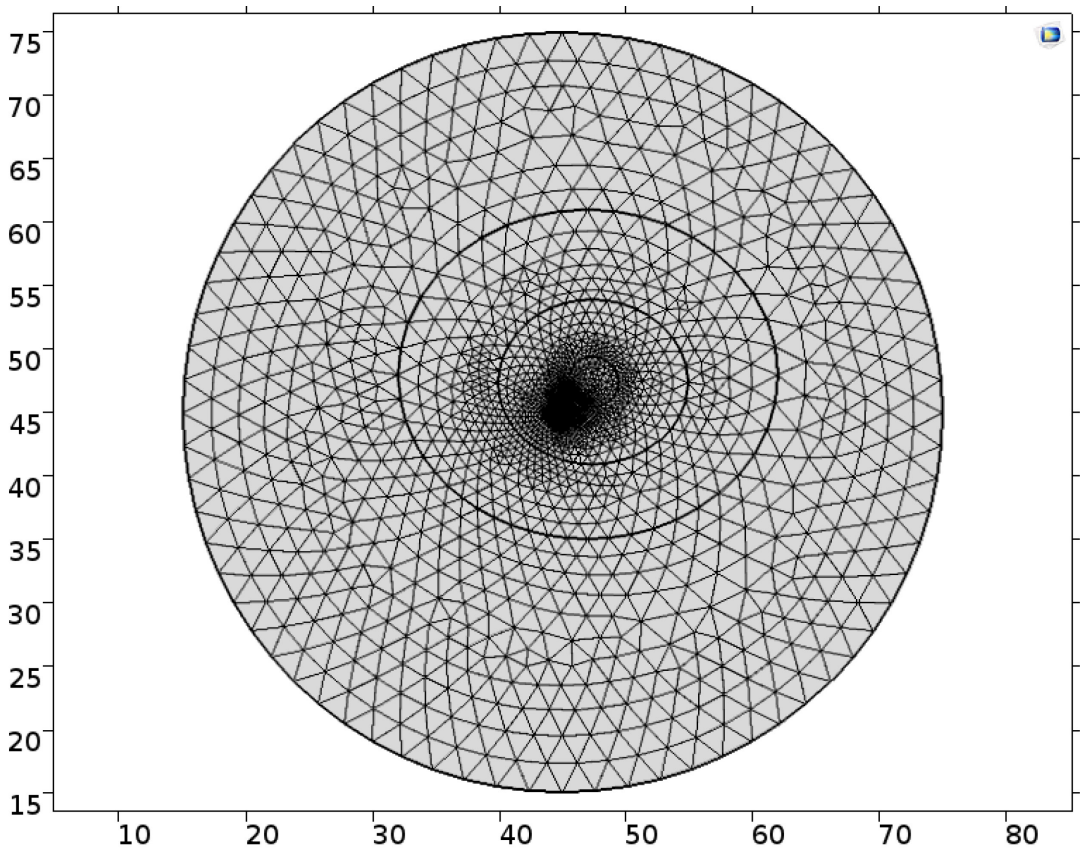

Figure 3-4. Meshing of the geometry domain used in the model simulations. The grid elements were refined near the injection well. Axis units are in meters.

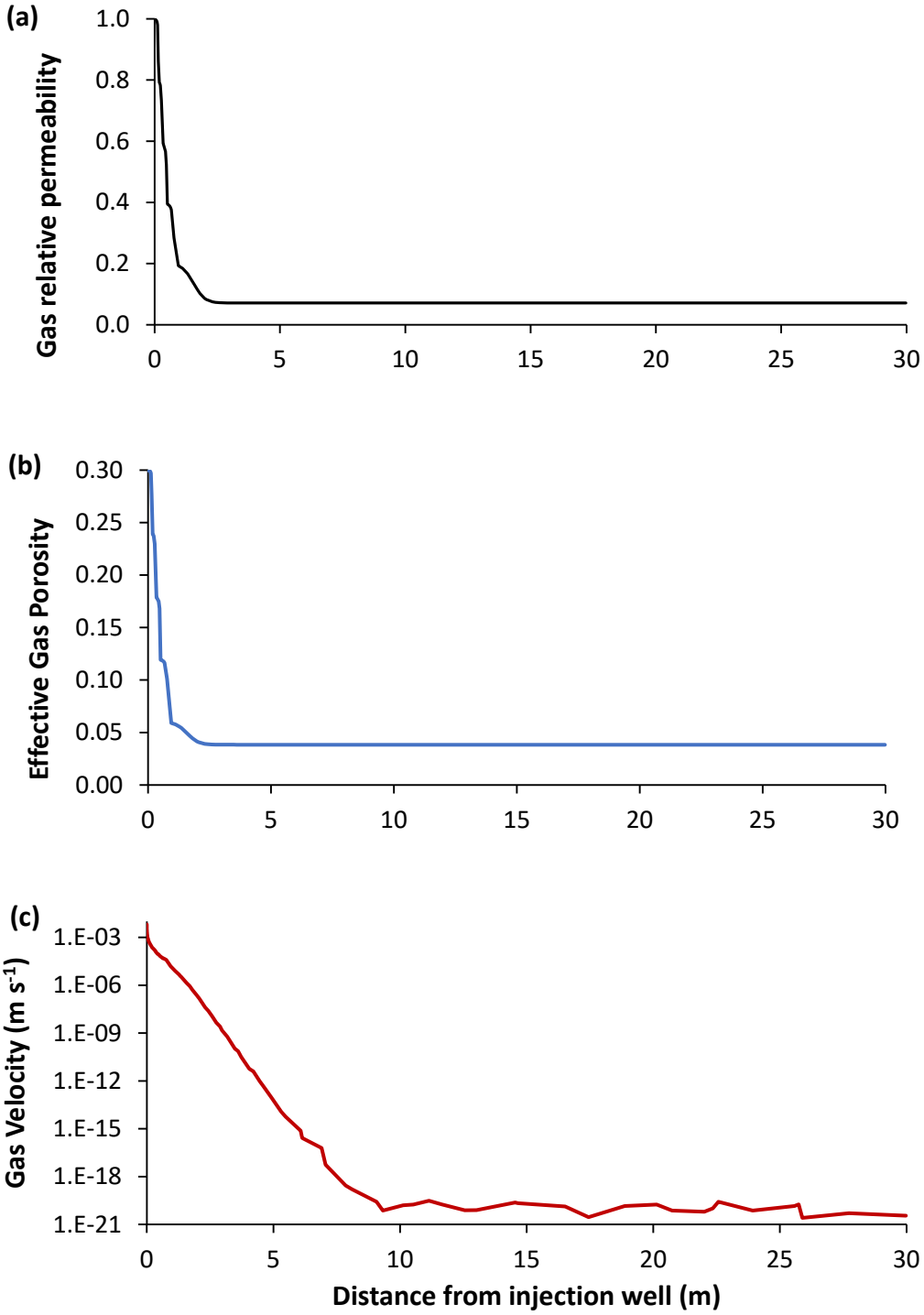

Figure 3-5 Relative permeability (a), effective gas porosity (b) and gas velocity (c) of the gas phase for a steady-state gas flow simulation.

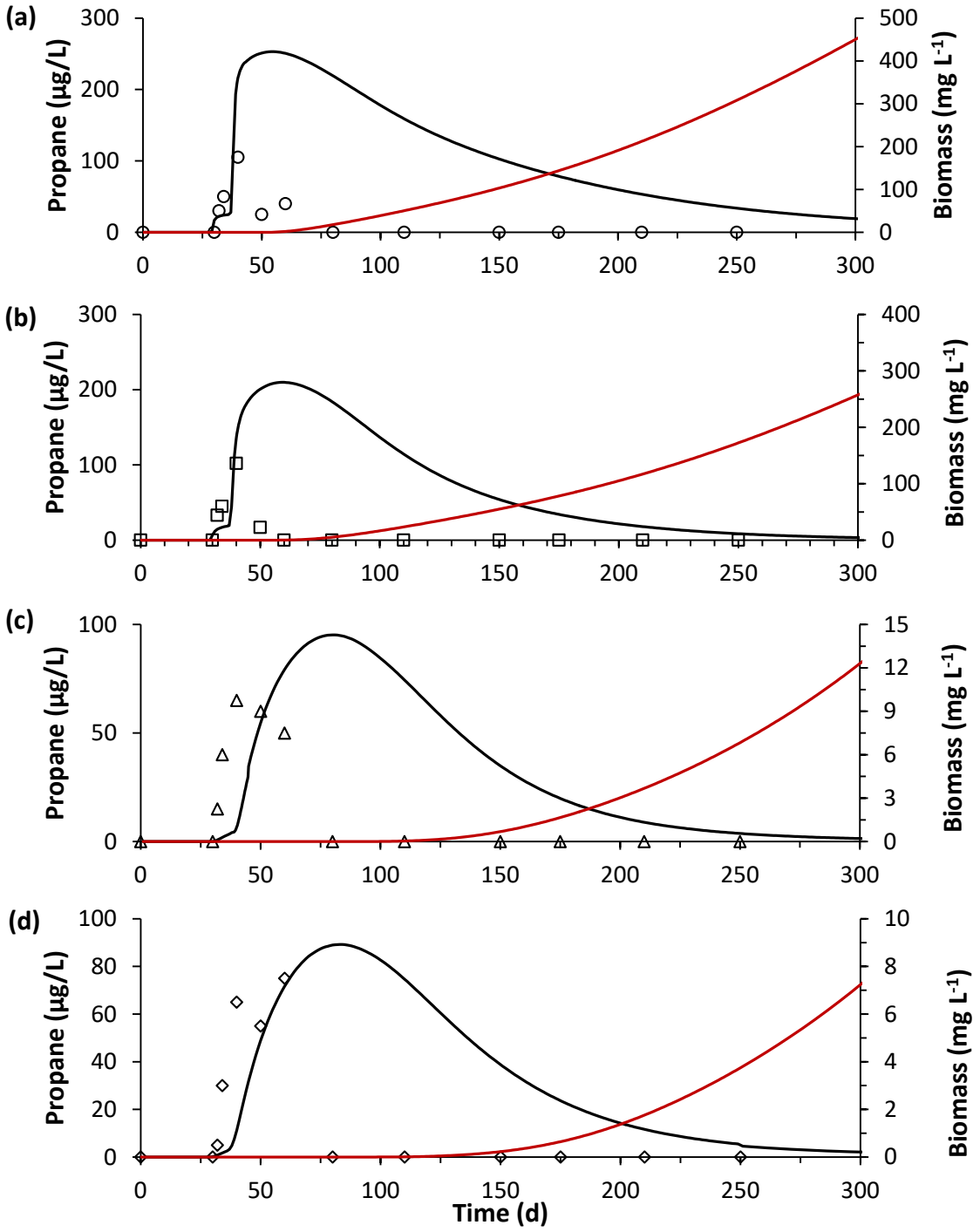

Figure 3-6 Propane (black) and biomass (red) predicted and measured concentrations in monitoring wells 47B (a), 2B (b), 34B (c) and 5B (d). Solid lines represent simulated values for propane and biomass whereas symbols indicate field measured concentrations of propane.

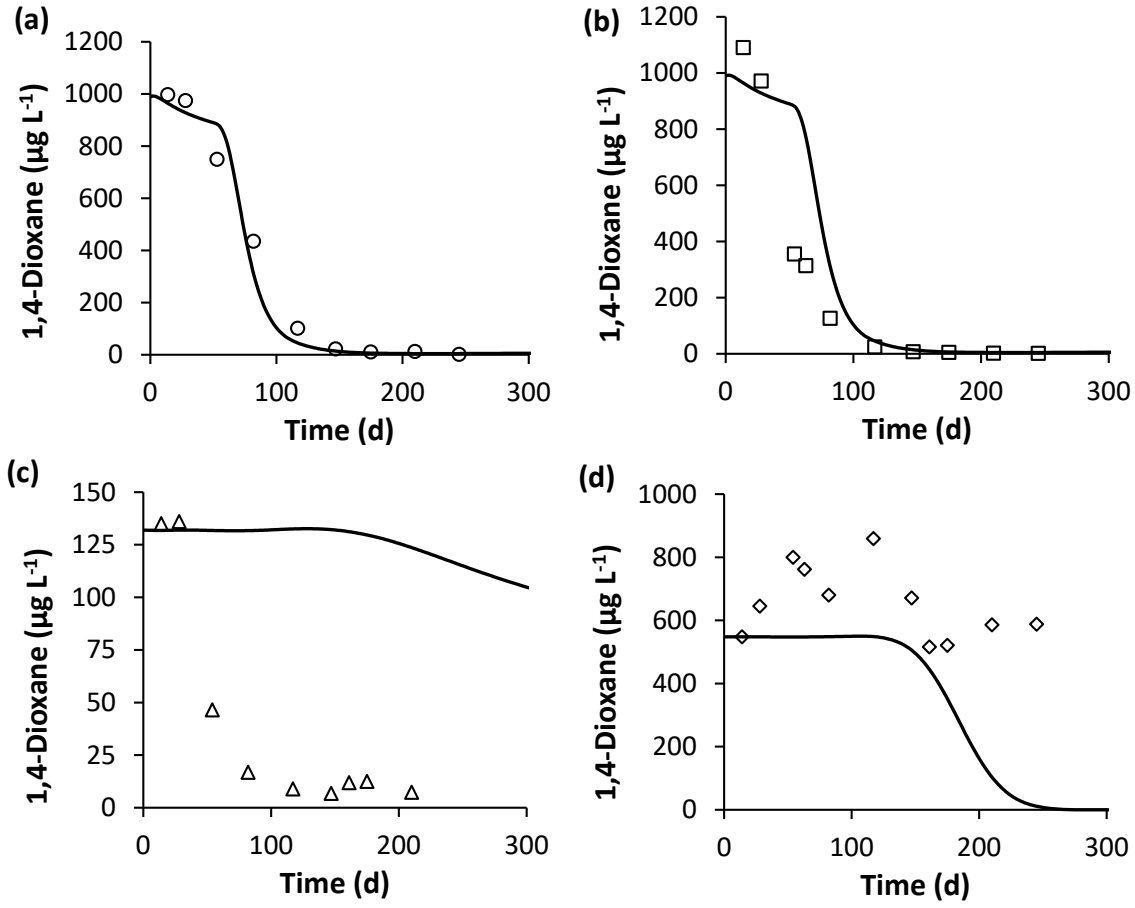

Figure 3-7 Model calibration fitting of 1,4-dioxane field data for monitoring wells 47B (a), 2B (b), 34B (c) and 5B (d). Solid lines represent simulated values whereas symbols indicate field measured concentrations of 1,4-dioxane.

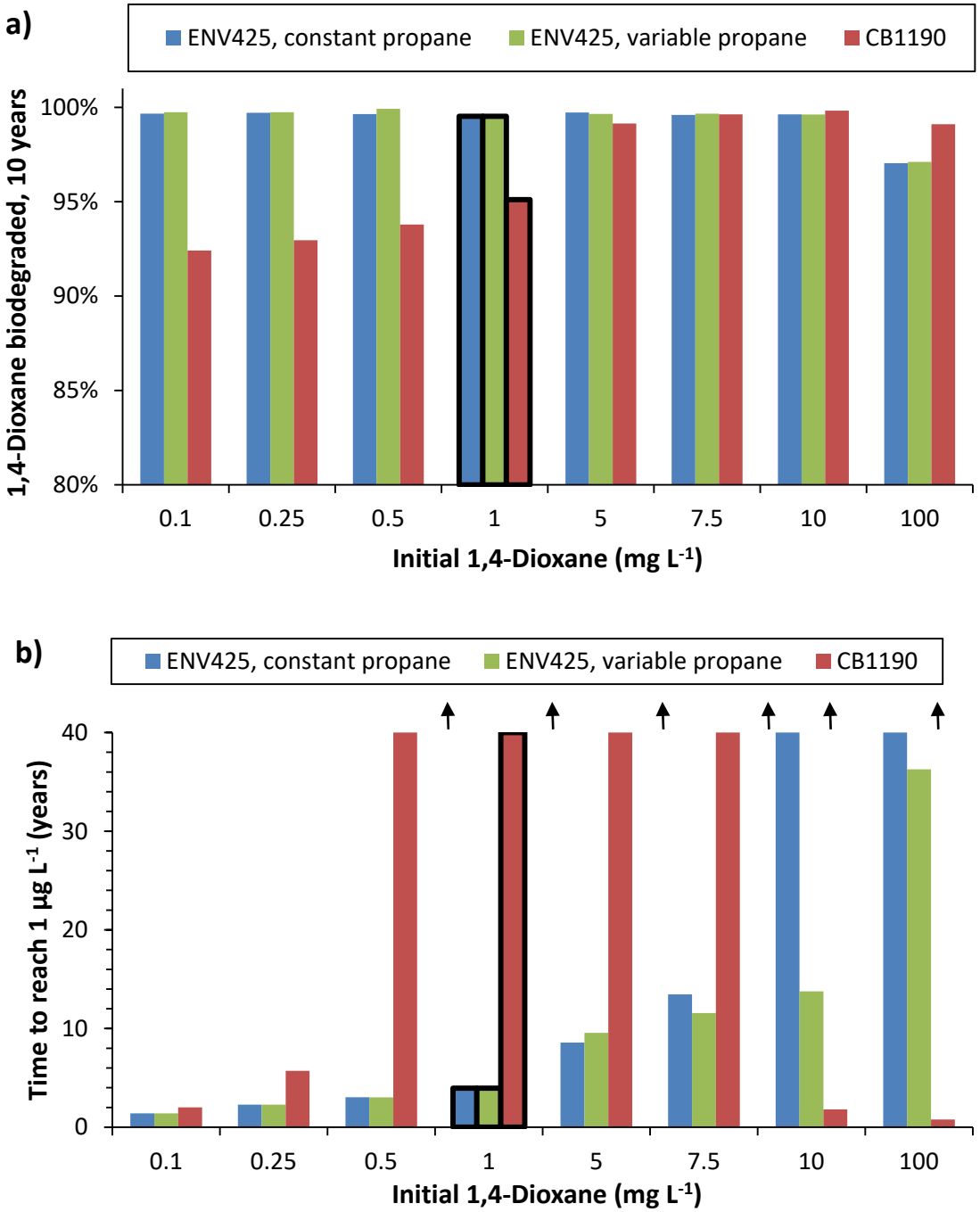

Figure 3-8 Influence of the initial 1,4-dioxane concentration at the source plume on: a) the biodegradation percentage after 10 years; and b) the time to reach an average concentration of 1 µg L^{-1} for metabolic and cometabolic bacteria with constant and variable propane input. Bars with bold outlines represent the base case results. Arrows indicate that the time to reach 1 µg L^{-1} was longer than 40 years.

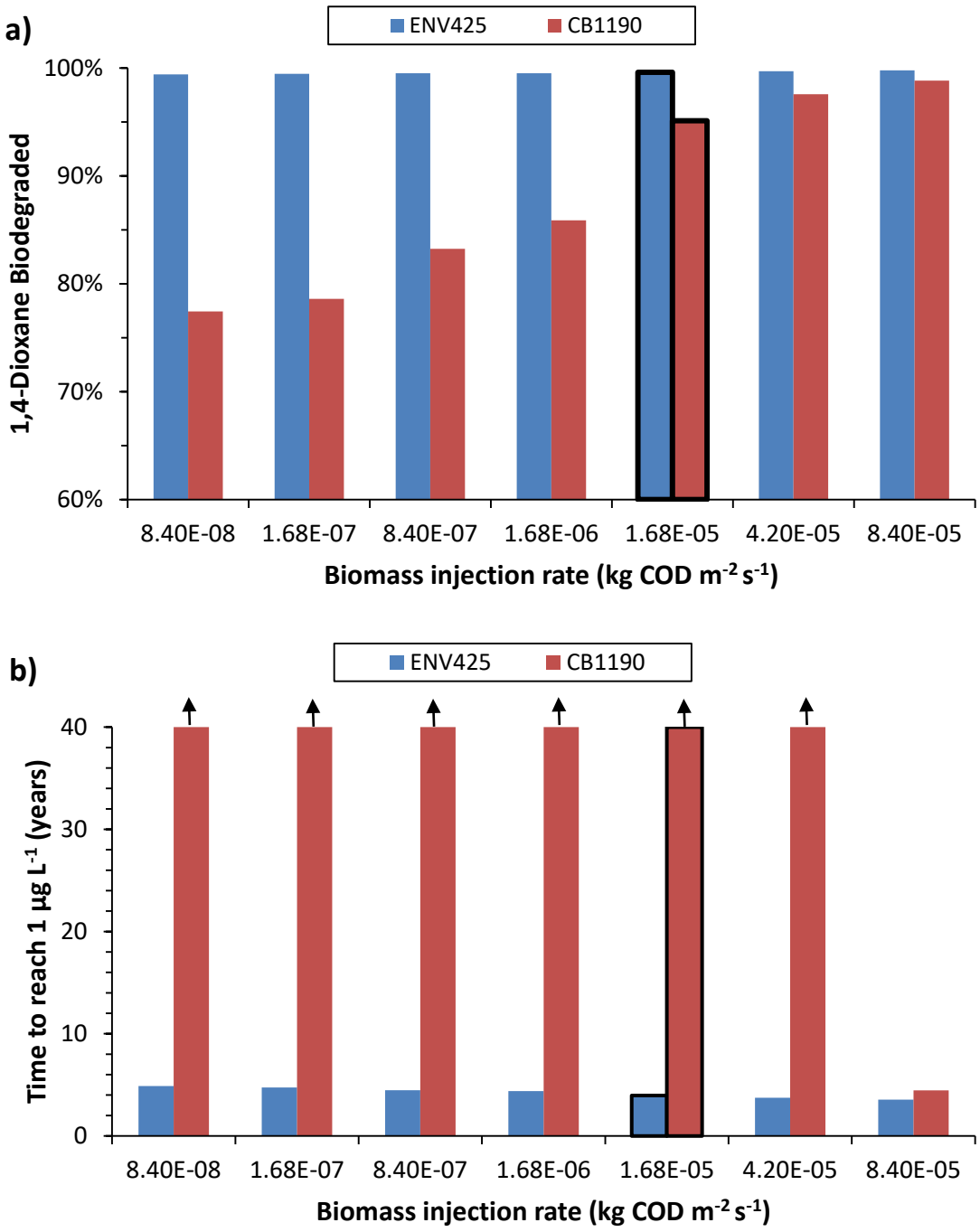

Figure 3-9 Influence of the biomass input rate on: a) the biodegradation percentage after 10 years; and b) the time to reach an average concentration of 1 µg L^{-1} for metabolic and cometabolic bacteria. Bars with bold outlines represent the base case results. Arrows indicate that the time to reach 1 µg L^{-1} was longer than 40 years.

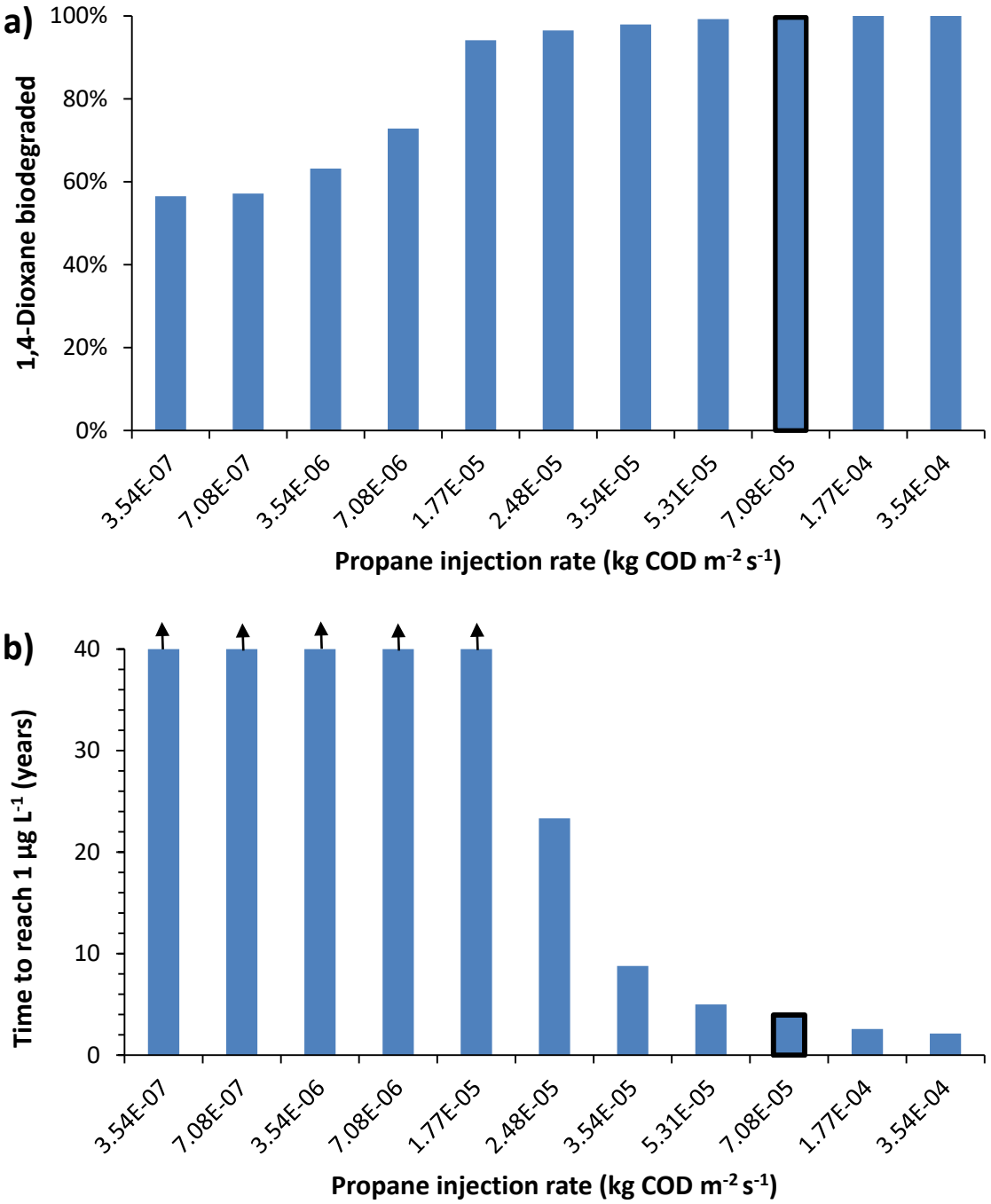

Figure 3-10 Influence of the propane input rate on: a) the biodegradation percentage after 10 years; and b) the time to reach an average concentration of 1 µg L^{-1} for cometabolic bacteria. Bars with bold outlines represent the base case results. Arrows indicate that the time to reach 1 µg L^{-1} was longer than 40 years.

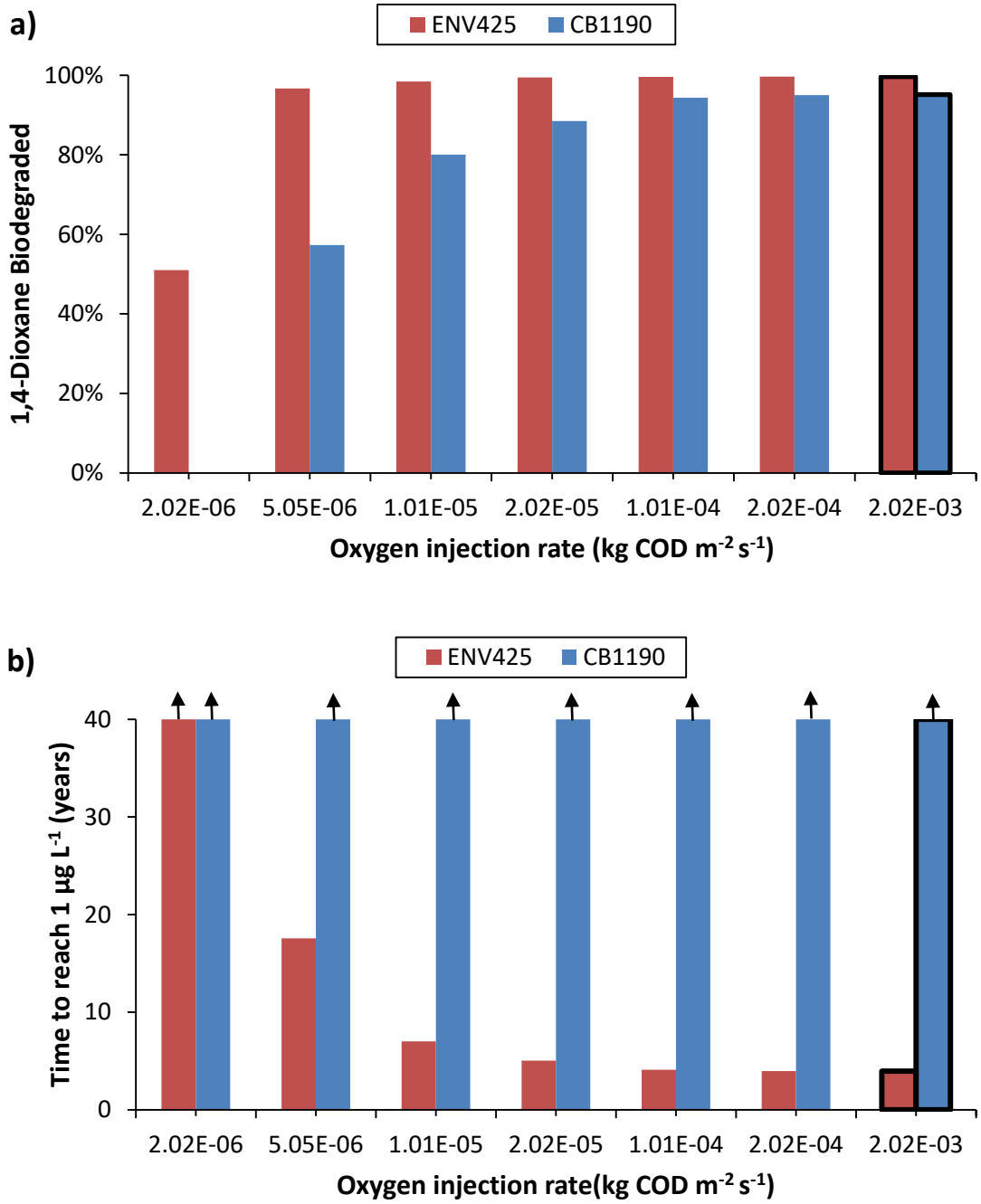

Figure 3-11 Influence of the oxygen input rate on: a) the biodegradation percentage after 10 years; and b) the time to reach an average concentration of 1 µg L^{-1} for metabolic and cometabolic bacteria. Bars with bold outlines represent the base case results.

4. LABORATORY EVALUATION OF BIODEGRADATION OF 1,4-DIOXANE UNDER ANAEROBIC CONDITIONS

4.1 Abstract

A laboratory study to evaluate the potential for anaerobic biodegradation of 1,4-dioxane was performed by constructing microcosms with groundwater and soil from two former industrial sites, referred to as Sites 1 and 2. The sites have been impacted with co-contaminants such as chlorinated solvents, freons, acetone and isopropyl alcohol. Field observations indicate that anaerobic conditions prevail within the plume, based on low dissolved oxygen and negative oxidation reduction potential levels.

Two types of microcosms were prepared (small and large) and amended with uniformly labeled ^{14}C-1,4-dioxane and different electron acceptors, including sulfate, Fe(III) oxide, Fe(III)-EDTA and anthraquinone disulfonic acid (AQDS). Biodegradation of acetone and isopropyl alcohol occurred in the Site 1 small microcosms. Small microcosms from Site 2 did not show any activity due to inhibitory levels of dichloromethane (DCM). No consistent or significant biodegradation of 1,4-dioxane was observed in live anaerobic microcosms after up to 4 years of incubation in comparison to autoclaved or water controls.

4.2 Introduction

Not long ago, 1,4-dioxane was considered to be a biologically recalcitrant compound. However, recent studies have shown that this contaminant can be degraded by several types of microorganisms. Biodegradation represents an important alternative to

other remediation approaches, such as physical and chemical processes that rely on the use of strong oxidants and high inputs of energy. In addition, by using a biological approach, contaminated sites can be treated *in situ*. However, in the groundwater present at most of the contaminated sites impacted with 1,4-dioxane, along with other contaminants such as chlorinated solvents, reducing conditions and the absence of oxygen prevail. Given the difficulty of delivering oxygen to an anaerobic aquifer, anaerobic biodegradation of 1,4-dioxane becomes an important issue to investigate.

Numerous studies have reported aerobic biodegradation of 1,4-dioxane (Li et al., 2010; Mahendra and Alvarez-Cohen, 2006; Parales et al., 1994; Sales et al., 2013; Zenker et al., 2002). For example, complete mineralization of 1,4-dioxane has been reported by Mahendra et al. (2007). Nevertheless, there is scarce evidence that 1,4-dioxane can be biodegraded anaerobically. Only one laboratory study describes anaerobic biodegradation, under iron-reducing conditions with inoculum from a wastewater treatment plant (Shen et al., 2008). After 40 days of incubation, 25% degradation was observed in the unamended treatment. In treatments amended with Fe(III) oxide and Fe(III) oxide + humic acids, the percentage of biodegradation increased to 37% and 62%, respectively. Chelation of iron with EDTA resulted in 62% biodegradation, whereas the treatment amended with Fe(III)-EDTA + humic acids reached 90% biodegradation. Dissolved Fe(II) increased along with the decrease in 1,4-dioxane. The levels of Fe(II) were lower in the treatments amended with Fe(III) oxide because of the limited availability of the iron, as opposed to chelated iron which is readily bioavailable; this is consistent with the limited biodegradation of 1,4-dioxane in the Fe(III) oxide amended treatments. The presence of humic acids enhanced

biodegradation and iron reduction when the Fe(III) chelating agent was present; humic acids can facilitate the transfer of electrons to Fe(III). The principal product observed from biodegradation of 1,4-dioxane was CO_2, based on measurements of HCO_3^- and CO_3^{2-} in the aqueous phase and CO_2 gas in the headspace (using thermal conductivity analysis of headspace samples). It was found that 59% of 1,4-dioxane was mineralized. However, since [^{14}C]1,4-dioxane was not used, it was not possible to confirm that the measured CO_2 came exclusively from 1,4-dioxane. Furthermore, no information was provided regarding the microbial community responsible for biodegradation of 1,4-dioxane, other than the fact that consumption occurred under iron-reducing conditions. Although Shen et al. (2008) provide preliminary evidence to suggest that 1,4-dioxane is biodegradable under anaerobic conditions, more lines of evidence and additional research are needed to better understand the process. The purpose of the present study was to evaluate the potential for anaerobic biodegradation of 1,4-dioxane under anaerobic conditions in the laboratory by constructing microcosms with soil and groundwater from two industrial sites impacted with 1,4-dioxane and other co-contaminants. In addition, radiolabeled [^{14}C]1,4-dioxane was used to confirm transformation and evaluate potential biodegradation products.

4.3 Site Observations of 1,4-Dioxane Degradation under Anaerobic Conditions

The motivation to evaluate anaerobic biodegradation of 1,4-dioxane as part of this dissertation is based on observations made at two contaminated industrial sites that suggest the occurrence of anaerobic biodegradation of 1,4-dioxane. Groundwater from the sites (Site 1 and Site 2) is contaminated with several halogenated volatile organic compounds

(VOCs) and non-halogenated compounds, including 1,4-dioxane. Figure 4-1 shows the concentration contours for 1,4-dioxane and 1,1-DCE for Site 2. Note that the 1,1-DCE plume is larger than the 1,4-dioxane plume. This is the opposite of what is expected. Since 1,4-dioxane adsorbs to a considerably lower extent than 1,1-DCE, it was anticipated that the 1,4-dioxane plume would be larger. This assumes that 1,4-dioxane was released at the same time as 1,1,1-TCA, which undergoes dehydrochlorination, an abiotic process resulting in 1,1-DCE. This is a reasonable expectation, since 1,4-dioxane was added to 1,1,1-TCA to reduce its reactivity with in metal storage containers. Concentrations of 1,4-dioxane in the source area are approximately 18.0 mg L^{-1} at Site 1 and 13.5 mg L^{-1} at Site 2. Acetone and isopropyl alcohol (IPA) are present at much high concentrations, with combined levels of 1,970 mg L^{-1} at Site 1 and 12,500 mg L^{-1} at Site 2. The concentration of acetone and IPA decreases significantly down gradient in a short distance. A comparison to the decrease in halogenated VOCs (i.e., freons at Site 1 and 1,1-DCE at Site 2) suggests that the decrease in 1,4-dioxane and other non-chlorinated compounds is due to biodegradation rather than simple dilution. In addition to 1,1-DCE, other related VOCs include 1,1-dichloroethane (1,1-DCA) and chloroethane (from reductive dechlorination of 1,1,1-trichloroethane), and TCE, *cis*-1,2-DCE, and VC. Most notably, Site 2 is also contaminated with high concentrations of DCM (~6,000 mg L^{-1}).

Acetone and IPA are readily biodegradable under aerobic conditions (Kilroy and Gray, 1992). Due to the high concentrations of acetone and IPA in the groundwater, any oxygen that enters the contaminated zone would be rapidly depleted, so anaerobic conditions are expected. The field oxidation-reduction potential data confirms this. Under

anaerobic conditions, acetone and IPA also undergo biodegradation, although not as quickly (Narayanan et al., 1993; Platen et al., 1990; Terzis and Diaper, 1990; Widdel, 1986). One potential pathway is partial oxidation of IPA to acetone and hydrogen (Appendix D, Figure 6-50), followed by oxidation of acetone to CO_2 plus assimilation into biomass. In the absence of inhibiting compounds or competing electron acceptors, hydrogen will be converted to methane.

Unlike acetone and IPA, 1,4-dioxane is generally considered to be refractory under anaerobic conditions (Shen et al., 2008; Steffan, 2007), consistent with the general expectation for ether-type compounds. Thus, it was notable that the field data suggest that 1,4-dioxane is undergoing biodegradation, apparently under anaerobic conditions. The high levels of IPA and acetone may be the key to this outcome; no similar sites were identified in the literature (i.e., with correspondingly high levels of IPA).

4.4 Materials and Methods

4.4.1 Microcosms Study

Using groundwater and soil samples from two contaminated sites (Site 1 and Site 2), microcosms were prepared to evaluate the hypothesized anaerobic biodegradation of 1,4-dioxane. The purpose of these microcosms was to find evidence of biodegradation and to determine if there is a specific terminal electron acceptor that is the most favorable. ^{14}C material was used to determine if biodegradation occurred. Two types of microcosms were prepared: small (160 mL serum bottles) and large (320 mL bottles); the larger bottles facilitated an increase in the frequency of sampling events.

4.4.2 Small Microcosms

Small microcosms were prepared using soil and groundwater from near the source areas at each site. The following treatments were prepared, in triplicate, for each site: unamended; addition of ferric iron; addition of chelated ferric iron; addition of anthraquinone 2,6-disulfonate (AQDS); addition of sulfate; aerobic; killed controls; and water controls.

The unamended treatment was designed to simulate *in situ* conditions. Addition of ferric iron, chelated ferric iron, AQDS (an analogue of humic acids), and sulfate was intended to determine if 1,4-dioxane biodegradation could be associated with these electron acceptors. IPA and acetone created a high oxygen demand at both sites, with a COD on the order of 4,500 and 29,000 mg L^{-1} at Sites 1 and 2, respectively.

Aerobic treatments were used to assess the potential for 1,4-dioxane biodegradation at the edges of the plume, where dissolved oxygen may be present in the groundwater. Killed controls were used to determine the extent of 1,4-dioxane loss due to abiotic processes, while water controls indicated the extent of losses solely by diffusion through the serum bottle septa.

The microcosms consisted of 160 mL serum bottles containing 20 g of sediment and 50 mL of groundwater, sealed with Teflon-lined red rubber septa and aluminum crimp caps.

Samples of the soil and groundwater were shipped on ice via an overnight carrier, within 24 hours of taking the samples. The cores samples from each site were cut open and the soil was discharged into a sterile plastic container; the composited samples were then

thoroughly mixed with a trowel, and the soil was transferred to an anaerobic chamber, where the soil underwent additional mixing. The groundwater and soil samples were handled aseptically, to ensure that any microbial activity observed in the microcosms was a result of organisms derived from the samples and not contaminants introduced during microcosm preparation. The groundwater was evaluated for 1,4-dioxane just prior to setting up the microcosms.

The 1,4-dioxane concentrations (12.6 mg L^{-1} for Site 1 and 10.7 mg L^{-1} for Site 2) were considered to be sufficiently high so that none was added to the live microcosms. Likewise, VOCs were sufficiently high such that none was added to the live microcosms. Autoclaving lowered the initial concentration of the contaminants for both sites. Consequently, 1,4-dioxane and VOCs were added to one set of autoclaved controls (Set A), in the amounts shown in Table 4-1. Similar amounts were added to the water controls (Table 4-1). As the results will show, the concentration of 1,4-dioxane and several of the other contaminants in the Set A autoclaved controls varied more than what was expected, perhaps due to a longer than anticipated time needed to reach equilibrium among the groundwater, soil and headspace. Consequently, a second set of autoclaved controls (Set B) was prepared (55 days later) without addition of any compounds and the levels remained more consistent over time.

All of the anaerobic microcosms were prepared in an anaerobic chamber. A small amount of hydrogen was introduced from the anaerobic chamber atmosphere (~1-5% hydrogen, the balance being nitrogen). This amount of hydrogen consumed no more than 13% of the electron acceptor added. When not being sampled, the bottles were stored in

the anaerobic chamber at room temperature (22-24°C) to minimize any opportunity for introducing oxygen via diffusion through the septa.

Two types of aerobic treatments (amended with oxygen) were prepared: Oxygen Set A was prepared in the same manner described above (i.e., under anaerobic conditions) and then pure oxygen (5.0 mL per bottle) was injected (Pressure Lok® Series A syringe) whereas Set B was prepared on the bench top rather than in the anaerobic chamber, so that the initial headspace consisted of room air. With both sets, the amount of oxygen present was monitored by headspace analysis; when the level in the headspace decreased below 5%, 5.0 mL of pure oxygen was injected.

Killed controls were prepared by autoclaving the microcosms for one hour on three consecutive days. After the third autoclaving, glutaraldehyde was added (14 g L^{-1}) to further reduce the potential for biotic activity (Rothermich et al., 2002). Water controls were prepared with autoclaved distilled deionized water and sufficient amounts of the neat contaminants to yield initial concentrations that were similar to the microcosms. In addition, glass beads were added, in order to displace the same volume of water that was displaced by 20 g of soil (~10 mL).

As the results for Site 2 will show, there was no indication of biodegradation of any of the compounds over the first two months of monitoring. In contrast, aerobic and anaerobic biodegradation of several compounds was evident in a number of the Site 1 microcosms. One hypothesis for the lack of biotic activity in the Site 2 microcosms was the high initial concentration of DCM in the groundwater (~6,000 mg L^{-1}). To evaluate this possibility, a second set of unamended microcosms (Unamended Set B) and a third set

of aerobic microcosms (Oxygen Set C) were prepared for Site 2. The new microcosms were assembled in the same manner described above. Next, the microcosms were sparged with nitrogen gas (99.998% purity) for 45-60 min per bottle; this significantly lowered the concentration of VOCs. Most notably, DCM was decreased to ~4.0 mg L^{-1}in unamended Set B treatment and ~9.7 mg L^{-1} in the Oxygen Set C treatment.

Resazurin was added to the groundwater in all microcosms (1 mg L^{-1}) for the purpose of monitoring the oxidation state of the bottles over time. A pink or blue color indicates if the E_h of the water is above -110 mV; a clear color indicates the E_h is below -110 mV.

All microcosms received approximately 1 μCi of uniformly labeled [^{14}C]1,4-dioxane (Moravek Biochemicals) dissolved in acetone. Addition of 1 μCi of [^{14}C]1,4-dioxane was accomplished by adding 5 μL of the stock solution, which increased the acetone concentration in the groundwater by ~75 mg L^{-1}. This was considered to be an acceptable increase given the high background levels present in the groundwater (i.e., 720-840 mg L^{-1} for Site 2 and 990-1,180 mg L^{-1} for Site 1).

4.4.3 Large Microcosms

A second set of microcosms was prepared with groundwater and soil samples from Sites 1 and 2. These microcosms contained 240 mL of groundwater and 96 g of soil and were prepared in 250 mL media bottles (Wheaton) with a total volume of 320 mL. The bottles were capped with black plastic caps containing grey butyl rubber septa. The purpose of having larger amounts of groundwater in this set was to allow for more frequent sampling from the liquid phase to determine the ^{14}C product distribution. In addition, two

additional treatments were included with this set. The treatments prepared for Site 1 microcosms were unamended; synthetic groundwater unamended; Fe(III) amended; Fe(III)-EDTA amended; AQDS amended; Fe(III)+AQDS amended; autoclaved controls; and water controls.

For the Fe(III) amended microcosms, 13 mM of Fe(III) oxide was added. In the Fe(III)-EDTA amended bottles, the concentration of Fe(III)-EDTA added was 13 mM. In the AQDS amended microcosms, 6.5 mM of AQDS was added. The synthetic groundwater unamended treatment received 20 mg L^{-1} of 1,4-dioxane. The synthetic groundwater consisted of 2.33 mM of $CaCl_2 \cdot 2H_2O$, 1.97 mM of Na_2SO_4, 2.10 mM of $NaHCO_3$, 1.28 mM of $MgCl_2 \cdot 6H_2O$, 0.17 mM of KCl and 0.01 mM of $MnSO_4(H_2O)$. These microcosms were also amended with [^{14}C]1,4-dioxane.

Large microcosms were also prepared with groundwater and soil from Site 2. The treatments evaluated were unamended; Fe(III)-EDTA-A amended; Fe(III)-EDTA-B amended; autoclaved controls; and water controls.

For the Fe(III)-EDTA-A and Fe(III)-EDTA-B amended microcosms, the concentration of Fe(III)-EDTA added was 13 mM. Groundwater was sparged with nitrogen in order to remove the VOCs, including acetone and IPA. Treatment Fe(III)-EDTA-B was spiked with 100 mg L^{-1} of acetone and 100 mg L^{-1} of IPA, while treatment Fe(III)-EDTA-A did not receive any additions, except for the acetone associated to [^{14}C]1,4-dioxane. This was done in order to evaluate if the presence of acetone and IPA affected biodegradation of 1,4-dioxane in the microcosms.

4.4.5 Chemicals

The sources and purity of chemicals used were: 1,4-dioxane (99%) from Aldrich; DCM (99.95%) from Omnisolve; acetone (99.5%) from Mallinckrodt; sodium acetate (99.7) from Mallinckrodt; 1,1-DCE (99.5%) from Chem Services; IPA (99.99%) from Omnisolve; 1,1-DCA (95%) from TCI America; *cis*-1,2-DCE (99%) from TCI America; 1,1,1-TCA (>99%) from Fisher Scientific; TCE (99.5%) from Aldrich; 1,1,2-trichloro-1,2,2-trifluoroethane (Freon 113, 99.9%) from American Refrigerants; 2,2-dichloro-1,1,1-trifluoroethane (Freon 123, ARI-700 certified) from American Refrigerants; methane (99.99%) from Matheson; chloromethane (99.9%) from Praxair; chloroethane (99.7%) from Aldrich; ethane (99.99%) from Matheson; ethene (99.5%) from National Welders; VC (<1 ppm of nitrogen) from Matheson; oxygen (99.5%) from National Welders; nitrogen (99.99%) from National Welders; anthraquinone-2,6-disulfonic acid (98%) from Pfaltz and Bauer; ferric chloride (97%) from Mallinckrodt, iron EDTA disodium salt (13% iron, 67% EDTA) from J.T. Baker; and glutaraldehyde (50% w/w) from Fisher Scientific. All other chemicals used were reagent grade or equivalent in purity.

[^{14}C]1,4-dioxane was custom synthesized by Moravek Biochemicals. It was provided as a stock solution in acetone, with a specific activity of 43 mCi mmol^{-1} and a radiochemical purity of at least 97%.

4.4.6 Analytical techniques

Although not regarded as a volatile organic compound, 1,4-dioxane is sufficiently volatile to permit estimates of the aqueous phase based on headspace analysis, with a detection limit of approximately 2 mg L^{-1} (Broske et al., 2002). The Agilent Application

Bulletin that describes headspace measurement of 1,4-dioxane (up to 100 mg L^{-1}) was also developed for measuring DCM, benzene, and 1,1,1-TCA, at concentrations up to 100 mg L^{-1}, and chloroform up to 50 mg L^{-1}. Thus, the method is compatible with compounds that are also found at Sites 1 and 2, in addition to 1,4-dioxane.

Initially, 1,4-dioxane was monitored in the microcosms by gas chromatographic analysis of headspace samples (1.0 mL) on a Hewlett Packard 5890 Series II gas chromatograph, equipped with a flame ionization detector and a 60-m x 0.32-mm ZB-624 capillary column (Phenomenex). Helium was delivered at 1.75 mL min^{-1} as the carrier gas. The temperature program was 40 ºC for 5 min, then increased to 90 ºC at 6.0 ºC min^{-1} and held for 5 min, for a total run time of 18.3 min. The injector and detector temperatures were set at 180 ºC and 260 ºC, respectively. The lowest quantifiable concentration was 2 mg L^{-1} with the headspace method.

Because of the high variability in headspace measurements of 1,4-dioxane observed, a more accurate method was subsequently used. Liquid injections (via an autosampler) using the same chromatographic method described above were performed with filtered (0.2 µm) samples. The filters were preconditioned with 650 µL of sample and 350 µL of the filtrate was placed in 500 µL glass inserts in 2.0 mL GC vials. With this method the lowest quantifiable concentration was 1 mg L^{-1}.

Two methods were used to quantify the VOCs. Method 1 employed the same GC conditions described above for 1,4-dioxane and was used to measure DCM, 1,1-DCA, Freon 123, *cis*-1,2-DCE, 1,1,1-TCA and TCE. Method 2 was used to quantify 1,1-DCE, Freon 113, methane, ethane, ethane, chloromethane, VC and chloroethane. This method

consisted of injecting 0.5 mL of headspace sample onto a Hewlett Packard 5890 Series II gas chromatograph, equipped with a flame ionization detector and a 2.44-m x 3.175-mm column packed with 1% SP-1000 on 60/80 Carbopak B (Supelco). The carrier gas was nitrogen at 30 mL min^{-1}. The temperature program was set at 60 ºC for 2 min, increased at 10.0 ºC min^{-1} to 200 ºC, then isothermal for 8 min, for a total time of 24 min. The injector and detector temperatures were set at 200 ºC.

For methods with headspace sampling, the gas chromatograph response to a headspace sample was calibrated to give the total mass of compound (*M*) in that bottle. Assuming the headspace and aqueous phases were in equilibrium, the total mass present was converted to an aqueous phase concentration (Equation 4-1):

$$C_l = \frac{M}{V_l + H_C V_g} \qquad 4\text{-}1$$

Where C_l = concentration in the aqueous phase (µM); M = total mass present (µmol $bottle^{-1}$); V_l = volume of the liquid in the bottle; V_g = volume of the headspace in the bottle; and H_c = Henry's constant ((mol·m^{-3} gas concentration)(mol·m^{-3} aqueous concentration)$^{-1}$) at 23 °C (LaGrega et al., 1994). For the volatile compounds other than 1,4-dioxane, the headspace method provided detection limits of approximately 2-5 µg L^{-1}.

Oxygen concentration was monitored by injecting a headspace sample (0.5 mL) onto a gas chromatograph equipped with a thermal conductivity detector and a 3.175-mm x 3.25-m 100/120 Carbosieve SII column (Supelco). Nitrogen was used as the carrier and reference gas at a rate of 50 mL min^{-1}. Two GC programs were used for oxygen analysis. For program 1, the oven temperature was set isothermal at 105 °C and the detector was set

to low sensitivity. The injector and detector temperature was set at 200 °C. This method was used for microcosms that were prepared in the anaerobic chamber and subsequently receive 5 mL of pure oxygen. Program 2 had the same settings as Program 1 but the detector was set to high sensitivity. This method was used for aerobic microcosms that were prepared on the bench top, with a headspace of room air.

IPA, acetone, and acetate were measured using a 3000 Ultimate Dionex HPLC system and an Aminex® HPX-87H ion exclusion column (300-mm×7.8-mm; BioRad). Eluent from the column passed in series through a UV/Vis detector set at 225 nm (to detect organic acids) followed by a Dionex Refractive Index Detector (to measure IPA and acetone). The eluent (0.01 N H_2SO_4) was delivered at 0.6 mL min^{-1}. Under these conditions, 1,4-dioxane co-elutes with acetone; however, since the acetone concentration is so much higher in groundwater from Sites 1 and 2, the comparatively lower amount of 1,4-dioxane did not present a significant interference.

The total amount of ^{14}C in the bottles at time zero was quantified by counting samples of the headspace (0.5 mL) and liquid (0.1 mL) in liquid scintillation cocktail. The distribution of ^{14}C in the liquid phase was periodically evaluated using the same HPLC system described above. Liquid samples (1000 µL) were filtered (0.2 µm, Acrodisk PTFE, pre-rinsed with 3 mL of DDI water); the first 750 µL of the filtrate was discarded and the remainder was collected in an HPLC vial. Samples (100 µL) were injected on the HPLC and the eluent was collected as it emerged from the RI detector. Two levels of fractionation were used. For the first method, only two fractions were collected: one corresponding to 1,4-dioxane (22.4-25.5 min, totaling 1.86 mL) and one corresponding to all other

compounds that eluted before 1,4-dioxane (0-22.4 min, totaling 13.4 mL) named "other soluble" fraction. The entire fraction corresponding to 1,4-dioxane was added directly to liquid scintillation cocktail and counted. For the "other soluble" fraction, a 2 mL aliquot of the total volume collected (13.4 mL) was added to liquid scintillation cocktail and counted.

Whenever any of the analyses indicated ^{14}C levels in the "other soluble" fraction that were sufficiently high (i.e., >5% of the initial ^{14}C added), a more detailed level of fractionation was performed. For this second method, nine fractions were collected prior to elution of 1,4-dioxane, followed by the fraction corresponding to 1,4-dioxane and one additional fraction after 1,4-dioxane (Table 4-2). Selection of these intervals was based on the elution times of organic acids that could hypothetically be formed from 1,4-dioxane biodegradation, including acetate and formate. Elution times for these compounds were evaluated using authentic compounds. The collection times were adjusted for the lag time from the RI detector to the point where the mobile phase discharged from tubing connected to the RI (0.66 min).

The percentage of 1,4-dioxane recovered (R) from the HPLC analysis at time t was calculated as follows:

$$R = \frac{C_{DXE,t}}{C_{to}} \times 100 \qquad 4\text{-}2$$

where $C_{DXE,t}$ is the amount of ^{14}C activity in the HPLC fraction for 1,4-dioxane at time t and C_{to} is the initial measured amount of ^{14}C added to the microcosms.

The percentage of other soluble ("OS") ^{14}C-labeled compounds at time *t* was calculated as follows:

$$OS = \frac{C_{x,t}}{C_{t0}} \times 100 \qquad 4\text{-}3$$

where $C_{x,t}$ is the amount of ^{14}C activity in the HPLC fraction for compound "*x*" at time *t*.

The efficiency of the HPLC fractionation method was evaluated based on the total ^{14}C in all fractions that were collected divided by a direct count of the total ^{14}C activity in an equivalent liquid sample injected onto the HPLC.

For the microcosms sacrificed at the end of their incubation period, the total amount of ^{14}C remaining in the microcosms was quantified in the same manner as at time zero. To determine the amount of $^{14}CO_2$ formed, the pH of the liquid in the serum bottles was raised above 11.5 (by adding 0.5 mL of 8 M NaOH) in order to drive the CO_2 in the headspace into the liquid phase. Then, a sample of the liquid phase (10 mL) was transferred to a test tube that was connected to a second test tube containing 10 mL 0.5 M NaOH. Nitrogen gas was sparged into the first tube and over into the second. The pH in the first tube was lowered by injecting 0.25 mL of 6 M HCl, to facilitate stripping of CO_2, which was trapped in the second tube. The presumptive amount of $^{14}CO_2$ trapped was determined by counting the ^{14}C level in a 2 mL sample from the second test tube. The percentage of $^{14}CO_2$ formed was calculated as follows:

$$\%CO_2 = \frac{C_{trapped}}{C_{to}} \times 100 \qquad 4\text{-}4$$

where $C_{trapped}$ is the amount of $^{14}CO_2$ present in a microcosm, based on the ^{14}C present in the trapping tube (dpm per bottle).

When the presumptive percentage of $^{14}CO_2$ was statistically higher (α=0.05) than at least one of the autoclaved sets and the water controls, the identity of this fraction was confirmed based on precipitation with barium hydroxide as follows: 6 mL volume of liquid remaining in the second test tube were transferred to a 15 mL centrifuge tube, 1.05 g of $Ba(OH)_2$ were added, and the contents were vortexed for 5 min. The tube was centrifuged (22,050 × *g*; Sorvall Centrifuge) for 20 min and a 2 mL sample of the centrate was transferred to liquid scintillation cocktail and evaluated for ^{14}C. When the centrate contained less than 5% of the ^{14}C in the sample prior to adding $Ba(OH)_2$, the contents of the second test tube were considered to be $^{14}CO_2$.

Dissolved Fe(II) in the groundwater was quantified by the ferrozine assay as described by Stookey (1970). Samples were removed from the liquid phase (0.05 mL) by using a 1 mL syringe that was previously flushed with nitrogen gas. The sample was filtered (0.25 μm) before being added into an HCl solution. An aliquot (0.05 mL) from the HCl plus sample mix was taken and added to the ferrozin reactant. Samples were immediately measured for absorbance at 562 nm using a UV-VIS spectrophotometer. Standards prepared with chemically reduced iron were used for calibration.

Reduced AQDS was measured by a spectrophotometric method, as described by Kwon and Finneran (2008). Samples (2.5 mL) were taken from the microcosms and placed in test tubes with 2.5 mL anoxic distilled deionized water. The tubes were previously sparged with nitrogen gas to remove oxygen. The tubes containing the mix of water and

sample were measured for absorbance at 450 nm using a UV-VIS spectrophotometer. Standard prepared with reduced AQDS were used for calibration.

4.5 Results

4.5.1 Small Microcosms: Site 1

Based on GC analysis of headspace samples, 1,4-dioxane concentrations decreased in most of the anaerobic live treatments over the first 100 days of incubation (Figure 4-2a). In spite of some fluctuations, the decreasing trend was clearly evident in the unamended treatment and the treatments amended with Fe(III), AQDS, Fe(III)-EDTA, and sulfate. The lowest concentration of 1,4-dioxane occurred in the Fe(III) amended treatment (5.15 mg L^{-1} by day 100). After day 100, 1,4-dioxane levels no longer exhibited a consistent decreasing trend in any of the treatments. This may have been related to the poor precision of the headspace method, or to a slow rate of establishing equilibrium in the soil, groundwater and headspace. The variability in headspace measurements for 1,4-dioxane was due to its low volatility.

Average percent decreases in 1,4-dioxane are shown for each treatment in Figure 4-2b. Statistically significant decreases occurred in all of the live anaerobic treatments except for the one amended with AQDS, while significant decreases did not occur in the aerobic treatments or in the autoclaved controls. The decrease in the water controls was significant, but lower than for the unamended treatment and the Fe(III), Fe(III)-EDTA, and sulfate amended treatments. Overall, these results suggest that the net decreases observed in four of the five live anaerobic treatments could be a consequence of biodegradation;

however, due to the variability of the method, the distribution of ^{14}C material was considered to be a more accurate approach to determine if 1,4-dioxane was anaerobically biodegraded.

Liquid samples from the microcosms were evaluated for the distribution of ^{14}C on days 103, 222, and 287. For days 103 and 222, sample analysis was limited to determining the percentage of ^{14}C in the liquid phase that was not attributable to 1,4-dioxane. The percentages are based on the ^{14}C activity in the HPLC fraction other than 1,4-dioxane, compared to the total ^{14}C added at time zero. On those sampling events, the Fe(III)-EDTA treatment had a significantly higher fraction of non-dioxane ^{14}C than any of the other treatments, including the controls. The AQDS amended treatment also had a non-dioxane fraction above the controls, although the magnitude of difference was notably smaller. These differences were significant with respect to the autoclaved and water controls.

The samples collected on day 287 were subjected to a more complete analysis, by separating the non-dioxane category into 11 fractions. The sum of these fractions is shown in Figure 4-3a. The highest level of ^{14}C associated with compounds other than 1,4-dioxane (22.5%) occurred in the Fe(III)-EDTA amended treatment, followed by the AQDS amended treatment.

The fractionation results are shown in Table 4-3. For the Fe(III)-EDTA treatment, acetate constituted the majority of the ^{14}C in non-dioxane fractions, followed by formate. These identifications are based on co-elution with authentic material.

The overall percent recovery of ^{14}C ranged from 81 to 97%, based on the ^{14}C counted at the end of the incubation period divided by the ^{14}C counted at time zero (Table

4-3). Given the long incubation time for the microcosms, this was an acceptable level of recovery. Table 4-3 also reports the efficiency of the HPLC fractionation procedure, by comparing the sum of ^{14}C in all fractions to the ^{14}C injected onto the HPLC; these ranged from 85 to 103%, indicating that the HPLC column retained little to none of the ^{14}C in the samples.

Results for $^{14}CO_2$ are shown in 4-3b. The only treatment exhibiting a statistically higher level compared to the controls was "Oxygen Set A", which also had a statistically significant level of ^{14}C in the HPLC fractions other than 1,4-dioxane. Confirmation that the ^{14}C activity obtained with this method was due to $^{14}CO_2$ was obtained by precipitation with barium hydroxide.

Decreases in IPA were highest in the aerobic treatments, as expected. Significant decreases also occurred in all of the anaerobic treatments (Appendix C, Figure 6-30). In contrast, IPA losses from the autoclaved controls were not significant. Percent decreases in IPA in the live anaerobic treatments were generally greater than for acetone (Appendix C, Figure 6-31). Acetone concentrations decreased the most in the aerobic treatments. Significant decreases also occurred in all of the live anaerobic treatments, in comparison to the Set B autoclaved controls.

The fate of the acetone and IPA was not evaluated. However, in the live anaerobic treatments, there was a significant increase in acetate over time (Appendix C, Figure 6-38), corresponding to the decreases in acetone and IPA. Since the amount of electron acceptor added was much lower than the total amount needed for oxidation of the acetone and IPA, the electron acceptor was likely consumed and thereafter biodegradation of acetone and

IPA in the anaerobic treatments occurred via fermentation. In the aerobic treatments, oxygen consumption was continuous (Appendix C, Figure 6-42a). Aerobic biodegradation of acetone and IPA would be expected to yield CO_2 and new cells. The total mass of acetone and IPA consumed was consistent with the amount of oxygen consumed, assuming a yield of 0.6 mg cell as COD per mg of acetone plus IPA in terms of COD (data not shown).

Regarding biodegradation results for DCM, statistically significant decreases occurred in all live treatments except for the AQDS amended microcosms (Appendix C, Figure 6-33). Anaerobic biodegradation of DCM has been demonstrated via fermentation to acetate and formate (Mägli et al., 1998) or when nitrate serves as the terminal electron acceptor (Freedman et al., 1997; Kohler-Staub et al., 1995), although nitrate was not present in the groundwater. Biodegradation of DCM under aerobic conditions has also been demonstrated (Scholtz et al., 1988), so the results for Site 1 are consistent with previously demonstrated processes. DCM has been shown to inhibit the degradation of TCE (Bone et al., 2009); accumulation of salts from HCl neutralization also causes inhibition (Gälli and Leisinger, 1985). The initial concentration of DCM (less than 7.5 mg L^{-1}) was sufficiently low such that inhibition of DCM, 1,4-dioxane, acetone, and IPA biodegradation was not evident.

Biodegradation results for 1,1,1-TCA and 1,1-DCE (Appendix C, Figure 6-40 and Figure 6-41) indicate that decreases in 1,1,1-TCA occurred in the live treatments in comparison to autoclaved control Set A (the level in Set B was too low to evaluate). However, no volatile daughter products were detected, including 1,1-DCE, 1,1-DCA,

chloroethane, and ethane. Since the level of 1,1,1-TCA remained stable in autoclaved control Set A, losses in the live treatments cannot be attributed to abiotic processes. Consequently, the process by which 1,1,1-TCA decreased in the live bottles is not known. Losses of 1,1-DCE were lower than for 1,1,1-TCA in all of the live treatments.

Results for the other VOCs that were monitored, including 1,1-DCA, *cis*-1,2-DCE, Freon 113, Freon 123, and TCE, were similar to 1,1-DCE, i.e., losses were lower than for 1,1,1-TCA in all of the treatments (data not shown).

Unlike Site 1, groundwater in all of the live microcosms from Site 2 remained pink for the entire incubation period. This indicated that the E_h remained above -110 mV at all times. As will be shown, this observation is consistent with the low level of biotic activity in the microcosms from Site 2, including the anaerobic and aerobic treatments. This observation motivated the preparation of a new subset of Site 2 microcosms (Unamended Set B and Oxygen Set C), based on the hypothesis that the high initial concentration of DCM was inhibitory. To address this, the groundwater was sparged with nitrogen to lower the DCM concentration. In these microcosms, the color of the groundwater did change from pink to clear between days 103 and 184. This was longer than for the Site 1 microcosms, but it did confirm that DCM was inhibiting biotic activity in the original microcosms. As with the Site 1 oxygen microcosms, the Oxygen Set C treatment of Site 2 cycled between a pink color (after adding oxygen) and clear. The color change in the resazurin for the Unamended Set B was consistent with anaerobic biodegradation of DCM. Evidence for biotic activity in the Oxygen Set C microcosms included a consistent level of oxygen consumption and biodegradation of DCM and IPA.

4.5.2 Small Microcosms: Site 2

1,4-Dioxane concentrations in the live microcosms from Site 2 were variable over the first 100 days of incubation and then the concentration leveled off (Figure 4-4a). In spite of the considerable variability in concentrations during the initial 100 days, a decrease in 1,4-dioxane was most evident for the FE(III) treatment, which decreased from ~52 mg L-1 at time zero to ~20 mg L-1 on day 85. For the Fe(III)-EDTA treatment, 1,4-dioxane decreased from ~26 mg L-1 to ~8 mg L-1 between days 48 and 85. The Autoclaved Control Set A microcosms had a time zero 1,4-dioxane concentration of ~120 mg L-1. By day 35, the concentration decreased to ~55 mg L-1 and there was no significant change thereafter. This suggests that the 1,4-dioxane was not yet in equilibrium for the first two headspace measurements. Results for autoclaved control Set B were more consistent over time.

Figure 4-4b shows the overall consumption of 1,4-dioxane at the end of the incubation period. Note that the overall consumption for the Autoclaved Control Set A is 50%, however if the actual concentration at time zero (55 mg L^{-1}) is considered instead, the overall consumption is 0%. Results for Autoclaved Control Set B show no net decrease in 1,4-dioxane, whereas there was an overall 11% decrease in the water controls. Decreases in 1,4-dioxane were highest in the Fe(III)-amended treatment (80%), followed by the sulfate, unamended, Fe(III)-EDTA, and AQDS amended treatments. However, the level of confidence in the percent decrease is compromised by the high level of variability in the time zero measurements. The reason for this trend is not known; it may have been related to the poor precision of the headspace method, a slow rate of establishing equilibrium

among the soil, groundwater and headspace, or some other factor. The variability in headspace measurements for 1,4-dioxane reflects its low volatility.

A major difference in behavior between the Site 1 and Site 2 microcosms was the lack of oxygen consumption and the corresponding lack of aerobic biodegradation of acetone and IPA, as shown below. Furthermore, there was no indication of anaerobic biodegradation of DCM in the Site 2 microcosms (see below). This was likely a consequence of the high initial concentration of DCM (~6,000 mg L-1). Consequently, two additional treatments were prepared for Site 2 to evaluate the effect of DCM. The Unamended Set B and Oxygen Set C treatments were prepared with groundwater that was sparged with N2 to remove most of the DCM. Lowering the initial concentration of DCM did result in aerobic biodegradation activity (see below) and anaerobic biodegradation of the remaining DCM. However, as shown in Figure 4-5, lowering the initial concentration of DCM did not result in better performance in terms of 1,4-dioxane biodegradation; in fact, the percent removal appears to be lower, but that was likely a consequence of variability in the time zero 1,4-dioxane measurements.

Liquid samples from the microcosms were evaluated for the distribution of ^{14}C on days 103, 222, and 287. Sample analysis was limited to determining the percentage of ^{14}C in the liquid phase that was not attributable to 1,4-dioxane. The percentages are based on the ^{14}C activity in the HPLC fraction other than 1,4-dioxane, compared to the total ^{14}C added at time zero.

The ^{14}C results for the live treatments from Site 2 were not significantly different from the autoclaved controls (Figure 4-8b). Thus, although the GC monitoring data

suggested some losses of 1,4-dioxane, the more definitive ^{14}C results indicated that no significant biodegradation occurred. For this reason, no attempt was made to fraction the HPLC eluent, as was done with the Site 1 samples on day 287. As indicated above, the low level of ^{14}C in the aqueous phase other than 1,4-dioxane in the autoclaved and water controls was likely a consequence of impurities in the [^{14}C]1,4-dioxane stock solution. The amount of ^{14}C in the non-dioxane fraction in the controls was less than 4%, which is consistent with the purity of the [^{14}C]1,4-dioxane stock solution as reported by the manufacturer.

The ^{14}C results for the Unamended Set B and Oxygen Set C treatments from Site 2 were also not significantly different from the autoclaved controls (Figure 4-5a). This indicated that lowering the initial DCM concentration did not improve biodegradation of the 1,4-dioxane, which is consistent with the results from the headspace monitoring.

There was no significant accumulation of $^{14}CO_2$ above what was detected in the autoclaved controls, either in the original set of treatments or in the Unamended Set B and Oxygen Set C treatments (Figure 4-5b).

IPA concentrations were an order of magnitude higher for Site 2 microcosms versus Site 1 (Appendix C, Figure 6-36). The significantly higher concentration of IPA may have been a factor in the overall inhibition of biodegradation activity, along with the high initial concentration of DCM (see below). IPA levels did not decrease significantly from the initial level. The exception was in Oxygen Set C; in this treatment, it appears that removal of most of the DCM allowed for the onset of IPA biodegradation, resulting in ~24% decrease over the full incubation period. The total mass of IPA removed from Oxygen Set

C was similar to the mass removed from the aerobic treatments for Site 1 (Appendix C, Figure 6-36b); however, since the initial concentration in the Site 2 microcosms was much higher, the percent decrease was lower.

Significant decreases in acetone were observed in the unamended treatment and those amended with Fe(III), Fe(III)-EDTA, AQDS and sulfate (Appendix C, Figure 6-37), while no significant losses were observed in the autoclaved controls. It should be noted, however, that there was considerable variability in the acetone measurements, with a decrease on one sampling date typically followed by an increase on the next sampling date. The behavior of the two treatments that were sparged to remove DCM was similarly erratic; the concentration of acetone in Oxygen Set C rose significantly over time, while Unamended Set B dropped to zero on day 220 and then rebounded to the highest level measured over the entire incubation period. The reason for the lack of a clear trend in acetone levels in the Site 2 microcosms is not known. One possibility is oxidation of IPA to acetone, followed by biodegradation of the acetone. Additional work is needed to better understand the possible interaction between IPA and acetone biodegradation at Site 2.

Consistent with the lack of IPA biodegradation in the oxygen treatments (Sets A and B), there was no significant consumption of oxygen in these microcosms (Appendix C, Figure 6-42b). This contrasts with the continuous consumption of oxygen in the Site 1 microcosms (Appendix C, Figure 6-42b). The lack of oxygen consumption was likely attributable to the inhibitory levels of DCM and possibly IPA. In the Oxygen Set C treatment, oxygen was consistently consumed and biodegradation of IPA was observed.

This suggests that sparging to remove most of the DCM and some of the IPA removed the inhibition that prevented aerobic biodegradation.

Acetate levels in the live microcosms started between ~190 and ~300 mg L^{-1} (Appendix C, Figure 6-38). After 30 days of incubation, the Fe(III)-EDTA amended treatment had a significant production of acetate and reached ~700 mg L^{-1}. The rest of the live treatments produced acetate only after day 100. After day 225 most of the treatments show a sharp decrease in acetate back to levels of ~200 to ~300 mg L^{-1}. The exception was for the oxygen Set C treatment, which reached a final concentration of ~1,000 mg L^{-1} on day 290. The acetate concentration in this treatment ended up being almost 5 times its initial value (Appendix C, Figure 6-38b).

Results for DCM monitoring data indicate that in the original set of microcosms (i.e., not sparged to lower the initial DCM level), there was no significant change in DCM over the 287 days of incubation (Appendix C, Figure 6-39). pH was not a factor; the initial pH was 7.2 (measured with a pH electrode meter) and was close to 7 at the end of the incubation period (measured with pH indicating strips).

In contrast, in the live treatments in which the initial concentration of DCM was lowered by sparging, DCM was completely consumed in oxygen Set C and ~66% was biodegraded in the Unamended Set B treatment. This, combined with the oxygen consumption observed in Oxygen Set C (Appendix C, Figure 6-42b), indicates that the high initial concentration of DCM was inhibitory to both aerobic and anaerobic activity in the Site 2 microcosms.

4.5.3 Large Microcosms: Site 1

Concentrations of 1,4-dioxane in these microcosms were measured by direct aqueous injection. After 1,473 days of incubation, no significant decrease was observed for any of the treatments (Figure 4-6a). The initial 1,4-dioxane concentrations ranged from 14.8 mg L^{-1} to 17.3 mg L^{-1} in the live treatments, with the exception of the "Synthetic Groundwater" treatment which started at 19 mg L^{-1}. The water control bottles had an initial concentration of 21.3 mg L^{-1}. During several sampling events, some treatments showed lower 1,4-dioxane concentrations: the Fe(III)-EDTA treatment showed the lowest concentration at 9.8 mg L^{-1} on day 403, followed by the Fe(III)+AQDS treatment which had 11.2 mg L^{-1} on day 1,007. The decreases were likely an artifact of improper handling of the samples, by exposing them to oxygen and allowing the F(II) to oxidize, creating a Fenton's reaction. However, the final values of 1,4-dioxane are not significantly different from those measured at time zero (Figure 4-6b), following use of better sampling handling practices to prevent oxidation of Fe(II). There is no evidence for anaerobic biodegradation of 1,4-dioxane according to these data.

Data from the analysis of ^{14}C distribution in the aqueous phase shows no significant biodegradation of 1,4-dioxane in any of the treatments with respect to the autoclaved and water controls after 1,473 days of incubation (Figure 4-7a). The percent of 1,4-dioxane present in the bottle is expressed as the amount of ^{14}C activity corresponding to the 1,4-dioxane fraction eluted from the HPLC divided by the total amount of ^{14}C measured at time zero. The 1,4-dioxane remaining in the microcosms varies between 74.1 and 87.9 %. Considering the long incubation time, the decrease in 1,4-dioxane is not significant and

thus it can be concluded that anaerobic biodegradation did not occur. To assess the appearance of any degradation products in the aqueous phase, the ^{14}C eluted from the HPLC other than 1,4-dioxane (called "Other soluble") is presented as a percentage of the total initial ^{14}C material measured in the aqueous phase (Figure 4-7b). On day 32 of incubation, first measurement of the rest of effluent fraction, the Fe(III)-EDTA treatment shows that 14.3% of ^{14}C corresponded to soluble products; however, this low level of conversion to soluble products was due to the intrusion of oxygen in the HPLC sample vial which triggered an iron oxidation and hydroxyl radical reaction that eventually degraded some of the 1,4-dioxane, as it occurred in samples from the small microcosms. No significant generation of soluble products with respect to the autoclaved or water controls is shown for the other treatments. On the final measurement, the soluble products fraction has similar or lower percentages than those of the experiment controls. This is in agreement with the data showing the percentage of [^{14}C]1,4-dioxane present in the liquid phase.

Reduced iron concentrations in the aqueous phase indicate that microbial reduction of Fe(III) occurred in the Fe(III)-EDTA amended treatment (Appendix C, Figure 6-43). Reduced iron was first observed on day 39 and it was followed by an addition of more Fe(III)-EDTA. The amount of iron reduced was approximately the same as the amount of added iron (63 mM). The sustained reduction of Fe(III)-EDTA can be attributed to the biodegradation of the main electron donors present in the microcosms, i.e., acetone and IPA.

Microbial reduction of AQDS was observed in the AQDS and AQDS plus Fe(III) treatments (Appendix C, Figure 6-44) only after 263 days of incubation. On day 408, the

concentration of reduced AQDS was 3.86 and 3.32 for the AQDS and AQDS plus Fe(III) amended treatments, respectively. This is slightly half of the initial amount of AQDS added. Even though these results indicate that usage of AQDS as an electron acceptor and electron shuttle was observed after a long incubation period, there was no significant effect on 1,4-dioxane biodegradation.

4.5.4 Large Microcosms: Site 2

Similarly to the treatments in the large microcosms from Site 1, the large microcosms from Site 2 showed no significant degradation of 1,4-dioxane. The final GC measurement point occurred on day 1,198 (Figure 4-8a). After an apparent initial drop of 1,4-dioxane in the Fe(III)-EDTA B (treatment amended with 100 mg L^{-1} of acetone and IPA), the last two measurements showed a rebound. The percentage of 1,4-dioxane remaining with respect to the initial concentration was between 78 and 94%, however, there is not a significant difference with respect to the autoclaved controls (Figure 4-8b).

According to measurements of ^{14}C distribution in the aqueous phase, the percentage of 1,4-dioxane present in the aqueous phase after 1,198 days of incubation ranged between 77.5 and 87.9 % (Figure 4-9a). Using this metric, no significant decrease in 1,4-dioxane occurred in the treatments with respect to the autoclaved and water controls. The "other soluble" fraction of ^{14}C material results show that no more than 5 % was recovered as degradation products (b). The unamended, Fe(III)-EDTA and autoclaved treatments have very similar levels of other soluble fraction measured at time zero. By day 1,198, none of these treatments surpassed the 5 % level for the other soluble fraction.

Reduced iron was also observed in the Fe(III)-EDTA treatments. On incubation day 300, both iron amended treatments show complete reduction of iron (Appendix C, Figure 6-45). Even though the Fe(III)-EDTA Set A treatment was not amended with acetone or IPA, there was approximately 90 mg L^{-1} of acetone present at time zero due to the addition of [^{14}C]1,4-dioxane. That amount of acetone was enough to provide electrons to promote iron reduction.

4.5 Discussion

As stated in the introduction, evidence for 1,4-dioxane biodegradation under anaerobic conditions is scarce. The study published by Shen et al. (2008) indicates that high percentages of biodegradation occurred in unamended anaerobic microcosms prepared with anaerobic sludge. An enhancement in this activity occurred when the microcosms were amended with humic acids. The present study attempted to recreate part of those conditions by adding the electron shuttle AQDS as a humic acid homologue. Even though reduction of AQDS and Fe(III)-EDTA was observed, no anaerobic biodegradation of 1,4-dioxane could be associated with it. No studies were found that verify the work by Shen et al. (2008). Since the results from ^{14}C measurements are more reliable than GC measurements of 1,4-dioxane, anaerobic biodegradation has not been proven in this study. Data from GC measurements tended to be variable, especially for the initial GC method that relied on headspace samples. Even though the direct aqueous injection method improved the detection limit and reduced the variability of the GC measurements, no substantial decrease on 1,4-dioxane was observed during the long incubation periods.

Unlike 1,4-dioxane, GC data for DCM and HPLC data for acetone and IPA unequivocally provided evidence that those compounds underwent biodegradation.

Results from ^{14}C measurements indicated partial degradation of 1,4-dioxane during some sampling events for treatments amended with chelated iron. In this case, the samples had been inadvertently exposed to oxygen for a few hours and the microbially reduced iron was oxidized; such reaction promoted the generation of hydroxyl radicals which were able to break the ring structure of 1,4-dioxane (Sekar and Dichristina, 2014). When oxygen intrusion was later prevented in the HPLC sample vials, no iron oxidation took place. Several batch experiments with addition of reduced iron and reduced chelated iron were performed to clarify and confirm the causes of this process (Appendix C, Figure 6-46, Figure 6-47, and Figure 6-48). Those experiments confirmed that a Fenton's reaction process was responsible for 1,4-dioxane abiotic degradation. In addition, the experiments showed that maintaining a circumneutral pH improved the extent of abiotic degradation. However, complete degradation of 1,4-dioxane was not achieved within a reasonable amount of time under the experimental conditions that were examined and no additional studies were performed based on abiotic degradation.

It was assumed when the microcosms were prepared that the high levels of acetone and IPA would provide an excess of electron donor that would keep the water anaerobic. However, oxidation of reduced iron was faster than biological oxidation of acetone or IPA. Under complete anaerobic conditions, none of the treatments showed conversion of ^{14}C material as soluble products, nor showed any significant 1,4-dioxane decrease.

It is unclear if 1,4-dioxane natural attenuation is occurring at the contaminated sites from which the microcosms were constructed. The observations in the field indicate a smaller 1,4-dioxane plume than predicted if it is assumed that 1,4-dioxane was released in the aquifer at the same time as the chlorinated co-contaminants. If that is the case, a different process is in charge of the attenuation of the 1,4-dioxane plume. As observed in this study, the slight introduction of oxygen can trigger abiotic degradation of 1,4-dioxane if microbially reduced iron is also present. Even though the sites are mostly anaerobic, one can speculate how low levels of oxygenated groundwater in the fringes of the anaerobic zones contribute to this abiotic degradation. Alternatively, aerobic conditions at the fringe may be supporting aerobic biodegradation of 1,4-dioxane, either via a cometabolic process or by microbes that grow on the contaminant.

4.6 Conclusions

Anaerobic biodegradation of 1,4-dioxane was evaluated for three sets of microcosms prepared with groundwater and soil from two contaminated sites. The longest incubation time was 1,473 days, for the large microcosms from Site 1. Several of the small microcosms from Site 1 showed biodegradation of acetone and IPA, whereas all of the small microcosms from Site 2 did not show any biological activity. The reason for the lack of activity in these bottles was a high level of DCM. When DCM was sparged out of the water in newer microcosms, oxygen utilization and biodegradation of acetone and IPA was observed.

Limited biodegradation of 1,4-dioxane into CO_2 was observed for the aerobic treatments in small microcosms from Site 1. None of the anaerobic microcosms treatments

across the different treatments showed any significant biodegradation of 1,4-dioxane. Apparent decreases in 1,4-dioxane measured by GC or ^{14}C counts were not different from the water or autoclaved controls. False positives for ^{14}C measurement of soluble products and 1,4-dioxane decreases were observed in small and large microcosms from Site 1, amended with Fe(III)-EDTA. Initially, it was believed that approximately 20 to 25% of 1,4-dioxane was being biodegraded anaerobically in these microcosms. However, it was discovered that the limited degradation of 1,4-dioxane was occurring due to the intrusion of oxygen in the sampling vials. Oxygen oxidized the microbially reduced iron in a few hours and triggered the production of hydroxyl radicals that degraded 1,4-dioxane. When ^{14}C samples were protected from any oxygen intrusion, no iron oxidation was observed and the higher ^{14}C levels for 1,4-dioxane and lower counts for the other soluble fraction indicated that there was no biodegradation.

After monitoring many of the anaerobic microcosms in excess of 5 years, no compelling evidence was found to support 1,4-dioxane biodegradation under anaerobic conditions, although microbial activity was observed in most of the treatments. It is speculated that the site observations that indicate natural attenuation of 1,4-dioxane may be attributable to an as yet undiscovered anaerobic process. Alternatively, aerobic degradation at the periphery of the plume may be preventing migration of the 1,4-dioxane, while any of the VOC contaminants present (e.g., Freons and 1,1-DCE) are recalcitrant under aerobic conditions and therefore may be spreading further in the plume.

4.7 Tables for Chapter 4

Table 4-1 Amounts of VOCs and 1,4-dioxane added to autoclaved control Set A.

	Target Concentration (mg L^{-1})			Volume Added (µL $bottle^{-1}$)		
Compound	**AC B-41**	**AC B-10**	**WC**	**AC B-41**	**AC B-10**	**WC**
DCM	5.71	6,737	6,664	16[b]	300[a]	300[a]
1,1-DCE	0.10	0.46	0.49	6[b]	33[b]	33[b]
1,1-DCA	0.75	2.11	2.14	15[b]	45[b]	46[b]
Freon 123	8.41	0.00	8.29	325[b]	0[b]	325[b]
Freon 113	2.13	0.01	1.11	2[a]	93[b]	2[s]
cis-1,2-DCE	1.30	1.37	1.70	16[b]	19[b]	24[b]
1,1,1-TCA	0.04	0.24	1.10	5[b]	28[b]	125[b]
TCE	0.23	0.47	0.51	17[b]	37[b]	41[b]
1,4-dioxane	63.0	55.0	54.7	3[a]	3[a]	3[a]

[a] Neat compound.
[b] Water-saturated solution.

Table 4-2 HPLC fractionation of collected eluent, soluble compounds and time intervals.

Fraction	Description	Trapping time interval (min)
1	Pre-injection	0.66-3.66
2	Pre-injection	3.66-6.96
3	AQDS	6.96-9.16
4	Unknown peak	9.16-10.16
5	No peak	10.16-11.89
6	Formate	11.89-15.48
7	Acetate	15.48-18.25
8	No peak	18.25-21.46
9	IPA	21.46-22.96
10	1,4-Dioxane	22.96-27.15
11	No peak	27.15-30

Table 4-3 Percent recoveries of ^{14}C and percent ^{14}C product distribution based on HPLC fractionation for Site 1 microcosms.

Treatment	Overall Recovery of ^{14}C (%)[a]	Recovery of ^{14}C in HPLC eluent (%)[b]	1,4-Dioxane (%)[c]	Formate (%)[c]	Acetate (%)[c]	Unknown (%)[c,d]
Unamended	90.8	101.6	98.3	0.2	2.1	1.1
Fe(III)	97.4	96.6	93.4	0.1	2.1	1.0
FE(III)-EDTA	95.5	97.3	74.8	4.7	16.1	1.7
AQDS	92.5	85.3	76.9	0.4	5.2	2.8
Sulfate	94.5	97.6	94.4	0.1	2.1	1.0
Oxygen Set A	86.6	99.7	90.6	4.1	1.1	4.0
Oxygen Set B	91.3	98.8	94.4	2.2	0.8	1.4
AC Set A	81.4	102.8	98.9	0.2	2.3	1.5
AC Set B	95.1	87.9	85.2	0.4	1.0	1.3
WC	94.3	96.5	93.7	0.1	1.4	1.3

[a] (^{14}C in liquid phase at final time) (^{14}C in liquid phase at time zero)$^{-1}$.
[b] (sum of dpm in all fractions) (dpm injected)$^{-1}$.
[c] (dpm in the fraction indicated) (dpm injected)$^{-1}$.
[d] (sum of ^{14}C in fractions #1-5, 8, 9, and 11) (dpm injected)$^{-1}$.

4.8 Figures for Chapter 4

(a)

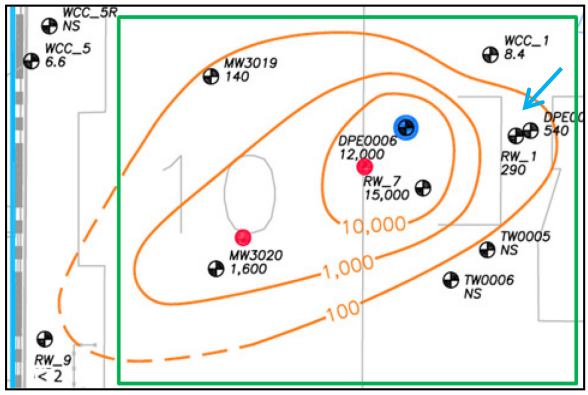

(b)

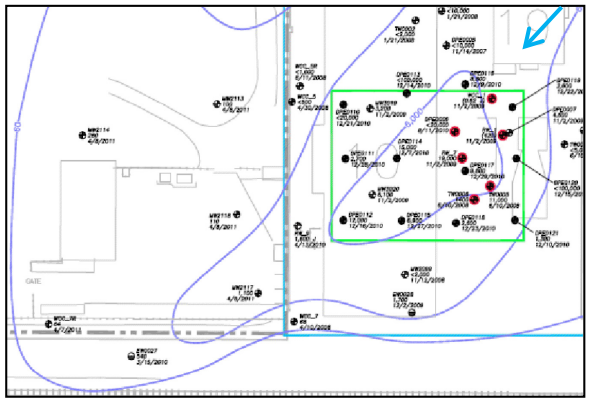

Figure 4-1. Plan view of contaminated area for Site 2 showing 1,4-Dioxane concentration contours (a) versus 1,1-DCE plume (b). Units are in µg L^{-1}. The green rectangle in (b) indicates the area and location of the 1,4-dioxane plume (a). The thick arrow shows the direction of the groundwater flow.

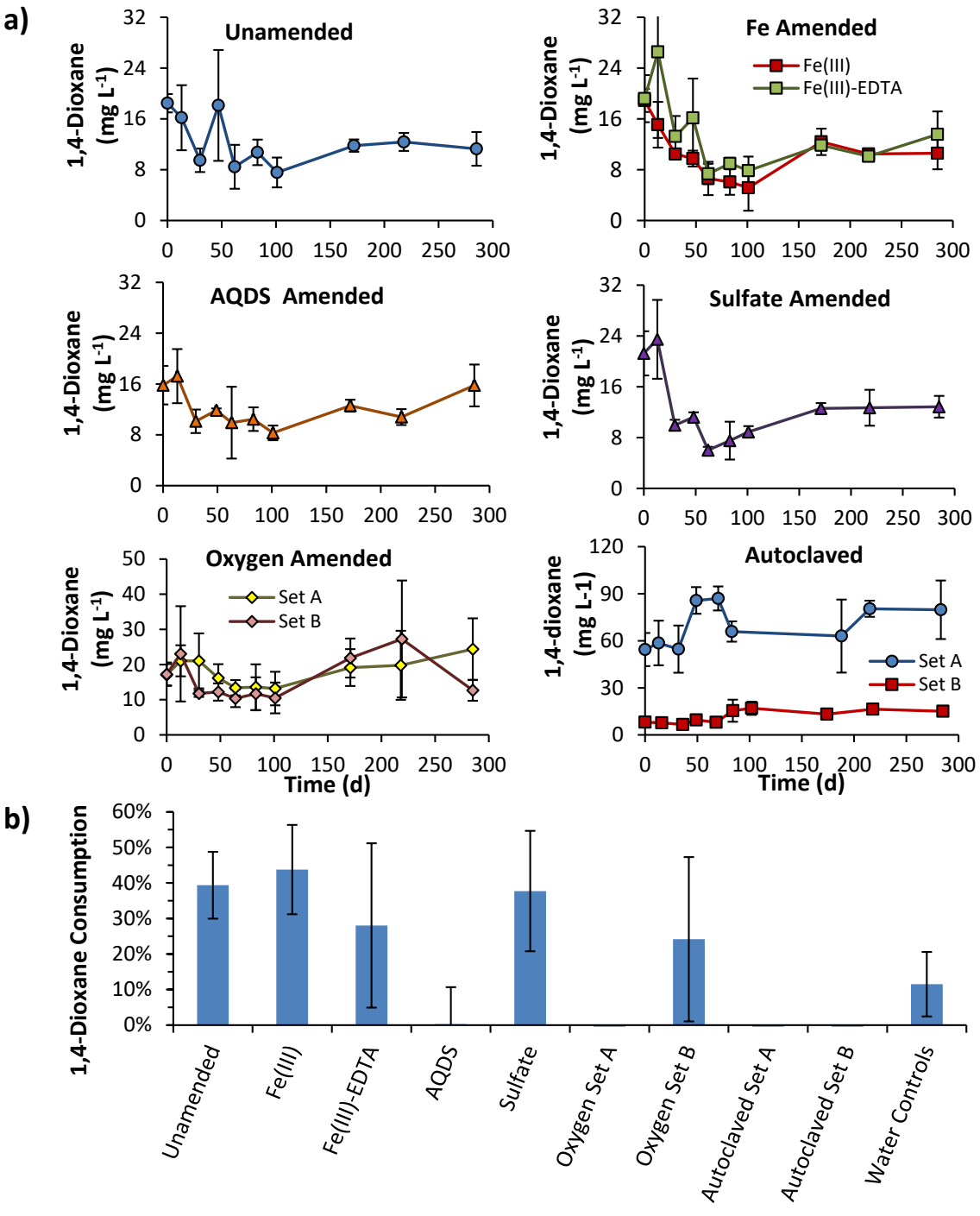

Figure 4-2 1,4-Dioxane in all treatments for small microcosms from Site 1 over time (a) and percent decreases at the end of incubation (b), based on GC analysis of headspace samples; averages for triplicates, error bars represent one standard deviation.

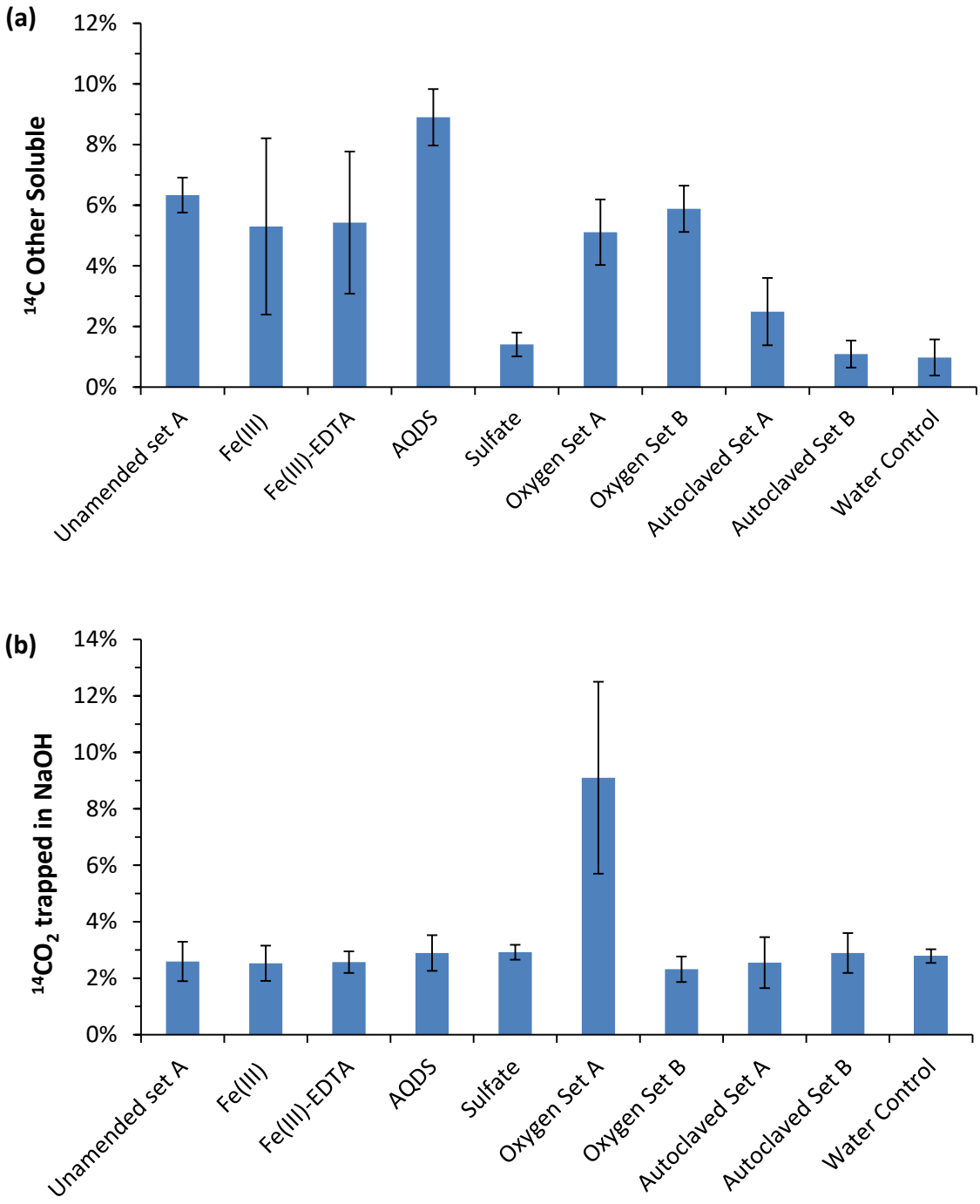

Figure 4-3. Percent of ^{14}C in HPLC eluent other than 1,4-dioxane (a) and $^{14}CO_2$ trapped in NaOH on day 287, relative to the initial [^{14}C]1,4-dioxane added, small microcosms from Site 1; averages for triplicate microcosms are shown; error bars represent one standard deviation.

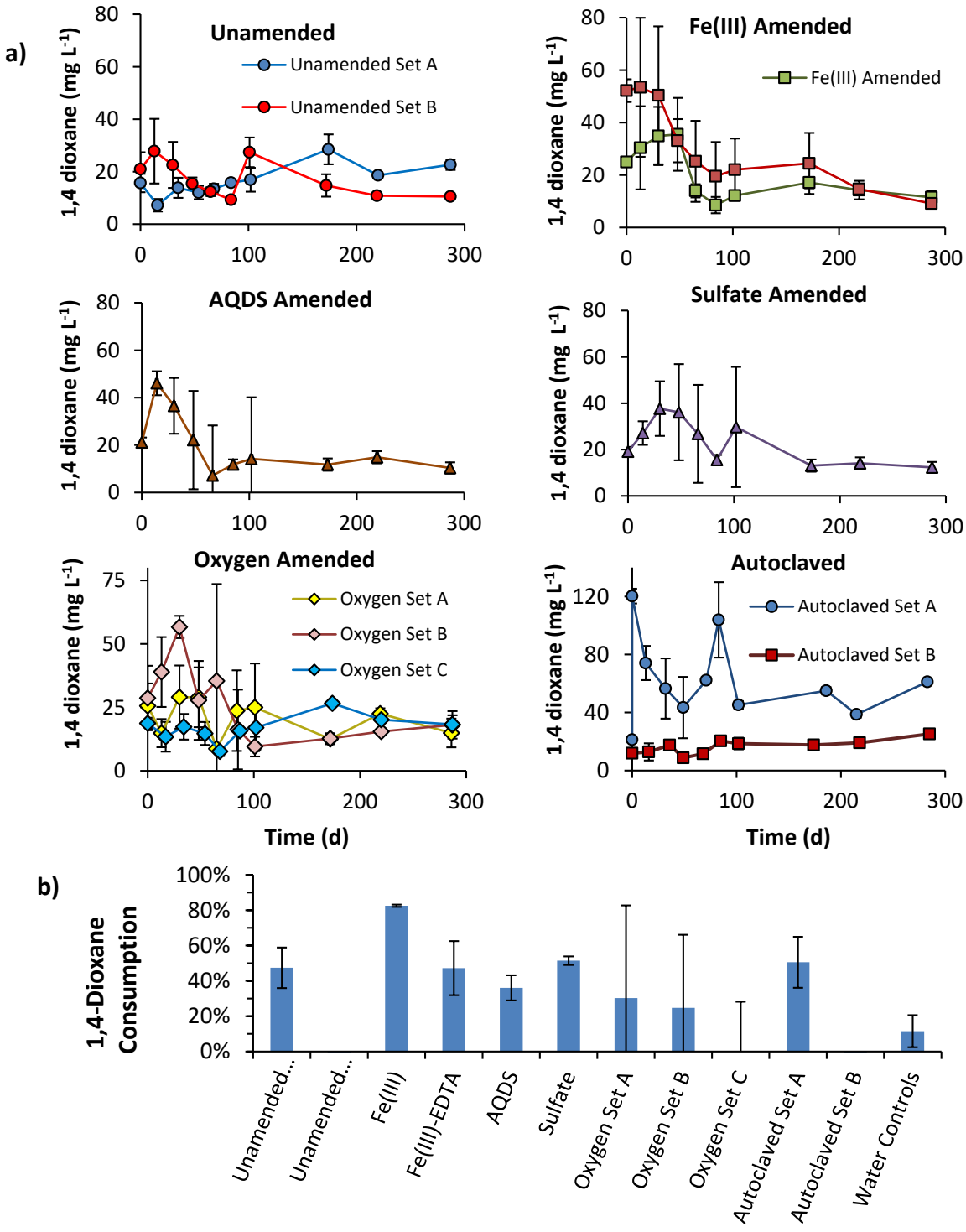

Figure 4-4. 1,4-dioxane concentration over time (a) and percent decreases (b) for small microcosms from Site 2; a bar is not shown for Autoclaved Set B because there was no net decrease compared to the initial concentration.

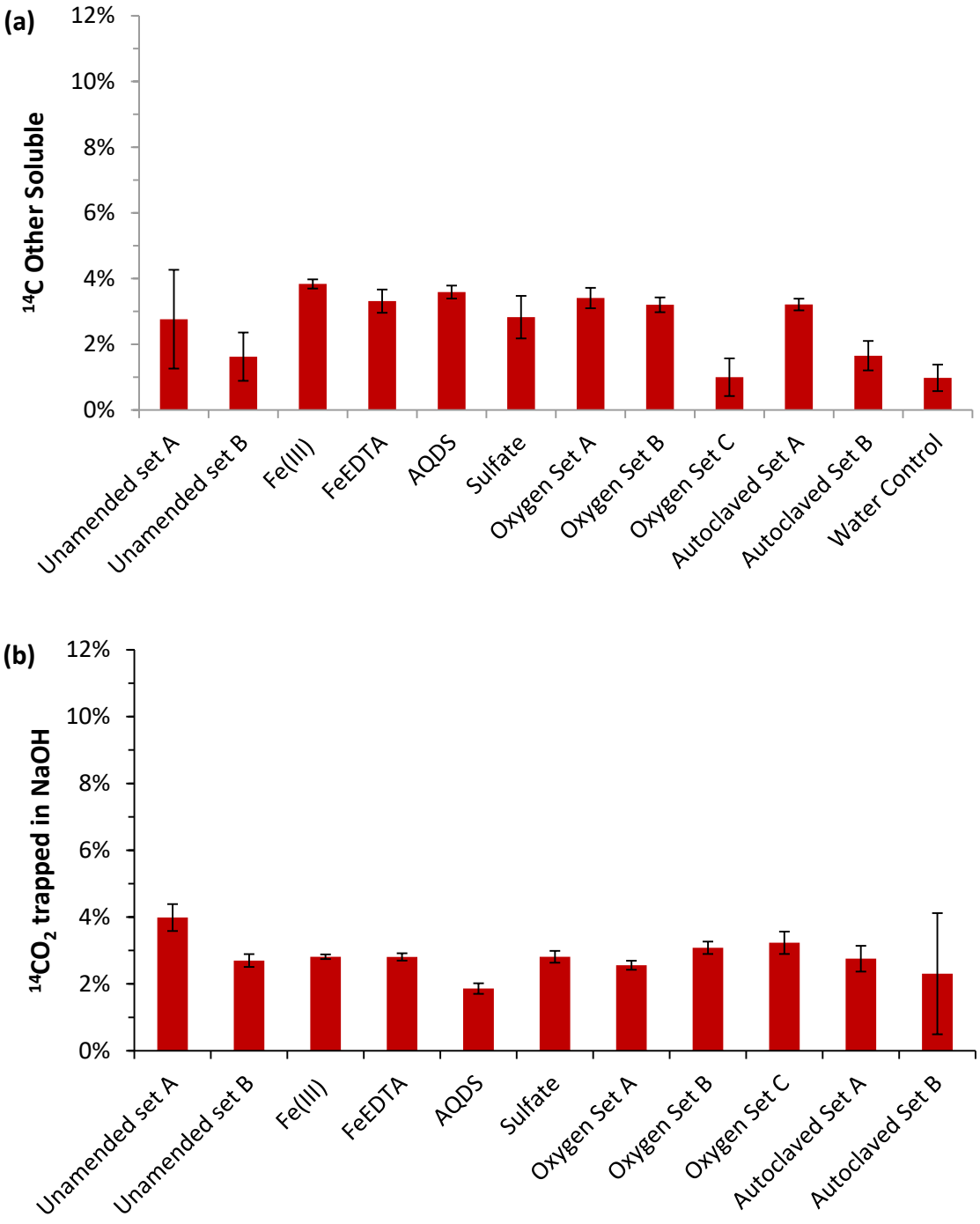

Figure 4-5. Percent of ^{14}C in HPLC eluent other than 1,4-dioxane (a) and $^{14}CO_2$ trapped in NaOH on day 287, relative to the initial [^{14}C]1,4-dioxane added, for small microcosms from Site 2; averages for triplicate microcosms.

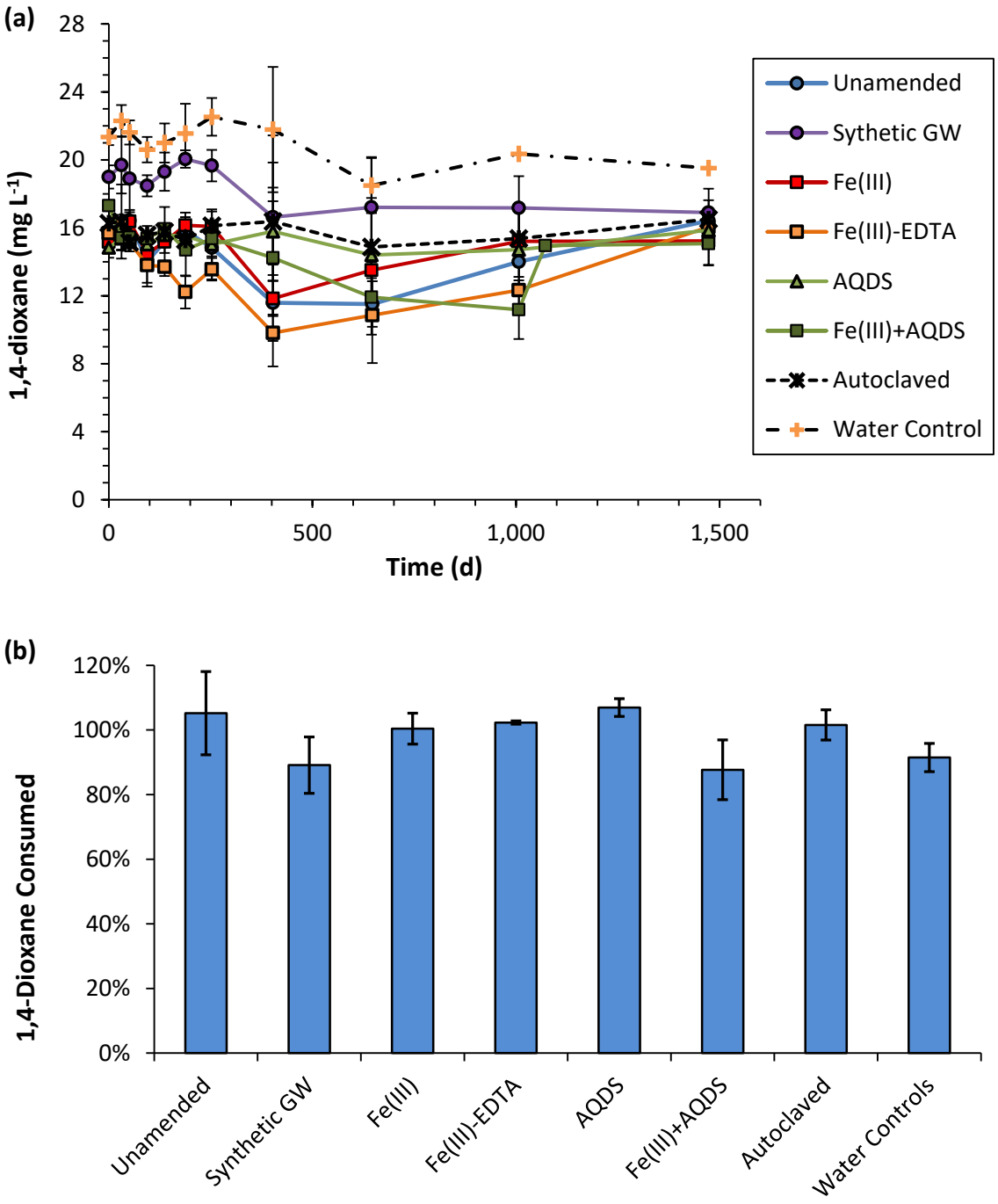

Figure 4-6. 1,4-Dioxane concentration over time (a) and percent decreases (b) for large microcosms from Site 1.

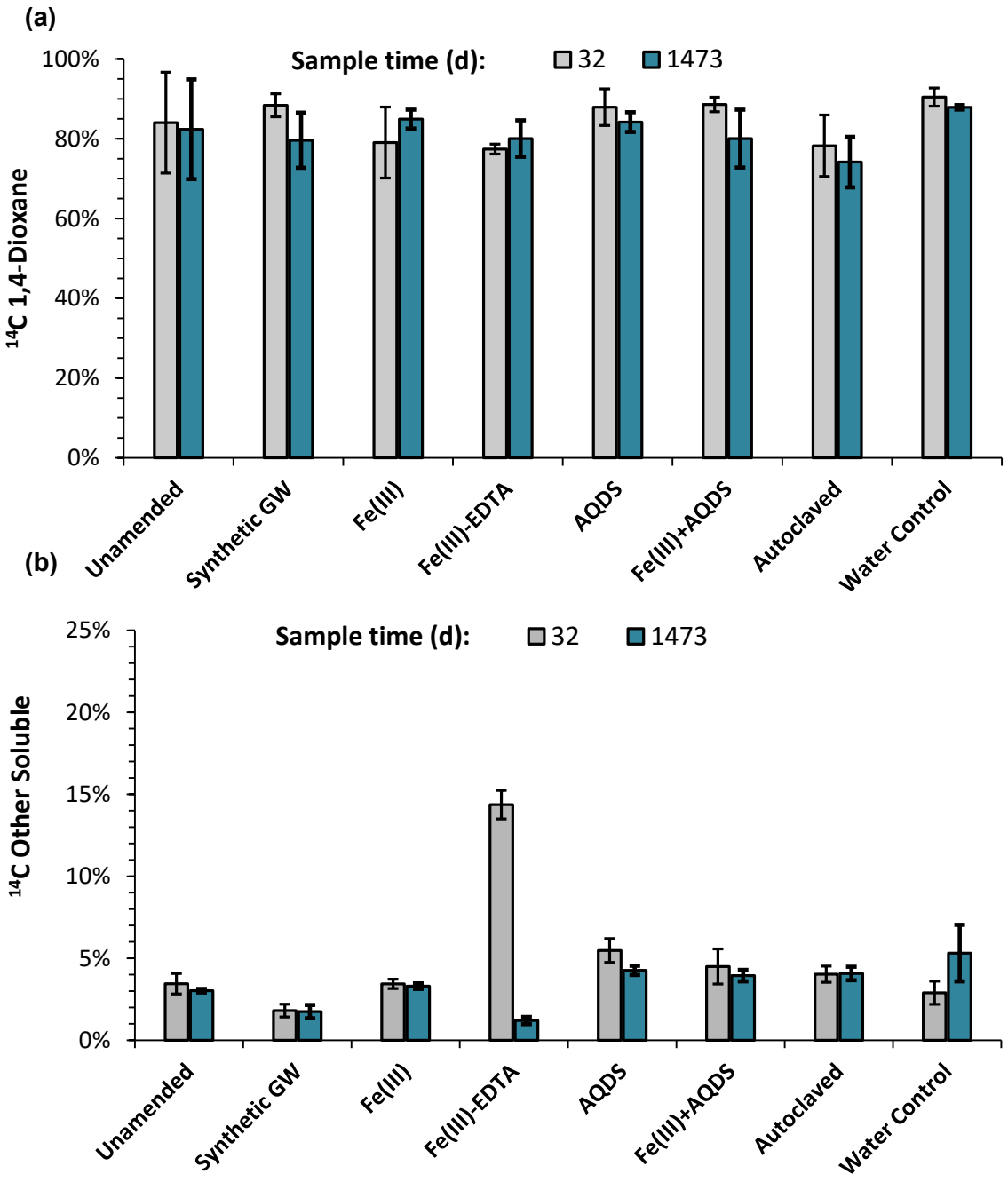

Figure 4-7. Percent ^{14}C in HPLC 1,4-dioxane eluent fraction (a) and other than 1,4-dioxane (b) on days 32 and 1,473, relative to the initial [^{14}C]1,4-dioxane added, for large microcosms from Site 1.

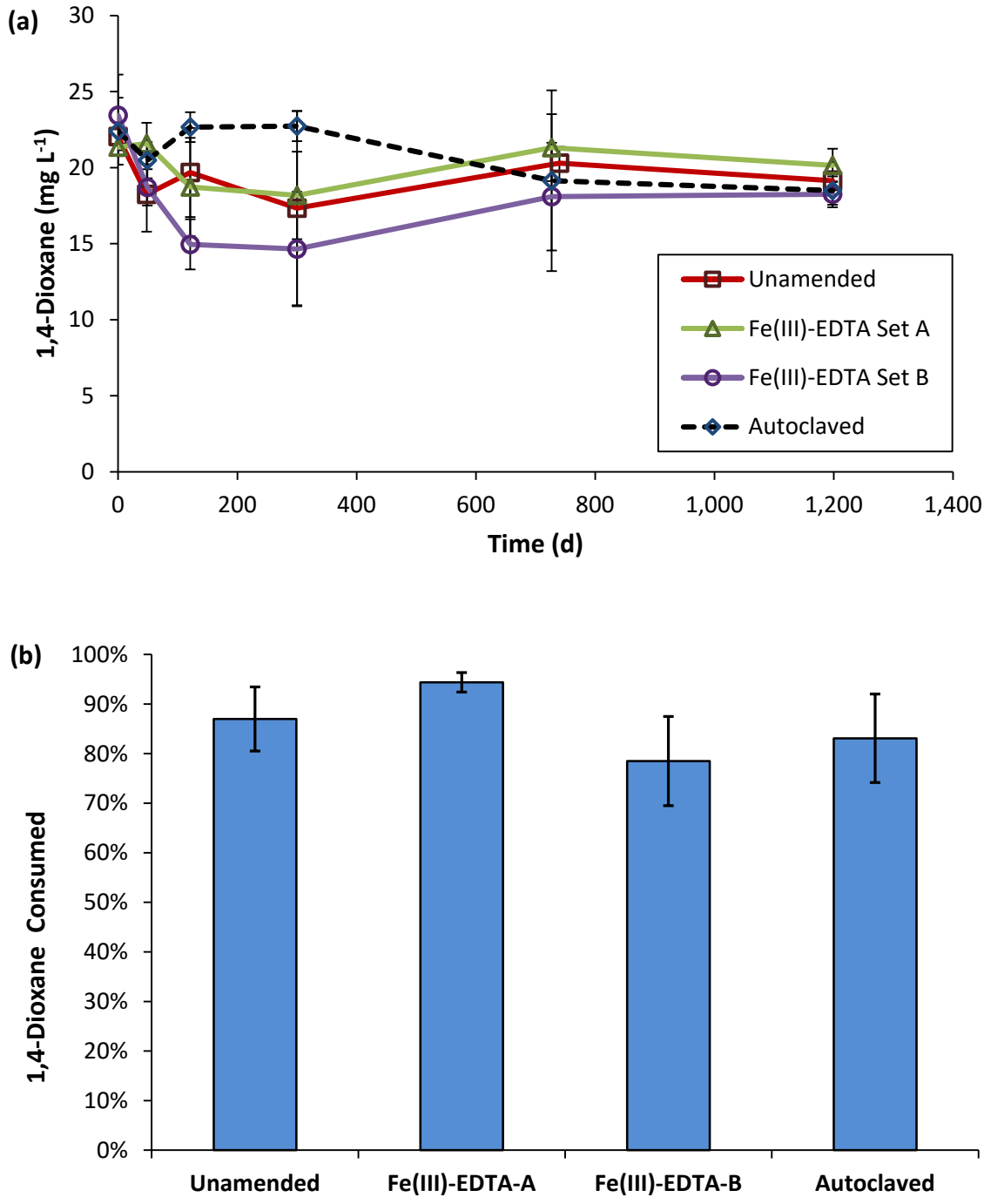

Figure 4-8. 1,4-Dioxane concentration over time (a) and percent remaining (b) for large microcosms from Site 2.

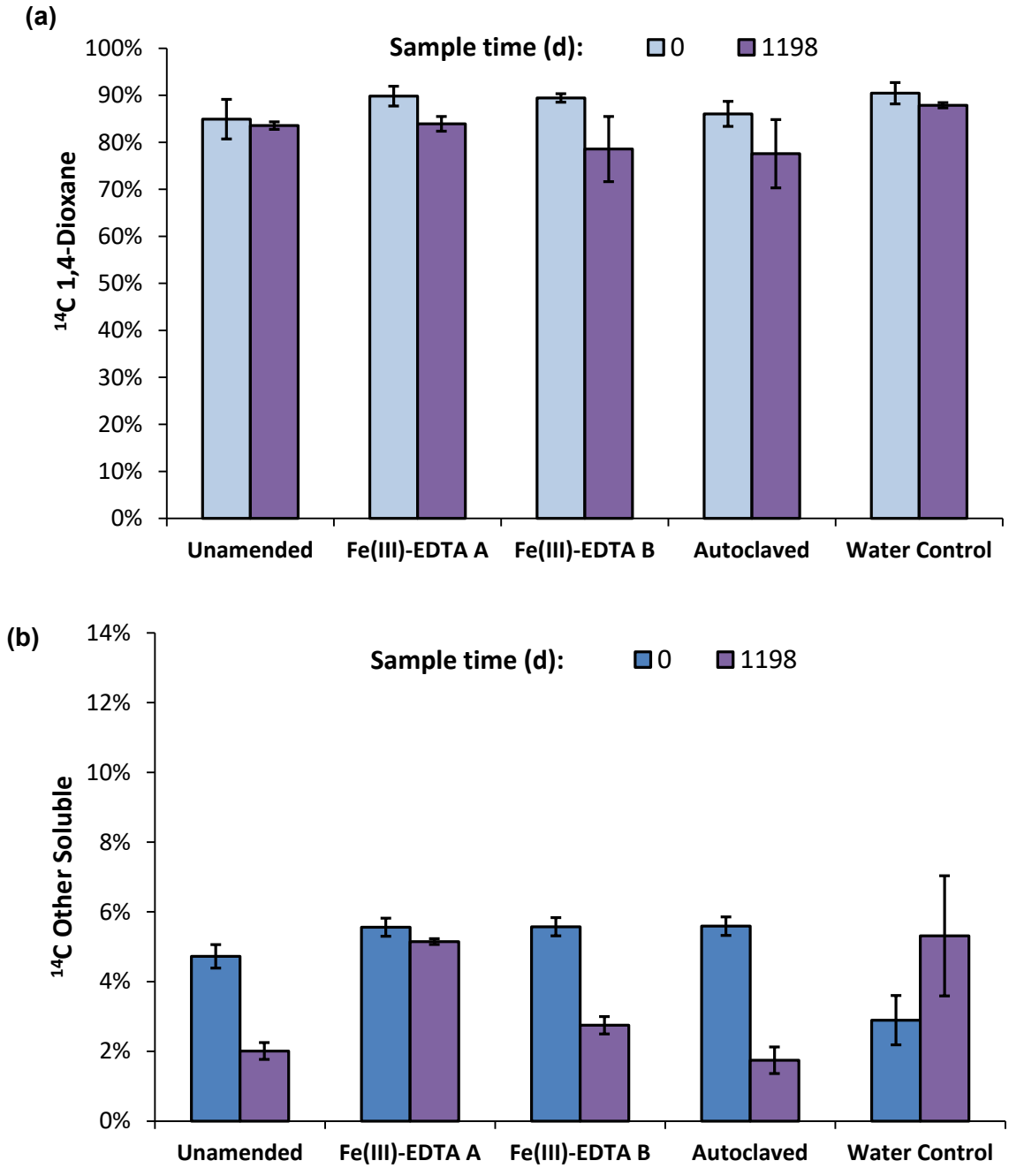

Figure 4-9. Percent ^{14}C in HPLC 1,4-dioxane eluent fraction (a) and other soluble (b) on days 32 and 1,198, relative to the initial [^{14}C]1,4-dioxane added, large microcosms from Site 2.

5. CONCLUSIONS AND RECOMMENDATIONS

This study evaluated the potential for biodegradation of 1,4-dioxane under aerobic and anaerobic conditions. Both approaches are of special interest for bioremediation practitioners. Aerobic biodegradation of 1,4-dioxane has been well studied under laboratory conditions. However, most contaminated aquifers have reducing conditions in which anaerobic biodegradation would be more advantageous due to the challenges of delivering oxygen to a deep aquifer. Therefore, this study explored the potential for both alternatives. Anaerobic biodegradation of 1,4-dioxane was evaluated in microcosms using a variety of amendments. Aerobic biodegradation was evaluated using propanotrophic cultures that cometabolize 1,4-dioxane, and with a culture (CB1190) that degrades 1,4-dioxane as a sole carbon and energy source. The kinetic constants obtained from these experiments were applied in a numerical model to compare the performance of cometabolic versus metabolic biodegradation via gas sparging and bioaugmentation.

Although much is already known about aerobic biodegradation of 1,4-dioxane, no prior studies were found that compared metabolic and cometabolic bioaugmentation. Aerobic biodegradation of 1,4-dioxane by metabolic and cometabolic bacteria was successfully characterized by obtaining 16 kinetic parameters which are key for predicting *in situ* bioremediation. These findings formed the foundation for developing a groundwater-contaminant transport model to predict the performance of these bacteria *in situ*. The specific conclusions obtained from this study are:

1. Regarding the kinetics of aerobic metabolic and cometabolic biodegradation of 1,4-dixoane, it was found that Y, b and q_{CMAX} rates were similar for the propanotrophic

cultures ENV425 and ENV487, whereas the CB1190 had a faster q_{SMAX} for 1,4-dioxane and a lower Y.

2. No self-inhibition by high concentrations of 1,4-dioxane was observed with the propanotrophs and their T_C values were consistent with values for cometabolism with other primary growth substrates.

3. The effect of dissolved oxygen on growth substrate and contaminant biodegradation were described by the K_{SO} and K_{CO} parameters, respectively. CB1190 had a lower affinity towards oxygen, K_{SO}, when compared to the propanotrophic cultures. There was no minimum oxygen concentration for ENV425 and ENV487 associated with propane consumption (O_{SMIN}) and the minimum oxygen concentration associated with 1,4-dioxane biodegradation (O_{CMIN}) was lower than that of CB1190 (O_{SMIN}).

4. Cometabolic biodegradation of 1,4-dioxane was inhibited by the presence of propane as reflected by the K_{iS} parameter. The inhibition was due to the preference of bacteria towards propane and it was reduced once the propane concentration was below 2 mg L^{-1}. Growth of the propanotrophic cultures was not inhibited by the presence of 1,4-dioxane, even at high concentrations (800 mg L^{-1}).

5. According to batch simulations based on the kinetic model at dissolved oxygen levels below 2 mg L^{-1}, the initial biomass concentration played a significant role in determining which culture was more effective for 1,4-dioxane biodegradation. The time to reach a bioremedation goal of 1 μg L^{-1} of contaminant was significantly increased for low dissolved oxygen levels and differences between the cultures

performance were magnified. When the initial concentration of 1,4-dioxane and biomass were increased, the performance of CB1190 became more competitive. On the other hand, for low concentrations of 1,4-dioxane cometabolic biodegradation is more advantageous, as long as adequate levels of propane are maintained with.

6. The kinetic parameters from the laboratory study were successfully utilized in a groundwater-contaminant transport model to determine the performance of 1,4-dioxane degrading bacteria (CB1190 and ENV425). The model used steady-state air sparging as a mean to deliver propane and oxygen into the water phase. Calibration of the model was made possible by using monitoring data from several wells from a pilot study in which bioaugmentation of ENV425 with propane was used to achieve bioremediation of 1,4-dioxane. Although several assumptions such as a constant air and propane injection rate and a homogeneous porous media had to be made, the model predicted the correct trends in propane and 1,4-dioxane concentrations.

7. The model was significantly sensitive to the biomass decay rate due to its impact on the extent of biodegradation and the time to reach 1 μg L^{-1} of contaminant for both metabolic and cometabolic bacteria. The effect on metabolic bacteria was so strong that for most of the simulation scenarios the remediation goal was not achieved within 40 years of simulation. The biomass decay coefficient, *b*, had to be adjusted to 10% of the value measured under laboratory conditions. This is justified due to the fact that *b* can be affected by environmental conditions such as low substrate concentrations. In addition, q_{CMAX} had a strong impact on the remediation

times for cometabolic bacteria. This parameter was adjusted to 50% of its laboratory determined value. The effective q_{CMAX} was reduced due to the presence of other co-contaminants that inhibit biodegradation of 1,4-dioxane. In the same manner, q_{SMAX} was reduced by 50% for CB1190 in order to maintain consistency regarding the assumption mentioned. The third most influential parameter was the biomass dispersion coefficient, which dictated the movement or spread of biomass in the simulated aquifer. Both CB1190 and ENV425 biodegradation percentages after 10 years of simulation were affected by biomass dispersion, as well as the time to reach a remediation goal of 1 μg L^{-1} for 1,4-dioxane. Other parameters that also influenced bioremediation outcomes were the permeability and porosity of the aquifer.

8. For initial concentrations of 1,4-dioxane below 10 mg L^{-1}, model simulations indicated that the time to reach a remediation goal of 1 μg L^{-1} for the propanotrophic culture was notably lower than for the CB1190. This is in agreement with the batch simulations using only the kinetic model. Metabolic biodegradation of 1,4-dioxane was not feasible at concentrations of 0.5 to 7.5 mg L^{-1}, since simulated remediation times were above 40 years. For concentrations below 0.5 mg L^{-1}, the performance of CB1190 improved but still fell behind of ENV425. When the initial concentration of 1,4-dioxane was above 10 mg L^{-1}, CB1190 outperformed ENV425 considerably. This information is key to determining which type of culture should be used for a given 1,4-dioxane plume.

9. Variations in the biomass injection rate had a greater effect on the performance of CB1190; the lowest biomass injection rates tested (8.4×10^{-8} kg COD m^2 s^{-1}) decreased the percentage of biodegradation to 77% and the highest biomass injection rate (8.4×10^{-5} kg COD m^2 s^{-1}) reduced the time to reach 1 µg L^{-1} of 1,4-dioxane to 4.5 years. On the other hand, ENV425 was not significantly affected by the biomass injection rate because the performance of cometabolism depended more on the addition of propane.

10. The oxygen injection rate had a greater impact on CB1190 compared to ENV425 although both cultures were affected by the lowest injection rate evaluated. CB1190 was more susceptible to changes in dissolved oxygen concentration because of its lower affinity to oxygen as indicated by O_{SMIN} and K_{SO}.

11. Increasing the propane injection rate reduced the remediation times to 2.1 years, although this effect plateaued when the injection rate reached 1.77×10^{-4} kg COD m^2 s^{-1}. Similarly, the extent of biodegradation after 10 years fell to 56% when the injection of propane was decreased to 3.54×10^{-7} kg COD m^2 s^{-1}. These results indicate that the propane injection rate applied at VAFB was in excess and ensured that biodegradation of 1,4-dioxane occurred within 10 years.

12. The groundwater-contaminant transport model constitutes a framework that can be used to determine bioremediation strategies involving metabolic or cometabolic biodegradation of 1,4-dioxane. The information gained from the model simulations under different environmental conditions indicated that the use of cometabolic bacteria is more advantageous for dilute plumes of 1,4-dioxane and that adequate

injection of primary growth substrate is essential to ensure proper performance. On the other hand, metabolic biodegradation should be used for higher concentration plumes of 1,4-dioxane and adequate amounts of biomass should be injected to prevent the decay rate from overcoming growth. In both strategies, adequate injection rates of oxygen should be procured to achieve remediation goals in an acceptable amount of time.

13. Anaerobic biodegradation of 1,4-dioxane was evaluated for microcosms prepared with groundwater and sediments from two contaminated sites. By using ^{14}C distribution data in the aqueous phase along with GC-FID monitoring data, it was determined that anaerobic biodegradation of 1,4-dioxane did not occur in any of the treatments. Partial mineralization (~10%) to CO_2 was observed in some of the treatments amended with oxygen. Microbial activity was observed in microcosms prepared for Site 1, whereas for microcosms from Site 2 no activity was observed due to inhibition by high levels of DCM. For microcosms from Site 2 with reduced levels of DCM, biological activity was detected. Biodegradation of DCM, IPA, and acetone as well as acetate production were observed in several microcosms. These results indicate that although biological activity was detected in most microcosms and some mineralization of 1,4-dioxane was observed when oxygen was present, anaerobic biodegradation did not occur.

Although this study provides critical information for predicting *in situ* bioremediation of 1,4-dioxane, some recommendations that could improve the body of work include:

1. The expansion of the air-sparging model to consider a transient state in which the initial gas pressure in the aquifer is zero. Although most air-sparging systems achieve steady state within a reasonable amount of time, the geological characteristics of the aquifer influence the extent and shape of the gas distribution. In addition, groundwater mounting is observed during the transient stage of air sparging and it could affect the contaminant distribution. By generating a velocity field in the water phase due to the transient changes in gas pressure, and therefore water pressure, the movement of species in the water phase would be then dominated by advection. Also, dispersion could be modeled by dispersivity and groundwater velocity. In addition the model could be converted to a 3D geometry in which gravity effects play a more important role.
2. Investigation of the transport mechanisms of biomass in porous media. Although several modeling approaches for bacteria movement in porous media exist, there is not enough quantification of these processes. On top of that, different literature sources utilize different mechanisms. Dispersion and attachment are two of the most mentioned mechanisms in which biomass movement is described. Additional evaluation by column laboratory experiments needs to be done in order to describe biomass movement in porous media for different types of bacteria cultures.

3. The contaminant transport model could be expanded to consider factors such as nutrient limitations into the growth kinetics term. In addition, batch experiments with other co-contaminants present could also bring insight on coinhibition effects on 1,4-dioxane biodegradation rates.
4. More exploration on anaerobic biodegradation of 1,4-dioxane needs to be done. Most contaminated sites with 1,4-dioxane present reducing conditions thus creating high oxygen demand making aerobic biodegradation a challenge. Variation in dose and type of amendments different to the ones used in this study could be experimented as well as the addition of different types of nutrient media.

6. APPENDICES

A. Supplementary Material for Chapter 2

A.1 Aerobic Biodegradation of 1,4-Dioxane

Table 6-1. Summary of microorganisms that utilize 1,4-dioxane as a sole source of carbon and energy.

Microorganism	**Reference**
Rhodococcus sp.	Bernhardt and Diekmann (1991)
Pseudonocardia dioxanivorans CB1190	Mahendra and Alvarez-Cohen (2006)
Pseudonocardia benzenivorans B5	Mahendra and Alvarez-Cohen (2006)
Pseudonocardia antarctica DVS 5a1	Li et al. (2010)
Mycobacterium vaccae PH-06	Kim et al. (2009)
Cordyceps sinensis	Nakamiya et al. (2005)

Table 6-2. Kinetic parameters of metabolic and cometabolic 1,4-dioxane biodegradation.

Microorganism	Growth Substrate	Half Saturation Coefficient (mg L^{-1})[a]	Maximum substrate degradation rate (mg 1,4-dioxane mg protein^{-1} h^{-1}) [b]	Reference
Pseudonocardia dioxanivorans CB1190	1,4-dioxane	160	1.09	Mahendra and Alvarez-Cohen (2006)
		-	1.98	Parales et al. (1994)
Pseudonocardia benzenivorans B5	1,4-dioxane	330	0.10	Mahendra and Alvarez-Cohen (2006)
Pseudonocardia ENV478	THF	-	0.049	Vainberg et al., (2006)
Rhodococcus ruber ENV425	THF	-	0.023	Vainberg et al., (2006)
Mixed culture	THF	12.6	0.008	Zenker et al. (2000)
Graphium sp.	THF	-	0.05	Skinner et al., (2009)
Pseudomonas mendocina KR-1	Toluene (TCA present)	0.0132	0.28	Mahendra and Alvarez-Cohen (2006)
	Toluene (DCE present)	0.0432	0.30	

[a] K_S when the growth substrate is 1,4-dioxane; K_C when the growth substrate is other than 1,4-dioxane.
[b] k_S when the growth substrate is 1,4-dioxane; k_C when the growth substrate is other than 1,4-dioxane.

A.2 Cultures growth

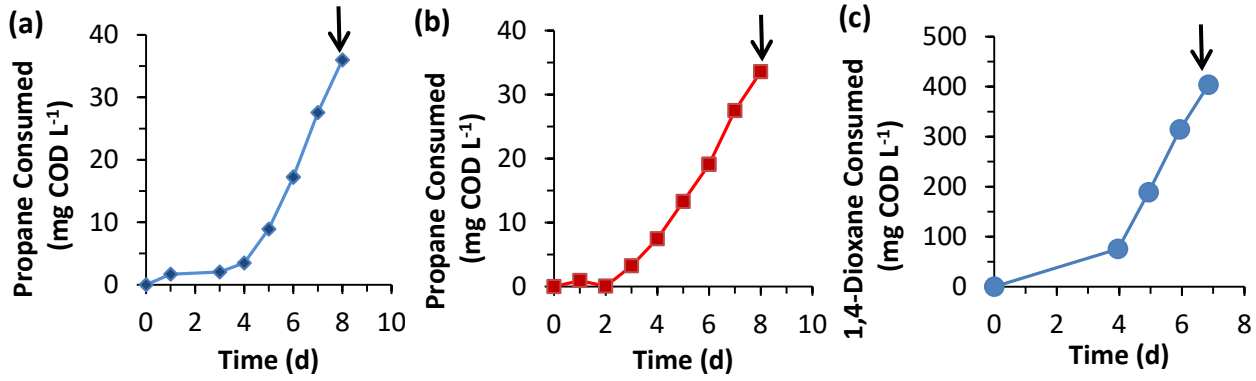

Figure 6-1. Consumption of primary growth substrate used to monitor the growth of cultures: (a) ENV425, (b) ENV487 and (c) CB1190. Arrows indicate the time when cells were harvested.

A.3 Yield

Data for biomass yield measurements is shown in Figure S.1. The plots show the biomass formed in the y-axis and the growth substrate (propane or 1,4-dioxane) consumed in the x-axis in COD units. Measurements of triplicate bottles were taken for total protein and growth substrate. Yield values for the propane-oxidizing cultures were similar and higher than the yield measured for the metabolizer CB1190.

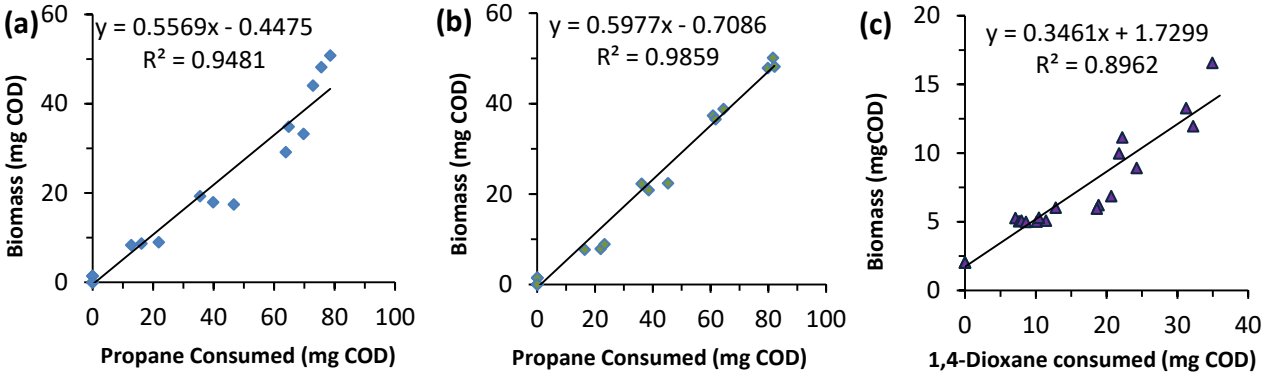

Figure 6-2. Biomass yield measurements in COD units for ENV425 (a), ENV487 (b) and CB1190 (c). The slope of the regression line corresponds to the yield value.

A.4 Endogenous decay

The endogenous decay coefficient (*b*) was obtained by plotting the natural logarithm of the oxygen uptake rates measured over different incubation days. The values were 0.11 ± 0.02, 0.14 ± 0.04, and 0.05 ± 0.01 d^{-1} for ENV425, ENV487 and CB1190, respectively. The magnitude of *b* plays an important role in biodegradation kinetics when the growth substrate is low, and could determine whether or not a microbial culture is capable of reaching contaminant goal levels.

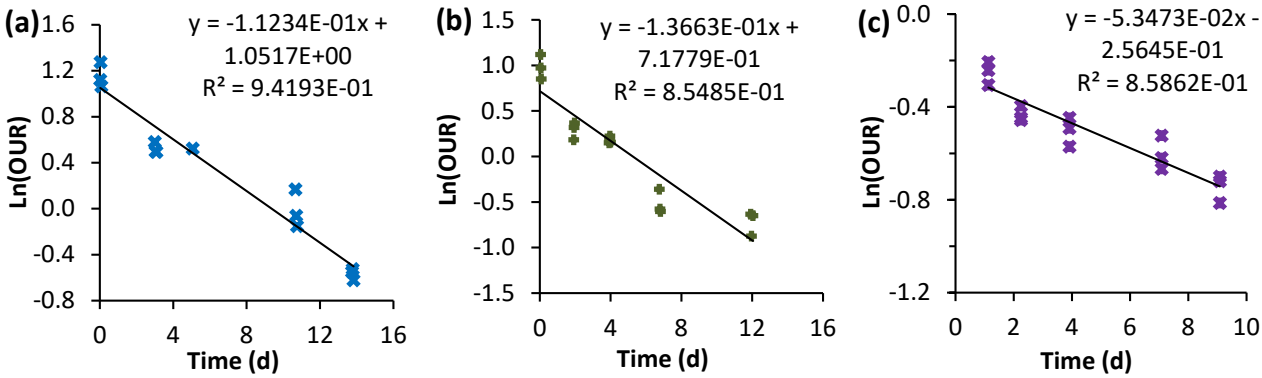

Figure 6-3. Endogenous biomass decay coefficient measurements for ENV425 (a), ENV487 (b) and CB1190 (c). Each point represents the natural logarithm of an oxygen uptake rate measured with a DO probe for periods of 20 to 4 minutes. The slope of the regression line corresponds to the b value.

A.5 Comparison of q_{SMAX} for 1,4-dioxane with Mahendra's study values

The maximum specific 1,4-dioxane biodegradation rate (q_{SMAX}) for the CB1190 obtained in this study differs significantly from the reported values in the literature. To demonstrate that the culture's performance was intrinsically unchanged and to account for environmental conditions, an experiment was designed to replicate the same conditions shown in a study by Mahendra et al. (2006) (Mahendra and Alvarez-Cohen, 2006) in which the incubation temperature was 30°C. Two treatments starting at 100 and 500 mg L^{-1} of 1,4-dioxane were set up with triplicate bottles for each treatment. The q_{SMAX} values were obtained as the average slope from the triplicates. Figure S.6 shows how the obtained q_{SMAX} values for each initial concentration are close to those obtained by the previous study. These results indicate that the variability in kinetics parameters observed for CB1190 are mainly due to environmental factors inherent to the experimental conditions of each study.

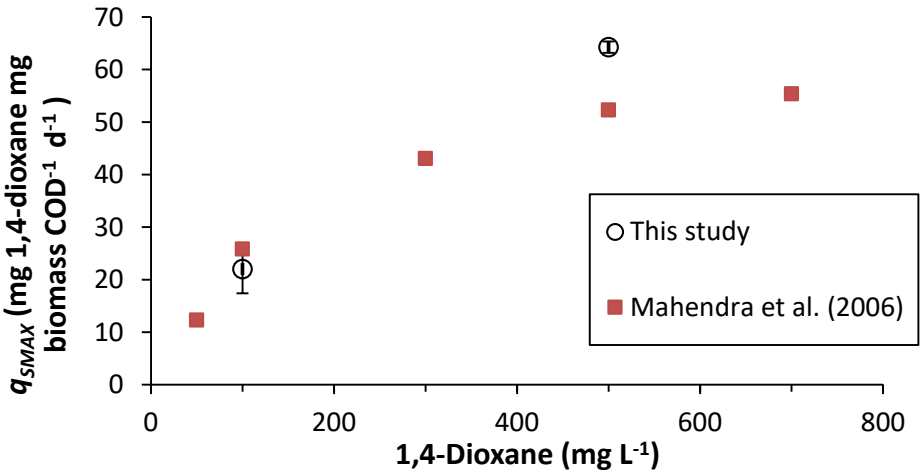

Figure 6-4. Maximum specific 1,4-dioxane utilization rates for CB1190 as a function of the initial 1,4-dioxane concentration. Filled squares are results from Mahendra's study (Mahendra and Alvarez-Cohen, 2006) whereas hollow circles represent the average value of triplicate bottles from this study incubated at 30°C. Error bars correspond to standard deviations.

A.6 Application of the Blackman Model for ENV425

Growth kinetics for the ENV425 were initially fit with a Monod model. Since model did not fit the data very well for propane concentrations below 2 mg COD L-1, the Blackman model was tested. This model is defined by the equation:

$$\frac{dS}{dt} = -q_{SMAX} \cdot \left(\frac{S}{K_S \left(1 + \frac{C}{K_{iC}}\right)} \right)^{n} \cdot \frac{O - O_{SMIN}}{K_{SO} + O - O_{SMIN}} \cdot X \qquad \text{A.1}$$

Where *n* is a power exponent that can be calibrated to adjust the model to the experimental data. This equation brings extra flexibility due to the introduction of the power exponent. Hence, the fitting of the model at low propane concentrations is improved.

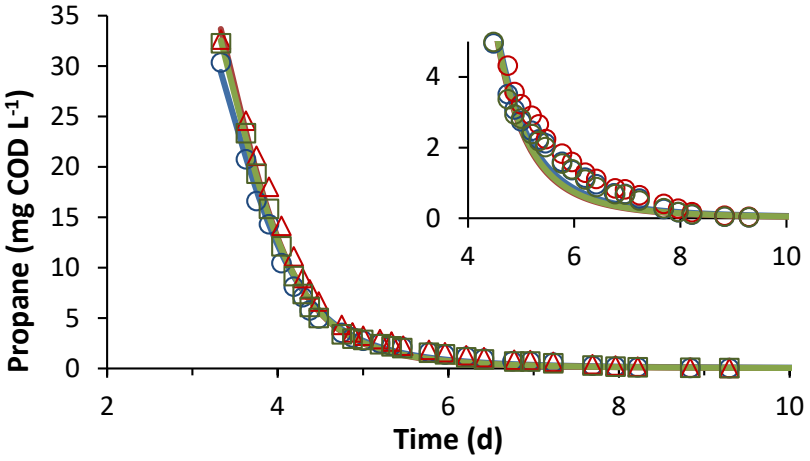

Figure 6-5. Batch depletion data for propane-oxidizing culture ENV425. Triplicate bottles were measured for propane and data was fit in Aquasim® to estimate KS with the Blackman model when oxygen was in excess and no contaminant was present. The amplified box indicates when the model fit the data adequately.

A.7 Coinhibition Experiment for ENV425

An initial data set of low batch depletion for experiments in which 1,4-dioxane and propane were simultaneously present was used to determine the co-inhibition coefficient by propane on 1,4-dioxane biodegradation (K_{iS}) for ENV425. All bottles had the same initial concentration of 1,4-dioxane of 18 mg COD L^{-1}, while initial propane concentrations varied as follows: 0, 3.6, 17, and 31 mg COD L^{-1}. Data for 1,4-dioxane depletion is matched by the fitting, although propane data did was not fit adequately.

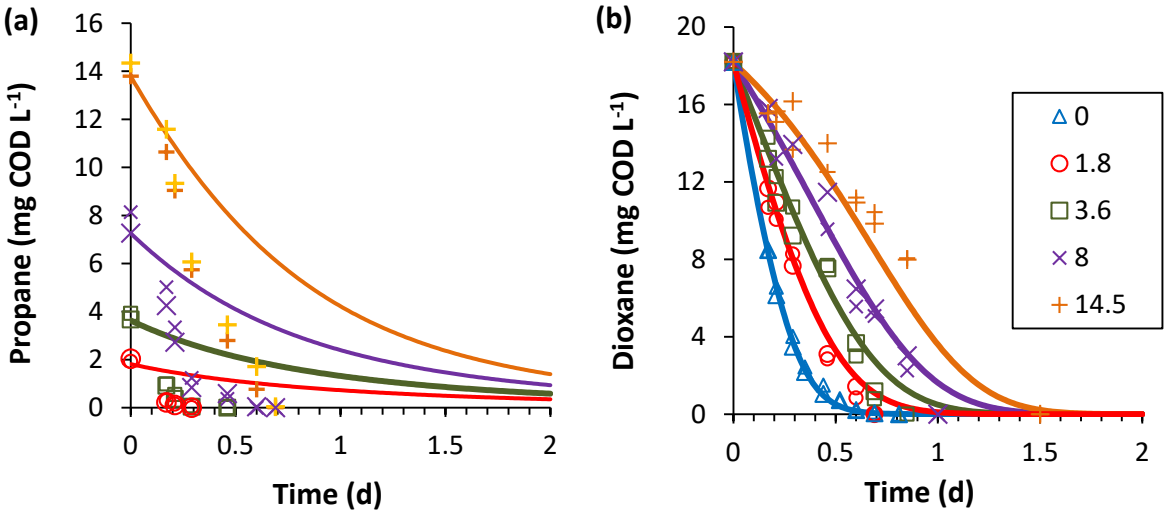

Figure 6-6. Propane (a) and 1,4-dioxane (b) depletion data for ENV425 used to estimate K_{iS}. Symbols indicate measurements for individual bottles with different initial propane concentrations.

A second data set to estimate the co-inhibition coefficient for propane presence on 1,4-dioxane cometabolism (K_{iS}) for ENV425 was obtained from batch experiments with a fixed initial 1,4-dioxane concentration of 15.8 mg COD L^{-1} and different initial propane concentrations (0, 3.6, 18.1, 36.3 and 175 mg COD L^{-1}) were prepared similarly to the experiment for ENV487. Batch depletion data for propane and 1,4-dioxane are shown in

Figure S.6. This time, consumption of propane data was also successfully fitted to the model. The estimated value for K_{iS} was 0.74 ± 0.03 mg COD L^{-1} of propane. When compared to K_{iC}, it is evident that K_{iS} demonstrates that propane has a more inhibitory effect than 1,4-dioxane. The reason is that propane-oxidizing bacteria prefer to consume propane in order to grow; once propane levels are low, the grown biomass expresses enough monooxygenase enzyme activity which results in cometabolic biodegradation of 1,4-dioxane. There is a lag in 1,4-dioxane biodegradation when propane levels approach 36.3 mg COD L^{-1}, however, which is an important fact to consider for *in situ* bioremediation of 1,4-dioxane.

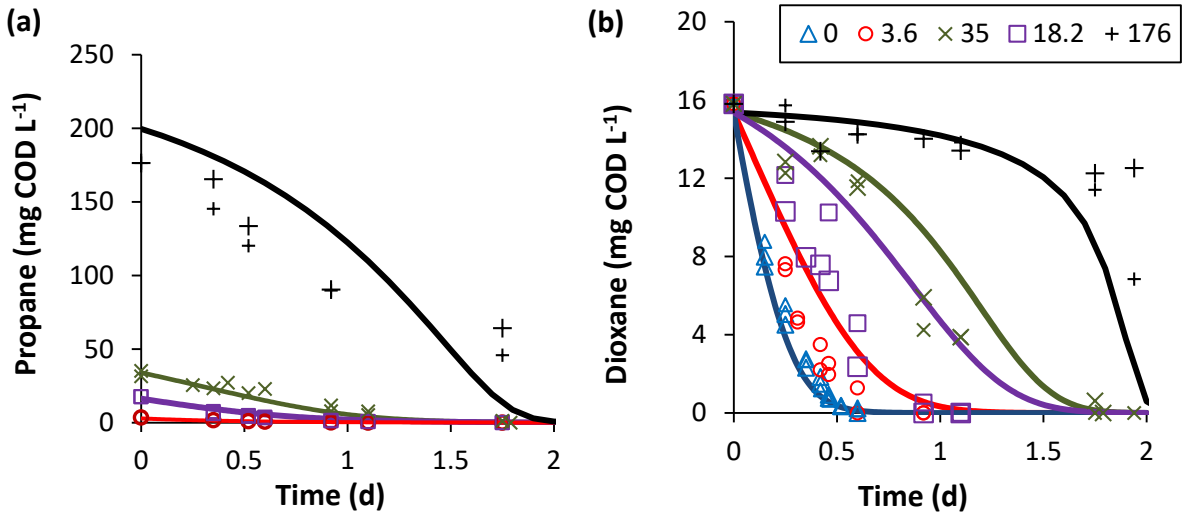

Figure 6-7. Propane (a) and 1,4-dioxane (b) depletion data for ENV425 used to estimate K_{iS}. Symbols indicate measurements for duplicate bottles with an initial propane concentration of: 0 mg COD L^{-1}, 3.6 mg COD L^{-1}, 18.1 mg COD L^{-1}, and 36.3 mg COD L^{-1} .

Batch depletion data for propane and 1,4-dioxane used to estimate the co-inhibition coefficient for 1,4-dioxane presence on propane utilization (K_{iC}) are shown in Figure S.4. Propane utilization was slightly affected when the initial concentration of 1,4-dioxane was 1,456 mg COD L^{-1}. At lower 1,4-dioxane concentrations, the effect was not significant. Both propane and 1,4-dioxane depletion data followed the model adequately.

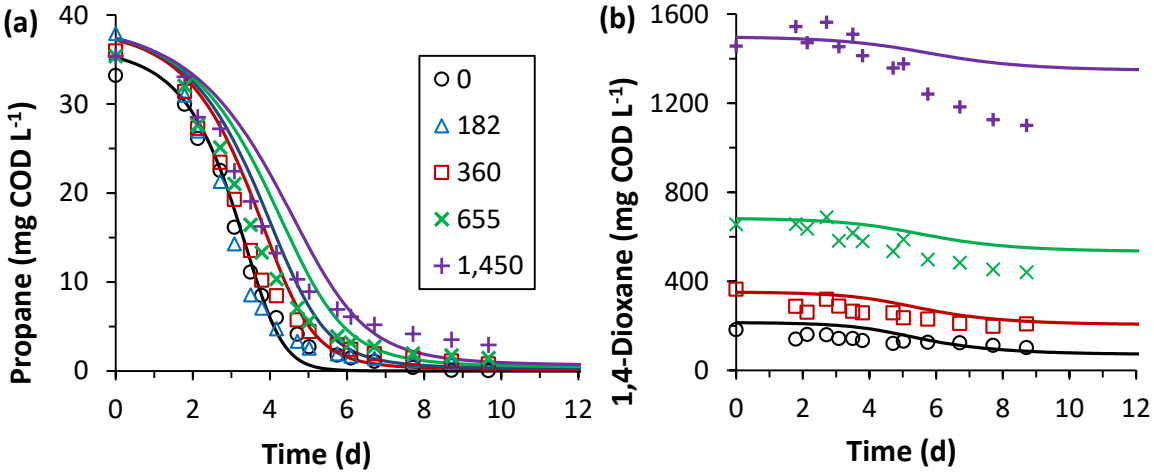

Figure 6-8. Propane (a) and 1,4-dioxane (b) depletion data for ENV425 used to estimate K_{iC}. Symbols indicate measurements for individual bottles with an initial concentration of 1,4-dioxane of: (Δ) 0 mg COD L^{-1}, (○) 182 mg COD L^{-1}, (□) 364 mg COD L^{-1}, (×) 655 mg COD L^{-1}, and (+) 1456 mg COD L^{-1}.

A.8 Oxygen saturation effects experiment for ENV425

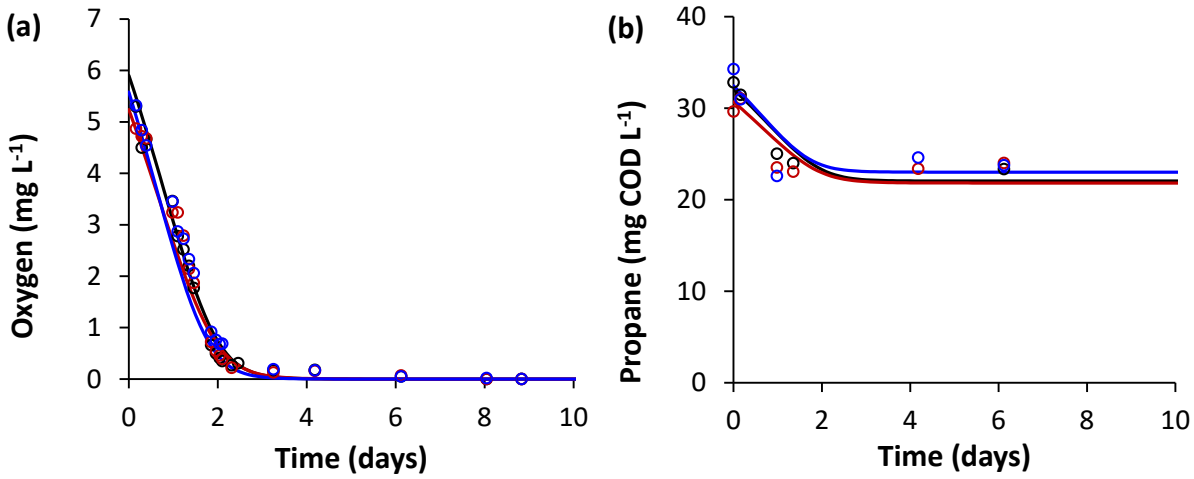

Figure 6-9. Batch depletion data for oxygen and propane concentrations to estimate K_{SO} and q_{SOMAX}. Symbols represent triplicate bottles.

A.9 Effect of decay coefficient on batch simulations for CB1190

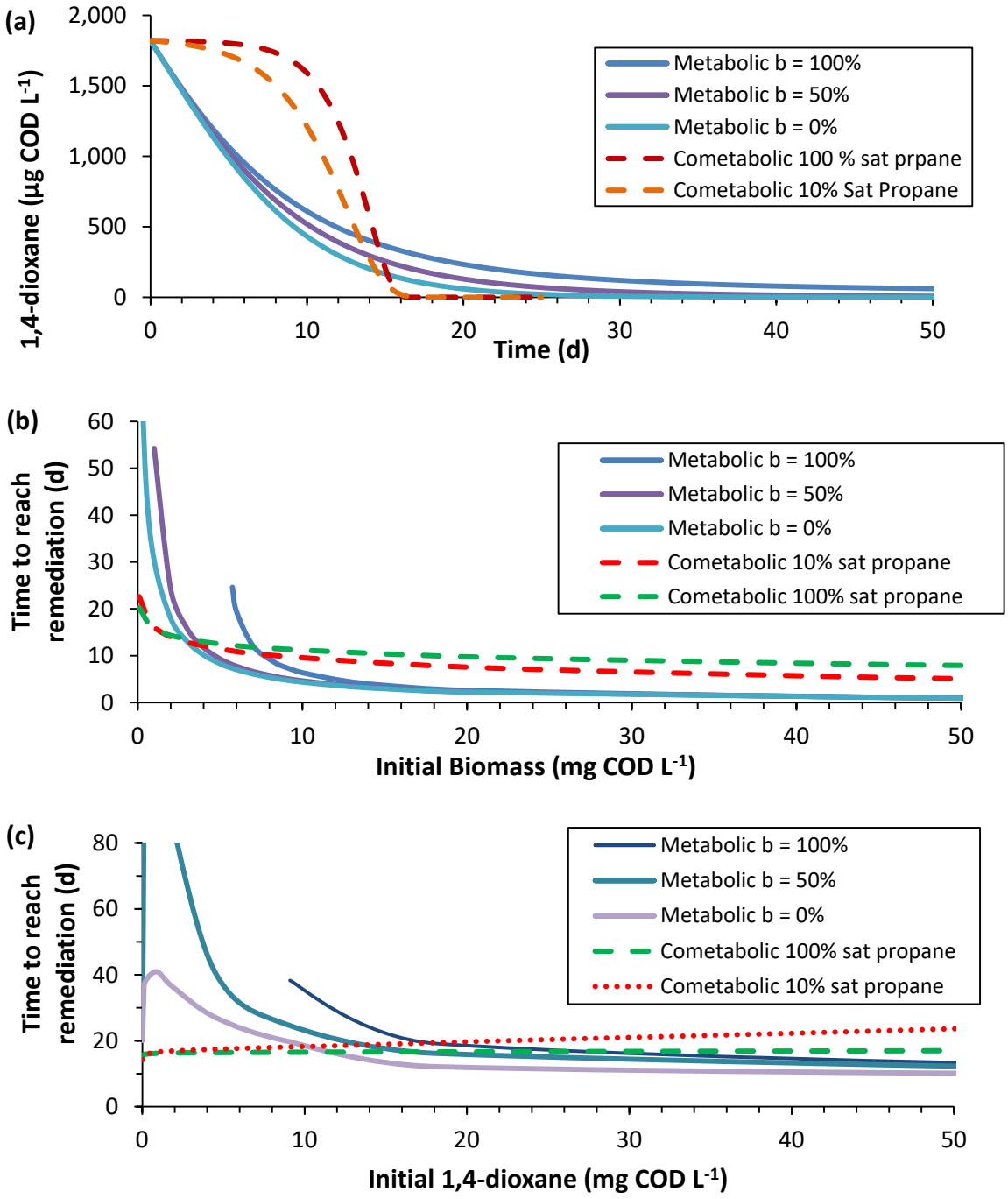

Figure 6-10. Effect of decay coefficient, b, on the performance of metabolic biodegradation of 1,4-dioxane.

B. Supplementary Material for Chapter 3

B1. Sensitivity Analysis

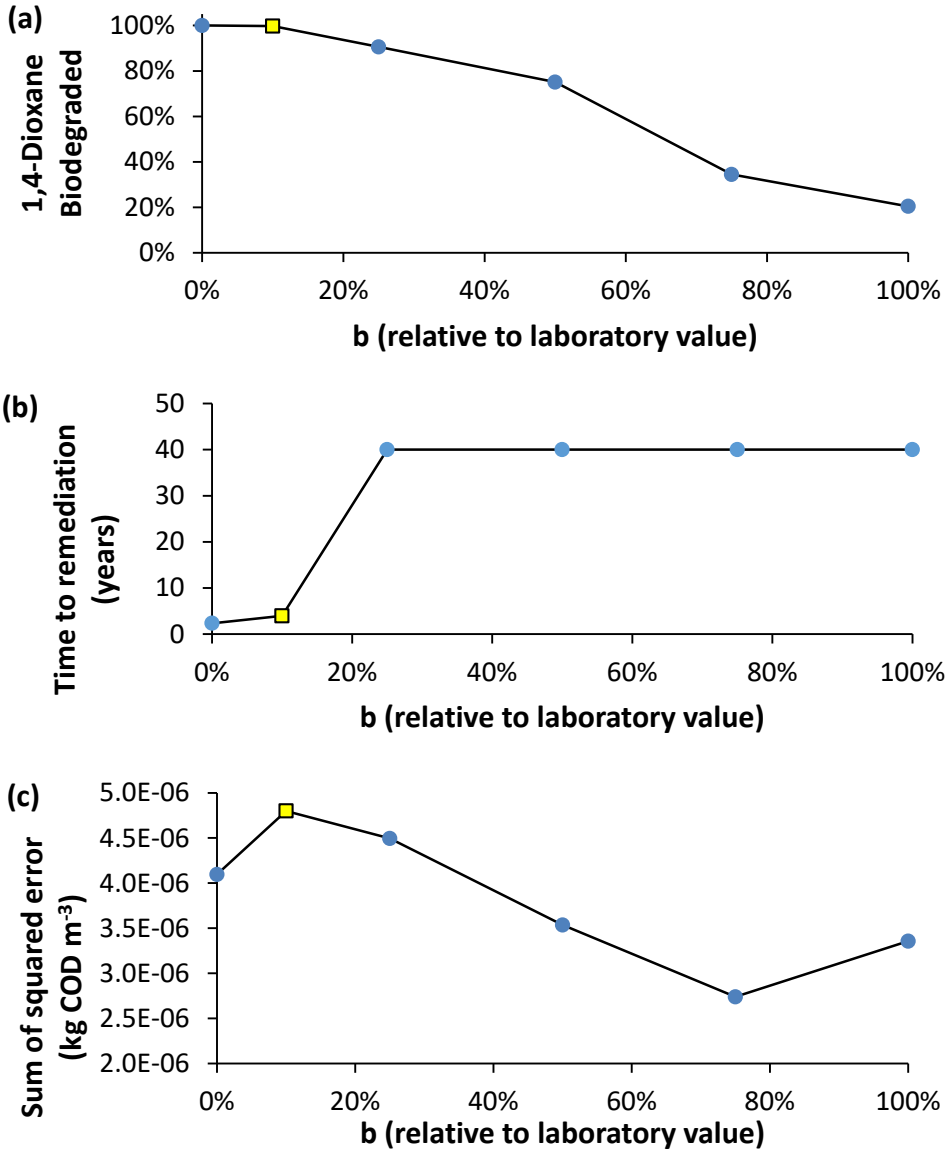

Figure 6-11. Effect of relative value of biomass decay coefficient (*b*) on 1,4-dioxane biodegradation percentage after 10 years (a), time to achieve remediation (b) and sum of squared errors (c) for ENV425. Square symbol corresponds to baseline scenario.

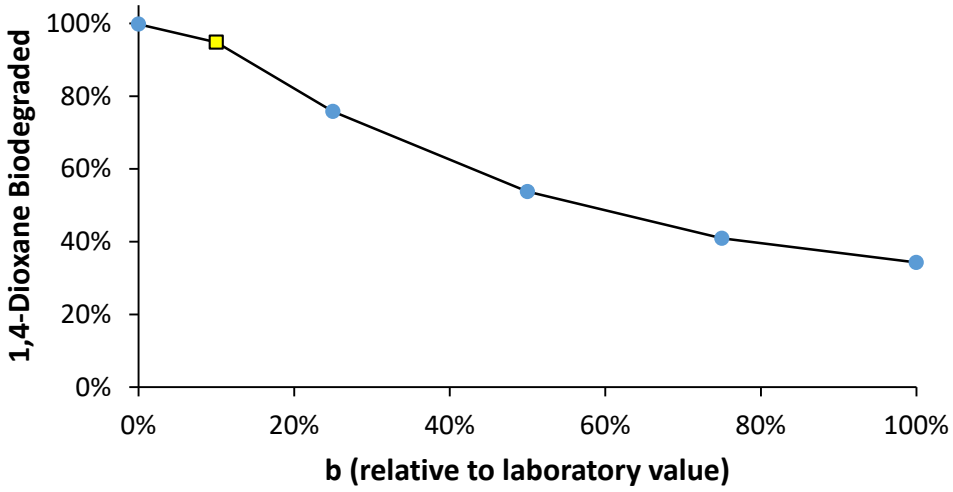

Figure 6-12. Effect of relative value of biomass decay coefficient (*b*) on 1,4-dioxane biodegradation percentage after 10 years for CB1190.

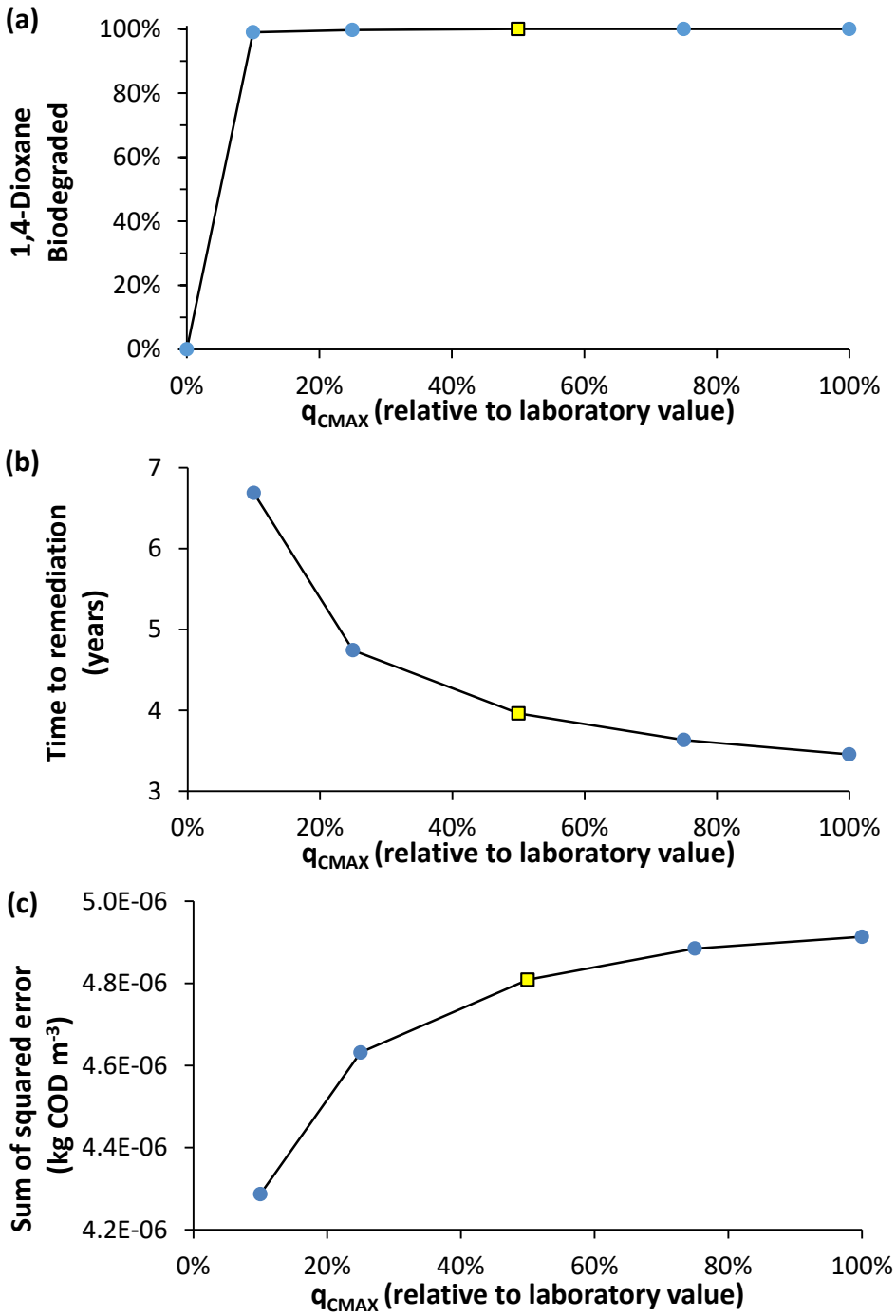

Figure 6-13. Effect of maximum specific 1,4-dioxane biodegradation rate (q_{CMAX}) on biodegradation percentage after 10 years (a), time to achieve remediation (b) and sum of squared errors (c) for ENV425.

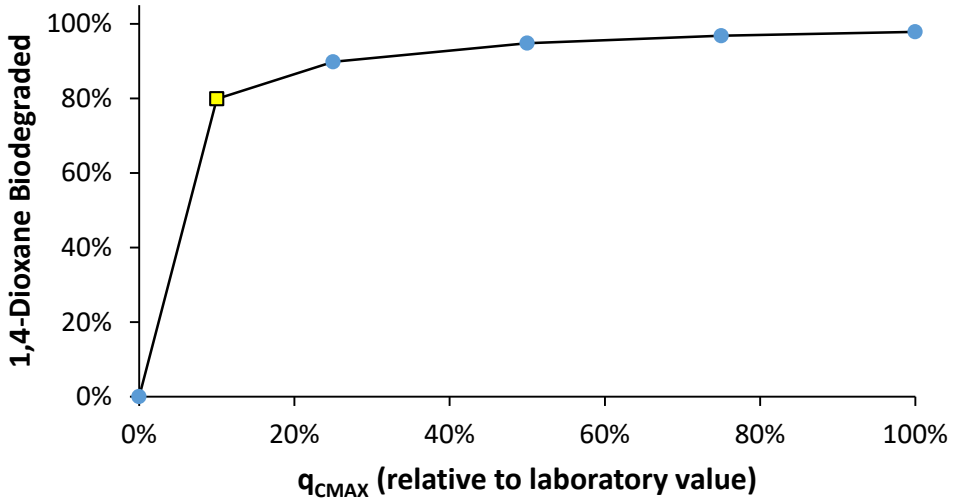

Figure 6-14. Effect of the maximum specific 1,4-dioxane biodegradation rate (q_{CMAX}) on biodegradation percentage after 10 years for CB1190.

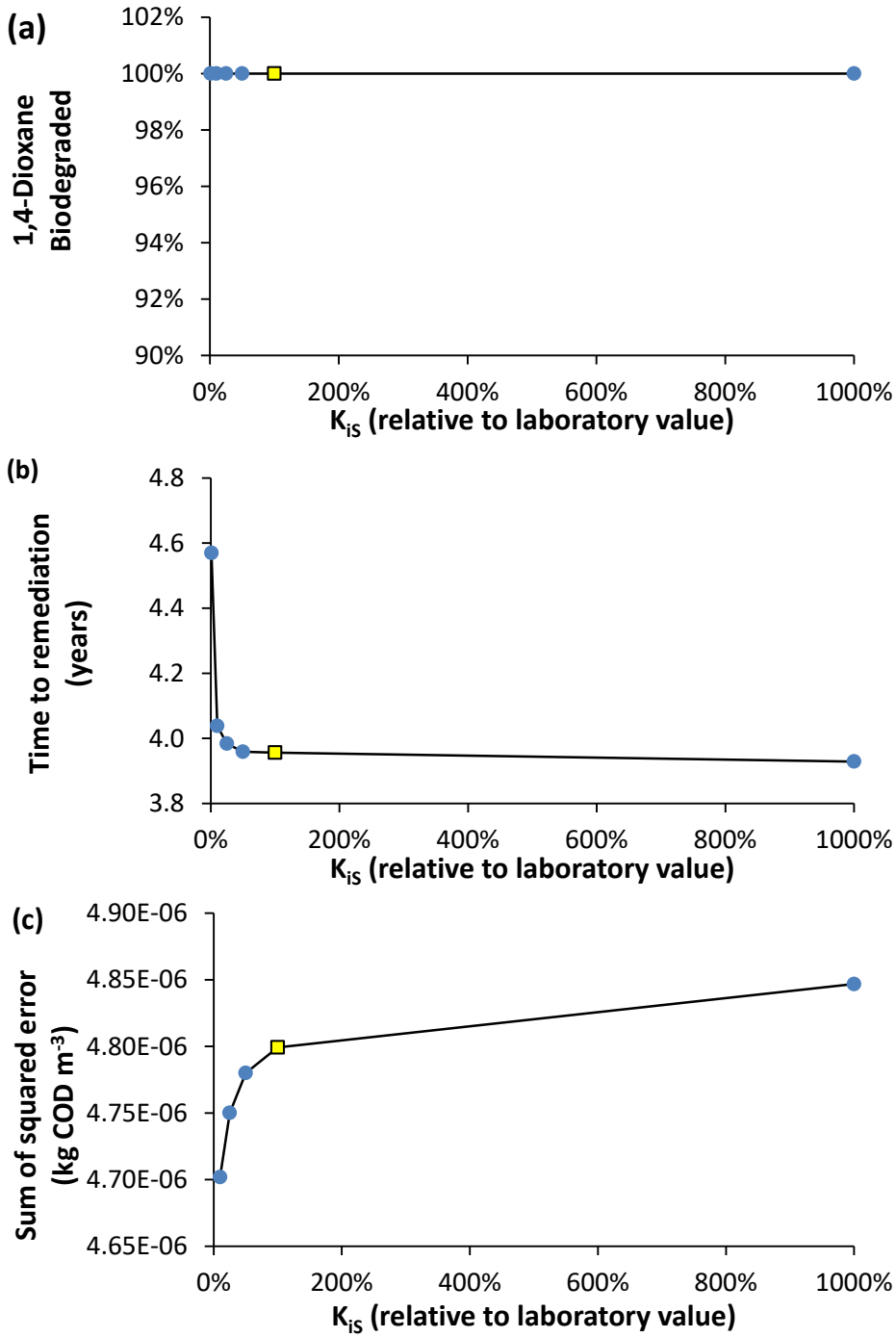

Figure 6-15. Effect of propane coinhibition coefficient (K_{iS}) on biodegradation percentage after 10 years (a), time to achieve remediation (b) and sum of squared errors (c) for ENV425.

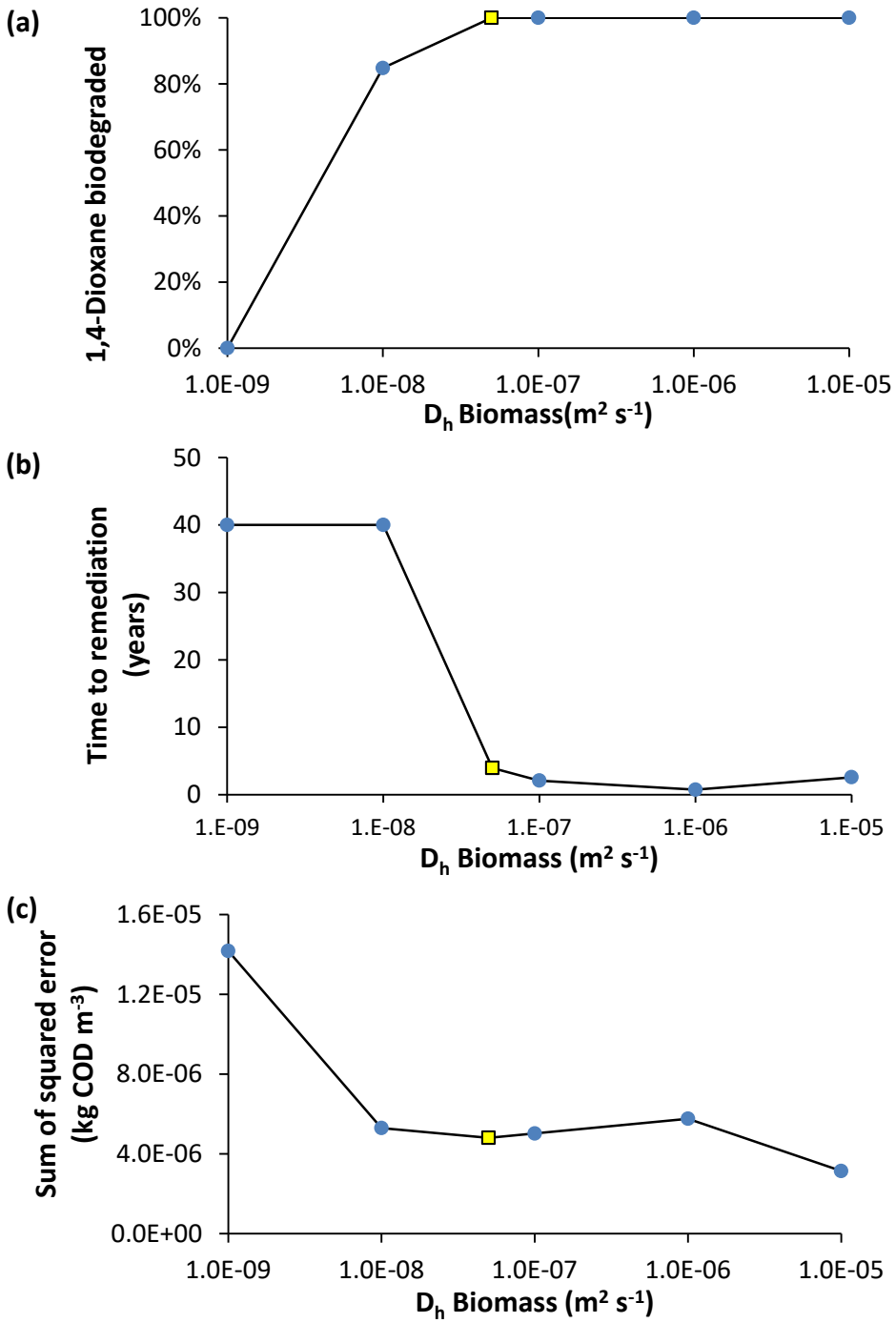

Figure 6-16. Effect of biomass dispersion coefficient in water (D_h) on biodegradation percentage after 10 years (a), time to achieve remediation (b) and sum of squared errors (c) for ENV425. Remediation times at 40 years indicate that the remediation goal was not achieved within that period.

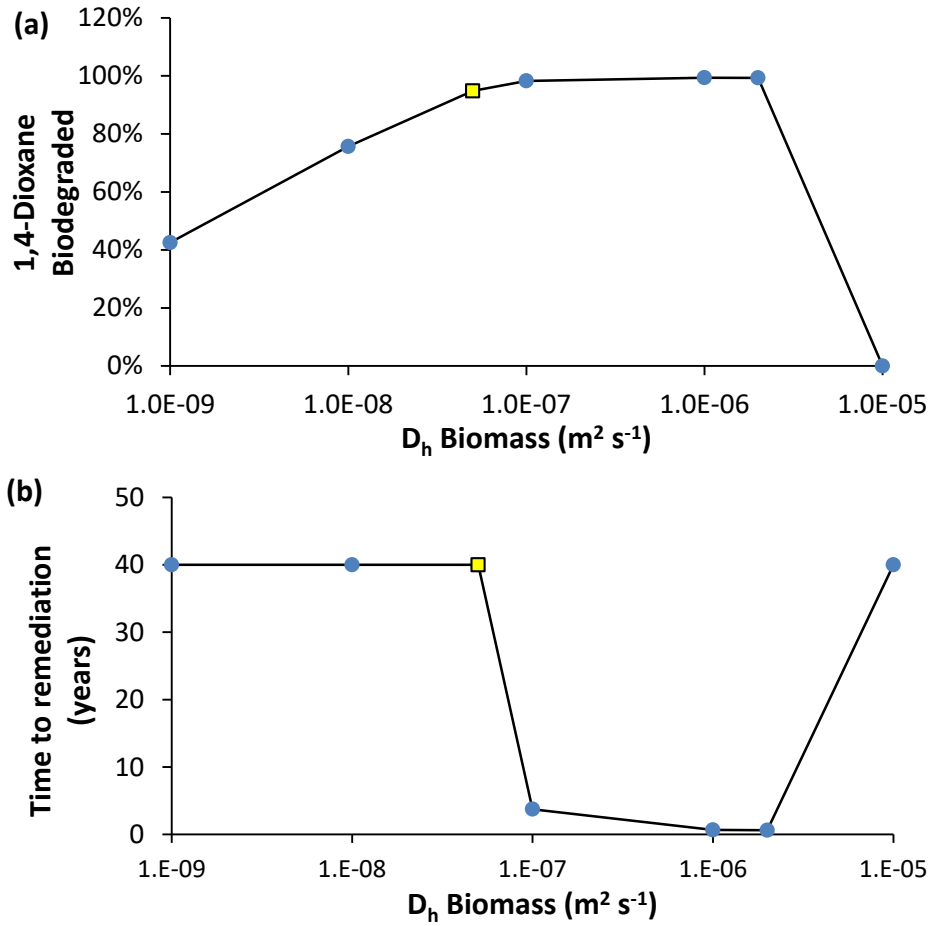

Figure 6-17. Effect of biomass dispersion coefficient in water (D_h) on biodegradation percentage after 10 years (a) and time to achieve remediation (b) for CB1190. Remediation times at 40 years indicate that the remediation goal was not achieved within that period.

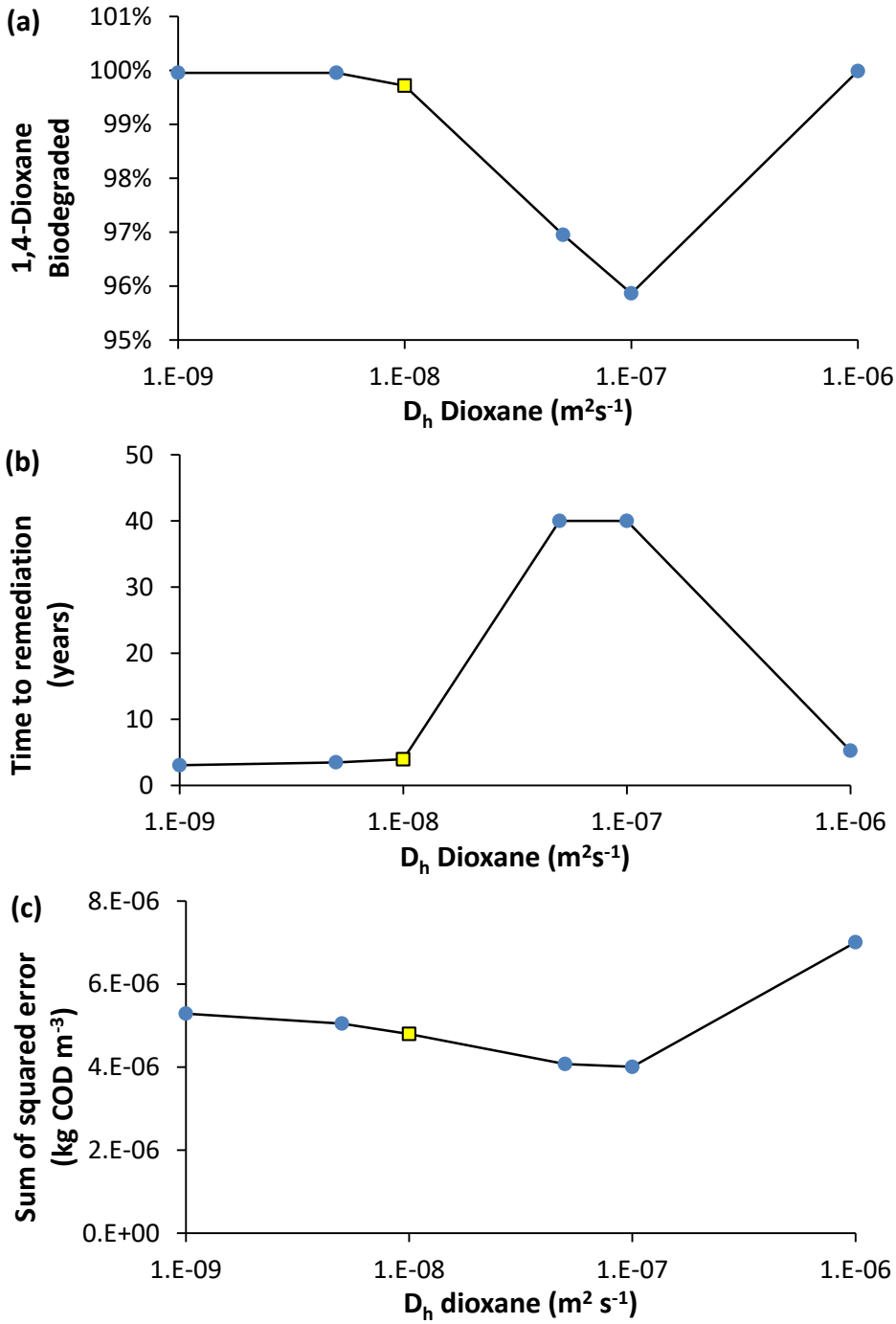

Figure 6-18. Effect of 1,4-dioxane dispersion coefficient (D_h) on biodegradation percentage after 10 years (a), time to achieve remediation (b), and sum of squared errors (c) for ENV425. Remediation times at 40 years indicate that the remediation goal was not achieved within that period.

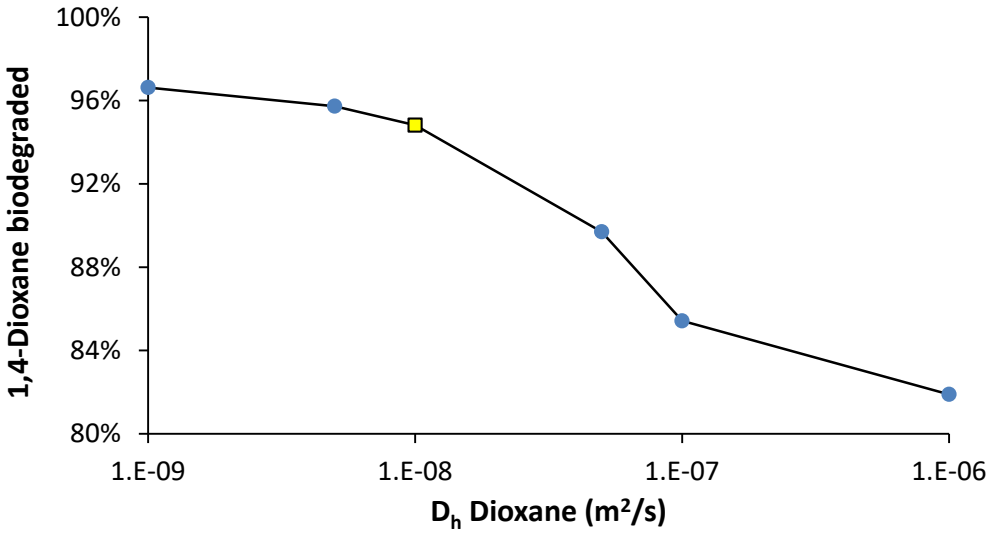

Figure 6-19. Effect of 1,4-dioxane dispersion coefficient (D_h) on biodegradation percentage after 10 years for CB1190.

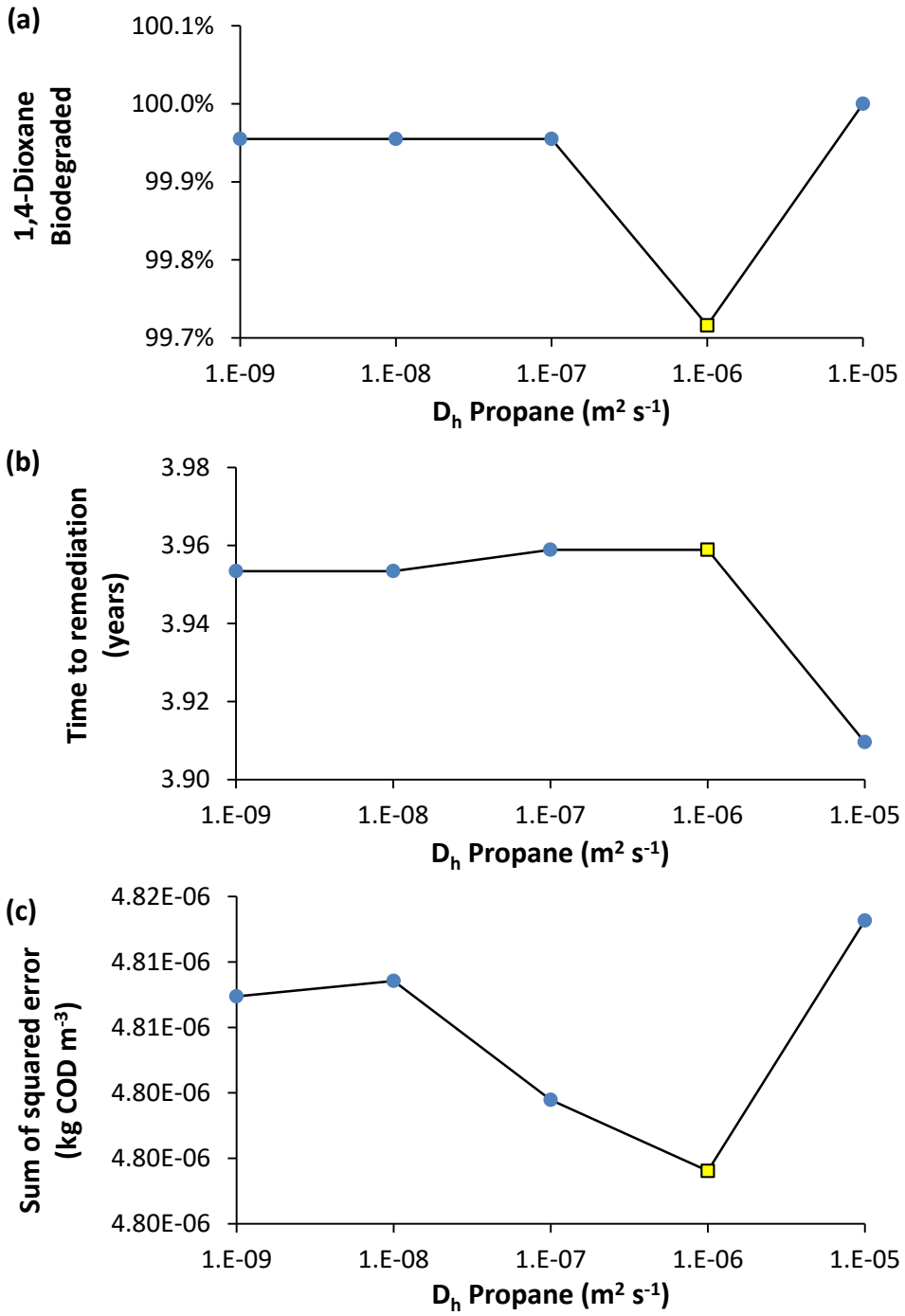

Figure 6-20. Effect of propane dispersion coefficient (D_h) on biodegradation percentage after 10 years (a), time to achieve remediation (b), and sum of squared errors (c) for ENV425.

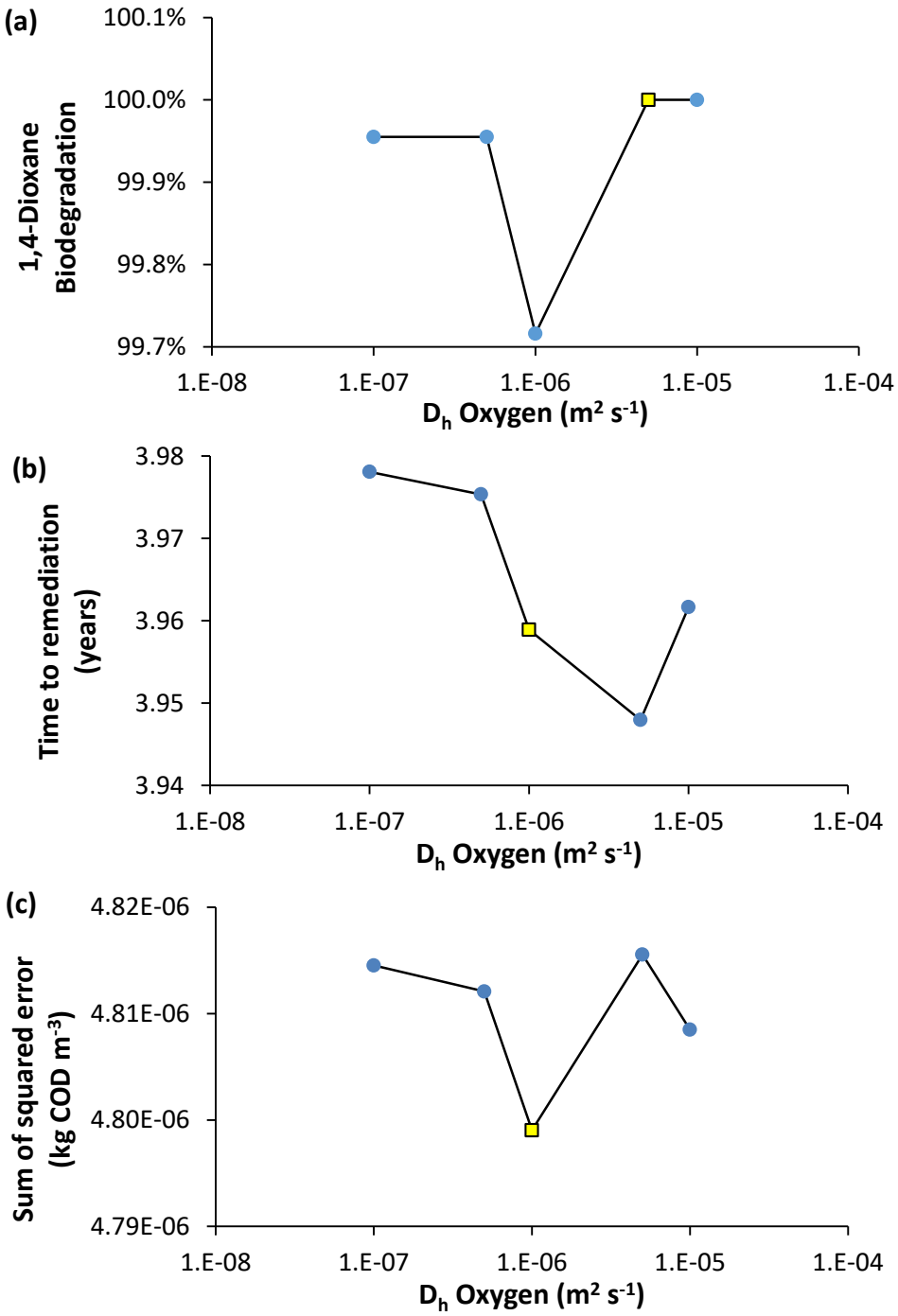

Figure 6-21. Effect of oxygen dispersion coefficient (D_h) on biodegradation percentage after 10 years (a), time to achieve remediation (b), and sum of squared errors (c) for ENV425.

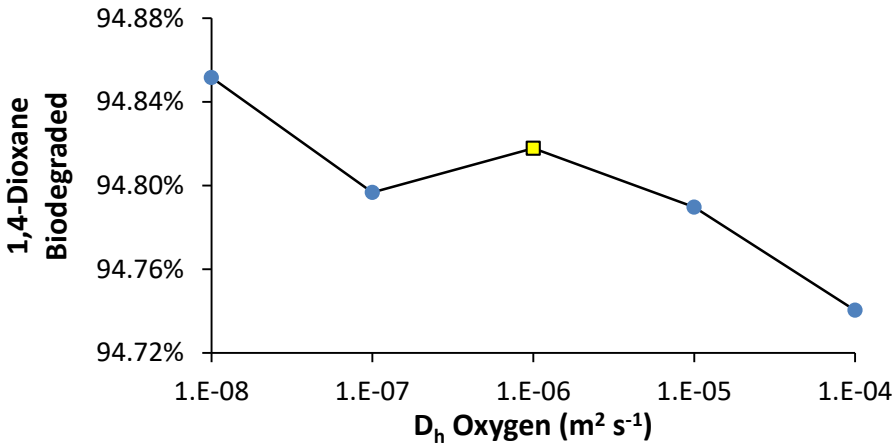

Figure 6-22. Effect of oxygen dispersion coefficient (D_h) on biodegradation percentage after 10 years for CB1190.

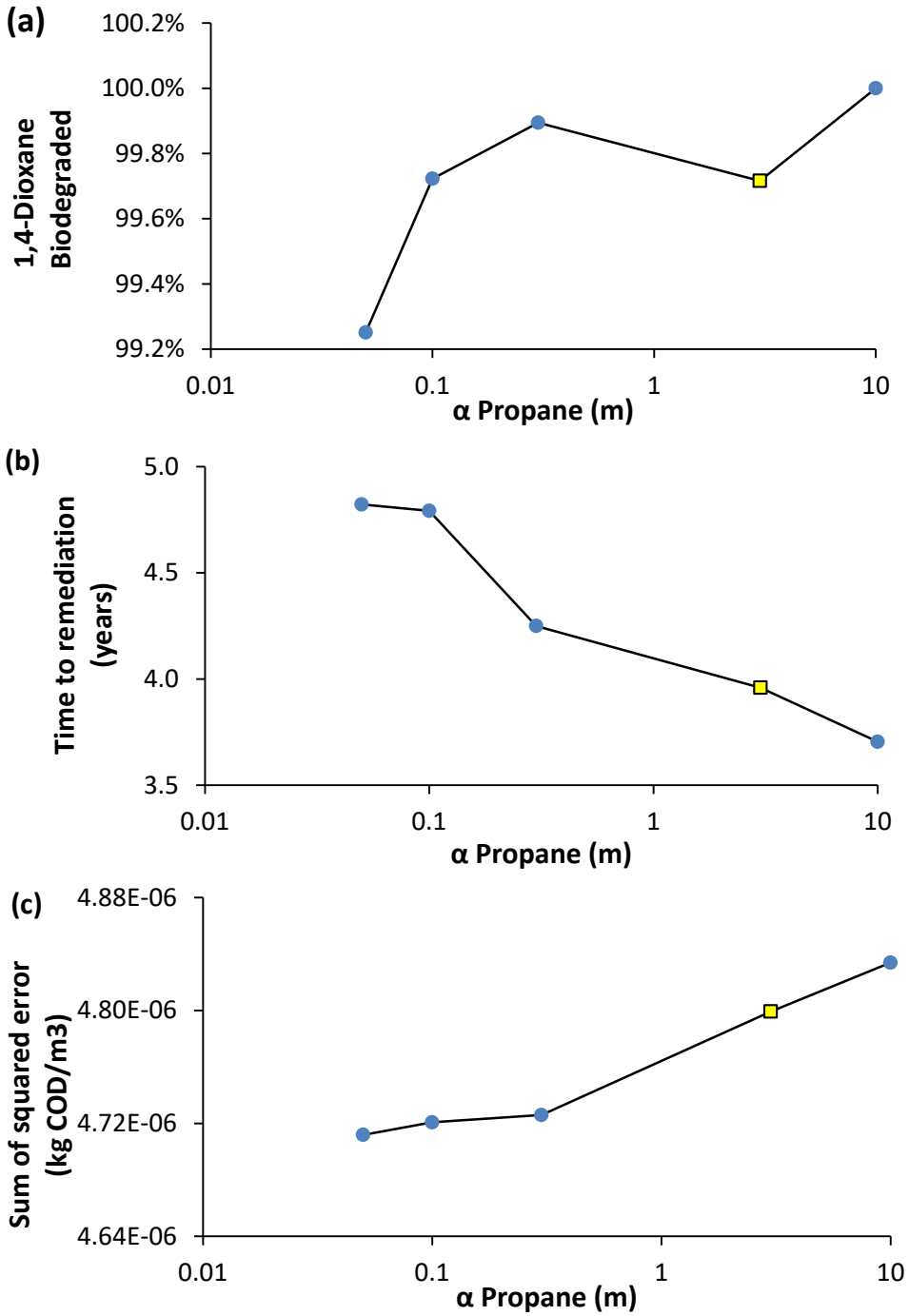

Figure 6-23. Effect of propane dispersivity in the gas phase (α) on biodegradation percentage after 10 years (a), time to achieve remediation (b), and sum of squared errors (c) for ENV425.

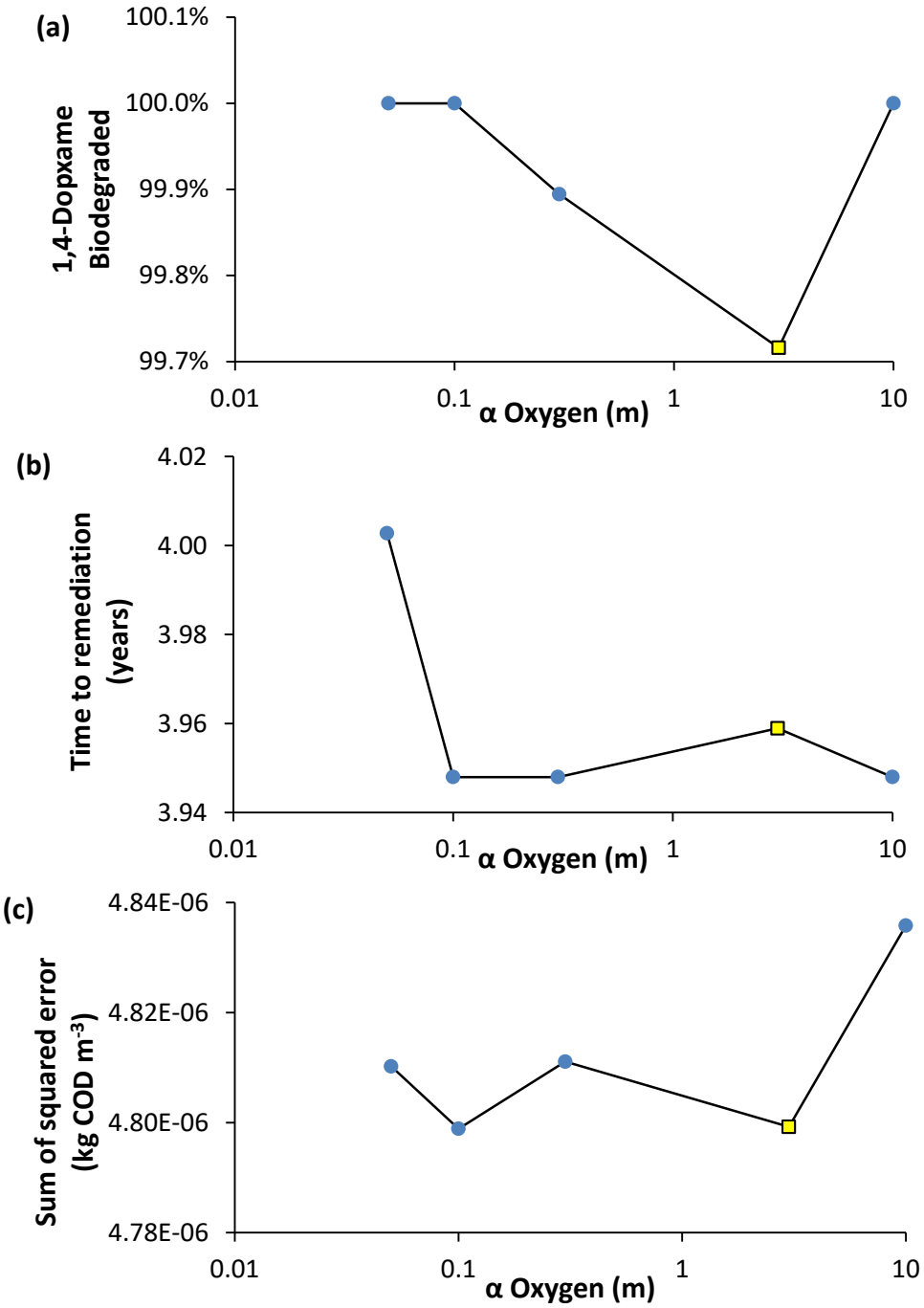

Figure 6-24. Effect of oxygen dispersivity in the gas phase (α) on biodegradation percentage after 10 years (a), time to achieve remediation (b), and sum of squared errors (c) for ENV425.

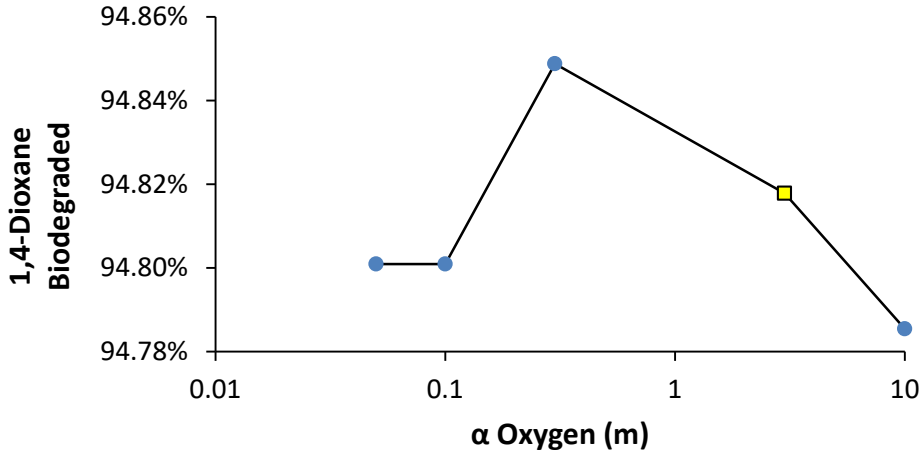

Figure 6-25. Effect of oxygen dispersivity in the gas phase (α) on biodegradation percentage after 10 years for CB1190.

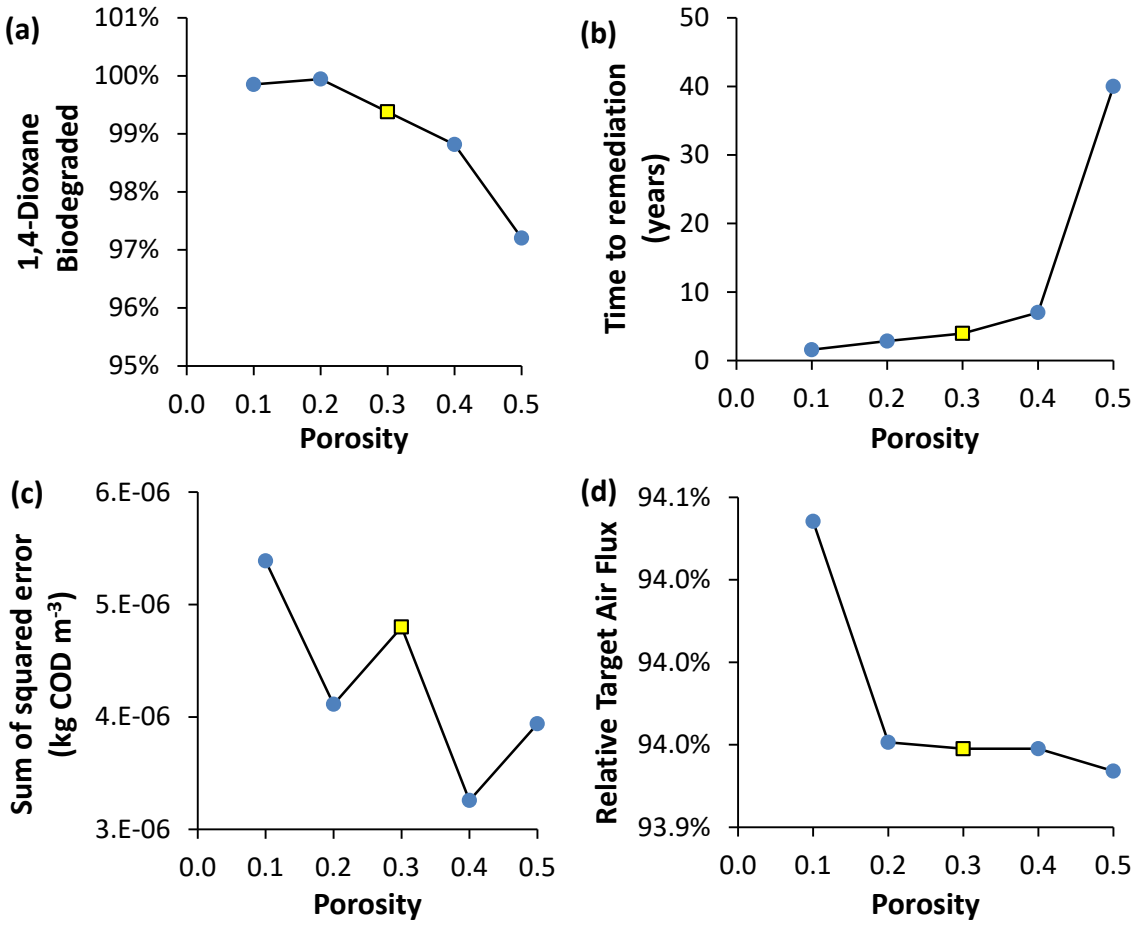

Figure 6-26. Effect of porosity on biodegradation percentage after 10 years (a), time to achieve remediation (b), sum of squared errors (c) and the air flux percentage relative to the base value (d) for ENV425.

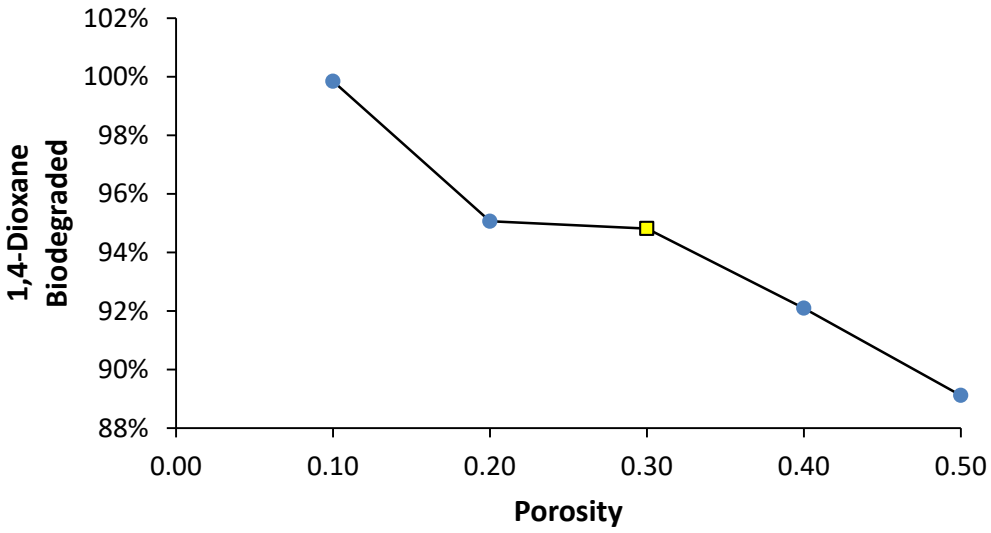

Figure 6-27. Effect of porosity on biodegradation percentage after 10 years for CB1190.

C. Supplementary Material for Chapter 4

C1. ^{14}C Monitoring results

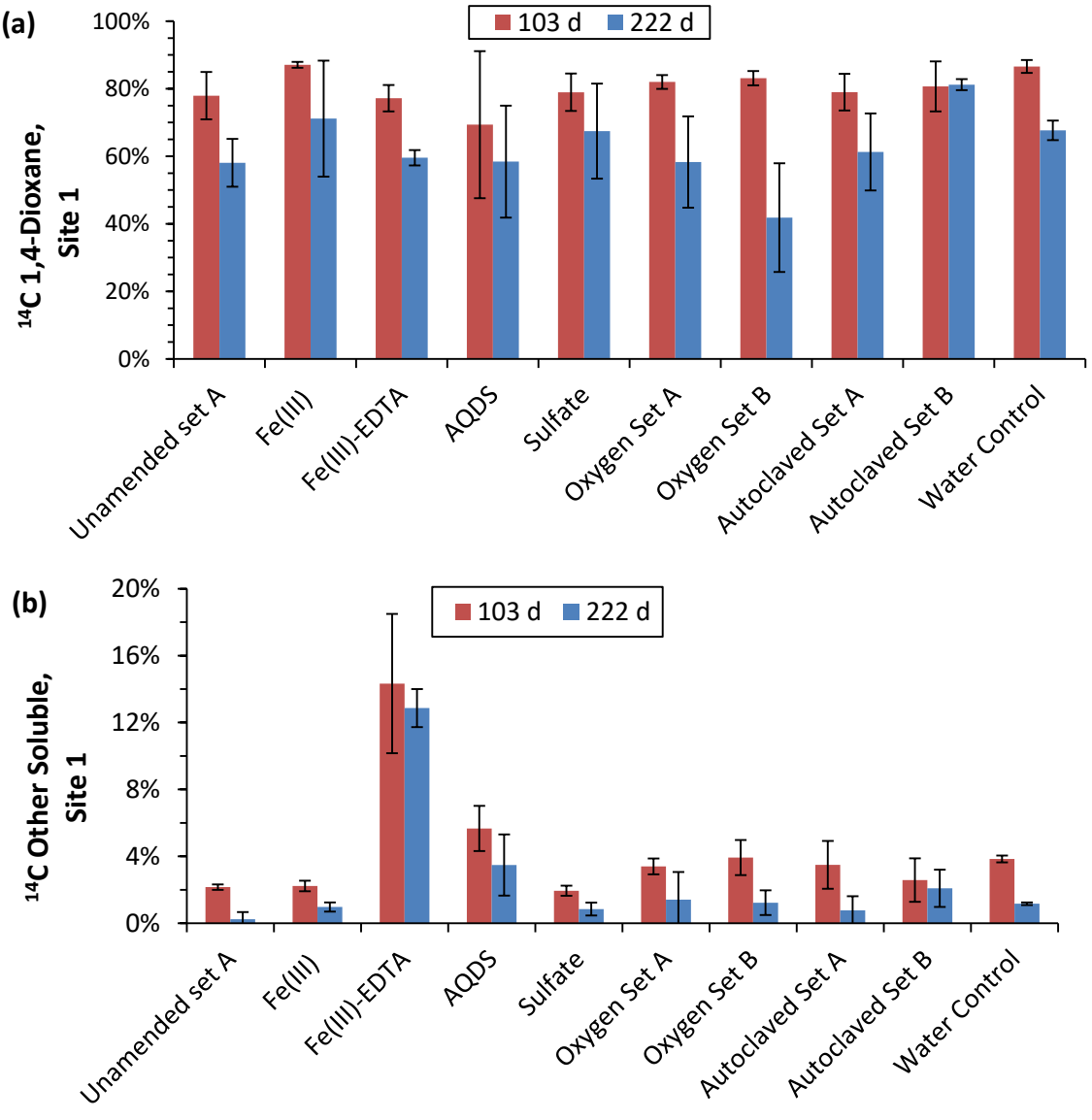

Figure 6-28. Percentage ^{14}C material corresponding to 1,4-dioxane (a) and other soluble compounds (b) with respect to the initial amount of ^{14}C added in small microcosms from Site 1, measured on days 103 and 222. Error bars represent the standard deviations from triplicate measurements.

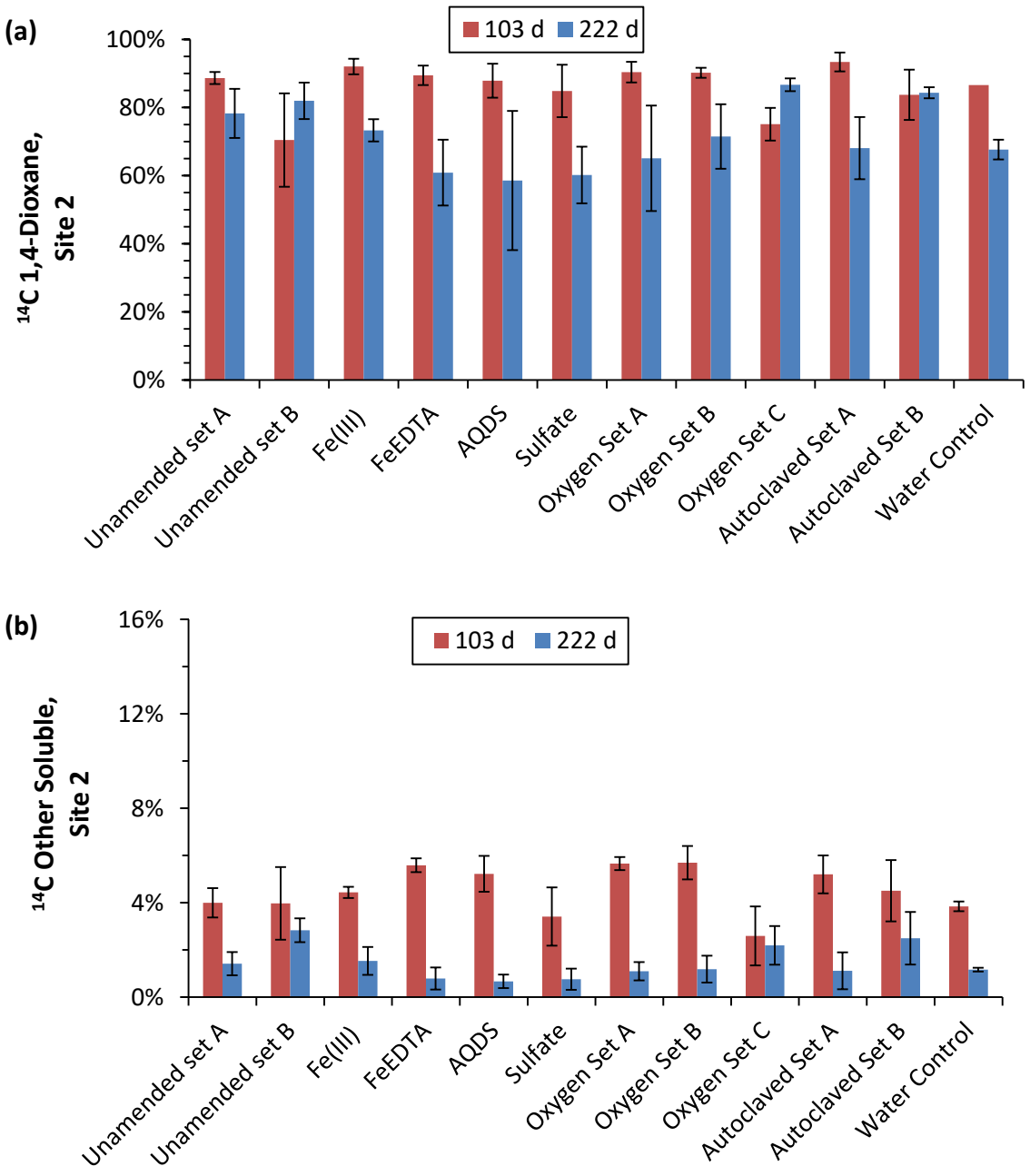

Figure 6-29. Percentage ^{14}C material corresponding to 1,4-dioxane (a) and other soluble compounds (b) with respect to the initial amount of ^{14}C added in small microcosms from Site 2, measured on days 103 and 222. Error bars represent the standard deviations from triplicate measurements.

C2. GC monitoring of VOCs

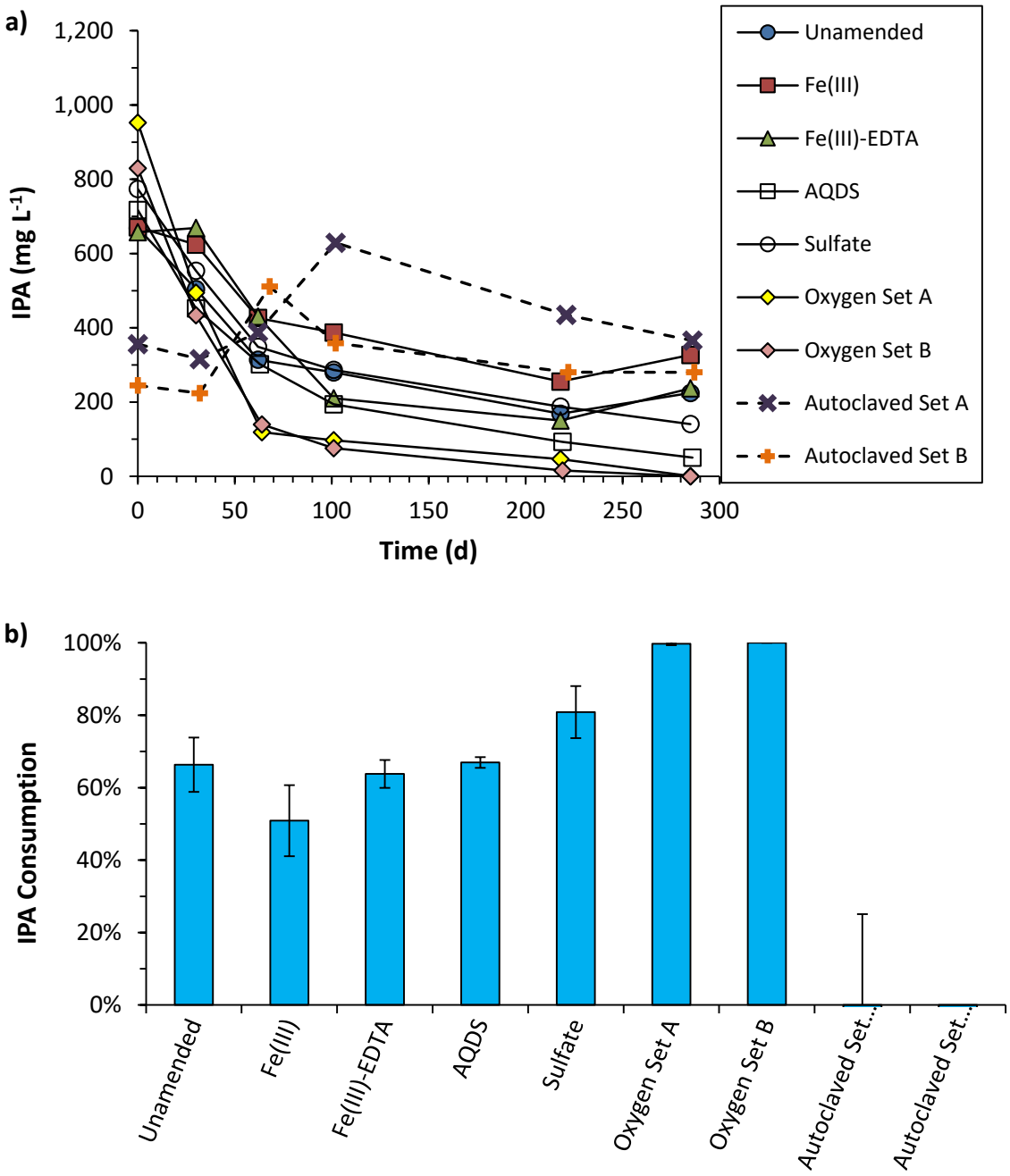

Figure 6-30. IPA concentration over time (a) and percent decreases at the end of incubation (b) for Site 1; averages of triplicate microcosms; error bars represent one standard deviation.

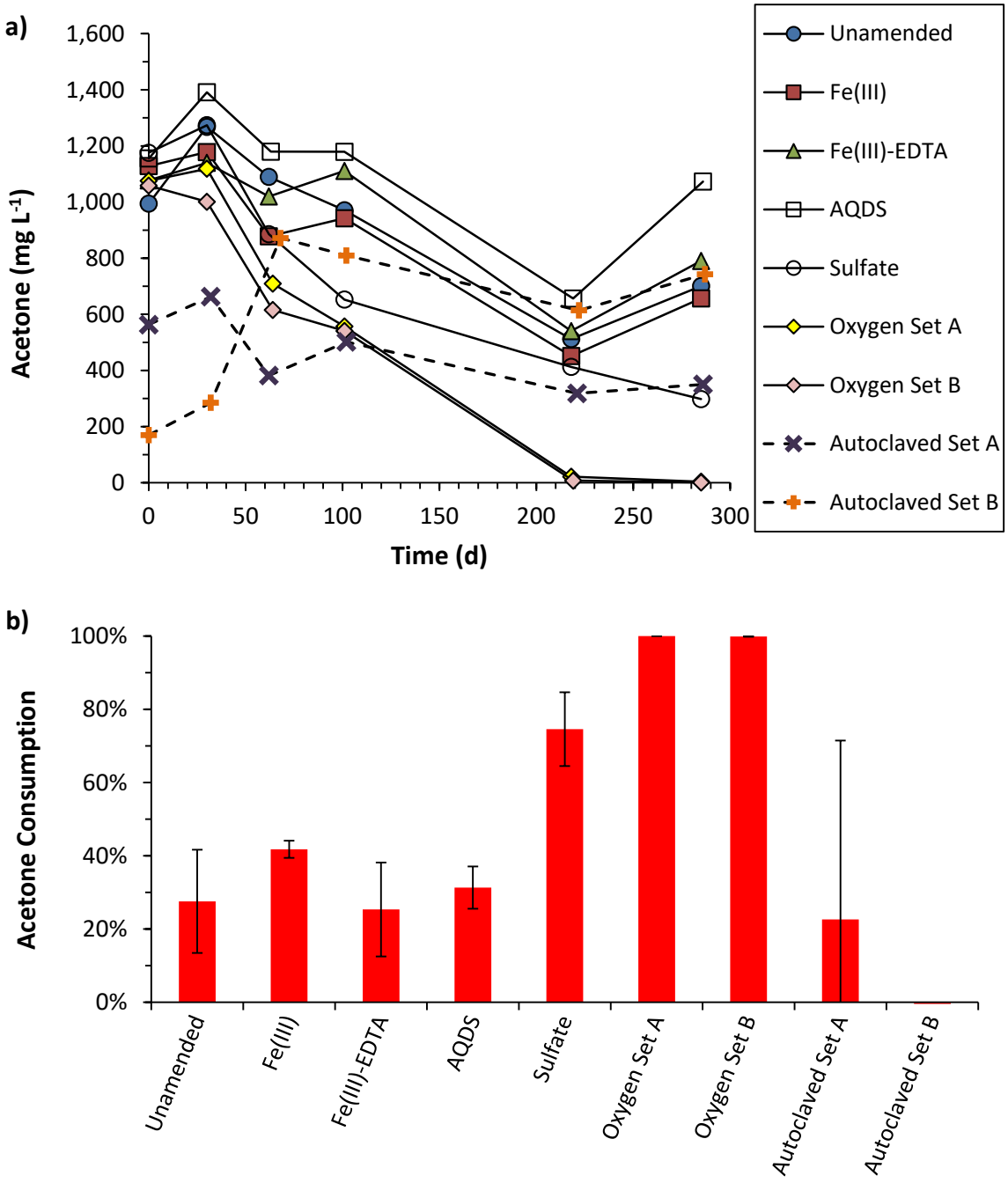

Figure 6-31. Acetone concentration over time (a) and percent decreases at the end of incubation (b) for Site 1; averages of triplicate microcosms; error bars represent one standard deviation.

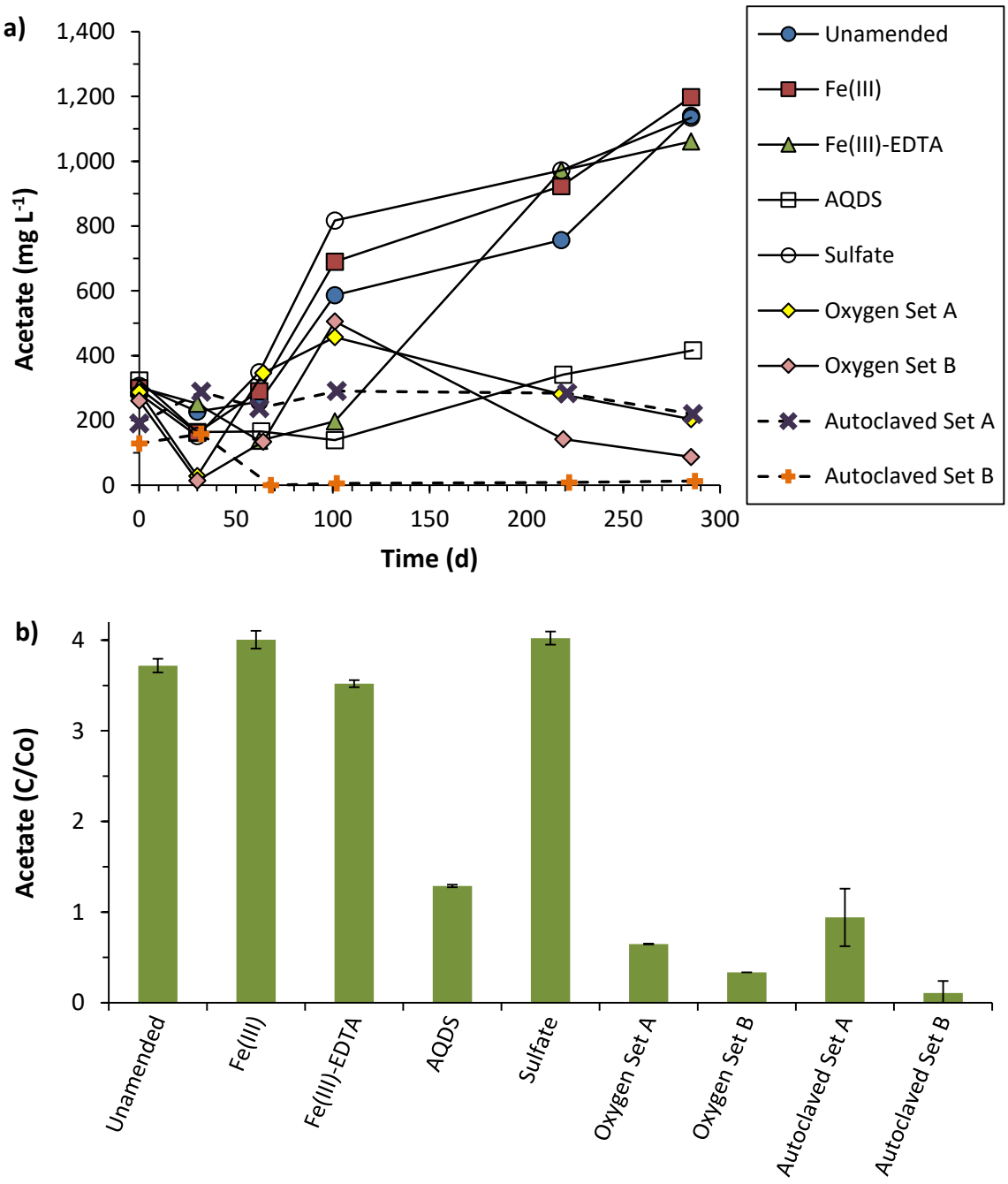

Figure 6-32. Acetate concentration over time (a) and the ratio of final to initial acetate concentration (b) in live microcosms, for Site 1; averages of triplicate microcosms; error bars represent one standard deviation.

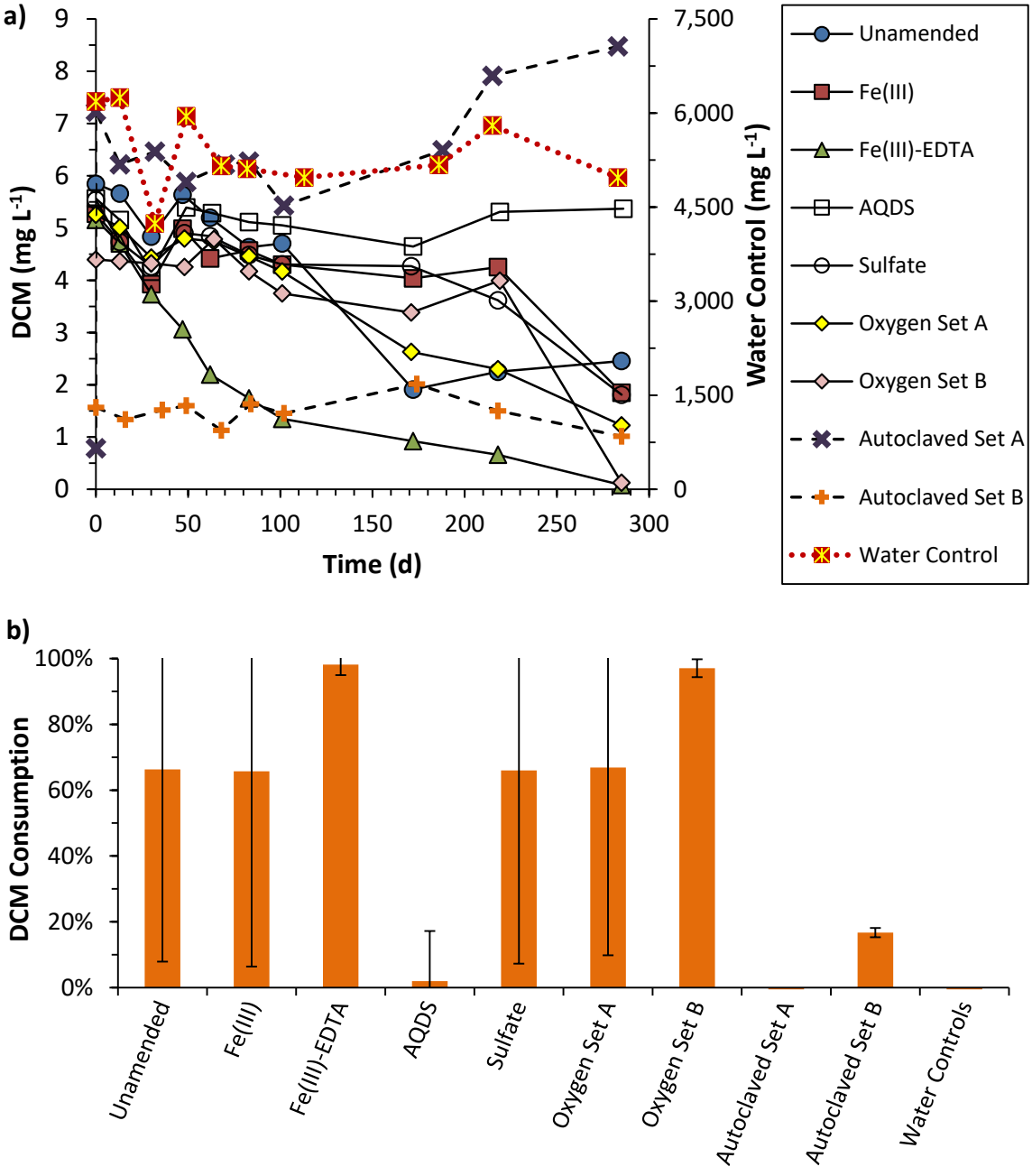

Figure 6-33. Average DCM concentration for triplicate microcosms (a) and percent decrease (b) for Site 1; averages of triplicate microcosms; error bars represent one standard deviation.

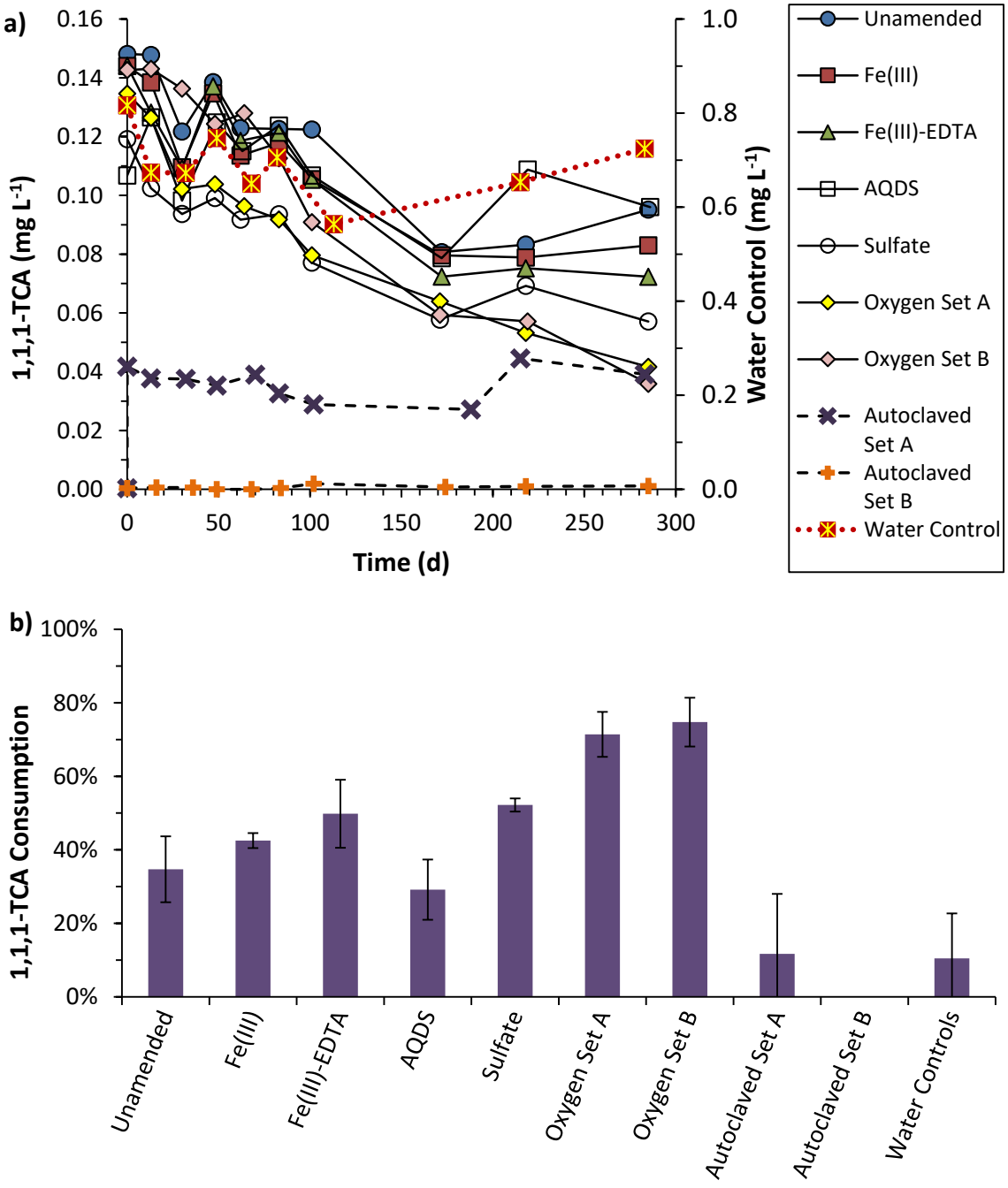

Figure 6-34. Average 1,1,1-TCA concentration for triplicate microcosms (a) and percent decrease (b) for Site 1; averages of triplicate microcosms; error bars represent one standard deviation.

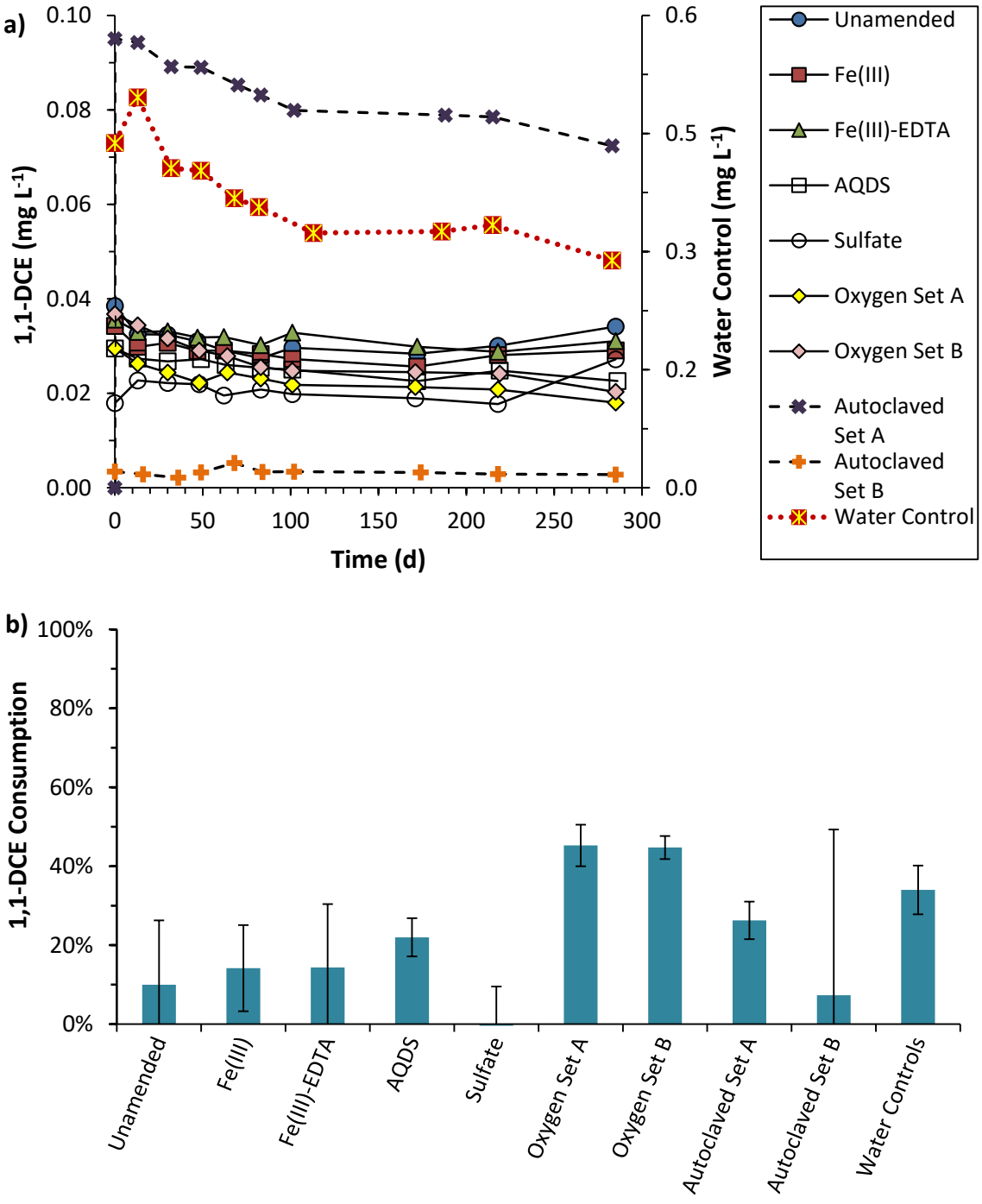

Figure 6-35. Average 1,1-DCE concentration for triplicate microcosms (a) and percent decrease (b) for Site 1; averages of triplicate microcosms; error bars represent one standard deviation.

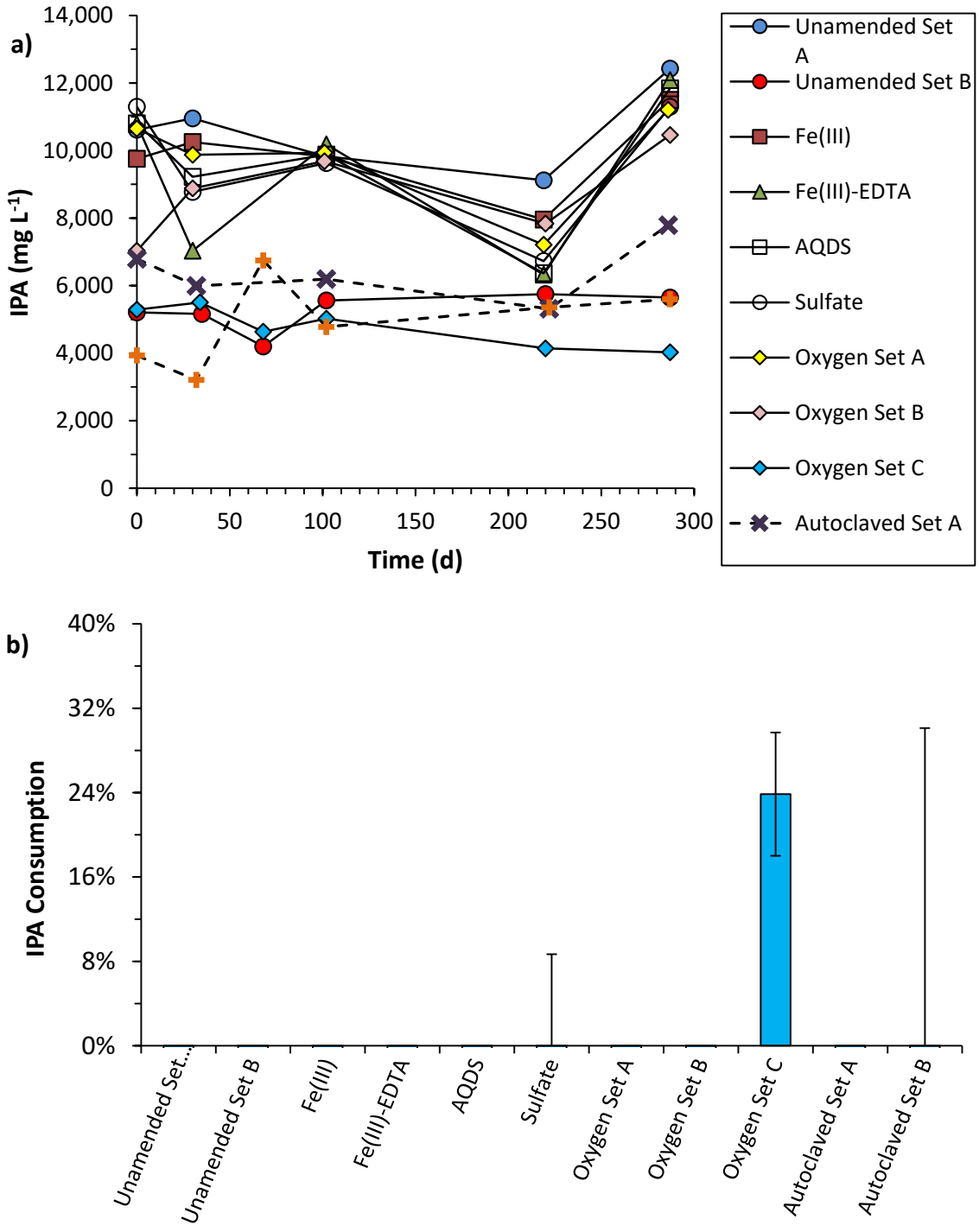

Figure 6-36. IPA concentration over time (a) and percent decreases at the end of incubation (b) for Site 2; averages of triplicate microcosms; error bars represent one standard deviation.

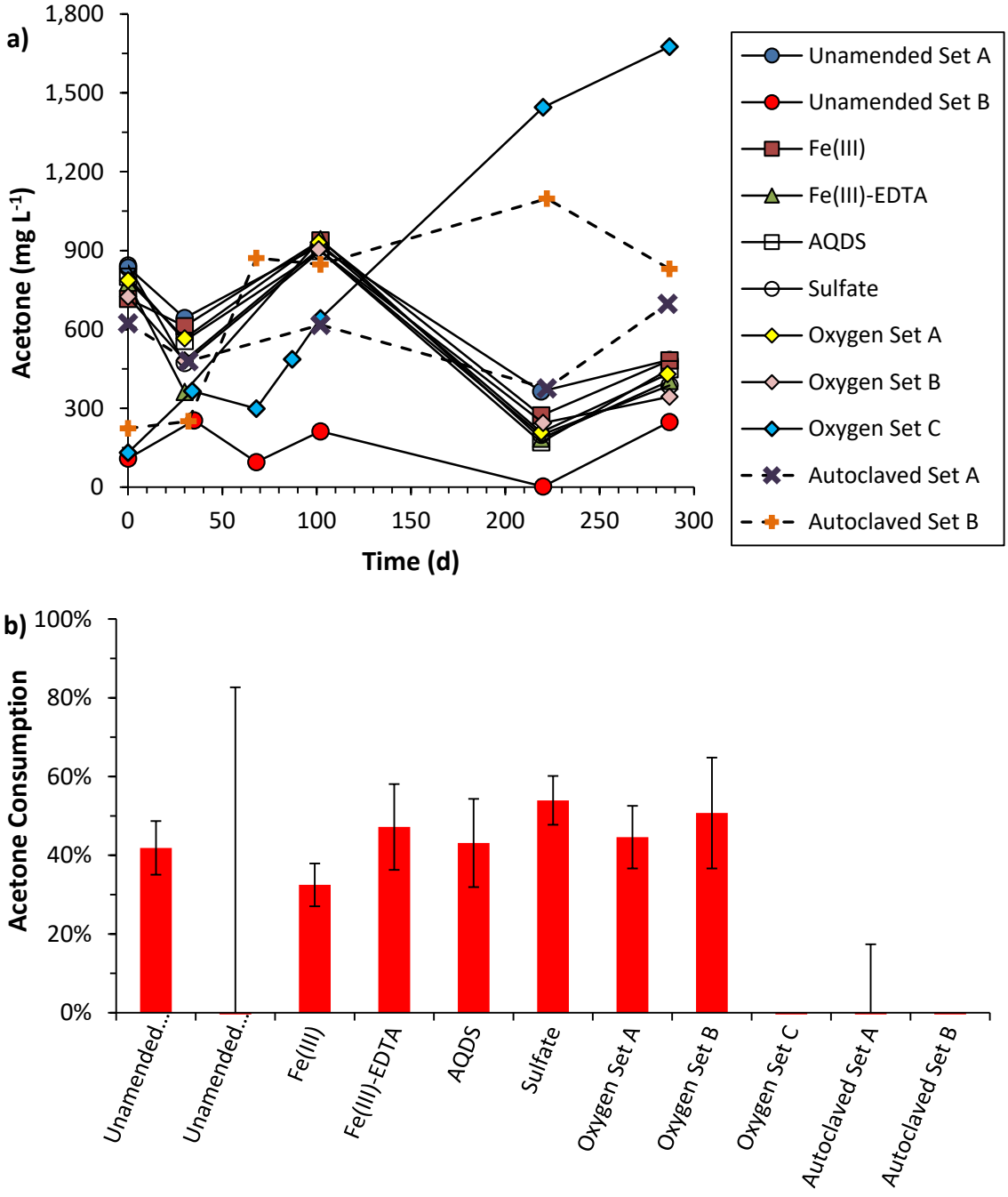

Figure 6-37. Acetone concentration over time (a) and percent decreases at the end of incubation (b) for Site 2; averages of triplicate microcosms; error bars represent one standard deviation.

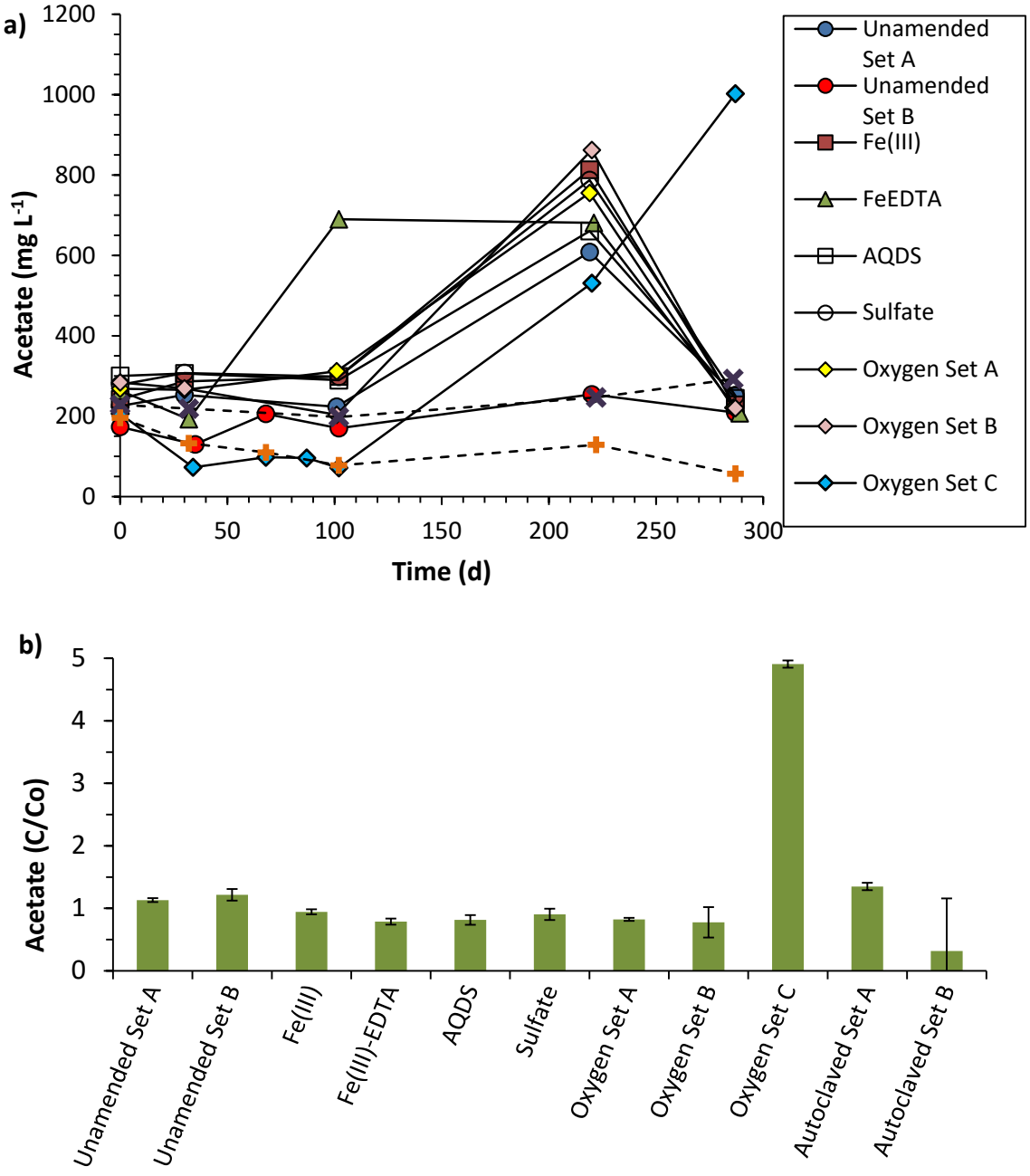

Figure 6-38. Acetate concentration over time (a) and percent decreases at the end of incubation (b) for Site 2; averages of triplicate microcosms; error bars represent one standard deviation.

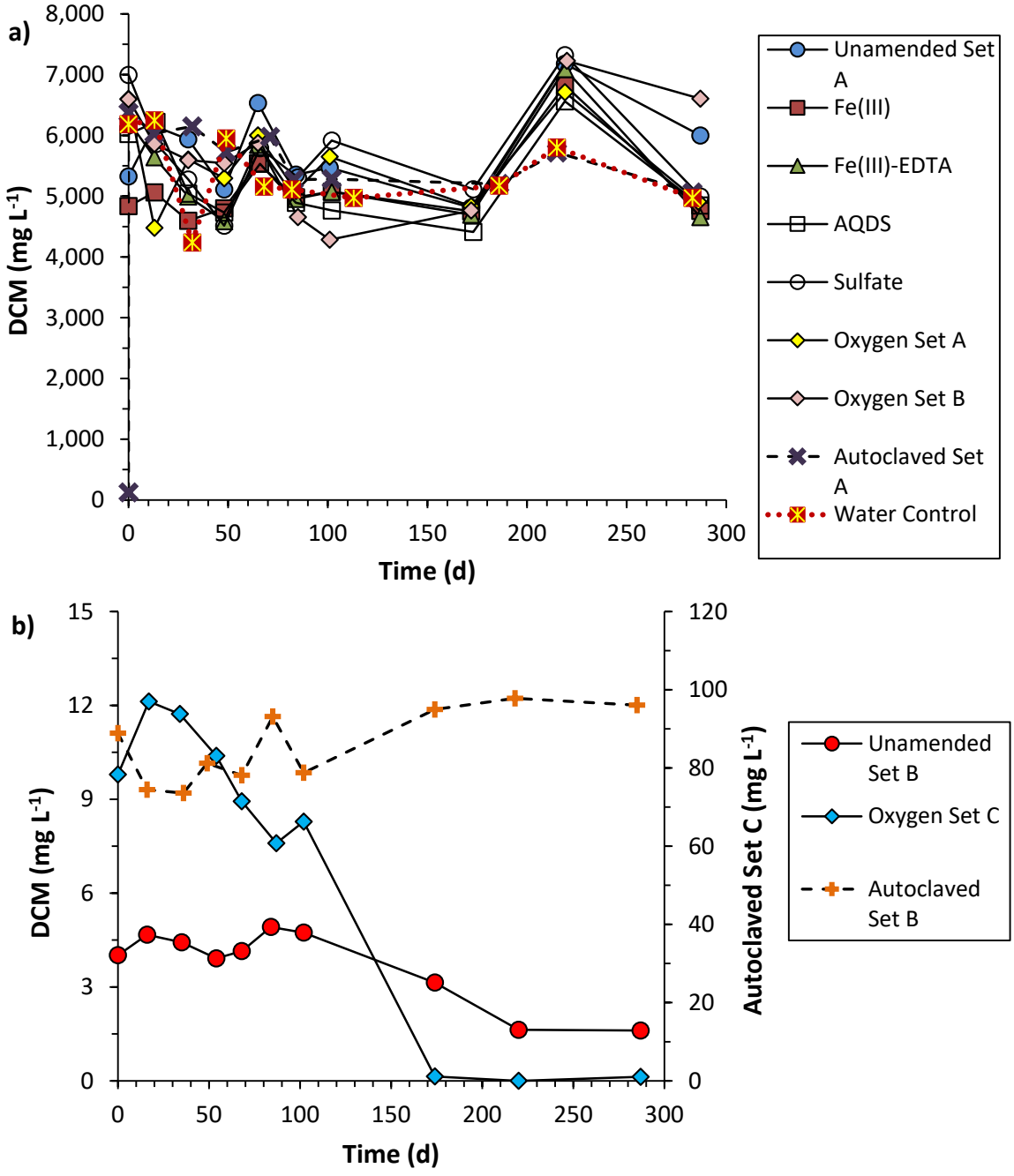

Figure 6-39. DCM concentration over time (a) and percent decreases at the end of incubation (b) for Site 2; averages of triplicate microcosms; error bars represent one standard deviation.

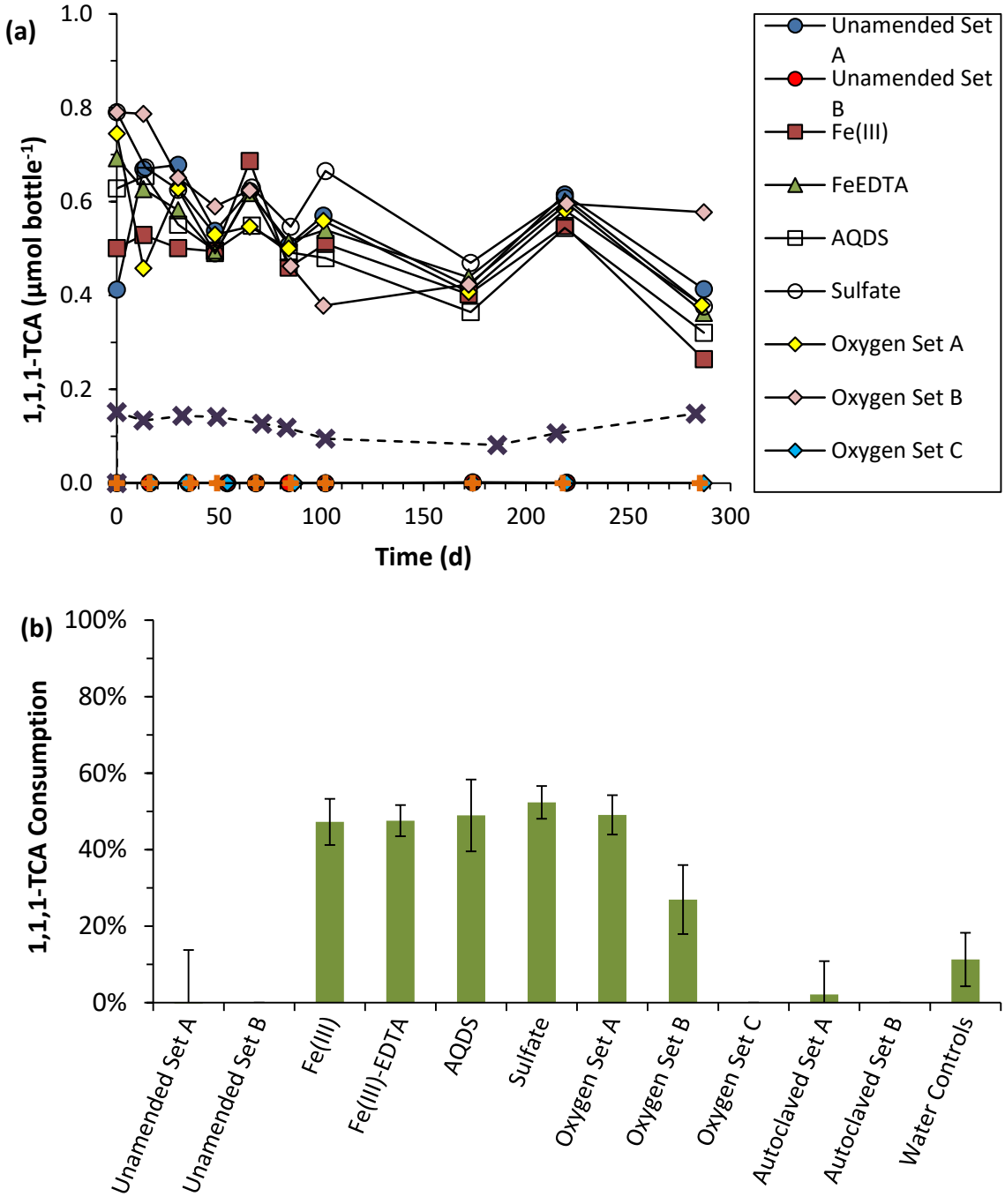

Figure 6-40. 1,1,1-TCA concentration over time (a) and percent decreases at the end of incubation (b) for Site 2; averages of triplicate microcosms; error bars represent one standard deviation.

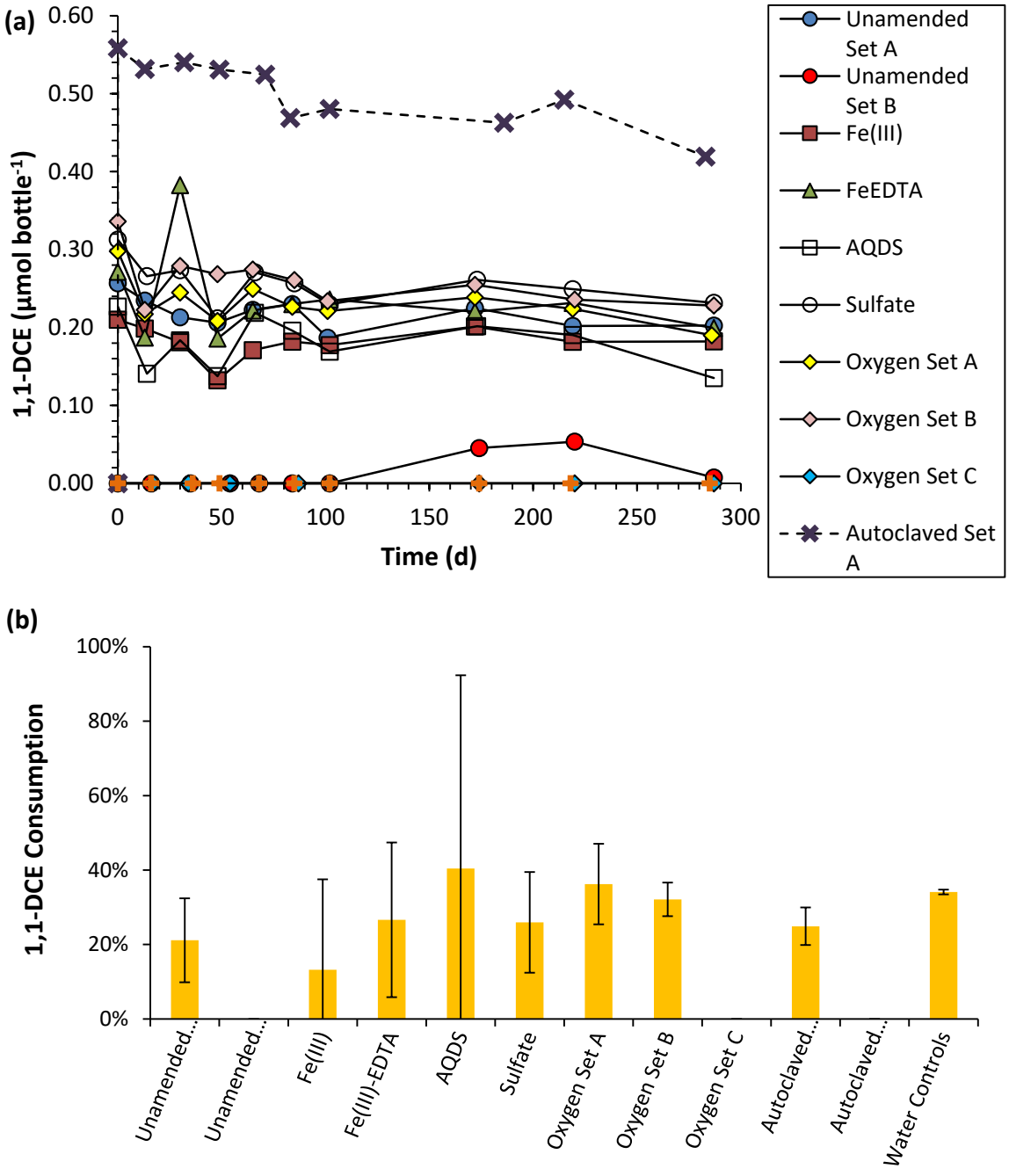

Figure 6-41. 1,1-DCE concentration over time (a) and percent decreases at the end of incubation (b) for Site 2; averages of triplicate microcosms; error bars represent one standard deviation.

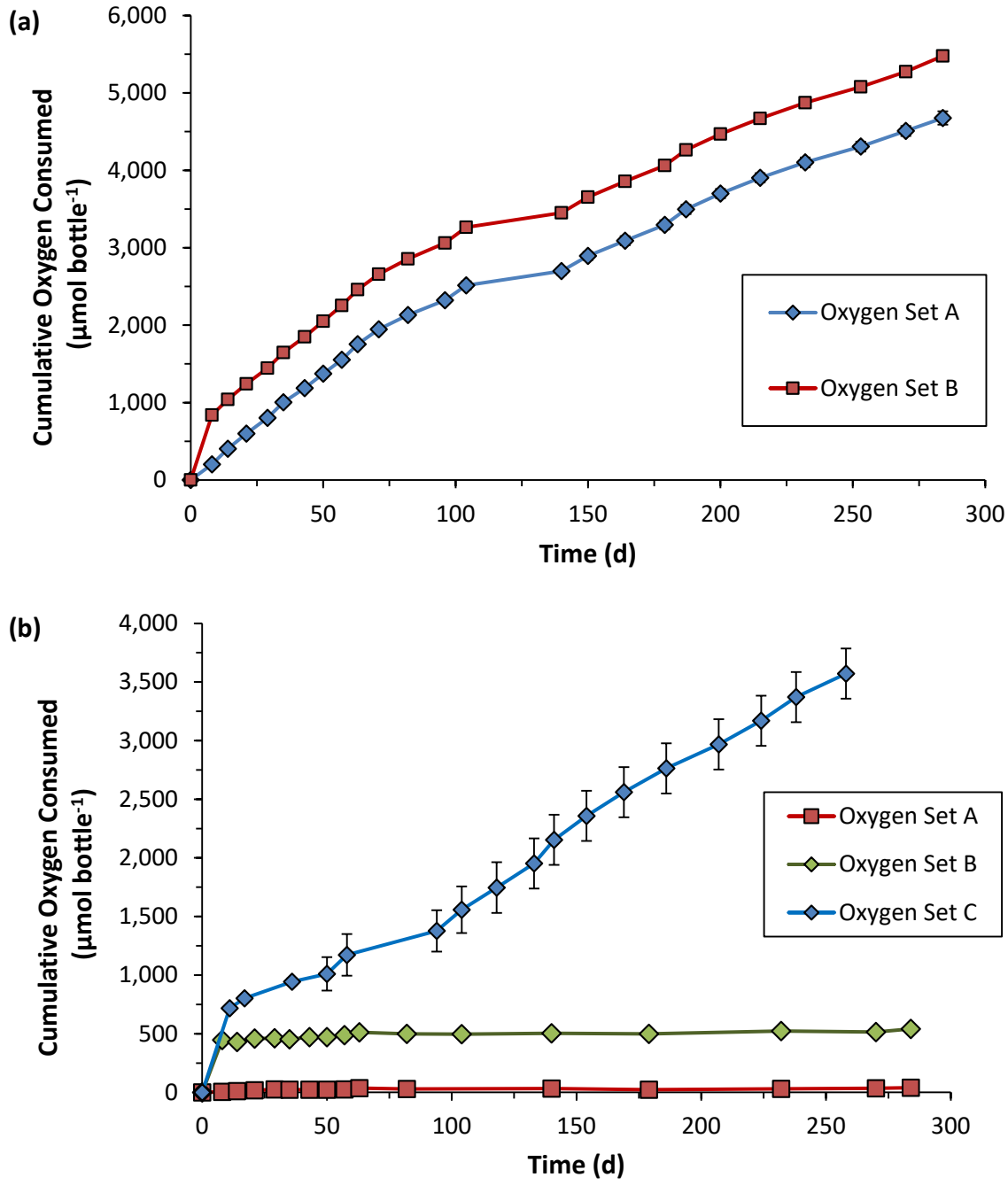

Figure 6-42. Average cumulative oxygen consumed for small microcosms from Site 1 (a) and Site 2 (b); averages of triplicate microcosms and error bars represent one standard deviation.

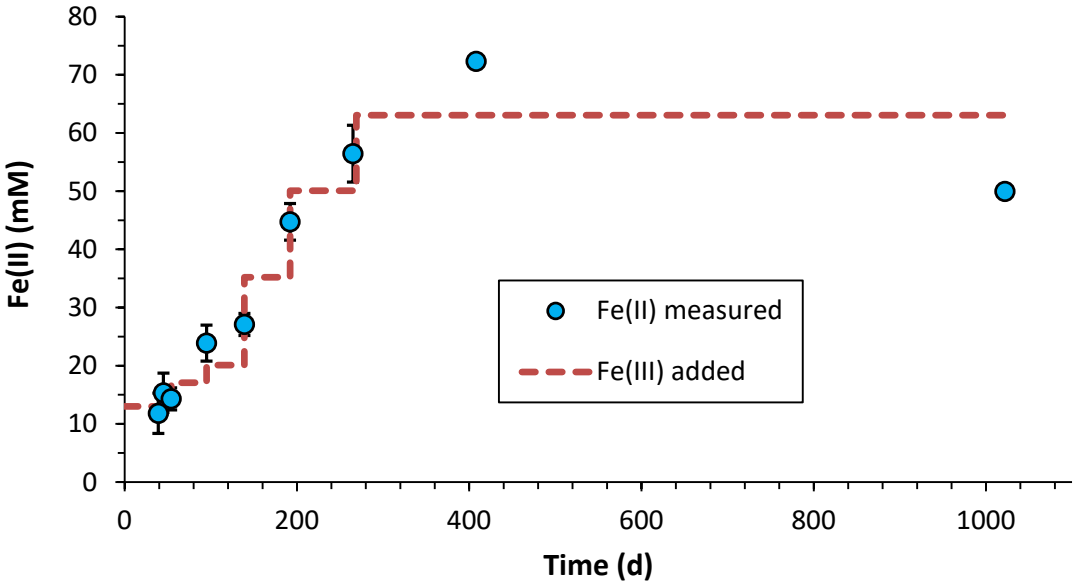

Figure 6-43. Concentration of reduced iron, Fe(II), in large microcosms from Site 1 that were amended with Fe(III)-EDTA. Circles represent triplicate measurements and dashed line is the concentration of iron added as Fe(III)-EDTA.

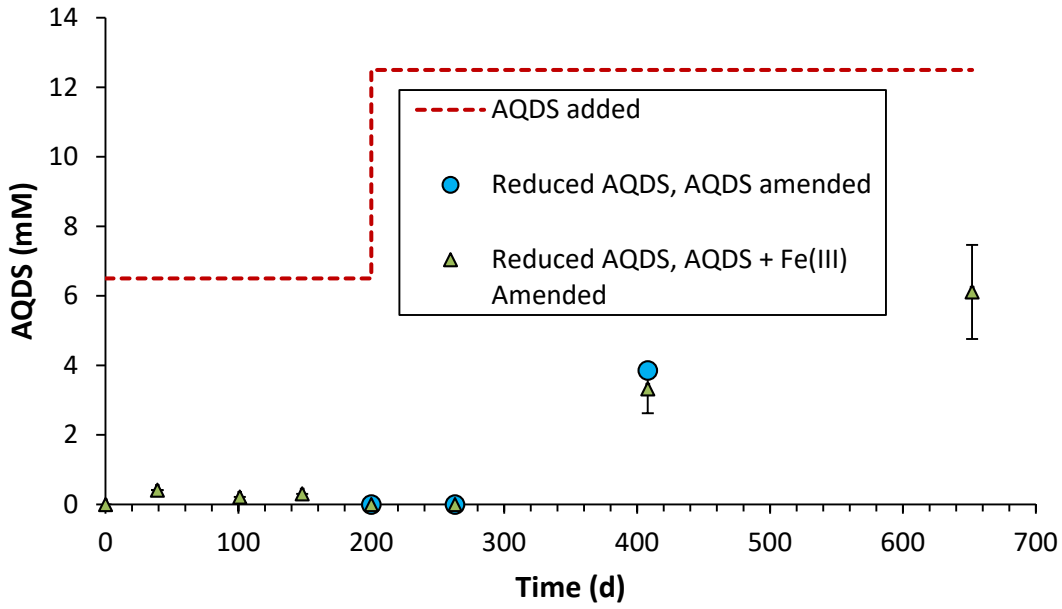

Figure 6-44. Concentration of reduced AQDS in large microcosms from Site 1 amended with AQDS (circles) and AQDS plus Fe(III) (triangles). Dashed line represents the amount of AQDS amended.

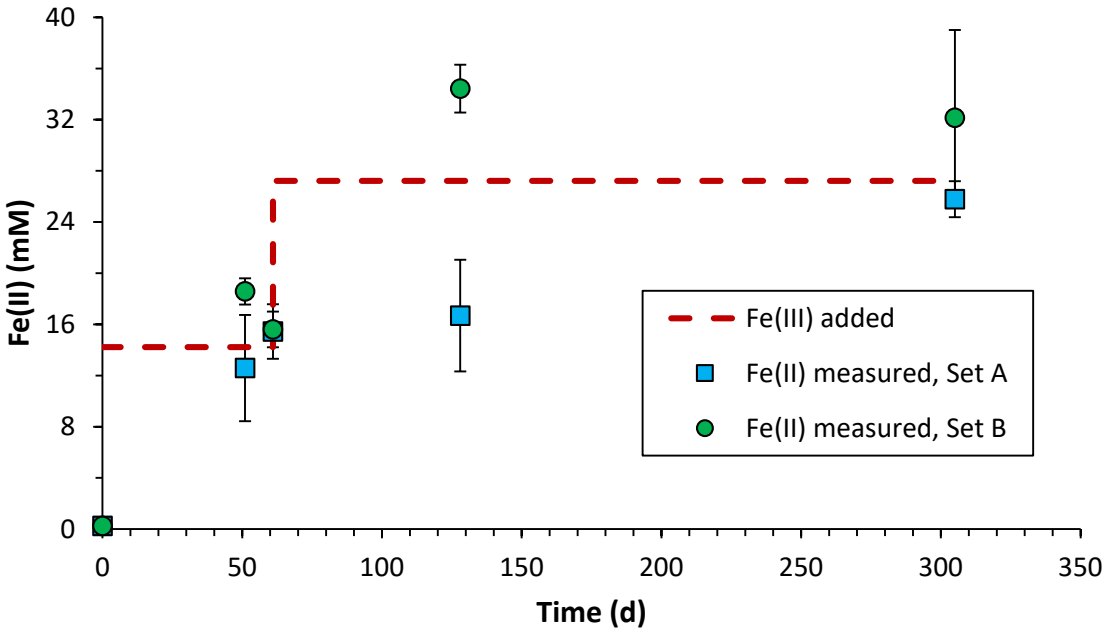

Figure 6-45. Concentration of reduced iron, Fe(II), in large microcosms from Site 2. Symbols represent triplicate measurements and dashed line is the concentration of iron added as Fe(III)-EDTA.

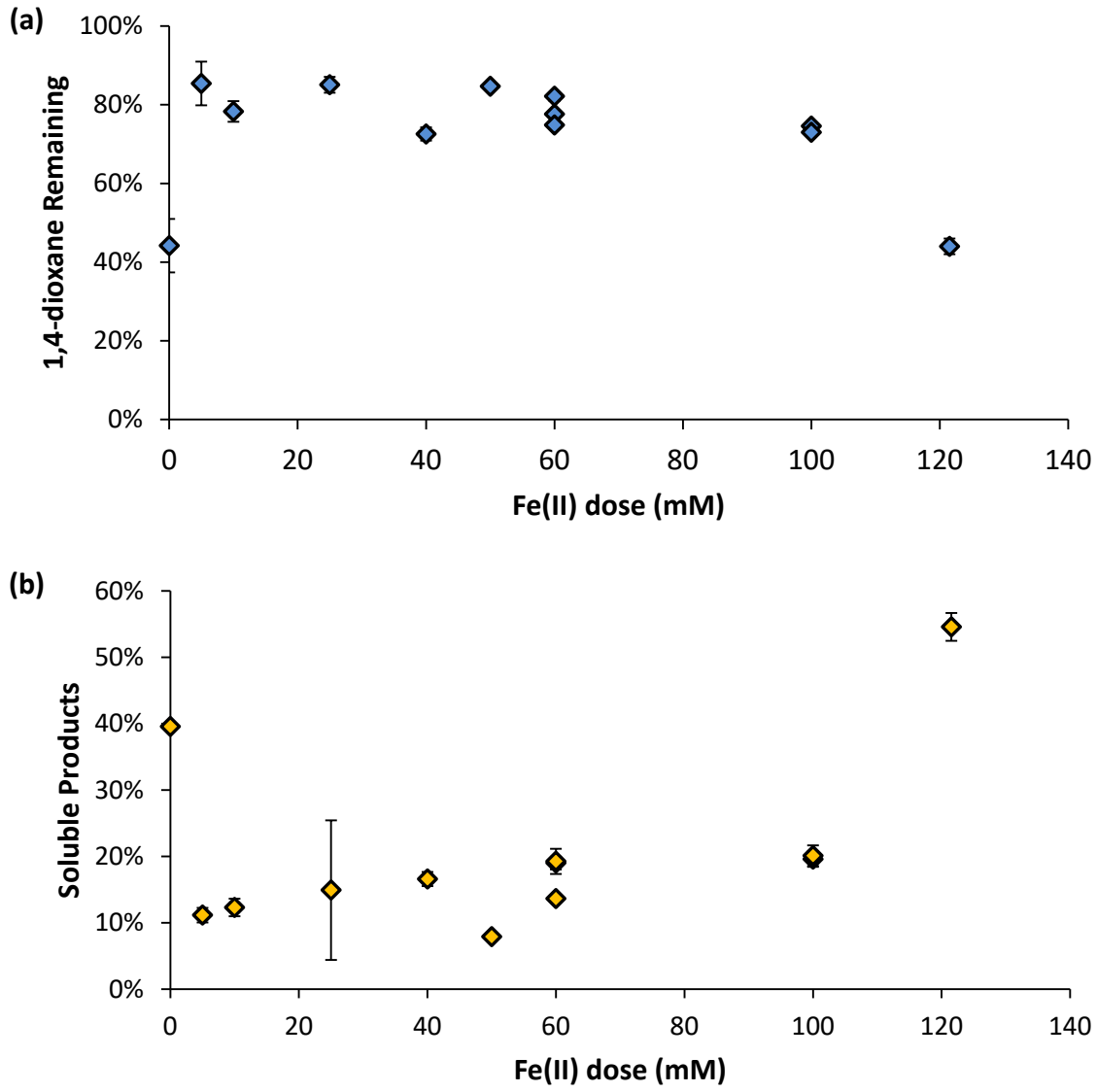

Figure 6-46. Percent of 1,4-dioxane remaining (a) and soluble products (b) after iron oxidation occurred for different doses of reduced iron in batch experiments.

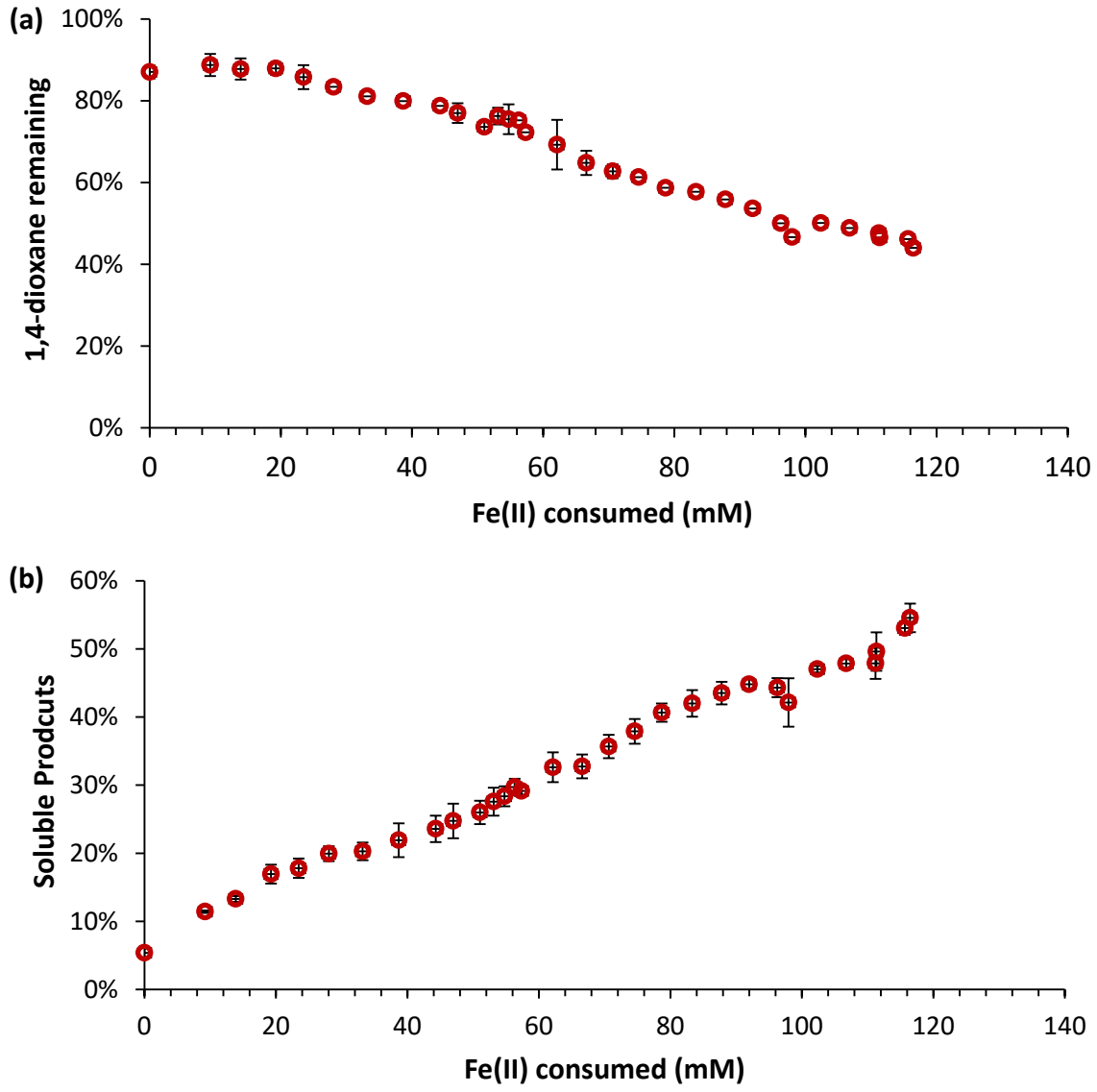

Figure 6-47. Percent of 1,4-dioxane remaining (a) and soluble products (b) after several repeated additions of reduced iron followed by oxidation. Data points indicate average of triplicate values.

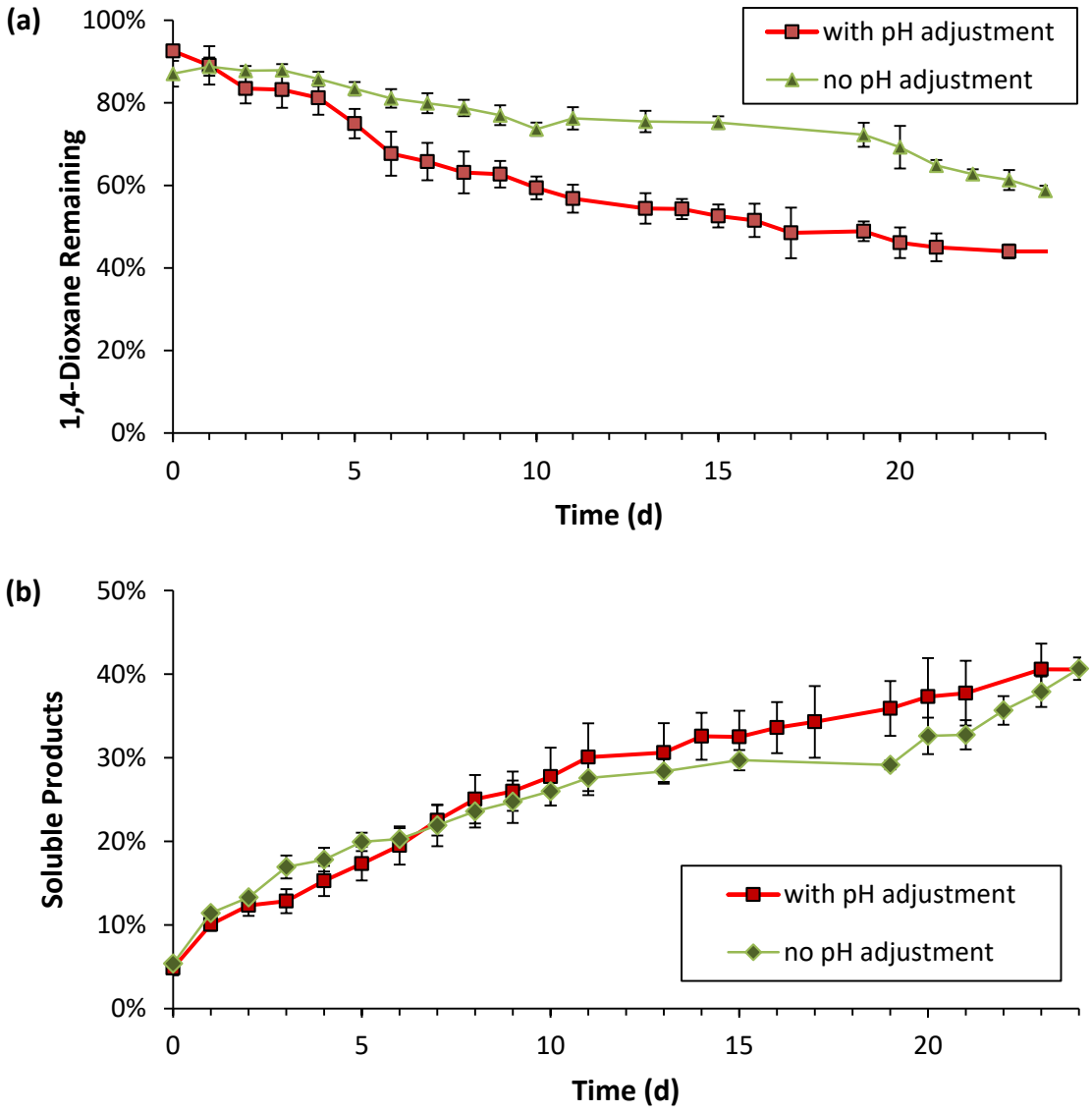

Figure 6-48. Percent of 1,4-Dioxane remaining (a) and soluble products (b) for batch experiments amended with reduced iron and exposed to oxidation, with and without pH adjustment.

D. Additional Figures

D1. Biodegradation Pathways

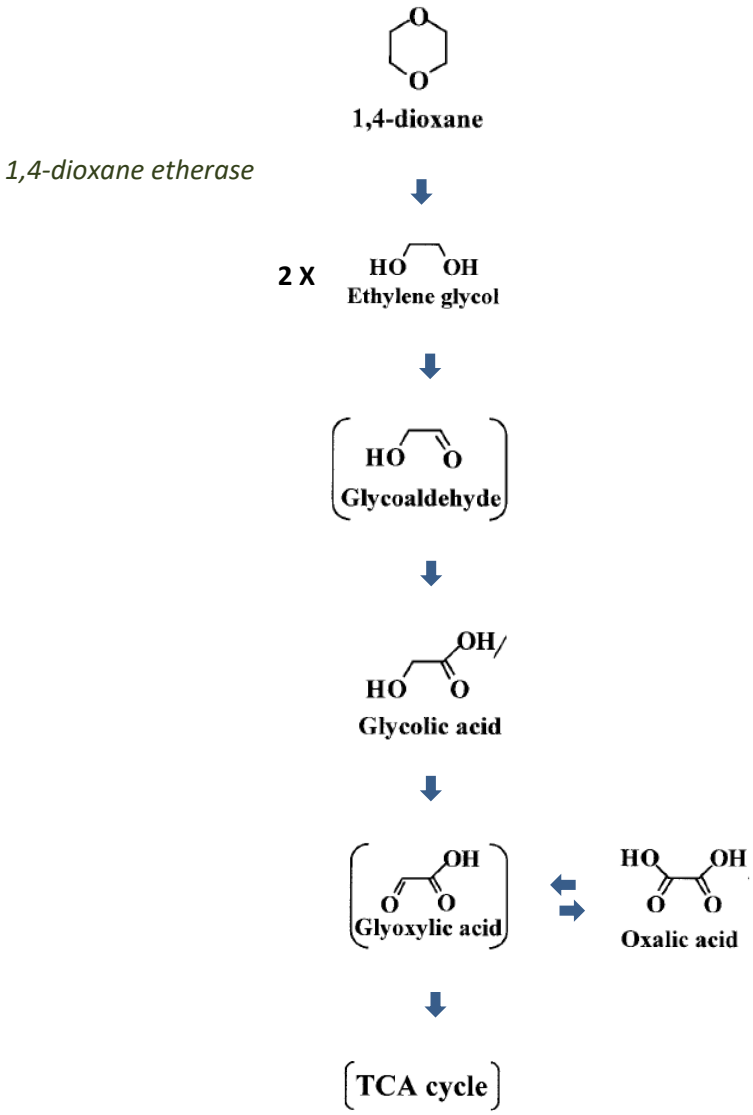

Figure 6-49. Biodegradation pathway of 1,4-dioxane by fungus *Cordyceps sinensis* (Nakamiya et al., 2005).

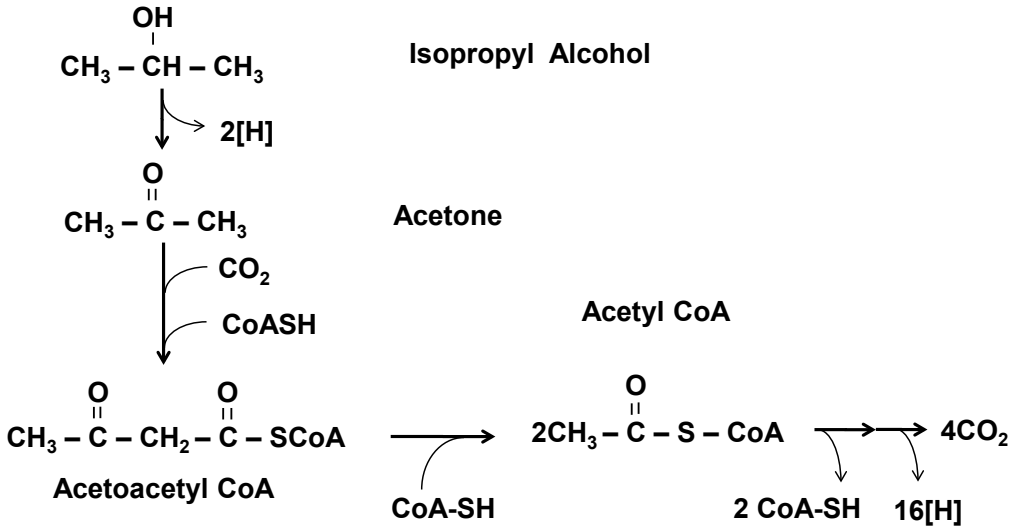

Figure 6-50. Pathway for oxidation of IPA to acetone and formation of acetyl CoA (Platen et al., 1990; Terzis and Diaper, 1990).

D2. Response Factors

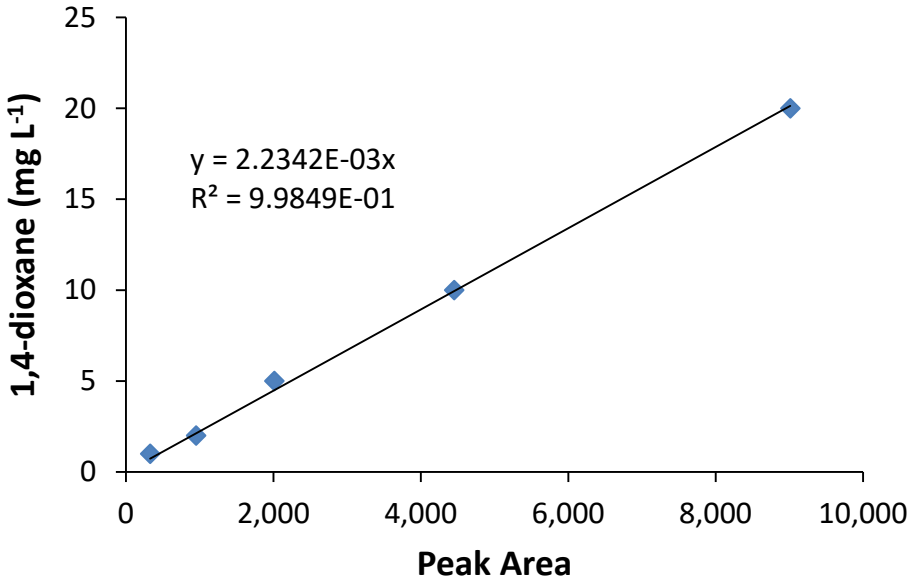

Figure 6-51. Standard calibration curve for 1,4-dioxane on GC-FID.

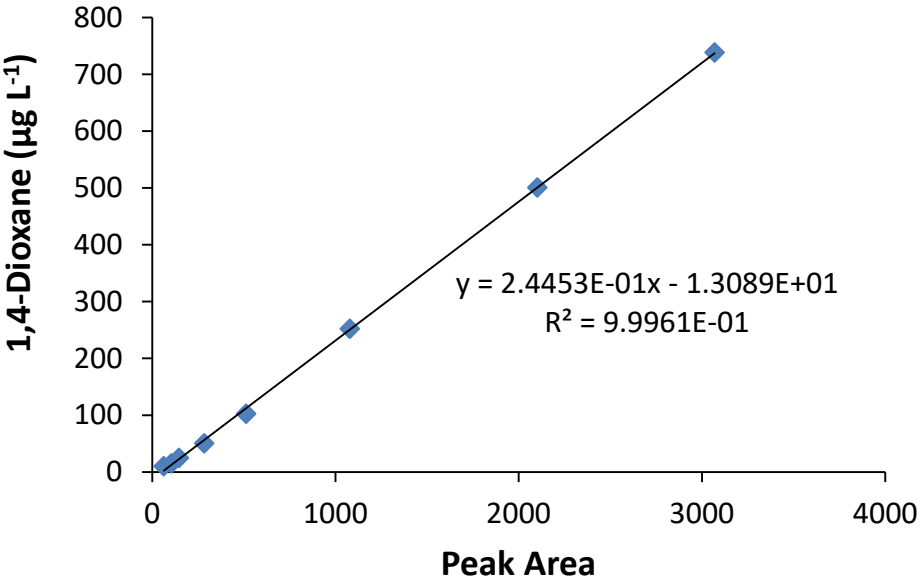

Figure 6-52. Standard calibration curve for 1,4-dioxane by the micro-frozen extraction in DCM method.

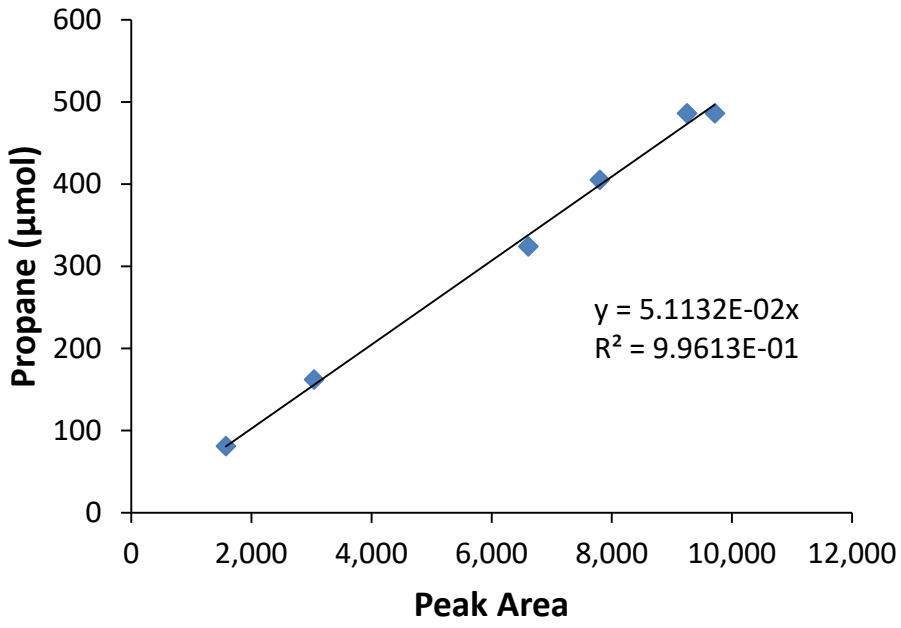

Figure 6-53. Standard calibration curve for propane on GC-FID.

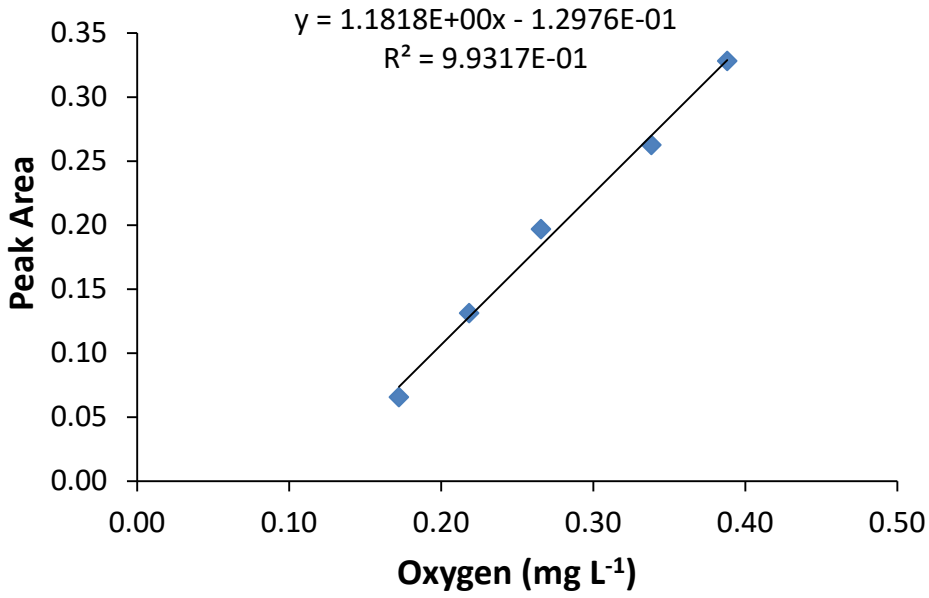

Figure 6-54. Standard calibration curve for measurements of oxygen using GC-TCD.

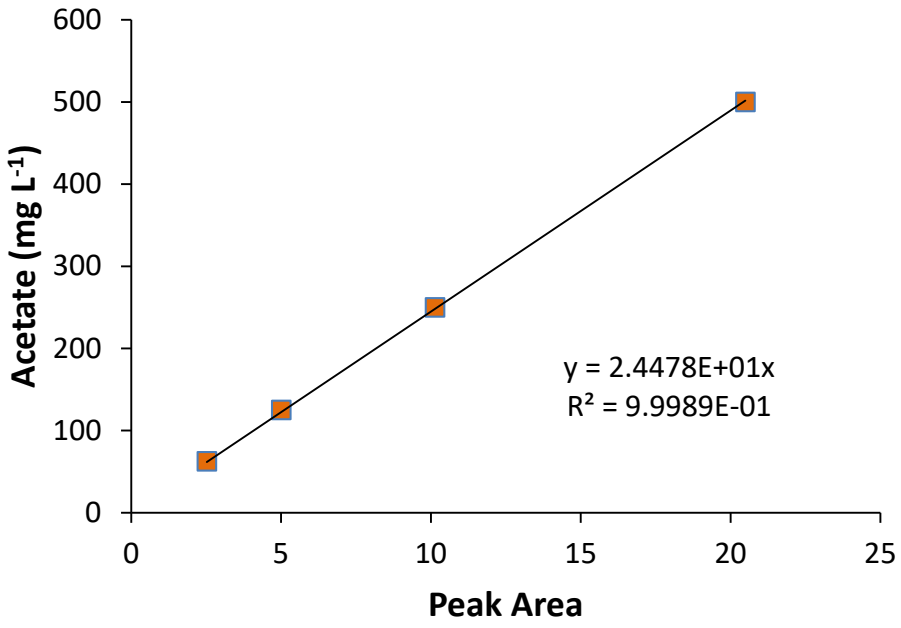

Figure 6-55. Standard calibration curve for acetate on HPLC UV at 225 nm.

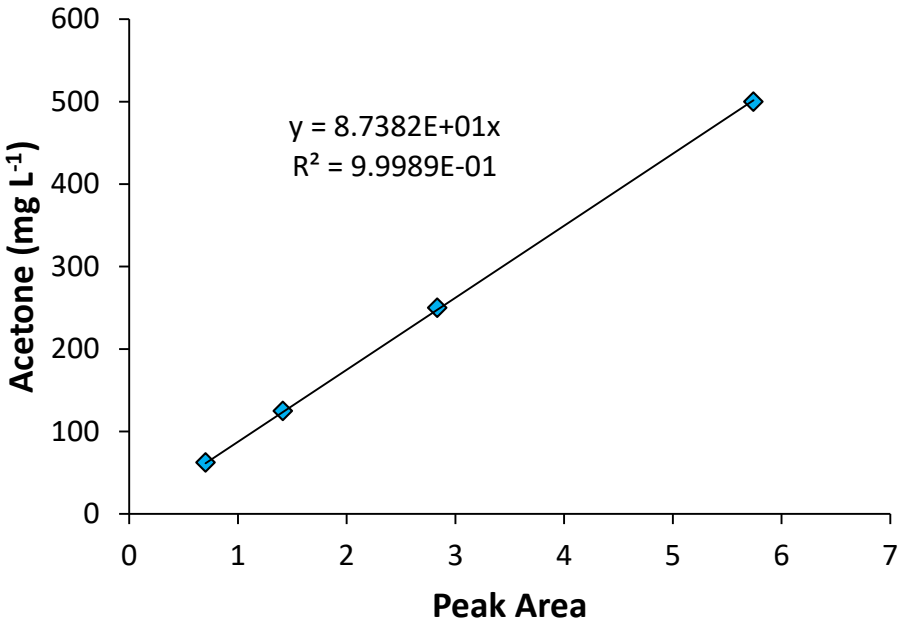

Figure 6-56. Standard calibration curve for acetone on HPLC RI.

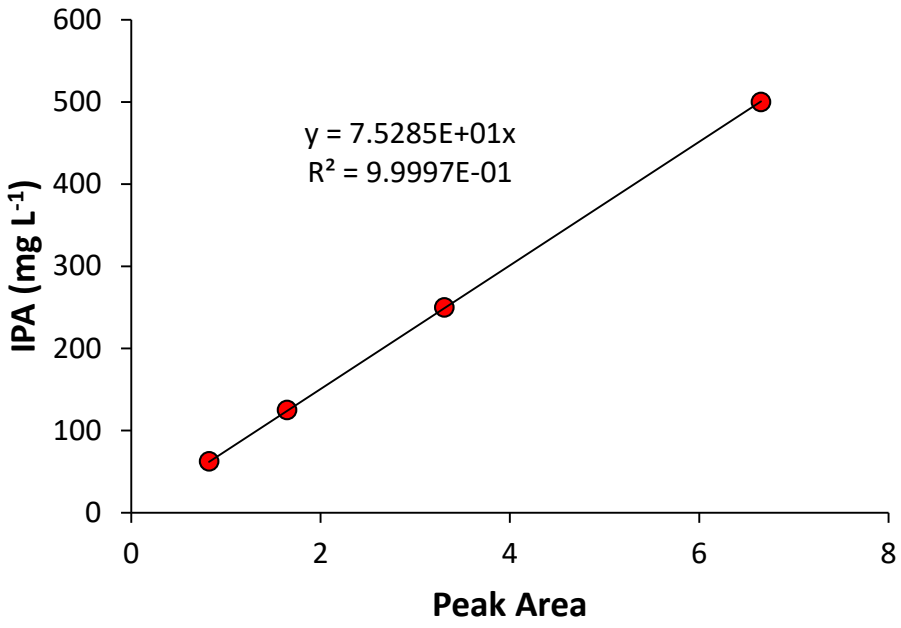

Figure 6-57. Standard calibration curve for IPA on HPLC RI.

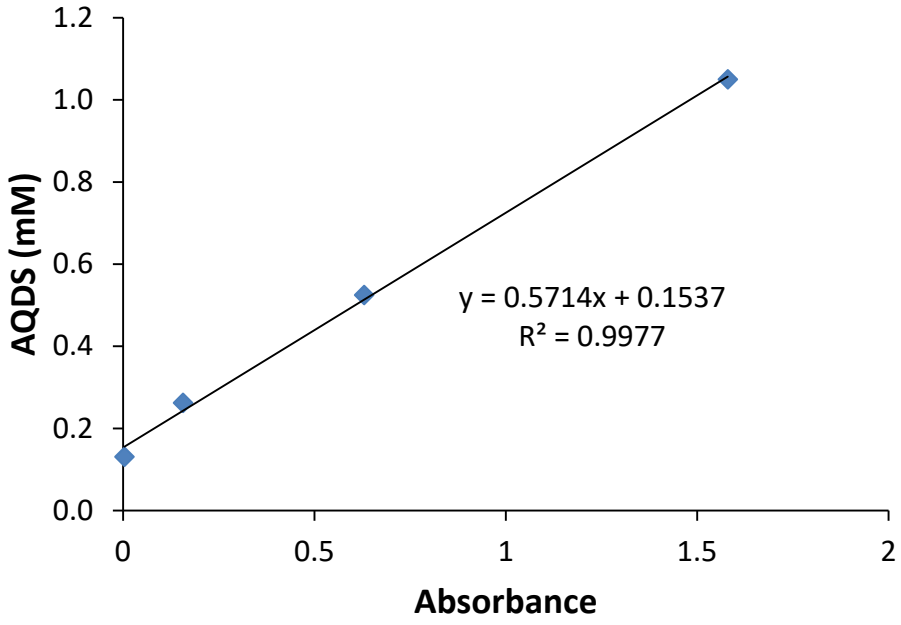

Figure 6-58. Standard calibration curve for reduced AQDS by UV absorbance.

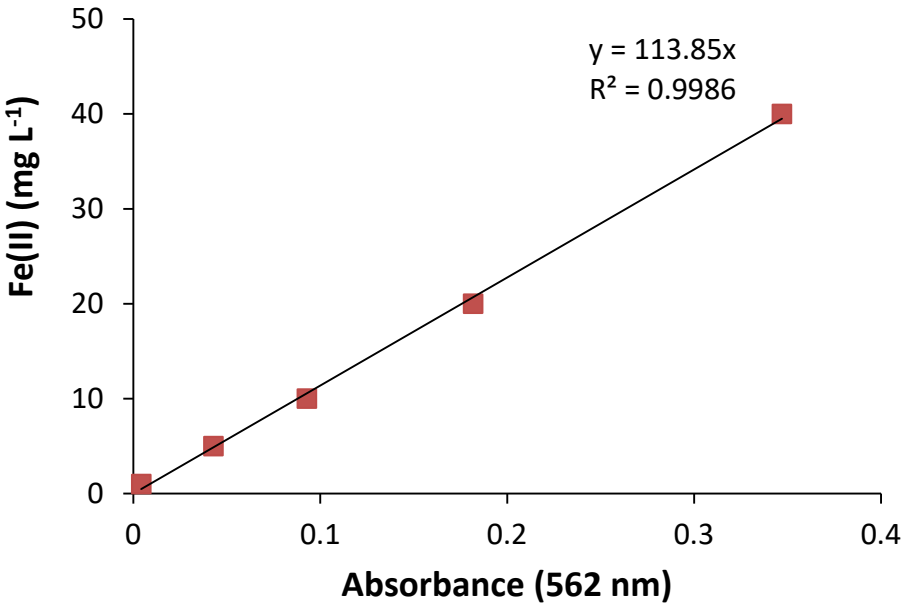

Figure 6-59. Standard calibration curve for reduced iron by UV absorbance.

7. REFERENCES

Adamson DT, Mahendra S, Walker KL, Rauch SR, Sengupta S, Newell CJ. 2014. A multisite survey to identify the scale of the 1,4-dioxane problem at contaminated groundwater sites. *Environ. Sci. Technol. Lett.* **1**:254–258.

Adamson DT, Anderson R, Mahendra S, Newell C. 2015. Evidence of 1 , 4-Dioxane Attenuation at Groundwater Sites Contaminated with Chlorinated Solvents and 1 , 4-Dioxane. *Environ. Sci. Technol.* **49**:6510–6518.

Anderson JE, Mccarty PL. 1997. Transformation yields of chlorinated ethenes by a methanotrophic mixed culture expressing particulate methane monooxygenase. *Appl. Environ. Microbiol.* **63**:687–693.

Anderson RH, Anderson JK, Bower P a. 2012. Co-occurrence of 1,4-dioxane with trichloroethylene in chlorinated solvent groundwater plumes at US air force installations: Fact or fiction. *Integr. Environ. Assess. Manag.* **8**:731–737.

Battersby NS, Wilson V. 1989. Survey of the anaerobic biodegradation potential of organic chemicals in digesting sludge. *Appl. Environ. Microbiol.* **55**:433–439.

Benner ML, Stanford SM, Lee LS, Mohtar RH. 2000. Field and numerical analysis of in-situ air sparging: A case study. *J. Hazard. Mater.* **72**:217–236.

Bernhardt D, Diekman H. 1991. Degradation of dioxane, tetrahydrofuran and other cyclic ehters by an environmental *Rhodococcus* strain. *Appl. Microbiol. Biotechnol.* **36**:120–123.

Bone A, Lehmicke L, Freedman DL. 2009. Dichloromethane inhibition of trichloroethene reductive dechlorination activity in bioaugmentation cultures. In: . *Tenth Int. Battelle Symp. situ on-site bioremediation*. Baltimore, MD.

Borden RC., Lee MD., Thomas MJ., Bedient PB., Ward HC. 1989. In situ measurment and numerical simulation of oxygen limited biotransformation. *Gr. Water Monit. Remediat.* **Winter**:83–91.

Brooks RH, Corey AT. 1964. Hydraulic Properties of Porous Media. Colorado State University. Vol. 92 61-87p. Colorado State University Hydrology Papers. http://cedb.asce.org/cgi/WWWdisplay.cgi?14175.

Broske AD, Diubaldo D, Gere DR. 2002. Headspace Analysis of Organic Volatile Impurities by USP <467> Using the DB-624 and the HP-Fast GC Residual Solvent Column. Agilent Technologies.

Bruce CL, Salanitro JP, Johnson PC, Spinner GE. 2013. Bioaugmentation for MTBE remediation. In: Stroo, HF, Leeson, A, Ward, CH, editors. *Bioaugmentation Groundw. Remediat.* Alexandria, VA: SERDP, ESTCP, pp. 289–312.

Chambon JC, Bjerg PL, Scheutz C, Bælum J, Jakobsen R, Binning PJ. 2013. Review of reactive kinetic models describing reductive dechlorination of chlorinated ethenes in soil and groundwater. *Biotechnol. Bioeng.* **110**:1–23.

Chang HL, Alvarez-Cohen L. 1995. Transformation capacities of chlorinated organics by mixed cultures enriched on methane, propane, toluene, or phenol. *Biotechnol. Bioeng.* **45**:440–449.

Chang WK, Criddle CS. 1997. Experimental evaluation of a model for cometabolism: Prediction of simultaneous degradation of trichloroethylene and methane by a methanotrophic mixed culture. *Biotechnol. Bioeng.* **56**:492–501.

Chen M, Abriola LM, Amos BK, Suchomel EJ, Pennell KD, Löffler FE, Christ J a. 2013. Microbially enhanced dissolution and reductive dechlorination of PCE by a mixed culture: Model validation and sensitivity analysis. *J. Contam. Hydrol.* **151**:117–130.

Chiang CY., Salanitro JP., Chai EY., Colthart JD., Klein CL. 1989. Aerobic biodegradation of benzene, yoluene, and xylene in a sandy aquifer-data analysis and computer modeling. *Ground Water* **27**:823–834.

Deeb RA, Scow KM, Alvarez-Cohen L. 2000. Aerobic MTBE biodegradation: An examination of past studies, current challenges and future research directions. *Biodegradation* **11**:171–186.

EPA. 2012. 1,4-Dioxane in the Environment. *Tech. Outreach Serv. Communities*. Environmental Protection Agency.

Essaid BHI, Bekins BA. 1997. BIOMOC, A Multispecies Solute-Transport Model with Biodegradation. Menlo Park, CA.

Finneran KT, Lovley DR. 2001. Anaerobic Degradation of Methyl tert-Butyl Ether (MTBE) and tert-Butyl Alcohol (TBA). *Environ. Sci. Technol.* **35**:1785–1790.

http://dx.doi.org/10.1021/es001596t.

Frascari D, Zanaroli G, Danko AS. 2015. In situ aerobic cometabolism of chlorinated solvents: A review. *J. Hazard. Mater.* **283**:382–399.

Freedman DL, Smith CR, Noguera DR. 1997. Dichloromethane biodegradation under nitrate-reducing conditions. *Water Environ. Res.* **69**:229–235.

Gälli R, Leisinger T. 1985. Specialized bacterial strains for the removal of dichloromethane from industrial waste. *Conserv. Recycl.* **8**:91–100.

Gelhar LW, Welty C, Rehfeldt KR. 1992. A Critical Review of Data on Field-Scale Dispersion in Aquifers. *Water Resour. Res.* **28**:1955–1974. http://dx.doi.org/10.1029/92WR00607.

Grady CPL, Daigger GT, Love NG, Filipe C. 2011. Biological wastewater treatment 3rd ed. IWA Publishing 324,325 p.

Grady CPL, Smets BF, Barbeau DS. 1996. Variability in kinetic parameter estimates: A review of possible causes and a proposed terminology. *Water Res.* **30**:742–748.

Harder W, Dijkhuizen L. 1984. Physiological responses to nutrient limitation. *Ann. Rev. Micriobiol.* **22**:1–23.

Hareland WA, Crawford RL, Chapman PJ, Dagley S. 1975. Metabolic function and properties of 4-hydroxyphenylacetic acid 1-hydroxylase from Pseudomonas acidovorans. *J. Bacteriol.* **121**:272–285.

Harter T. 2003. Basic Concepts of Groundwater Hydrology. *Agric. Nat. Resour. Univ. Calif.*

Hartung R. 1989. Health and environmental effects assessment for 1,4-dioxane. Ann Arbor: Gelman Sciences, Inc 1-124 p.

Heijnen J, Romein B. 1995. Derivation of kinetic equations for growth on single substrates based on general properties of a simple metabolic network. *Biotechnol. Prog.* **11**:712–716.

Hongwei Y, Zhanpeng J, Shaoqi S. 2004. Anaerobic biodegradability of aliphatic

compounds and their quantitative structure biodegradability relationship. *Sci. Total Environ.* **322**:209–19. http://www.ncbi.nlm.nih.gov/pubmed/15081749.

Hornberger GM, Milis AL, Herman J. 1992. Bacterial transport in porous media. *Water Resour. Res.* **28**:9. http://www.opengrey.eu/item/display/10068/822397?lang=fr.

Huang H, Shen D, Li N, Shan D, Shentu J, Zhou Y. 2014. Biodegradation of 1,4-dioxane by a novel strain and its biodegradation pathway. *Water. Air. Soil Pollut.* **225**.

Hunter KS, Wang Y, Papenguth HW. 2001. Kinetic modeling of microbially-driven redox chemistry of radionuclides in subsurface environments: Coupling transport, microbial metabolism and geochemistry. *J. Contam. Hydrol.* **47**:297–309.

Ji W, Dahmani A, Ahlfeld DP, Lin JD, Hill E. 1993. Laboratory Study of Air Sparging: Air Flow Visualization. *Ground Water Monit. Remediat.* **13**:115–126. http://dx.doi.org/10.1111/j.1745-6592.1993.tb00455.x.

Johnson PC, Johnson RL, Bruce CL, Leeson A. 2001. Advances in In Situ Air Sparging/Biosparging. *Bioremediat. J.* **5**:251–266. http://www.tandfonline.com/doi/abs/10.1080/20018891079311.

Kelley SL, Aitchison EW, Deshpande M, Schnoor JL, Alvarez PJJ. 2001. Biodegradation of 1,4-dioxane in planted and unplanted soil: Effect of bioaugmentation with *Amycolata* sp. CB1190. *Water Res.* **35**:3791–3800.

Kilroy AC, Gray NF. 1992. The toxicity of four organic solvents commonly used in the pharmaceutical industry to activated sludge. *Water Res.* **26**:887–892. http://www.sciencedirect.com/science/article/pii/0043135492901938.

Kim YM, Jeon JR, Murugesan K, Kim EJ, Chang YS. 2009. Biodegradation of 1,4-dioxane and transformation of related cyclic compounds by a newly isolated *Mycobacterium* sp. PH-06. *Biodegradation* **20**:511–519.

Kohler-Staub D, Frank S, Leisinger T. 1995. Dichloromethane as the sole carbon source for Hyphomicrobium sp. strain DM2 under denitrification conditions. *Biodegradation* **6**:229–235.

Kohlweyer U, Thiemer B, Schräder T, Andreesen JR. 2000. Tetrahydrofuran degradation by a newly isolated culture of *Pseudonocardia* sp. strain K1. *FEMS Microbiol. Lett.* **186**:301–306.

Kovárová-Kovar K, Egli T. 1998. Growth kinetics of suspended microbial cells: from single-substrate-controlled growth to mixed-substrate kinetics. *Microbiol. Mol. Biol. Rev.* **62**:646–666.

Kwon MJ, Finneran KT. 2008. Biotransformation products and mineralization potential for hexahydro-1,3,5-trinitro-1,3,5-triazine (RDX) in abiotic versus biological degradation pathways with anthraquinone-2,6-disulfonate (AQDS) and *Geobacter metallireducens*. *Biodegradation* **19**:705–15. http://www.ncbi.nlm.nih.gov/pubmed/18239998.

LaGrega MD, Buckingham PL, Evans JC. 1994. Hazardous Waste Management. New York: McGraw-Hill.

Li M, Conlon P, Fiorenza S, Vitale R, Alvarez PJJ. 2011. Rapid Analysis of 1,4-Dioxane in Groundwater by Frozen Micro-Extraction with Gas Chromatography/Mass Spectrometry. *Ground Water* **31**:70–76. http://onlinelibrary.wiley.com/doi/10.1111/j.1745-6592.2011. 01346.x/abstract.

Li M, Fiorenza S, Chatham JR, Mahendra S, Alvarez PJJ. 2010. 1,4-Dioxane biodegradation at low temperatures in Arctic groundwater samples. *Water Res.* **44**:2894–2900.

Lippincott D, Streger SH, Schaefer CE, Hinkle J, Stormo J, Steffan RJ. 2015. Bioaugmentation and propane biosparging for in situ biodegradation of 1,4-dioxane. *Gr. Water Monit. Remediat.* **35**:1–12.

Lobos J, Wisniewski C, Heran M, Grasmick A. 2005. Effects of starvation conditions on biomass behaviour for minimization of sludge production in membrane bioreactors. *Water Sci. Technol.* **51**:35–44.

Lourenço A V. 1863. Recherches sur les composes polyatomiques. *Ann. Chim. Phys.* **67**:257–339.

Lu H, Keller J, Yuan Z. 2007. Endogenous metabolism of Candidatus Accumulibacter phosphatis under various starvation conditions. *Water Res.* **41**:4646–4656.

Lundergard PD, Andersen G. 1993. Numerical simulation of air sparging performance. In: *Proc. Pet. Hydrocarb. Org. Chem. Gr. Water Prev. Detect. Restor.*, pp. 461–476.

Mägli A, Messmer M, Leisinger T. 1998. Metabolism of dichloromethane by the strict

anaerobe Dehalobacterium formicoaceticum. *Appl. Environ. Microbiol.* **64**:646–650.

Mahendra S, Alvarez-Cohen L. 2005. *Pseudonocardia dioxanivorans* sp. nov., a novel actinomycete that grows on 1,4-dioxane. *Int. J. Syst. Evol. Microbiol.* **55**:593–598.

Mahendra S, Alvarez-Cohen L. 2006. Kinetics of 1,4-dioxane biodegradation by monooxygenase-expressing bacteria. *Environ. Sci. Technol.* **40**:5435–5442.

Mahendra S, Grostern A, Alvarez-Cohen L. 2013. The impact of chlorinated solvent co-contaminants on the biodegradation kinetics of 1,4-dioxane. *Chemosphere* **91**:88–92. http://dx.doi.org/10.1016/j.chemosphere.2012.10.104.

Mahendra S, Petzold CJ, Baidoo EE, Keasling JD, Alvarez-Cohen L. 2007. Identification of the intermediates of in vivo oxidation of 1,4-dioxane by monooxygenase-containing bacteria. *Environ. Sci. Technol.* **41**:7330–7336.

Manger EG. 1963. Porosity and Bulk Density of Sedimentary Rocks. *Geol. Survery Bull. 1144-E*.

Mayer KU, Benner SG, Frind EO, Thornton SF, Lerner DN. 2001. Reactive transport modelling of processes controlling the distribution and natural attenuation of phenolic compounds in a deep sandstone aquifer. *J. Contam. Hydrol.* **53**:341—368.

McCray JE, Falta RW. 1996. Defining the air sparging radius of influence for groundwater remediation. *J. Contam. Hydrol.* **24**:25–52.

McCray JE, Falta RW. 1997. Numerical Simulation of air sparging for remediation of NAPL contamination. *Ground Water* **35**:99–110.

Mohr TKG. 2010a. Environmental Investigacion and Remediation; 1,4-dioxane and other solvent stabilizers. Boca Raton: CRC Press.

Mohr TKG. 2010b. Detections of 1,4-Dioxane in Ambient Surface Water, Groundwater, and Air. In: . *Environ. Investig. Remediat.* Boca Raton: CRC Press, pp. 102–103.

Nakamiya K, Hashimoto S, Ito H, Edmonds JS, Morita M. 2005. Degradation of 1, 4-dioxane and cyclic ethers by an isolated fungus. *Appl. Environ. Microbiol.* **71**:1254. http://aem.asm.org/cgi/content/abstract/71/3/1254.

Narayanan B, Suidan MT, Gelderloos AB, Brenner RC. 1993. Treatment of VOCs in high strength wastes using an anaerobic expanded-bed GAC reactor. *Wat. Res.* **27**:181–194. http://www.sciencedirect.com/science/article/B6V73-48BDRVK-XM/2/51c3d034632abe2c 411c7e46f775f2d3.

Neter J, Kutner MH., Nactsheim CJ., Wasserman W. 1996. Applied linear statistical models. Ed. John Neter 4th ed. Homewoood, IL: Irwim.

Parales RE, Adamus JE, White N, May HD. 1994. Degradation of 1,4-dioxane by an actinomycete in pure culture. *Appl. Environ. Micriobiol.* **60**:4527–4530.

Perez Padilla GG. 1996. Effects of synthetic organic chemicals on microbial death and lysis; Clemson University.

Platen H, Temmes A, Schink B. 1990. Anaerobic degradation of acetone by *Desulfococcus biacutus* spec. nov. *Arch. Microbiol.* **154**:355–361.

Pugazhendi A, Rajesh Banu J, Dhavamani J, Yeom IT. 2015. Biodegradation of 1,4-dioxane by *Rhodanobacter* AYS5 and the role of additional substrates. *Ann. Microbiol.* **65**:2201–2208. http://link.springer.com/10.1007/s13213-015-1060-y.

Rashid M, Kaluarachchi JJ. 1999. A simplified numerical algorithm for oxygen- and nitrate-based biodegradation of hydrocarbons using Monod expressions. *J. Contam. Hydrol.* **40**:53–77.

Reichert P. 1994. Aquasim - a Tool for Simulation and Data-Analysis of Aquatic Systems. *Water Sci. Technol.* Vol. 30 21-30p.

Rothermich MM, Hayes L a., Lovley DR. 2002. Anaerobic, sulfate-dependent degradation of polycyclic aromatic hydrocarbons in petroleum-contaminated harbor sediment. *Environ. Sci. Technol.* **36**:4811–4817.

Roy D, Anagnostu G, Chaphalkar P. 1994. Biodegradation of dioxane and diglyme in industrial waste. *J. Environ. Sci. Heal. . Part A Environ. Sci. Eng. Toxicol.* **29**:129–147.

Sales CM, Grostern A, Parales J V., Parales RE, Alvarez-Cohen L. 2013. Oxidation of the cyclic ethers 1,4-dioxane and tetrahydrofuran by a monooxygenase in two *Pseudonocardia* species. *Appl. Environ. Microbiol.* **79**.

Sander R. 1999. Compilation of Henry ' s Law Constants for Inorganic and Organic Species of Potential Importance in Environmental Chemistry. *Database*. http://www.mpch-mainz.mpg.de/~sander/res/henry.html.

Scholtz R, Wackett LP, Egli C, Cook AM, Leisinger T. 1988. Dichloromethane dehalogenase with improved catalytic activity isolated from a fast-growing dichloromethane-utilizing bacterium. *J. Bacteriol.* **170**:5698–5704.

Sei K, Miyagaki K, Kakinoki T, Fukugasako K, Inoue D, Ike M. 2013. Isolation and characterization of bacterial strains that have high ability to degrade 1,4-dioxane as a sole carbon and energy source. *Biodegradation* **24**:665–674.

Sekar R, Dichristina TJ. 2014. Microbially driven fenton reaction for degradation of the widespread environmental contaminant 1,4-dioxane. *Environ. Sci. Technol.* **48**:12858–12867.

Sellers KL, Schreiber RP. 1992. Air sparging model for predicting groundwater clean up rate. In: . *Proc. Conf. Pet. Hydrocarb. Org. Chem. Gr. Water Prev. Detect. Restoration, East. Reg. Gr. Water Issues*. Dublin, Ohio: National Ground Water Association, pp. 365–376.

Semprini L, McCarty PL. 1991a. Comparison between model simulations and field results for in-situ biorestoration of chlorinated aliphatics: Part 1. Biostimulation of methanotrophic bacteria. *Ground Water* **29**:365–374.

Semprini L, McCarty PL. 1991b. Comparison between model simulations and field results for in-situ biorestoration of chlorinated aliphatics: Part 2. Cometabolic transformations. *Ground Water* **30**:37–44.

Shen W, Chen H, Pan S. 2008. Anaerobic biodegradation of 1,4-dioxane by sludge enriched with iron-reducing microorganisms. *Bioresour. Technol.* **99**:2483–2487.

Skinner K, Cuiffetti L, Hyman M. 2009. Metabolism and cometabolism of cyclic ethers by a filamentous fungus, a *Graphium* sp. *Appl. Environ. Microbiol.* **75**:5514–5522.

Steffan RJ. 2007. Biodegradation of 1,4-Dioxane 1-53 p. http://hdl.handle.net/2060/19970012342.

Steffan RJ, McClay K, Vainberg S, Condee CW, Zhang D. 1997. Biodegradation of the gasoline oxygenates methyl tert-butyl ether, ethyl tert-butyl ether, and tert-amyl

methyl ether by propane-oxidizing bacteria. *Appl. Environ. Microbiol.* **63**:4216–4222.

Stookey LL. 1970. Ferrozine: a new spectrophotometric reagent for iron. *Anal. Chem.* **42**:779–781. http://pubs.acs.org/doi/pdf/10.1021/ac60289a016.

Sun B, Ko K, Ramsay J a. 2011. Biodegradation of 1,4-dioxane by a *Flavobacterium*. *Biodegradation* **22**:651–659.

Suthersan SS. 1999. In situ air sparging. In: . *Remediat. Eng. Des. concepts*. Boca Raton, FL: CRC Press.

Terzis E, Diaper J. 1990. Anaerobic biodegradation of industrial solvents: the case of acetone and iso-propanol. In: . *Proc. 45th Ind. Waste Conf.* Purdue University, pp. 387–394.

Vainberg S, McClay K, Masuda H, Root D, Condee C, Zylstra GJ, Steffan RJ. 2006. Biodegradation of ether pollutants by *Pseudonocardia* sp. strain ENV478. *Appl. Environ. Microbiol.* **72**:5218–5224.

Vanderborght J, Vereecken H. 2007. Review of dispersivities for transport modeling in soils. *Vadose Zo. J.* **6**:29.

Verce MF, Freedman DL. 2001. Modeling the kinetics of vinyl chloride by an ethane-grown *Pseudomonas* sp. *Biotechnol. Bioeng.* **71**:274–285.

Widdel F. 1986. Growth of methanogenic bacteria in pure culture with 2-propanol and other alcohols as hydrogen donors. *Appl. Environ. Microbiol.* **51**:1056–1062.

Wilcox D, Autentrieth R, Bonner J. 1995. Propane-induced biodegradation of vapor phase trichloroethylene. *Biotechnol. Bioeng.* **46**:333–342.

Wilson JT, Adair C, Kaiser PM, Kolhatkar R. 2005. Anaerobic biodegradation of MTBE at a gasoline spill site. *Gr. Water Monit. Remediat.* **25**:103–115.

Wilson LP, Bouwer EJ. 1997. Biodegradation of aromatic compounds under mixed oxygen/denitrifying conditions: a review. *J. Ind. Microbiol. Biotechnol.* **18**:116–130.

Yao Y, Lv Z, Min H, Lv Z, Jiao H. 2009. Isolation, identification and characterization of a novel *Rhodococcus* sp. strain in biodegradation of tetrahydrofuran and its medium

optimization using sequential statistics-based experimental designs. *Bioresour. Technol.* **100**:2762–2769. http://dx.doi.org/10.1016/j.biortech.2009.01.006.

Yeh CK, Novak JT. 1994. Anaerobic biodegradation of gasoline oxygenates in soils. *Water Environ. Res.* **66**:744–752.

Zenker MJ, Borden RC, Barlaz M a. 2000. Mineralization of 1,4-dioxane in the presence of a structural analog. *Biodegradation* **11**:239–246.

Zenker MJ, Borden RC, Barlaz MA. 2002. Modeling cometabolism of cyclic ethers. *Environ. Eng. Sci.* **19**:215–228.